An Investigation of Lipid Modulation of Low Voltage Activated Currents in Spiral Ganglion Neurons

Thesis submitted to UCL by

Lorcan Browne

For the degree of

Doctor of Philosophy, PhD

Declaration

I, **Lorcan Padraig Browne**, confirm that the work presented in this thesis is my own. Where information has been derived from other sources, I confirm that this has been indicated in the thesis.

Abstract

Type I spiral ganglion neurons (SGNs) synapse onto cochlear inner hair cells and constitute the majority of afferent fibres in the auditory nerve (AN). Better characterisation of their biophysical properties may identify therapeutic targets for optimising AN sensitivity. This study aimed to characterise the membrane physiology underlying the firing properties of post-hearing onset SGNs and investigated whether their properties could be modified by the presence of native and synthetic lipids.

In dissociated ganglionic cultures, SGNs displayed an intrinsic variation in their firing properties; this could be correlated with the magnitudes of specific membrane currents. SGNs were categorised by their response to depolarising current injection; SGNs either adapted to the stimulus rapidly, slowly or not at all. Rapid adaptation, a mechanism that preserves temporal precision throughout the auditory system, was found to be regulated by a dendrotoxin-K (DTX-K) and tityustoxin-Kα (TsTx)-sensitive low-threshold voltage-activated (LVA) K^+ current, suggesting contribution by Kv1.1 and Kv1.2 subunits. As Kv1.2 channels were known to be positively modulated by membrane phosphoinositides, we investigated the influence of phosphatidylinositol-4,5-bisphosphate (PIP_2) availability on SGN K^+ currents. Inhibiting PIP_2 production using wortmannin, or sequestration using a palmitoylated peptide (PIP_2-PP), slowed or abolished adaptation in SGNs. PIP_2-PP specifically reduced SGN LVA currents in a manner that was partly rescued by intracellular dialysis with diC_8PIP_2, a non-hydrolysable analogue of PIP_2. PIP_2-PP application induced similar levels of current inhibition in Kv1.1/Kv1.2 channels heterologously expressed in HEK293 cells. Accordingly, the lipid sensitivity of the Kv1.2 channel was further explored with a range of native and synthetic free fatty acids. Polyunsaturated fatty acids were found to be strong inhibitors of Kv1.2 currents, offering further potential candidates for SGN modulation.

Collectively, this data identifies Kv1.1 and Kv1.2 containing K^+ channels as key regulators of excitability in the AN, and potential targets for pharmacological modulation.

Acknowledgements

I would like to thank my supervisors; Dan Jagger, David Selwood and David McAlpine. Their constant kindness, support and patience were invaluable throughout my PhD. In particular, I would like to thank Dan for the time and effort he took in introducing me to the world of electrophysiology and for his constant help and encouragement thereafter. I would also like to thank Katie Smith who helped me immeasurably since her arrival. Without her input and advice my work would have been considerably poorer.

I would like to thank everyone at Ear Institute and the Wolfson Institute who helped me in one way or another in my work over the four years. At the Ear institute I would like to thank Miriam Gomez, Ruth Taylor, Andy Forge, Jimena Ballestero, Anwen Bullen, Warren Bakay, Katherine Wood, Piotr Sirko, Paromita Majumder and Robert Knight for their help and advice around the lab. At the Wolfson Institute, I would like to thank everyone in the Selwood lab especially Edith Chan, Filipa Mota, Justin Warne, David Steadman, Jennie Hutton, Christelle Soudy, Ioanna Sevastou and Paul Gane. Your friendliness and help made working there a pleasure.

I would like to thank all of my family and friends. It goes without saying I couldn't have done it without you. To my Mom, Emmett, Declan and Mary, your constant support, genuine interest and unwavering enthusiasm were all very much appreciated. Padraig and Barry, who always made Ireland feel that much closer, thank you. Finally, I would like to thank Elaine, without whom I could never have made it this far.

Contributors to work presented in this thesis

Once more, I would like Katie Smith for her contribution to the overall project. In particular, for her generation of the Kv1.1 and Kv1.2 constructs used in this study, and for sacrificing the time and effort to take me through the theory and practice of making them.

Table of contents

List of figures

Chapter 1

Chapter 3

Chapter 4

Chapter 5

List of tables

List of chemical schematics

Abbreviations

µW	Microwave
AA	Arachidonic acid
acac	Acetylacetone group (chemistry)
ACh	Acetylcholine
AEA	Anandamide
AKT	v-akt murine thymoma viral oncogene homolog (kinase)
ANF	Auditory nerve fibre
ANOVA	Analysis of variance
AP	Action potential
ArA	Arachidic Acid
ATP	Adenosine triphosphate
AVCN	Anteroventral cochlear nucleus
BDNF	Brain-derived neurotrophic factor
BK	Large-conductance calcium-activated K^+ (channel)
BPLB	Blood-perilymph barrier
CA	Caprylic acid
CCD	Charge-coupled devices (camera)
ccH_2O	Cell culture grade H_2O
cDNA	Complementary deoxyribonucleic acid
CF	Characteristic frequency
C_m	Whole-cell membrane capacitance
CNS	Central nervous system
COX	Cyclooxygenase
DAG	Diacylglycerol
DAPI	(4',6-diamidino-2-phenylindole)
dB	Decibels
DCN	Dorsal cochlear nucleus
ddH2O	Double Distilled Water
DHA	Docosahexaenoic acid
DIC	Differential interference contrast
diC_8PIP_2	Dioctanyl phosphatidylinositol 4,5-bisphosphate
DIPEA	N,N-Diisopropylethylamine

DMEM	Dulbecco's modified eagle medium
DMF	Dimethylformamide
DMSO	Dimethyl sulphoxide
DNA	Deoxyribonucleic acid
DTX-K	Dendrotoxin-K
ECS	Extracellular solution
EDTA	Ethylenediaminetetraacetic acid
EGFP	Enhanced green fluorescent protein
EGTA	Ethyleneglycol-bis(β-aminoethyl)-N,N,N′,N′-tetraacetic acid
EI	Electron ionisation (Mass spectroscopy)
EPA	Eicosapentaenoic acid
EPSC	Excitatory postsynaptic current
EPSP	Excitatory postsynaptic potential
ER	Endoplasmic reticulum
ErA	Erucic acid
FCS	Foetal calf serum
G	Conductance
GPCR	G-protein coupled receptor
G_s	Slope conductance
GTP	Guanosine triphosphate
HA	Hexadecatrienoic acid
HCN	Hyperpolarisation-activated cyclic nucleotide-gated (channel)
HEK	Human embryonic kidney
HEPES	(4-(2-hydroxyethyl)-1-piperazineethanesulfonic acid)
hERG	human ether-à-go-go-related gene (channel)
HVA	High voltage activated
I	Current
ICS	Intracellular solution
I_h	Hyperpolarisation-activated cation current
IHC	Inner hair cell
I_k	K^+ Current
IR	Infra-red
K2P	Two-pore domain potassium channel
K_{Ca}	Calcium-activated K^+ channel

Kir	Inwardly rectifying K^+ channel
Kv	Voltage-gated potassium (subunit/channel)
LA	Linoleic acid
LaA	Lauric acid
LCFA	Long-chain fatty acid
LCMS	Liquid chromatography-mass spectrometer
LnA	Linolenic Acid
LOX	Lipooxygenase
LTP	Long-term potentiation
LVA	Low voltage-activated
mAChR	muscarinic acetylcholine receptors
mAEA	Methandamide
MAP	microtubule-associated protein channel;
MBP	Myelin basic protein;
MSC	Myelinating Schwann cells
mTor	Mechanistic target of rapamycin (kinase)
MUFA	Monounsaturated fatty acid
NA	Nervonic acid
NMR	Nuclear magnetic resonance
OA	Oleic acid
OAc	Acetoxy group (chemistry)
OC	Organ of Corti
OHC	Outer hair cell
o-tol	o-tolyl group (chemistry)
Oxo-M	Oxotremorine-M
PA	Palmitoleic acid
PaA	Palmitic acid
PBS	Phosphate buffered saline
PD	Pore domain
Ph	Phenyl group (chemistry)
PI	Phosphoinositide
PI3K	Phosphatidylinositol 3-kinase
PI4K	Phosphatidylinositol 4-kinase
PI5K	Phosphatidylinositol 5-kinase

PIP_2	Phosphatidylinositol 4,5-bisphosphate
PIP_3	Phosphatidylinositol 3,4,5-bisphosphate
PLC	Phospholipase C
PNS	Peripheral nervous system
PSA	Petroselinic acid
PTEN	Phosphatase and tensin homolog
PUFA	Polyunsaturated fatty acid
rpm	Revolutions per minute
RT-PCR	Reverse transcription polymerase chain reaction
S1-S6	Transmembrane segment 1-6
SA	Stearic acid
SFA	Saturated fatty acid
SG	Spiral ganglion
SGN	Spiral ganglion neuron
SK	Small conductance calcium-activated K^+ (channel)
SR	Spontaneous discharge rate
T1	Kv first tetramerisation (domain)
TASK	TWIK-related acid-sensitive K^+ channel
TC	Thalamocortical relay (neurons)
THF	Tetrahydrofuran
THIK	Tandem pore domain halothane-inhibited K^+ (channel)
TLC	Thin-layer chromatography
TM	Transmembrane
TPGS	DL-a-Tocopherol methoxypolyethylene glycol succinate
TRAAK	TWIK-related arachidonic acid-stimulated K^+ (channel)
TRP	Transient receptor potential (channel)
TsTx	Tityustoxin-Kα
TTX	Tetrodotoxin
TWIK	Two-pore domain K^+ (channel)
v/v	Volume/volume (solutions)
VDM11	(N-(4-hydroxy-2-methylphenyl)arachidonylamide).
VLCFA	Very long-chain fatty acid
V_m	Membrane potential
VSD	Voltage-sensing domain

w/v	Weight/volume (solutions)
αLA	α-Linolenic acid

Units

Measurements conforming to the international system of units (SI) are used throughout.

Peptide amino acids:

The single letter amino acid code is used throughout.

Chapter 1

Introduction

1.1 The physiology of hearing

1.1.1 Transmission of sound to the inner ear

The mammalian ear can be broadly divided into three anatomical regions based on their function in transmitting and processing sound: the outer, middle and inner ear (Figure 1.1). The outer ear provides two important functions in hearing. Firstly, it acts to collect sound waves from a large area and concentrates them into the auditory canal. This significantly increases the sound pressure level (SPL) at the tympanic membrane. This can be as much as 20-30 decibels (dB) for some frequencies (Bergevin and Olson, 2014). Secondly, the outer ear helps to localise sound. The pinna offers complex ridges and edges that reflect sound into the auditory canal. Waves reflected from these rims will travel further than if they enter into the auditory canal directly, offering interference patterns that can be used as spatial cues (Grothe and Pecka, 2014). These spatial cues are only available when the wavelength of the sound is short compared to the dimensions of the pinna; the ability of the outer ear to aid in sound localisation drops off sharply below 2 kHz in humans (Pickles, 2008).

The middle ear couples the sound energy from the auditory canal to the cochlea. The primary role of the middle ear is to act as a transformer to match the impedance of the auditory canal to that of the cochlear fluids (without this, much of the sound would be reflected). Sound energy is conveyed to the inner ear by the cone-shaped tympanic membrane. The architecture of the tympanic membrane and ossicles ensure that sound waves are transmitted solely to the oval window of the cochlea and not the round window ensuring unidirectional entry of sound to the cochlea (Bergevin and Olson, 2014). Furthermore, the actions of the middle ear muscles can modulate the stiffness of the middle ear bones. Many functions have been suggested for this modulation including protecting the inner ear from acoustic overexposure, improving the frequency response of the middle ear and reducing the masking effect of high intensity, low frequency stimuli on higher frequencies. For a fuller discussion of the role of the outer and middle ear in hearing see (Pickles, 2012).

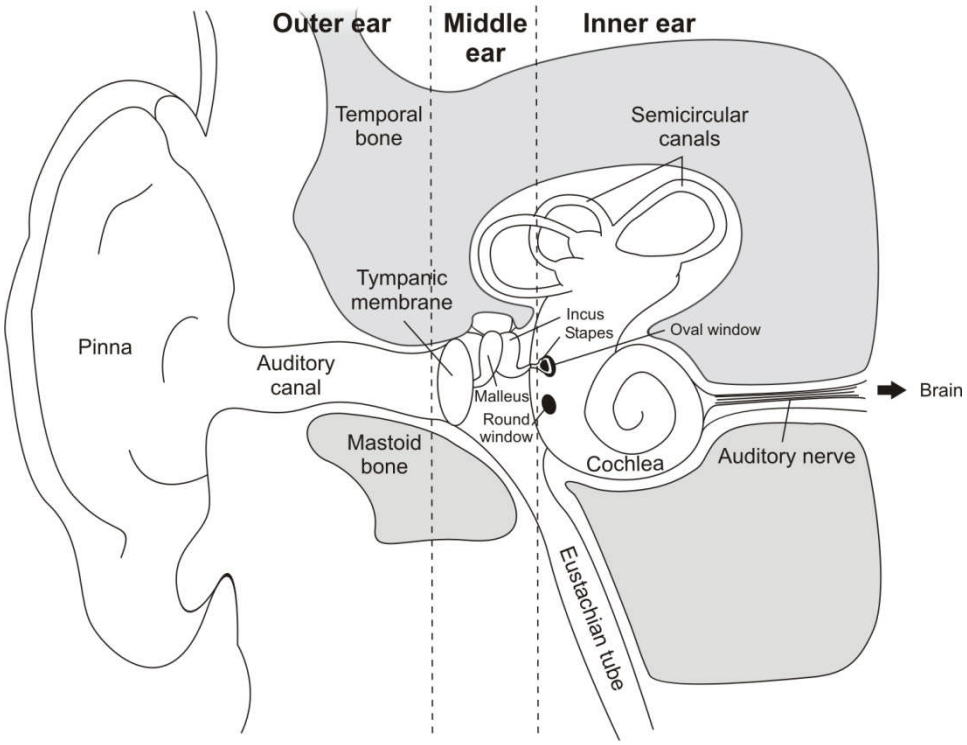

Figure 1.1 Anatomy of the peripheral auditory system. A schematic of the gross anatomical features of the outer, middle and inner ear and the beginning of the central auditory system.

1.1.2 Anatomy of the cochlea

The cochlea is embedded deep in the mammalian temporal bone (Figure 1.1). It consists of a spiral cavity divided longitudinally into three fluid filled compartments. The central compartment, the scala media, is divided from the scala vestibuli above by a partition known as the Reissner's membrane and from the scala tympani below by the basilar membrane. The two outer scalae are joined at the apex of the cochlea at a point termed the helicotrema (Figure 1.2). These outer scalae are filled with an extracellular-like fluid called perilymph. The scala media in contrast is filled with endolymph, a solution which is more akin to intracellular solution as it has a high K^+ and low Na^+ concentration. Consequently, endolymph has a highly positive potential (+80 mV) (Patuzzi, 2011).

The vibrations of the stapes are transferred onto a membrane covered opening in the cochlea called the oval window, resulting in a displacement of the fluid in the scala vestibuli and scala tympani. This, in turn, results in a wave-like displacement of the

basilar membrane and organ of Corti (OC; Figure 1.2A, *dotted line*) (Sohmer, 2015). The OC sits on the basilar membrane and contains the mechanosensory hair cells that are central to the transduction of the physical sound wave into neuronal signals (Lim, 1986). The OC contains a single row of inner hair cells (IHCs) and between three and five rows of outer hair cells (OHCs) and is covered by a gelatinous flap known as the tectorial membrane. The hair cell stereociliary bundles contact this membrane so that vibrations of the basilar membrane and OC result in the physical deflection of the hair cells' bundles.

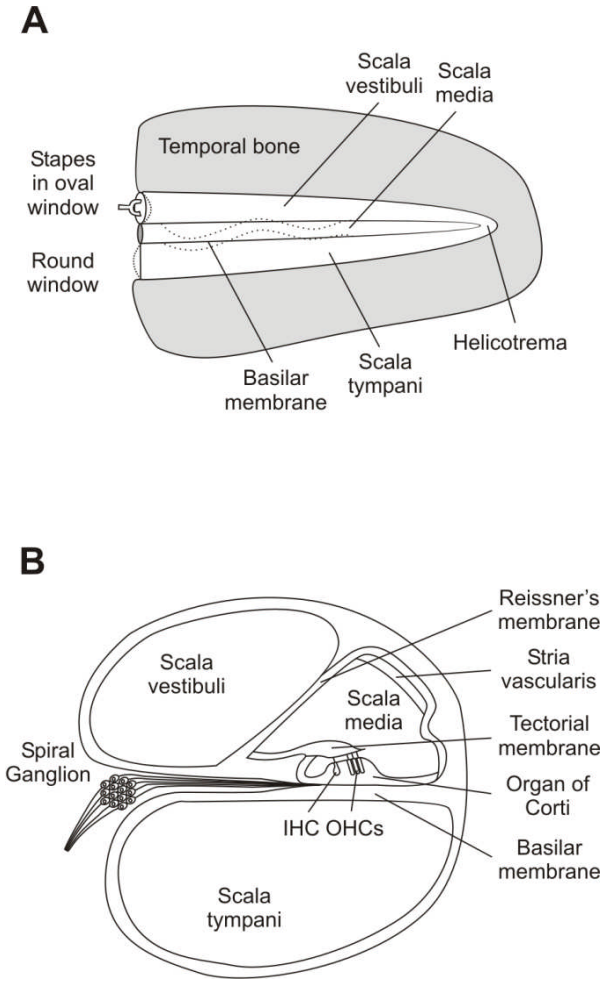

Figure 1.2 Anatomy of the cochlea. A Diagram of the "unrolled" cochlea. The dotted lines show the effects of fluid displacement as a result of vibrations of the middle ear bones on the membrane of the oval window. This displacement takes the form of a travelling wave which causes physical vibrations along the basilar membrane. **B** Transverse section of the cochlea duct. The three scalae and associated structures are shown.

The displacement of the basilar membrane follows a travelling wave which moves from the base to the apex of the cochlea (Sohmer, 2015). This is important as the position and pattern of the wave depends on the frequency of the sound. In the case of a single frequency tone, the vibrations of the basilar membrane are confined to a narrow region of the cochlea. A functional consequence of the travelling wave is that as the frequency of the stimulus increases, the position of the vibration maximum moves nearer the base of the cochlea (Bekesy, 1960, Olson et al., 2012). High frequency tones cause the most vibration near the base of the cochlea whist low frequency tones cause the most vibration near the apex. This is the basis for a frequency specific response in the cochlea. This tuning of the wave is further sharpened by active cochlear mechanics which feed in additional mechanical energy to the travelling wave producing additional stimulation of the cochlear hair cells (Neely and Kim, 1986). The exact processes that underlie this are still unclear. It is understood however that these mechanical processes are mediated, either directly or indirectly, by OHCs (De Boer, 1996).

In vitro recordings from IHCs reveal that displacement of the stereocilia modulates current flow through the cell (Russell and Sellick, 1978). Displacement of the hair cell bundles in the excitatory direction (in the direction of the largest stereocilia) produces large currents and depolarisation of the cell membrane. Deflections of the IHC stereocilia open ion channels on the tips of individual stereocilia. Once open, ions (mainly K^+) are driven into the hair cell by a combination of the highly positive endocochlear potential and the negative intracellular potential of the IHC. This results in rapid depolarisation of the IHC and Ca^{2+} channel mediated release of neurotransmitter onto the terminals of the auditory nerve fibres (ANFs) (Fettiplace and Kim, 2014).

1.1.3 Structure and organisation of the spiral ganglion

The cell bodies (somata) of the SGNs reside in a spiral cavity within the modiolus of the cochlea. This cavity, called Rosenthal's canal, runs parallel to the coiled labyrinths of the cochlea. From here, SGNs project neurites peripherally to the OC as well as centrally into the auditory nerve (AN) (Figure 1.2 & 1.3). Two distinct populations of neurons have been described in the SG: type I and type II. These neurons differ in their

peripheral and central targets, as well as in their size, abundance, protein expression and electrophysiology (Bernard and Spoendlin, 1973, Jagger and Housley, 2003, Liberman and Kiang, 1984, Nadol, 1988a) underscoring their divergent function in the auditory system. Type I SGNs constitute 90-95% of SGN. They are characterised by their large bipolar structure, prominent organelles and the presence of lipid bodies (Rosenbluth, 1962, Spoendlin, 1981). In contrast, type II SGNs are smaller, bipolar or pseudo-monopolar structures, highly filamentous and absent the usual organelles (Bernard and Spoendlin, 1973, Spoendlin, 1971). The central and peripheral processes of type I neurons are highly myelinated (Thomsen, 1966). Myelination of SGN somata is observed in some mammalian species but seems to be largely absent in human type I SGN. Type II SGNs are mostly unmyelinated (Ota and Kimura, 1980) (Figure 1.3).

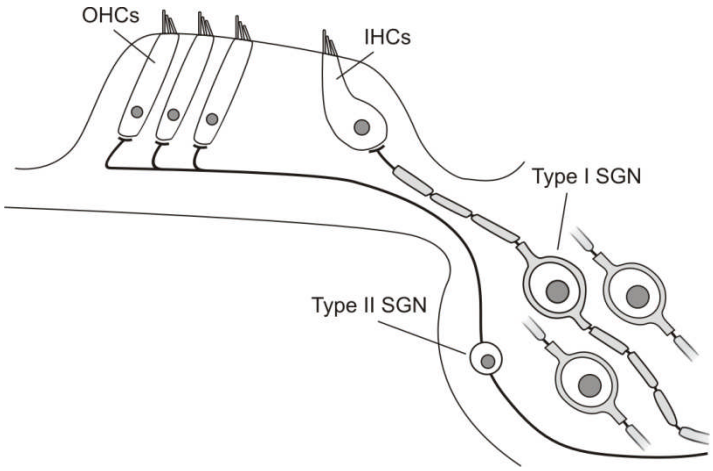

Figure 1.3 Organisation of SGNs in the inner ear. SGN somata occupy a spiral cavity within the modiolus of the cochlea. Their processes extend peripherally to the organ of Corti and centrally to the brainstem. The SG houses two major subpopulations of SGNs: type I and type II. Type I SGNs are large and highly myelinated. They make up the majority of the total SGNs and provide afferent innervation to IHCs. Type II SGNs are smaller and less prevalent than type I neurons and synapse onto the OHCs.

The peripheral target for type I SGNs are the IHCs of the OC. The peripheral processes of the SGN, called radial fibres, travel through the bony spiral lamina and extend out through a hole known as the habenula perforate, into the OC. The fibres, now

demyelinated, synapse onto the bottom of IHCs (Figure 1.3) (Kiang et al., 1982). Here they form a specialised type of synapse known as a ribbon synapse, named after the ribbon-like presynaptic projections originally observed at the presynaptic terminal in the retina (De Robertis and Franchi, 1956). These synapses are equipped with a presynaptic electron-dense structure known as a "ribbon" to which synaptic vesicles are tethered. These specialised synapses allow high temporal precision and sustained neurotransmitter release in response to IHC depolarisation, consistent with their function in coding acoustic information (Safieddine et al., 2012).

Each type I SGN makes a lone synapse onto an IHC. However individual IHCs are innervated by multiple type I SGNs. This manifold innervation is thought to enable the auditory system to encode a wider degree of auditory information (see also *Physiology of the Auditory nerve*). Type II peripheral neurites form similar radial projections into the OC but unlike type I SGN that turn upwards toward the IHCs, type II fibres cross the tunnel of Corti and then turn toward the basal end of the cochlea (Figure 1.4). These fibres can travel hundreds of micrometres, and give rise to multiple large boutons under OHCs (Brown et al., 1988, Kiang et al., 1982). Individual fibres vary in their process length and number of OHCs innervated. Ultrastructural studies of afferent type II-OHC interactions also reveal the presence of reciprocal synapses, where a classical "afferent" synapse, is paired with an "efferent" synapse within the same terminal bouton (Simmons et al., 1998). Type II SGN reciprocal synapses have been observed across mammalian species where they mediate bidirectional signalling with OHCs and have been proposed to constitute a local neural network within OHCs, enabling them to communicate with each other (Thiers et al., 2008). This is supported by findings that synaptic vesicle release from OHCs offers only small depolarisation at type II terminals (Weisz et al., 2009). Given the considerable distance between a SGN's peripheral and central target and the fact that type II neurons are unmyelinated, it seems unlikely type II SGNs would code auditory information directly. Interestingly, type II SGNs receive both axosomatic and dentritic synapses (Nadol, 1988a, Thiers et al., 2000). This has raised the possibility of efferent control of type II neurons. These efferent fibres originate from neurons whose somata reside in the medial and superior olivary complexes. The exact function of this efferent signalling is still under investigation.

The exact numbers of IHCs, OHCs and SGNs is highly species dependent. The number of SGN varies considerably from ~50,000 in cats (Chen et al., 2010) to ~15,000 in rats (Keithley and Feldman, 1979). Humans and other primates have ~30,000 (Nadol, 1988b). IHC and OHC numbers vary similarly; humans typically have ~3,500 IHCs and ~11,000 OHCs per cochlea (Bredberg, 1968), whilst rats contain ~3,500 OHCs and ~1,000 IHCs respectively (Keithley and Feldman, 1982). Finally, the density of type I SGN innervation shows a similar species dependence. Initial work on cats estimated that a single IHC is innervated by ~20 SGNs (Liberman, 1980, Spoendlin, 1979). This seems to be higher than what is found in humans (9-11) (Dunn and Morest, 1975).

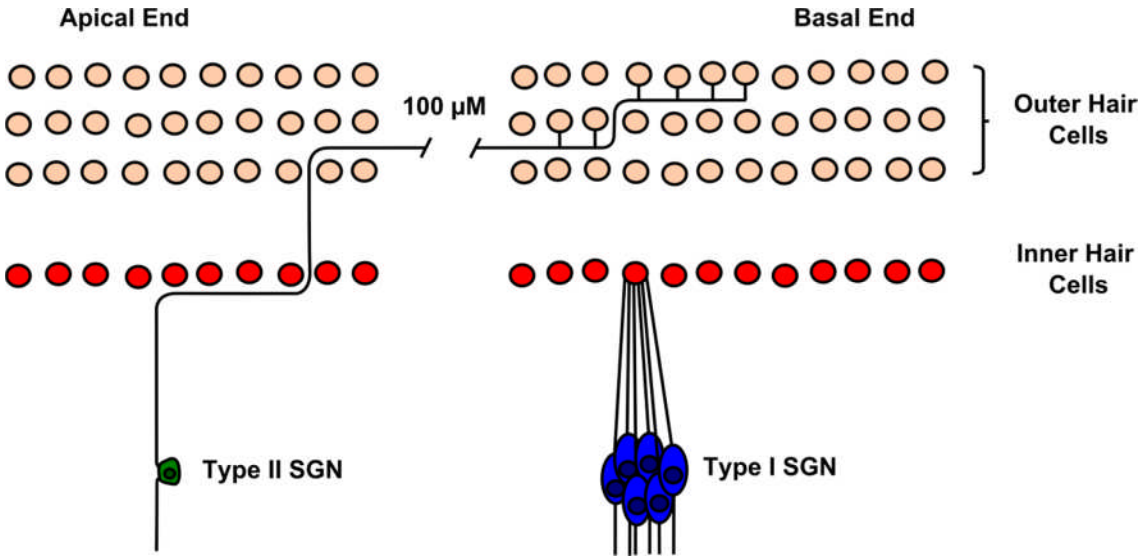

Figure 1.4 Type I and type II SGNs have different peripheral targets and innervation patterns. Each IHC is the target of multiple type I SGNs. In cats, each IHC is innervated by between 20-30 type I SGNs (Spoendlin 1979). OHCs, in contrast, are targeted by type II SGNs. Unlike type I SGNs, type II SGNs can innervate multiple hair cell targets making both *en passant* and terminal synapses with their targets.

The central axons of the type I and type II SGNs bundle together to form the AN and exit the cochlea via the modiolus (Figure 1.2). Both neuron types ascend towards the brainstem, enter the cochlear nucleus and subsequently bifurcate. This creates two branches which project to the anteroventral cochlear nucleus (AVCN) and the dorsal

cochlear nucleus (DCN) respectively (Nayagam et al., 2011). These branches, in turn, can project multiple smaller collateral projections, creating both *en passant* and terminal synapses with the cochlear nucleus (CN). The locations of the SGNs' central targets are also related to their frequency organisation. In general, low frequency fibres innervate the CN ventrally, with progressively higher frequency neurons innervating progressively more dorsally located regions (Berglund and Brown, 1994). Three dimensional reconstructions of SGN innervations show the presence of spatially separate tonotopic or "isofrequency sheets" (Nayagam et al., 2011). SGN branching in the AVCN terminates at a large, axosomatic terminal, known as the endbulb of Held (Ryugo and Fekete, 1982). This enormous neuronal junction contains up to 2000 different synaptic release sites in cats (Ryugo et al., 1996). Such a structure suggests that electrical signalling is carried out at very high fidelity; ensuring neurotransmission is tightly coupled to acoustic events. This has been suggested to be important in order for the brain to utilise interaural time cues to localise sound in space (Smith et al., 1993).

1.1.4 Physiology of the auditory nerve

The activity of single ANFs can be measured by placing an electrode close to the individual fibres exiting the cochlea. Many fibres exhibit random spontaneous activity. These spikes are generated at the initial segment of afferent SGN near the synaptic bouton (Hossain et al., 2005). This region contains a high density of voltage-gated Na^+ (Nav) channels that are activated in response to depolarising neurotransmitter (glutamate) from the ribbon synapse. Recordings from SGN boutons reveal that excitatory postsynaptic currents (EPSCs) and potentials (EPSPs) are regularly large enough that almost every depolarising event is sufficient to trigger a spike (Glowatzki and Fuchs, 2002, Rutherford et al., 2012). This maintains the precise timing needed to code acoustic information by ensuring short spike latencies that vary little. The spontaneously active fibres are exclusively made up of type 1 fibres which synapse onto the cochlear IHCs. Type II fibres display no spontaneous or evoked activity in response to sound (Robertson, 1984). Single tones presented to the ear during recordings affect the timing and the rate of ANF spiking. This evoked response is not uniform across

sound frequency however. A plot of ANF activity vs the frequency and sound level (dB) gives a characteristic V-shaped plot known as a representative tuning curve. Each fibre exhibits particular sensitivity to certain frequencies known as the fibre's characteristic frequency (CF). This CF is correlated largely with the position along the cochlea of the IHC it contacts (Greenwood, 1996). For a recent review of the basic response properties of ANFs see Heil and Peterson, 2015.

The spontaneous activities of ANFs exhibit a bimodal distribution of spontaneous discharge rates (SRs). In cats, approximately one quarter of fibres fire at a rate of <20 spikes/sec. A second broader group has an average discharge rate of around 60-80 spikes/sec with some fibres showing as much as 120 spikes/sec (Evans, 1972, Liberman, 1978). These SRs are correlated with the sound threshold for the fibre. On this basis, Liberman and colleagues categorised three subpopulations of afferent fibres: high SR fibres (>18 spikes/sec) with a low sound threshold, medium SR (0.5–18 spikes/sec) fibres with a moderate sound threshold and low SR fibres (<0.5 spikes/sec) with a high sound threshold. These subpopulations of firing types were also observed in rabbit (Borg et al., 1988), chinchilla (Relkin and Doucet, 1991), ferret (Sumner and Palmer, 2012) and guinea pig (Furman et al., 2013). Structurally, differences have also been reported; high SR fibres typically have a thicker fibre diameter and higher mitochondrial number than low or medium SR fibres (Kiang et al., 1982, Liberman, 1980). This is consistent with the need for higher metabolism and rapid signal conduction. The size and location of the afferent bouton at the IHC is also correlated with SR and threshold (Kiang et al., 1982, Liberman and Kiang, 1984). Boutons from fibres with low or medium SR synapse predominantly on the modiolar side of the IHCs, have large post-synaptic terminals and smaller pre-synaptic ribbons. Conversely, fibres with high SR and low thresholds terminate on the pillar side of the IHCs, have smaller post-synaptic terminals and larger pre-synaptic ribbons (Figure 1.5). Interestingly, acoustic overexposure in guinea pigs seems to cause selective loss of fibres with low SR (Furman et al., 2013).

For any applied frequency, the average spike rate varies as a function of sound pressure level (SPL). As SPL increases past threshold, ANF spiking increases from the basal SR. This spike rate increases monotonically before saturating at high SPL. A plot of this

activity vs SPL (dB) is known as the rate-level function or rate-intensity function (Figure 1.5B) (Yates et al., 1990). The shape and position of this function varies with the frequency of sound as well as the afferent type. Low threshold/high SR fibres at or near the CF display a high sound sensitivity and steep rate-level function, sometimes called a saturating response (Winter et al., 1990). This period of increase from the basal spontaneous rate until saturation is termed the dynamic range (Figure 1.5B, *grey area*). This reflects the range of sounds pressure level to which an individual fibre can respond with changes in its spike rate. Figure 1.5B also shows the typical response of a moderate threshold/medium SR fibre and high threshold/low SR fibre. High threshold/low SR fibres exhibit a response to sound that is right-shifted compared to low threshold fibres. High threshold/low SR fibres typically display shallower rate-intensity functions and a wider dynamic range allowing them to track increases in sound well above the limit of high SR fibres.

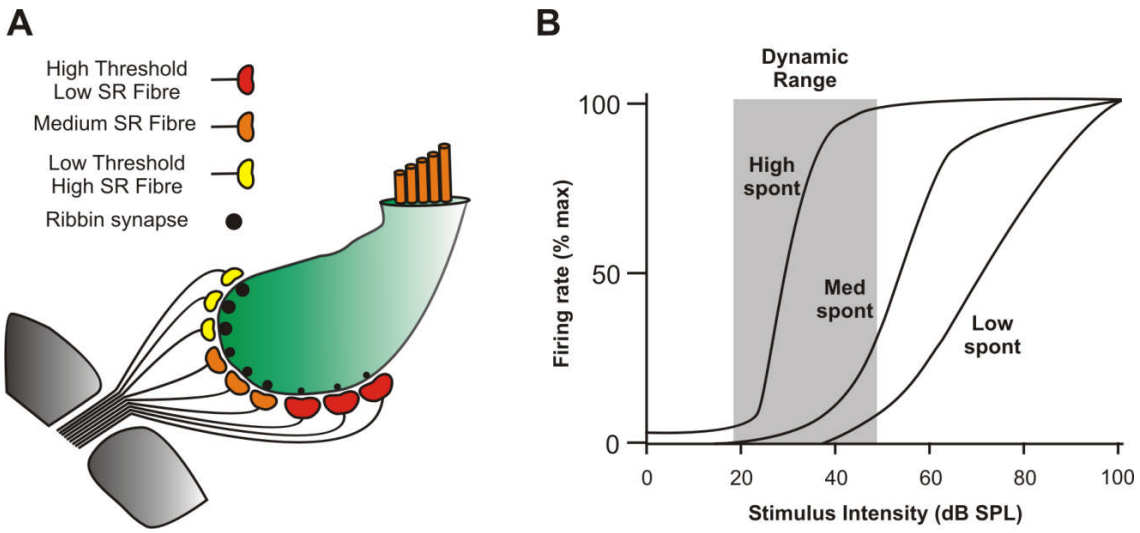

Figure 1.5 IHC afferents exibit heterogeneous physical and physiological properties. A Animation of a typical IHC and its innervations. High SR fibres synapse onto the modiolar side of the IHC and typically have a smaller bouton area, thicker peripheral neurites and larger synaptic ribbons. Low SR fibres, in contrast, synapse onto the pillar side of the IHC and have larger boutons, thinner peripheral neurites and smaller synaptic ribbons. **B** Model rate-intensity plot showing the different afferent responces. High SR fibres typically respond to low sound pressure level (SPL) and exhibit a steep rate-intensity relationship. This steep response that reaches plateau rapidly (saturating response) has a narrow dynamic range (grey area). Medium and low SR fibres exhibit lower sensitivity to sound and a shallower rate-intensity relationship (wider dynamic range).

The utility of such organisation is clear. Manifold innervation of IHCs from fibres with different rate-level functions allows individual ANFs to code different degrees of sound intensity from the same IHC. Low threshold/high SR fibres respond to low sound but saturate at higher levels where high threshold/low SR fibres are only near the bottom of their rate-intensity functions (Figure 1.5B). In this way the cochlea can sample a wide range of sound intensities whilst still remaining sensitive to small changes in sound level (Yates et al., 1990).

The various afferent types have distinct organisations of their central processes, further vindicating their categorisation into different fibre types. Whilst the main branches of high and low SR nerve fibres are remarkably similar in their layout and location in the CN (see *Structure and organisation of the Spiral Ganglion*), high SR fibres show considerable less axonal arborisations within the AVCN region compared to low SR fibres (Fekete et al., 1984). Interestingly, some of this branching from low SR fibres penetrates into the peripheral borders of the CN, and specifically to a structure called the small cell cap where they synapse onto the soma and dendrites of small cells (Ryugo, 2008). These small cell fibres have been shown to send axons to the medial olivocochlear efferent system (Ye et al., 2000) and implicates low SR fibres in mediating a high threshold feedback circuit to the inner ear.

Differences in fibre SRs have been ascribed to differences in the rate of neurotransmitter release at the ribbon synapses (Frank et al., 2009). Differences in ribbon size and density of voltage-gated Ca^{2+} channels (Cav), which form Ca^{2+} microdomains, likely contribute to the differential release of neurotransmitter from synapses present on the same IHC (Frank et al., 2009). The membrane properties of the different afferent fibres still remain to be elucidated however. For example, it is unclear if there are differences between the intrinsic membrane properties of high and low SR fibres. The principal limitation has been the inability to make whole cell recordings from SGNs *in vivo*. SGNs have been studied *in vitro* however. Interestingly there seems to be significant variability in the native ionic conductance of these cells suggesting that some of the heterogeneity observed *in vitro* may be replicated in the membrane properties of afferent SGNs (Davis and Crozier, 2015). *In vitro* studies have already shown significant differences in the ionic conductances of type I and type II SGNs (Jagger and Housley, 2003, Reid et al., 2004) underlining their functional diversity.

Further research is needed on the membrane properties of Type I SGNs to determine if it contribute to the observed heterogeneity in firing. A comprehensive understanding of how the AN functions requires an appreciation of how membrane conductances shape the generation and propagation of action potentials (APs) in the nerve.

1.2 Ion channels

Ion channels are macromolecular, protein pores in the membranes of living cells. They contain a central narrow, water-filled tunnel which facilitates the diffusion of ions down their electrochemical gradient. This central pore is often exclusive to a single ion type, excluding other ions based on their size and charge. They differ from other ion transport proteins, which involve active processes, by facilitating the passive diffusion of ions across the membrane. The rate of movement through ion channels is also vastly greater than in other ion transport proteins, often nearing diffusion-limited rates (10^7 ions channel^{-1}s^{-1}) (Sansom et al., 2002).

As early as 1902, Julius Bernstein correctly proposed that excitable cells such as neurons were selectively permeable to K^+ ions at rest. This "membrane hypothesis" explained how the highly polarised membrane potentials of muscles and nerves could be established (De Palma and Pareti, 2011). The resting membrane potential is now known to result from differences in the concentration of a few such ions: Na^+, K^+, Cl^- and Ca^{2+}. The observed transient excitability which Bernstein referred to as "Membrane breakdown" in these cells would also later be explained by the opening and closing, or "gating" of specific sets of ion channels. This gating is controlled by many factors including changes in membrane voltage and the presence or absence of various ligands.

As well as an electrical gradient, there is also an ion concentration gradient across the cell membrane. Cells maintain a high concentration of K^+ inside the cell relative to the extracellular solutions. Conversely Na^+ and Cl^- are kept at relatively low concentrations. Along with the effects of a selectively permeable membrane, the active transport of ions by pumps and exchange proteins help establish this gradient (Kurachi and North, 2004). Under these conditions, the opening of K^+ selective channels leads to a rapid efflux of

K^+ ions from the cell. In this way K^+ channels play a crucial role in the membranes of excitable cells; setting the resting membrane potential, establishing the excitatory threshold at which APs fire and determining the length the AP once fired (Johnston et al., 2010).

1.2.1 Potassium channel classification

K^+ selective channels represent the single largest and most varied family of ion channels. They are encoded by more than 70 distinct genes within the mammalian genome and include the voltage-gated (Kv), Calcium-activated (K_{Ca}), inward-rectifying (Kir), and two-pore (K2P) K^+ channel families (Figure 1.6) (Gutman et al., 2005). The largest of these families is the Kv family which include some 40 distinct genes in humans. K^+ channels are principally classified by the architecture of the pore-forming α-subunits which assemble in the membrane as tetrameric complexes. These ion channels are classified by the number of helical transmembrane (TM) domains which make up the α-subunits; typically 2, 4 or 6 TM domains (Gutman et al., 2005).

2-TM K^+ channels comprise two TM helical domains connected by a short loop region, known as the P-loop (Figure 1.7). In mammals 2-TM channels are encoded by 15 distinct genes and include the inward rectifying K^+ channel family, Kir. The structure of these channels has been largely determined by solving the KirBac1.1 crystal structure, a bacterial homolog (Kuo et al., 2003). Several of these channels have important physiological roles and mutations in their genes have been linked to a number of human diseases. Kir1.1 channels are involved in recycling K^+ in the lumen of the kidneys and mutations in this gene can cause “Bartter syndrome”, characterised by low potassium levels or hypokalaemia (Heitzmann and Warth, 2008). These channels lack a voltage sensor region and therefore their activity is unaffected by changes in membrane voltage, however some Kir channels are regulated by other signalling pathways such as the G-protein-coupled Kir3 and the ATP-sensitive Kir6 (Kubo et al., 2005). For a full review of the structure, functions, and roles of Kir channels, see Hibino et al., 2010.

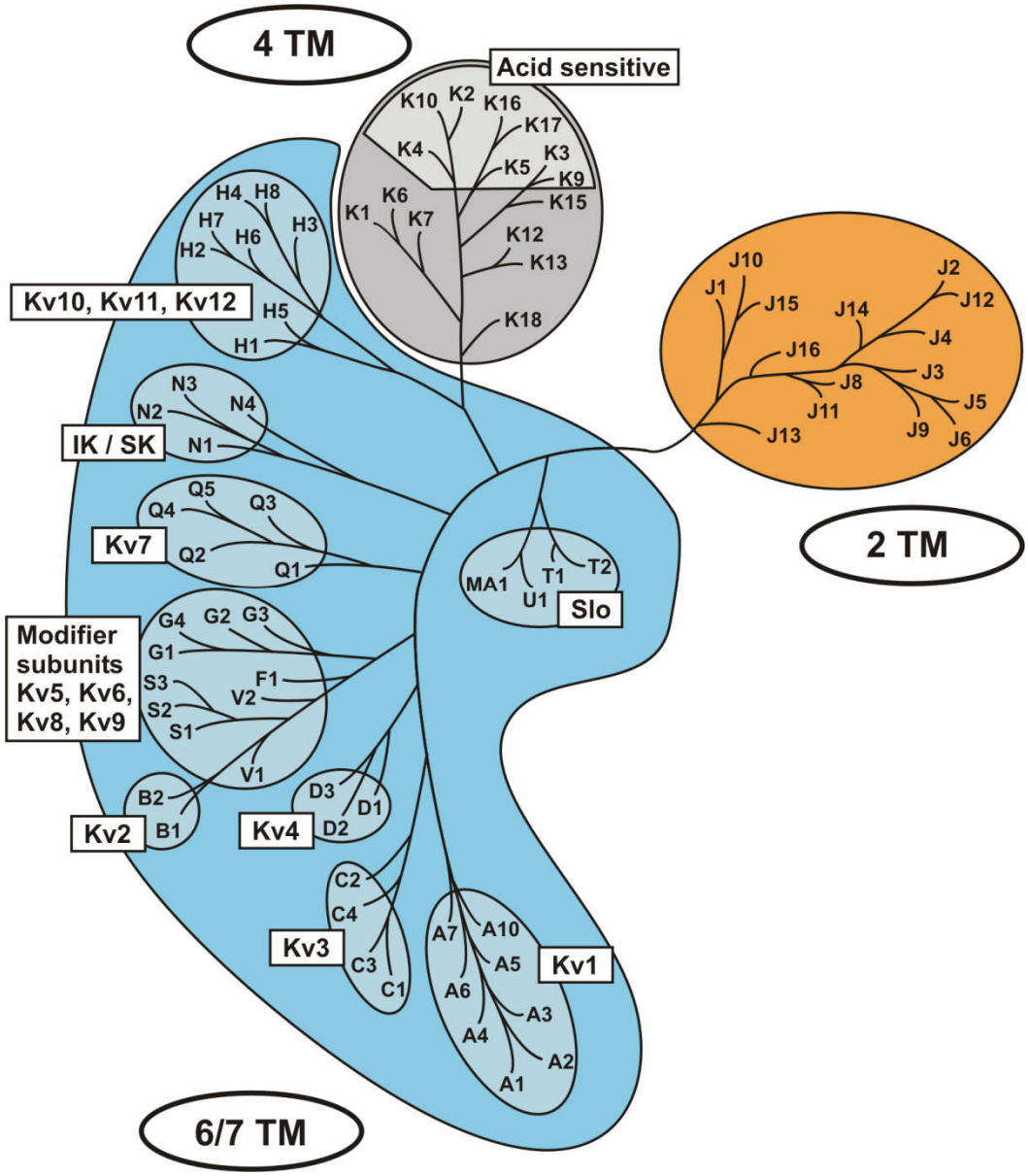

Figure 1.6 Phylogenetic tree of human K^+ channel genes. K^+ channels fall broadly into 3 classes based on the architecture of their pore-forming α-subunits: 2, 4 and 6/7 TM domain K^+ channels. K+ genes are detailed here using the 'KCN' nomenclature. For simplicity, KCN has been omitted from the channel name i.e. KCNA1 is A1 (Adapted from Heitzmann 2008).

K^+ channels from the 4-TM family include the leak channels TWIK, TREK and TASK. The naming of these channels, the "two-pore domain" potassium (K2P) channels, arises from the distinct topology of their channel subunits. Unlike the 2-TM and 6-TM K^+ channels, 4-TM proteins contain two pore-forming loop domains in each subunit.

Accordingly, K2P subunits dimerise as opposed to tetramerise to yield a functional channel with four pore loop domains (reviewed in Enyedi and Czirjak, 2010).

Kv and K_{Ca} channels combined make up the 6/7-TM family of K^+ selective channels. In humans 40 different genes contribute to this family and their structure is characterised by 6 TM domains, or 7 in the case of the "slo" family of genes (which include the large conductance BK channel). 6/7-TM channels contain a voltage-sensing S4 segment, conferring upon them sensitivity to local changes in membrane voltage. They also contain two pore-forming TM segments connected by an extracellular loop region, which can assemble into tetramers in a manner similar to the 2-TM channels (Figure 1.7).

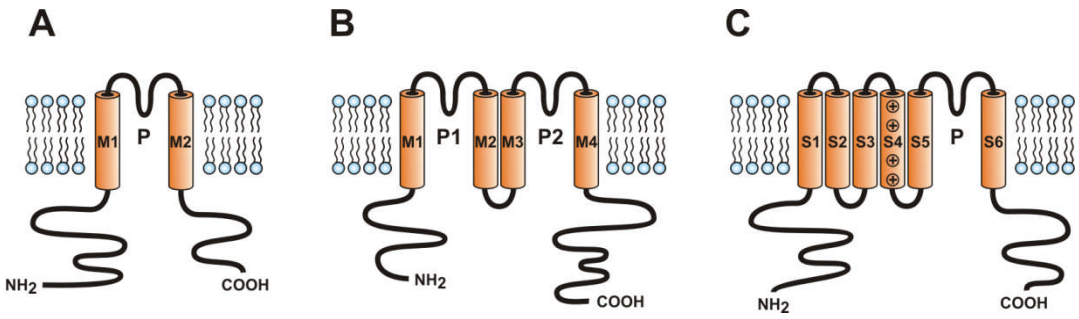

Figure 1.7 Membrane topology of mammalian K^+ channel α-subunits. A 2-TM channels consist of 2 helical transmembrane segments (M1 and M2) connected by an extracellular P-loop and are exemplified by the Kir channels. Four subunits combine to make up a functional channel. **B** 4-TM channels consist of two 2-TM motifs connected in tandem within a single subunit. As a result each subunit contains two P-loops and only two subunits are required to form functional channels. The 4TM family include the leak channels TASK and TREK. **C** 6/7TM channels make up the largest family of potassium channels and include in the Kv and K_{Ca} channels. As with all K^+ channels the central pore region is formed from two 2 helical TM segments (named S5 and S6) connected by the P-loop region. S4 is known as the voltage sensor region due to its role in controlling channel gating through its response to changes in surrounding membrane potential.

1.2.2 Structure of the K^+ channel

The basic structure of a K^+ channel is a tetramer with each α-subunit contributing one pore-forming domain (Yellen, 2002). The general structure of the pore-forming domain consists of two TM helices connected by a short loop region, known as the P-loop (Figure 1.7). This canonical motif is a universal feature of all K^+ channels regardless of the total number of TM domains (Choe, 2002). The central P-loop region, sometimes known as the H5 region, is composed of four conserved signature sequences (TVGYG) and serves as an "ion selectivity filter", a motif it shares with all K^+ selective ion channels (Heginbotham et al., 1994).

1.2.2.1 K^+ conduction and ion selectivity

The defining feature of K^+ channels is their ability to efficiently and selectively conduct K^+ ions across the membrane in the presence of multiple other small ions in the system. Despite their similar charge and size K^+ channels can effectively discriminate for K^+ ions (ionic radius of 1.33 Å) against the smaller Na^+ ions (ionic radius of 0.95 Å) whilst conducting K^+ ions at a rate close to the diffusion limit (Nimigean and Allen, 2011). The exact mechanism of selectivity and conductivity remained speculative until the solution of the crystal structure of KcsA, a bacterial K^+ channel from *Streptomyces lividans* (Doyle et al., 1998, Morais-Cabral et al., 2001, Zhou et al., 2001b). The structure of KcsA revealed that the selectivity filter (SF) essentially consists of four K^+ binding sites termed S1–S4 as well as a partly hydrated and partly coordinated site termed S0 (Figure 1.8). As ions move through the channel they encounter different ionic environments. From the intracellular side through to the central cavity, ions are hydrated by a shell of water molecules. K^+ ions are then dehydrated in the SF, and subsequently rehydrated as they enter the extracellular mouth of the pore. Dehydration of ions is an energetically expensive transition. This energy loss is compensated for by the presence and orientation of carbonyl oxygens in the TVGYG filter (Figure 1.8B). Each of these sites provides a cage of tightly packed electronegative oxygen atoms arranged in a square antiprism geometry for the bound K^+ ions, which is able to mimic the hydration shell of the ion in the water-filled cavity of the channel (5–7 hydrating

water molecules) (Neilson and Skipper, 1985). This stabilises the free cation and helps overcome the strong energy barrier of dehydration.

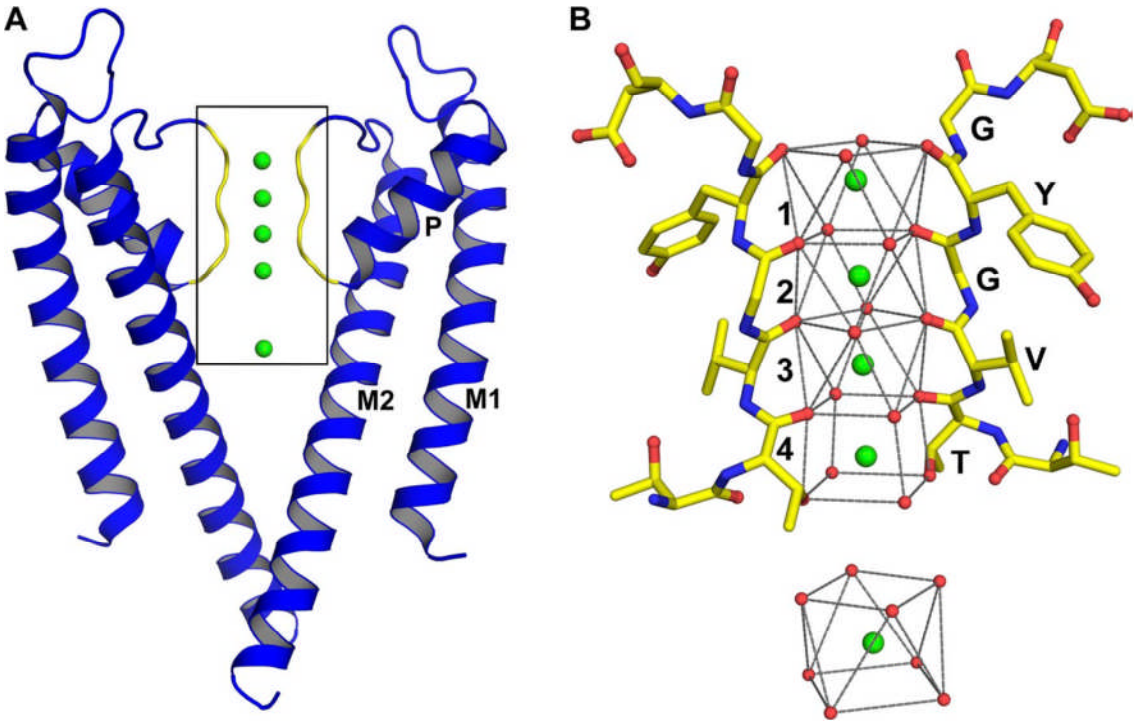

Figure 1.8 Structure of the KcsA channel in complex with K^+ ions. A Structure of KcsA, with the front and rear subunits removed for clarity. Selectivity filter: yellow; K^+ ions: green. M1 and M2 represent the outer and inner helix respectively. **B** Magnified view showing the region boxed in A. The K^+ ion in the cavity is shown hydrated by eight water molecules (red spheres). This ionic environment is recapitulated in the channel's filter region by amino acid backbone carbonyls. The four ion binding sites are labeled 1–4 and the amino acid residues are shown by letters (Adapted from Alam and Jiang, 2011).

If these K^+ sites bind so tightly however, how does the channel promote the rapid transfer of ions from one side of the selectivity pore to the other? The near diffusion-limited rate of ion conductance would suggest a very weak binding of ions to the channel (Kuang et al., 2015). It has been proposed that only two K^+ ions occupy the SF at any given time (Zhou and MacKinnon, 2004, Zhou and MacKinnon, 2003). K^+ ions

simultaneously occupy either the S2 and S4 sites or alternatively the S1 and S3 sites (Sites 1-4, Figure 1.8B). The corresponding vacant binding sites are thought to be occupied by two water molecules. The movement of K^+ ions is facilitated by the change of the 2,4-configuration of K^+ ions to a 1,3-configuration. The energy cost of such a transfer is predicted to be very low (Morais-Cabral et al., 2001). K^+ movement through the channel may be driven by the entry of new ions into the SF or by the repulsive effects between occupying cations within SF (Zhou and MacKinnon, 2003).

Structural determination has also been used to rationalise the selectivity of the channel. The identified K^+ binding sites, with its cages of carbonyl oxygen ligands, offer a thermodynamically favourable environment for the cycle of K^+ ion dehydration, transfer, and rehydration. The Na^+ ions are thought to be too small to effectively coordinate with the K^+ binding sites, making Na^+ binding to the channel thermodynamically unfavourable (Bezanilla and Armstrong, 1972, Doyle et al., 1998, Zhou et al., 2001b). This thermodynamically driven process is sometimes called the "snug-fit hypothesis". This hypothesis is supported by the inability to detect Na^+ in the SF even when vast excesses of Na^+ are employed. Furthermore, observation that high Na^+ conditions were seen to "collapse" the KcsA channel into a non-conducting conformation has led to the proposal that K^+ ions are required to stabilise the SF of K^+ channels in a conductive conformation (Valiyaveetil et al., 2006, Zhou et al., 2001b). However this "snug-fit hypothesis" has been challenged by more recent findings that that suggest KcsA can bind monovalent ions such as Li^+ and Na^+ (Thompson et al., 2009). These results have led to a competing kinetics-based model of ion selectivity. The evidence for kinetic vs thermodynamic based ion selectivity is comprehensively discussed in (Nimigean and Allen, 2011).

1.2.2.2 The voltage sensor domain and gating in voltage-gated K^+ channels

K^+ channels usually occupy one of three conformational states: Activated, inactivated or rest. Channels move, upon stimulation, from a non-conductive, resting state to a conductive activated state. Activation is often temporary and followed by the adoption of one or more non-conducting, inactivated states (Kuang et al., 2015). The opening and

closing of K^+ channels is called “gating” and the mechanisms that control it depend on the K^+ channel under investigation. Some K^+ channels open in response to the binding of specific small molecules, and are known as ligand-gated K^+ channels. Other K^+ channels open in response to changes in membrane voltage and these are termed voltage-gated K^+ (Kv) channels.

The first successfully cloned K^+ channel was the voltage-gated Shaker channel from *Drosophila melanogaster* (Papazian et al., 1987). Vertebrates express 12 Shaker-like channels known as the Kv1 channel proteins, termed Kv1.1, Kv1.2, Kv1.3 etc. encoded by 12 separate genes (KCNA) (Revest and Longstaff, 1998). Three more Kv channels, Shab, Shaw, and Shal, were further identified in *Drosophila melanogaster* (Butler et al., 1989) and are mirrored in vertebrates in the form of KCNB (Kv2), KCNC (Kv3) and KCND (Kv4) respectively. In all, 40 genes in all are now known, and according to the Allen Brain Map (http://brain-map.org/), at least 26 of these Kv subunits have been detailed in the mammalian brain.

The Kv channel α-subunit is composed of sic TM helices containing five linker regions, and an intracellular C and N terminus. The last two TM helices (S5 and S6) are positioned at the centre of the tetramer and make up the above-mentioned pore region, with the S5 and S6 helices corresponding approximately to the outer and inner helices in KcsA respectively (Figure 1.7). The first four TM helices (S1-S4) form the characteristic voltage-sensing domain (VSD) at the periphery of the channel (Jiang et al., 2003, Long et al., 2005). The VSD and pore domain (PD) can be viewed as essentially separate units linked by an intracellular chain termed the “S4-S5 linker”. Access to the water-filled cavity and SF of the Kv channel is controlled by a gate at the intracellular side of the channel protein (Figure 1.8). This intracellular gate is comprised of four S6 helices, one from each monomer, which protrude out into the intracellular cavity and form a bundle which obstructs ion flow in the closed channel state (Doyle et al., 1998).

The majority of Kv channels open in response to the depolarisation of its constitutive membrane and close when the membrane is hyperpolarised (Swartz, 2008). The function of the VSD therefore is to be responsive to changes in membrane voltage and couple these changes with the mechanical gating of the central pore. Each VSD is

composed of four to six basic residues separated by two hydrophobic residues which create a surface of positive charge along the S4 helix (Blunck and Batulan, 2012). This feature is what gives rise to the important voltage sensitivity of the channel. Depolarisation of the membrane results in the S4 helix undergoing conformational changes within the membrane which eventually results in pore opening. The S4 helix must negotiate several closed states before attaining the activated state, and only upon activation of all four S4 helices will the pore open (Zagotta et al., 1994a, Zagotta et al., 1994b). This voltage sensor movement can be detected experimentally as "gating currents" caused by the movement of the S4 electrostatic charges though an electrical field. The exact mechanism of gating after that is somewhat more contentions. Various models of channel reorientation including a "sliding helix" (Larsson et al., 1996), "helical screw" (Ahern and Horn, 2005) and "paddle" (Jiang et al., 2003) model have all been suggested. The current favoured model for the gating movement of the voltage sensor through the membrane is the single consensus model (Blunck and Batulan, 2012, Jensen et al., 2012, Yarov-Yarovoy et al., 2012). Briefly, in this model the positive charges in the S4 helix are paired with corresponding negative charges from the S1-S3 regions. During activation these positive charges move from one negative charge to the next resulting in the translocation of the S4 domain across the membrane. Subsequent movements are thought to involve tilting of the S4 helix and rotation around its helical axis as well as vertical and radial movement within the membrane. This results in displacement of the S4-S5 linker and consequently pore opening (Blunck and Batulan, 2012). The opening of the pore itself is a result of an uncrossing of the S6 bundle at the base of the Kv channel. In many Kv channels the S6 bundle contains a kink in its axis as a result of a strongly conserved proline sequence (PxP or PxG). It is thought that the movement of the C-terminus to PxP motif away from the central pore facilitates ion entry to the water-filled cavity of the channel.

Opening of the pore itself however, often results in the subsequent inactivation of the channel. Channels which enter an inactivated state cease conducting K^+ ions freely and cannot be re-stimulated by membrane depolarisation to open. Two primary forms of inactivation have been described. Rapid, N-type inactivation is a feature of some Kv channels and is a result of a flexible ball peptide bound to the N-terminus of the channel. This N-terminus ball peptide is proposed to interact with the open K^+ channel through electrostatic interactions (Fan et al., 2012, Hoshi et al., 1990, Zhou et al.,

2001b). N-type inactivation is necessarily limited to K^+ subunits which contain the required ball peptide. In contrast, nearly all K^+ channels, both prokaryotic and eukaryotic, undergo slower C-type inactivation. C-type inactivation results from activation induced changes in the SF, as well as the elimination of water and K^+ ions from the channel protein (Cuello et al., 2010). Studies on the Shaker K^+ channel indicate C-type inactivation is dependent upon external K^+ concentration as well as mutations in the pore region of the channel (Lopez-Barneo et al., 1993). Studies on bacterial KcsA suggest that the first inactivation step may be the pinching together of SF backbone carbonyls (Cuello et al., 2010). This slower inactivation response most likely plays a role in determining Kv channel function in the context of repetitive electrical activity or in modulating physiological responses to the accumulation of extracellular K^+ (Yellen, 2002).

1.2.2.3 Ancillary subunits associated with Kv channels

In vivo, the tetrameric assembly of four α-subunits is often complexed with accessory subunits. These proteins serve a number of functions including modulating channel kinetics and surface expression (reviewed in Pongs and Schwarz, 2010). Mutations in these proteins are associated with a range of human diseases including hypertension, epilepsy, and paralysis (Abbott et al., 2001, Brenner et al., 2000, Schulte et al., 2006). Accessory Kv channel proteins exhibit varied structure and expression patterns reflecting their diverse biological roles. Some accessory subunits are integral membrane proteins (Orio et al., 2006) whilst other accessory proteins are cytosolic and bind to cytoplasmic domains of Kv channel (Rettig et al., 1994). Auxiliary subunits include the Kvβ subunit (Pongs et al., 1999), the BKβ-subunits (Orio et al., 2006) the Kv4 Channels auxiliary subunits, KChIP and DPPL (An et al., 2000) and the KCNE subunit (Barhanin et al., 1996).

In mammals, the Kvβ subunits are encoded by three distinct genes: *KCNAB1* (Kvβ1), *KCNAB1* (Kvβ2) and *KCNAB1* (Kvβ3) (Heinemann et al., 1995, Leicher et al., 1996, Schultz et al., 1996). The genes, *KCNAB1* and *KCNAB2* also give rise to splice variants resulting in Kvβ1 and Kvβ2 subunits with varying NH_2-terminal sequences (Kvβ1.1-

1.3). Kvβ subunits associate into octameric complexes with Kv1 α-subunits in a 1:1 ratio (Heinemann et al., 1996, Long et al., 2005, Rettig et al., 1994). The site of interaction is formed by a short loop region in the Kv1α tetramerisation domain and complementary interacting sites on the Kvβ protein (Gulbis et al., 2000, Long et al., 2005). This sequence is highly conserved across Kv1α subunits, providing an explanation for the specificity of Kvβ proteins for the Kv1α subunit family.

Kvβ subunits are members of the oxidoreductase superfamily of proteins (Gulbis et al., 1999), a fact nicely exemplified by its complex with NADPH in the Kv1.2 crystal structure (Long et al., 2005). This implicates Kvβ subunits in coupling the function of the channel to the redox state of the intracellular environment (Pongs and Schwarz, 2010). Kvβ subunits can also influence the gating properties and voltage sensitivity of the Kv channel, most notably by conferring rapid inactivation to otherwise non-inactivating Kv channels (Rettig et al., 1994). Kvβ subunits also alter the pharmacological profile of the channel; for instance, by reducing the effects of the intracellular acting anaesthetics, Bupivacaine and Quinidine (Gonzalez et al., 2002). A final role has also been proposed for Kvβ proteins in determining surface expression and subunit localisation of Kv1 channels (see also *Kv channel biogenesis*). Kvβ has been observed to increase Kv1.2α surface expression and macroscopic currents in heterologous expression systems (Accili et al., 1997). Further, Kvβ has been shown to target Kv1α subunit to the axonal segments of cultured hippocampal neurons (Gu et al., 2006). However this is still controversial and knockout studies of Kvβ2 knockout mice and Kvβ1/Kvβ2 double knockout mice describe unchanged expression patterns of Kv1.1 and Kv1.2 subunits at the surface of cerebellar neurons (Connor et al., 2005, McCormack et al., 2002).

1.2.3.4 Kv channel biogenesis

Kv channels begin their life at the endoplasmic reticulum (ER). Specific amino acid sequences in the nascent α-subunit peptide (signal peptide) target the peptide/ribosome complex to the ER membrane where synthesis of the peptide is completed. Alternatively, nascent proteins can be targeted to other organelles such as mitochondria

by the presence of specific mitochondrial presequences (Stojanovski et al., 2012). At the ER, the ribosome/polypeptide binds to a translocon, an aqueous pore through which polypeptides enters the ER lumen (Johnson and van Waes, 1999). Along with providing access to the ER lumen, the translocon actively facilitates the incorporation of the TM peptide segments into the ER membrane (Figure 1.9) (Crowley et al., 1994). Translocation dictates the TM topology or "sidedness" of the growing channel and, along with chaperone proteins and other topological determinants, ensures the correct folding and orientation of the channel in the membrane (Deutsch, 2003). Even whilst the formation of this tertiary structure is still taking place, tetramerisation of Kv recognition domains is thought to initiate (Deutsch, 2003, Liu et al., 2001). The coupling of primary, secondary, tertiary and quaternary structural assembly is enabled by the functioning of multiple intracellular protein complexes in close proximity and in concert along the length of the polypeptide chain (Deutsch, 2003).

Whilst this translation and incorporation into the ER is taking place, post translational modification of the peptide occurs. Cleavage of the signal peptide is followed by glycosylation and oxidation of the peptide (Deutsch, 2002). Kv channels are glycosylated at important core residues and subsequently undergo further glycosylation at the Golgi. The cell surface expression, localisation and biophysical function of the channel are largely unaffected by these modifications (Deutsch, 2003, Liu et al., 2001, Zhu et al., 2014). Interestingly, S-acylation has been shown to be important in the cell surface expression of some Kv channels (Zhang et al., 2007).

The ER is also the site where Kv channels are coupled with their partner α-subunits and accessory subunits (Nagaya and Papazian, 1997). In fact, excepting some gap junction proteins, the ER is the site of most ion channel oligomerisation (Das Sarma et al., 2002). The choice of partner subunit will be determined by many factors, not least the presence and availability of other subunits within the ER at the time of synthesis. The choice of partner is not free either; only members of the same Kv1-Kv4 α-subunit family can co-assemble to from functional tetrameric channels (Covarrubias et al., 1991). This subunit specificity is primarily driven by recognition domains present on the channel proteins themselves (Xu et al., 1995). In Kv channels this is a highly conserved hydrophilic motif near the cytosolic N terminus of the protein. This is called the first tetramerisation domain or "T1 domain" (Lee et al., 1994, Li et al., 1992). If this recognition domain is

deleted, Kv subunits will still form stable, functional channels. However, T1-deleted Kv subunits associate promiscuously with other Kv family proteins (Tu et al., 1996). The T1 domain prevents homogenisation of Kv channels through random mixing, persevering discrete repertoires of Kv channels (Deutsch, 2002). Although not ultimately necessary for the association of Kv subunits the T1 domain is suggested to police channel assembly by bringing T1-compatible subunits into close proximity, consequently favouring their assembly kinetically over T1-incompatible monomers (Zerangue et al., 2000). The specific mechanisms of oligomerisation likely depend on the specific channel of under investigation, varying with the topology and folding sequence of the protein.

Of similar interest are the associations which govern the assembly of Kv channel subunits which contain the same T1 recognition domain. The organising principles which underlie homo vs heteromeric assembly are of great importance to understand how cells establish their electrophysiological properties. On one hand, an unbiased association of T1-compatible monomers might predict a binomial distribution of subunit containing channels with random stoichiometry (Panyi and Deutsch, 1996). Conversely, preferential association of some subunits could lead to discrete population of homomeric channels or non-random association of distinct heteromeric complexes with discrete stoichiometry. How these subunits assemble at the ER or whether they do so with any preference is still unclear. What is better understood is the expression of these functional homo/heteromeric channels at the plasma membranes of biological tissues. Experimental tools such as immunoprecipitation (Coleman et al., 1999), Kv α-subunit concatemerisation (Sokolov et al., 2007) and subunit specific toxins (Dodson et al., 2002) allow the molecular identity and composition of the native electrophysiology to be determined. However, as will be discussed, this ultimate distribution and expression is not just determined by the assembly of subunits at the ER, but by ER retention, trafficking and subcellular localisation.

After assembly of the Kv α-subunits and auxillary proteins into their channel complexes, Kv channels undergo so-called “quality control checkpoint” (Braakman and Bulleid, 2011). This ensures channels with the correct configuration can leave the ER membrane and is the major determinant of cell surface expression. The ability of various Kv1 homo- and heteromeric complexes to reach the plasma membrane is not

uniform. The subunit composition and stoichiometric as well as the presence or absence of auxillary proteins have a significant effect on ER exportation of the channels. This presumably leads to a much narrower range of possible channel types and subunit combinations than are formed at the ER (Vacher et al., 2008).

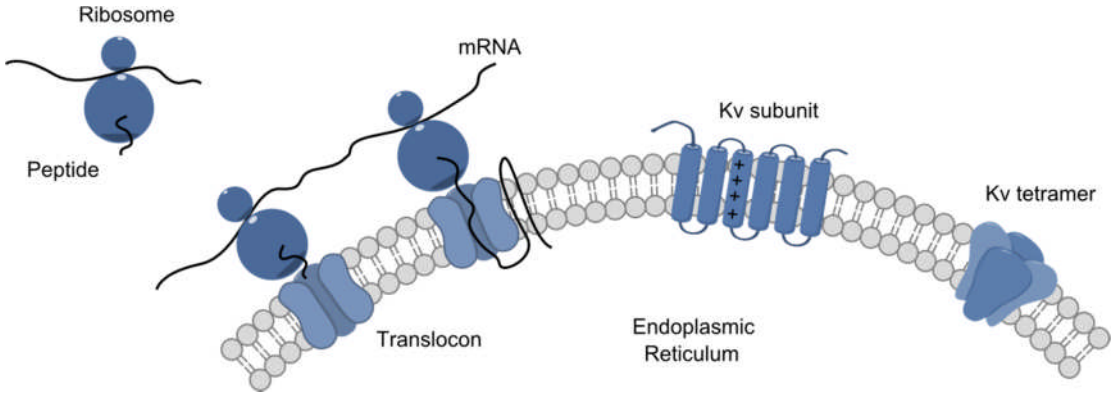

Figure 1.9 Kv channel biogenesis. After gene transcription and export of mRNA from the nucleus, translation of Kv channel peptides is initiated by cytosolic ribosomes. This peptide/ribosome complex is targeted to the nucleus where the growing peptide is integrated into the ER membrane by a translocon. Further peptide synthesis and folding occurs, forming the characteristic 6-TM domain architecture. T1-domain mediated tetramerisation follows, along with the association with auxiliary proteins. If it has the correct ER export signal, channel complexes will be transported to the Golgi for distribution to the cell surface.

The Kv1.1 subunit contains a strong ER retention signal within the pore domain of the channel (Manganas et al., 2001). Homomeric Kv1.1 channels show negligible surface expression in a mammalian cell line. Furthermore, coexpression of the Kv1.1 subunit with other Kv1 family members reduces the surface expression of the hybrid channel (Manganas and Trimmer, 2000). Other channels such as Kv1.4, which do not share this motif, readily reach the cell surface. Similar to Kv1.1, Kv7.3 subunits displays strong ER retention and must form heteromeric complexes with other Kv7 members to reach the cell surface (Schwake et al., 2000). Moreover, export of Kv7.2 from the ER has shown a dependence on the Ca^{2+} sensitive protein calmodulin, suggesting that intracellular Ca^{2+} levels may play a role in determining Kv7 surface expression. The

Kv4 family of subunit are largely retained at the ER and require binding of accessory protein in order to reach the cell surface. K^+ channel interacting proteins (KChIPs) stimulate significant cell surface expression of Kv4 α-subunits and can increase Kv4 current density by up to 100-fold in expression studies (An et al., 2000).

Once a Kv channel is successfully exported from the ER, it is transported to the Golgi apparatus. From here Kv channels are assigned to specific post-Golgi transport vesicles and distributed to various neuronal compartments (Jensen et al., 2011). Precise subcellular localisation of Kv channels is achieved by unique peptide signals encoded within the Kv channel polypeptide. In neurons the most fundamental demarcation is between proteins destined for the dendrites and those for the axon. In Kv1 channels axonal localisation is determined by the N-terminal tetramerisation (T1) domain (Campomanes et al., 2002, Gu et al., 2006). In other channels these signals are conserved peptide sequences and motifs such as the PRC signal present at the C-terminus of the Kv2 channels (Lim et al., 2000), which help localise the channel to the soma and dendrites of the neuronal structure. Similar targeting sequences have been identified for Kv4 channels (Rivera et al., 2003) and Kv7.2/Kv7.3 (Chung et al., 2006).

Finally, Kv channels are inserted at the cell surface through the fusion of Kv-containing transport vesicles with the plasma membrane. This may also contribute to the localisation of ion channels by limiting the insertion event to specific microdomains (Jensen et al., 2011). However, very little is known about these ion channel fusion events. Once inserted Kv channels are most likely tethered to large molecular scaffolds or kept in place by molecular crowding (Jensen et al., 2011). Kv7 tethering in the axon initial segment is most likely effected by their binding to ankyrin-G (Chung et al., 2006, Pan et al., 2006, Rasmussen et al., 2007) whilst Kv1 channels are able to bind a number of PDZ-domain scaffolding proteins by virtue of a PDZ binding motif at the intracellular C-terminus (Ogawa et al., 2008).

1.2.4 Kv channels in neuronal firing

Voltage-gated K^+ channels play a major role in the function of excitable cells. They help set the resting membrane potential of the cell and aid the rapid repolarisation of the membrane once an AP has been triggered. Mutations in Kv channel genes result in various forms of neuronal and cardiac dysfunction including epilepsy, episodic ataxia, cardiac arrhythmias, and congenital deafness (Adelman et al., 1995, Imbrici et al., 2006, Jentsch, 2000, Neyroud et al., 1997).

1.2.4.1 Determining the role of Kv channel function in neurons

The role of Kv channels in neurons has been primarily driven by the discoveries of the biophysical properties of recombinant Kv channels in heterologous expression systems. However these studies provide only a limited understanding of the role of the Kv channel complexes in functional nerves. Assortments of molecular and pharmacological tools are now available to dissect out the role of different Kv channel subtypes *in situ*. Channel specific toxins can be employed to block specific Kv channel subtypes. This allows the relative contribution of various Kv channel subtypes to be assessed in native tissue. Knockdown or knockout of Kv genes has also been used extensively to try and assess the role of Kv channels. However interpretation of these experiments is notoriously challenging. The tetrameric nature of Kv channels and their ability to heteromerise means that knockout of specific Kv genes may not significantly alter the level of functional ion channel available but rather alter the channel composition. This can lead to contradictory or unexpected changes in ion channel biophysics and expression. A good example of this is the finding that knocking out low-voltage-activated (LVA) Kv channel, Kv1.2, paradoxically results in enlarged neuronal LVA currents (Brew et al., 2007). This is thought to arise due to the increased contribution of the more hyperpolarised Kv1.1 subunit in the knockout animal, adjusting the biophysical properties of the channel accordingly, rather than altering Kv1 channel density. As discussed above, altering subunit composition and stoichiometry through gene knockout or knockdown could drastically change the export and trafficking of channels to the cell surface. Results from knockout/knockdown studies should be

interpreted with caution and validated with other available tools where possible. Transgenic and "Knockin" mice have offered a somewhat more subtle approach to examining Kv channel function; the introduction of specific genetic aberrations into the Kv channel subunit *in vivo* allows the examination of non-functional channel mutants without the confounding effects introduced by simple genetic ablation i.e. differences in channel composition and stoichiometry or differences in membrane trafficking (Doyle et al., 2012).

Another difficulty in analysing Kv channel contribution to neuronal electrophysiology is the membrane architecture of the cell. High quality voltage-clamp data can be difficult to obtain for large or arborous neurons which make space-clamp imperfect. Furthermore, neurons often display large magnitudes of outward current resulting in large voltage-clamp errors, even with series resistance compensation (Williams and Mitchell, 2008).

1.2.4.1 Kv channels shape the action potential in of a nerve

Neurons use the distinct biophysical and gating properties of Kv channel subfamilies to regulate excitability and determine the shape of APs. Some channels, such as Kv1, Kv4 and Kv7 are sensitive to changes in voltage close to the neuron's resting membrane potential and respond to small depolarisations of the membrane to prevent AP firing, i.e. during an EPSP (Figure 1.10) (Coetzee et al., 1999, Johnston et al., 2010). LVA Kv channels also help set the resting membrane potential of the cell by opening at or near the RMP of the cell. Effective pharmacological blockers now exist and the effect of blocking these Kv subfamilies can be assessed in neuronal tissues. In some cases, where toxins are available, it is even possible to assess the relative contributions of a single channel subtype to the firing of a neuron (Dodson et al., 2002).

In contrast, high-voltage-activated (HVA) channels such as the Kv2 and Kv3 family of channel proteins only open in response to significant depolarisations of the membrane, like those seen during AP firing (Figure 1.10). In combination with the rapid inactivation of Nav channels, HVA Kv channels act to repolarise the neuronal

membrane (Johnston et al., 2010). TEA is a cationic blocker of all Kv channels, but at low concentrations, TEA can act as an effective blocker of the HVA Kv3 channels. In rapidly firing neurons, inhibition of Kv3 current increases the length of the AP and reduces the frequency of firing (Winlove and Roberts, 2011).

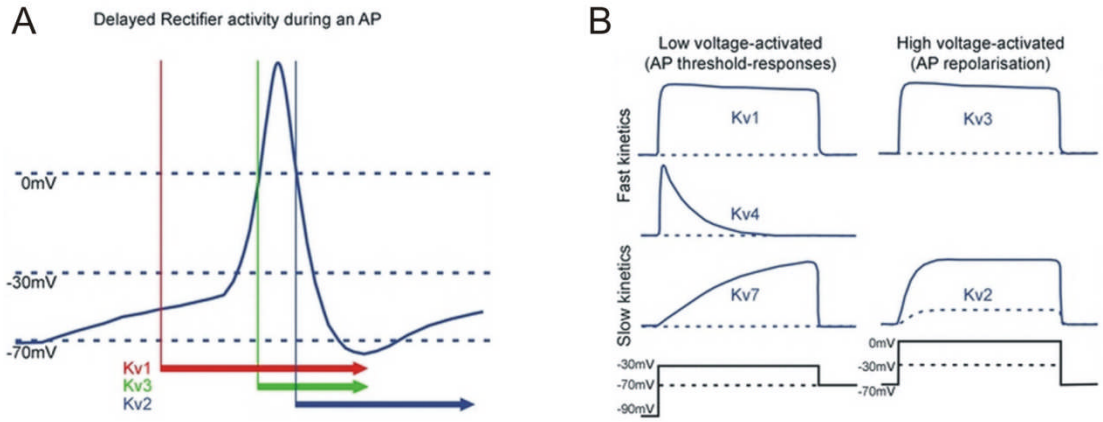

Figure 1.10 The different biophysical characteristics of Kv channels underlie their utility in excitable cells. A Under voltage clamp it is possible to examine biophysical properties of Kv channels in heterologous expression systems. Some channels, such as Kv1, 4 and 7 are activated by small membrane depolarisations whilst others (Kv2 and 3) require much higher depolarisations (such as those encountered during an AP) to open. **B** The different biophysical properties of Kv channels means they contribute differently to the initiation and propagation of an AP. The temporal activities of the different Kv channel families are roughly demonstrated here by the coloured bars/arrows: Low-threshold voltage-activated (LVA) channels, as exemplified by the Kv1 channels (red) open on depolarisation from typical resting potentials, therefore influencing the threshold for AP firing. High Voltage Activated (HVA) channels, exemplified here by the Kv3 family of channels, need further depolarisation, and hence activate during an AP to aid repolarisation. Kv2 channels (blue) act even later in the waveform due to their slower kinetics. It is the action of different populations of Kv channels working in concert that give rise to the characteristic AP waveform, as well as the length of the AP duration and threshold at which it fires (adapted from Johnston et al., 2010).

The kinetics of the channel is also important; slowly activating Kv channels do not play a significant role in shaping the immediate AP due to their slower response properties.

Kv channels with slower response kinetics often serve other functions such as setting the resting membrane potential of the neuron (Kv7) or influencing the firing properties of neurons in response to repeated electrical activity (Kv2; see Figure 1.10B). Some Kv channels such as Kv4 exhibit "A-type" behaviour. They display a significant initial conductance upon depolarisation which inactivates as depolarisation persists, requiring hyperpolarisation before becoming available for conduction again (Maffie and Rudy, 2008).

Finally, the targeting of Kv channels to specific subcellular locations is a key determinant for their biological function. Kv1 family subunits are localised to multiplicity of microdomains in both the central nervous system (CNS) and the peripheral nervous system (PNS; reviewed in Lai and Jan, 2006) where they likely influence different aspects of neuronal activity. Kv1 expression at the presynaptic terminals of CNS neurons helps regulate neurotransmitter release (Lambe and Aghajanian, 2001) whilst Kv channels located to axonal and dendritic compartments influence AP propagation along the neuron (Trimmer and Rhodes, 2004). Kv1 currents at the post synaptic side of the calyx of Held determine the threshold of depolarisation required for AP generation (Ishikawa et al., 2003) ensuring only large EPSCs result in APs. The biophysical properties of Kv channels and their distinct spatial localisation combine to create a neuron's unique response properties.

1.2.5 Lipid modulation of Kv channels

Lipids are fundamental biomolecules for life. Thousands of different lipids have now been identified in mammalian cells with eukaryotes dedicating ~5% of all genes to their synthesis (Fahy et al., 2009). Lipids serve three primary functions in mammals: energy storage, as a basis for the plasma membranes and as a first or secondary messenger system in signal transduction (for review see van Meer et al., 2008). Polar lipids, which contain both hydrophilic and hydrophobic elements, spontaneously self-assemble into micelles and bilayers in aqueous environments providing the physical basic for the formation of plasma membranes. The six TM segments of the Kv channel structure traverse this lipid bilayer in functional channels and the gating of these channels

involves the movement of TM domains through this hydrophobic environment. This fact makes Kv channels (and ion channels in general) ideal candidates for lipid modulation.

The major lipids in eukaryotic membranes are glycerophospholipids which include phosphatidyl, phosphatidylethanolamine, phosphatidylserine, phosphatidic acid and phosphatidylinositol (PI). Phosphatidylcholine accounts for more than 50% of membrane phospholipids in most eukaryotes (van Meer et al., 2008). Other membrane lipids include sterols, sphingolipids, glycolipids and free fatty acids. Many models have been proposed to explain lipid regulation of membrane ion channels. The direct interaction of negatively charged lipids with K^+ channels may facilitate gating and prevent C-type inactivation (Valiyaveetil et al., 2002), raising the possibility of conserved lipid interaction sites within K^+ channels. Furthermore lipids may be necessary for electromechanical gating. Kv7 channels have been shown to require the presence of anionic lipid for VSD coupling to the pore (Zaydman et al., 2013). But these broad explanations most likely do not account for the molecule specific effects observed between lipids.

1.2.5.1 Phosphoinositides

Phosphoinositides (PIs) are a family of closely related phospholipid molecules which play a number of keys roles across a range of biological processes. They are involved in the control of intracellular vesicle trafficking, lipid transport, cytoskeleton organisation, ion channel regulation and are also substrates for both receptor-stimulated phospholipase C (PLC) signalling cascades as well as phosphoinositide 3-kinase (PI3K) signalling pathways (Balla, 2013). PIs are amphiphilic, ensuring they localise to the intracellular leaflet of the plasma membranes of cells. Their chemical structure comprises a glycerol backbone, with two non-polar fatty acids which embed in the hydrophobic cell membrane, and a phosphate group linking this backbone to an inositol head group. The inositol head group may also be phosphorylated at the 3-, 4-, or 5-position on the inositol ring. There are seven PIs excluding the parent molecule phosphatidylinositol, PI (Figure 1.11). The seven family members; PI(4)P; PI(4,5)P_2;

PI(3,4,5)P_3; PI(3,4)P_2; PI(3,5)P_2; PI(3)P and PI(5)P differ in their relative abundance and location within cells. The different PIPs are synthesised and broken down by specific phosphoinositide kinases and phosphatases that catalyse phosphorylation and dephosphorylation at different positions on the inositol head group (Figure 1.11) (Lemmon, 2008).

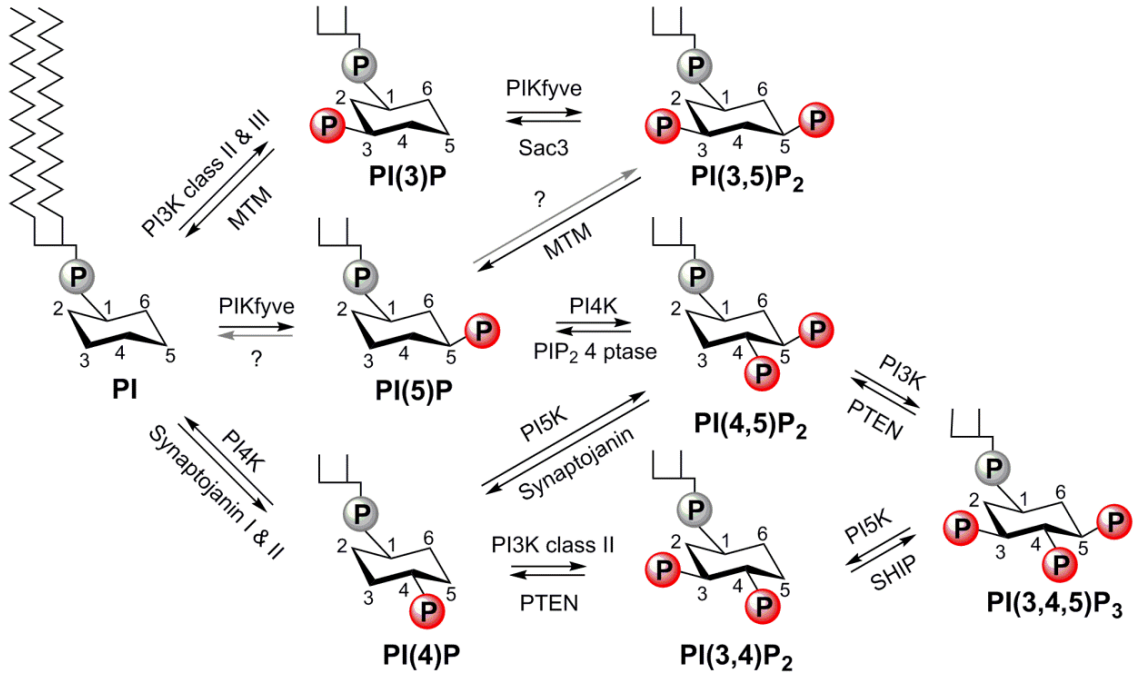

Figure 1.11 Phosphoinositides and their metabolism. The basic phosphoinositide (PI) molecule is comprised of a highly polar inositol 1-phosphate group and a hydrophobic diacylglycerol moiety (Acyl groups are shown for phosphatidylinositol (PI) but were otherwise cropped out for clarity). Shown are the major pathways and important enzymes for the synthesis and breakdown of the phosphoinositide family members. P, phosphate; PI3K, PI4K, and PI5K, phosphoinositide 3-kinase, phosphoinositide 4-kinase, and phosphoinositide 5-kinase, respectively; MTM, myotubularin; PI(3)P, phosphatidylinositol 3-phosphate; PI(3,5)P_2, phosphatidylinositol 3,5-bisphosphate; PI(5)P, phosphatidylinositol 5-phosphate; PI(4,5)P_2, phosphatidylinositol 4,5-bisphosphate; PIP_2 4 ptase, phosphatidylinositol 4,5-bisphosphate-4-phospatase; PTEN, phosphatase and tensin homolog; PIKfyve, FYVE finger-containing phosphoinositide kinase; SHIP, Src homology 2 containing inositol 5-phosphatase; PI(3,4,5)P_3, phosphatidylinositol 3,4,5-trisphosphate; PI(4)P, phosphatidylinositol 4-phosphate; PI(3,4)P_2, phosphatidylinositol 3,4-bisphosphate.

$PI(4,5)P_2$, commonly known as "PIP_2" is the most abundant of the phosphoinositides outside of the parent PI, and is arguably the best studied of the PIPs in mammalian tissues (Lemmon, 2008). PIP_2 interacts with a large variety of cellular proteins and processes including membrane bound ion channels and receptors, GTPases and actin regulatory proteins (McLaughlin et al., 2002), as well as nuclear proteins (Barlow et al., 2010). PIP_2 is also an important regulator of ionic membrane properties (Hilgemann and Ball, 1996, Zhang et al., 1999, Suh and Hille, 2002). PIP_2 directly binds and enhances the activity many K^+ channels; its presence is obligatory for the functioning of many of these channels (for a full review see Suh and Hille, 2008). PIP_2 can also regulate ion channel activity through downstream effector pathways. Similarly, mutations in ion channel proteins which directly affect the affinity of the channel for PIP_2 has been linked to important channelopathies and diseases (Logothetis et al., 2010).

1.2.5.2 Free fatty acids

Fatty acids are ubiquitous within the plasma membrane. However the vast majority of the fatty acid motif is bound up as fatty acid tails, esterified to glycerol. In this form they make up the carbon backbone of membrane glycerophospholipids (Figure 1.12). Here they play a structural role making up the hydrophobic interior of the lipid bilayer. The influence of fatty acids on membrane proteins in this form is limited; however the phospholipid fatty acid length and the degree of saturation can impact physical properties of membranes such as the lateral mobility and fluidity of lipids and proteins (Lee, 2004).

Free fatty acids (FFAs) only exist as a fraction of the total fatty acid motif in the membrane but temporal and local increases in the FFA concentration is possible by cleavage from membrane glycerophospholipids. These temporary and inducible increases in FFA concentration make it an ideal signalling molecule. Activation of specific G-protein coupled receptors results in the enzyme-mediated hydrolysis of membrane phospholipids, which liberates non-esterified fatty acids. Phospholipase A_2 (PLA_2) generated FFAs in a single step by hydrolysis of an acylester bond in phospholipids, yielding a FFA (mostly arachidonic acid and docosahexaenoic acid) and

a lysophospholipid (Figure 1.12) (Farooqui and Horrocks, 2004). FFA can also be produced in a two-step process by the actions of Phospholipase C and phospholipase D (PLD) producing diacylglycerol or monoacylglycerol respectively. The subsequent actions of diacylglycerol- or monoacylglycerol-lipase yield further FFAs.

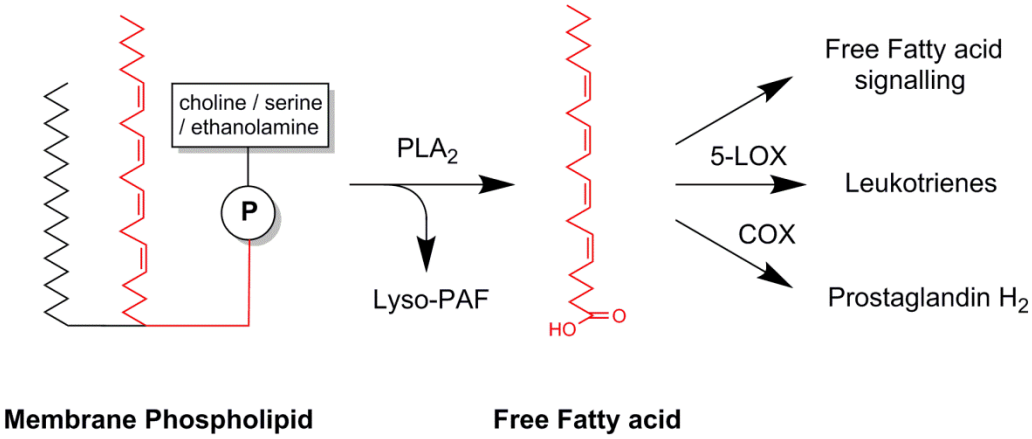

Figure 1.12 Receptor-mediated release of fatty acids from membrane phospholipids. Fatty acids can be formed in a single enzymatic step by the action of phospholipase A_2 on membrane phospholipids. In this example free arachidonic acid (AA) is liberated from one of phosphatidylcholine, phosphatidylserine or phosphatidylethanolamine giving the free fatty acid and a lysophospholipid (Lyso-PAF). AA can, in turn, act as a substrate for other signalling pathways. AA can be used to synthesis the important inflammatory mediator prostaglandin H_2 and leukotriene through the actions of cyclooxygenases (COX) and lipooxygenases (LOX) respectively. Alternately, AA can signal directly through a variety of methods

Once cleaved, FFAs diffuse through the membrane where they may enter into further metabolic pathways as substrates for the production of diglycerides, ceramides, prostaglandins, leukotrienes and thromboxanes (Figure 1.12) (Tassoni et al., 2008). Unlike other membrane lipids, fatty acids have intrinsically high dissociation rates from the membrane and can diffuse into aqueous environments (Balsinde et al., 2002). Therefore in addition to providing the basis for other bioactive molecules, some FFAs may function directly as second messengers. Free arachidonic acid has been shown to have direct modulatory effects on a range of cellular proteins, including protein kinase

C (Khan et al., 1995), G proteins (Abramson et al., 1991) and adenylate cyclase (Murphy, 1985). Furthermore, FFAs can directly regulate cellular events such as exocytosis by their direct interaction with the cellular machinery involved (Darios et al., 2007). Finally, FFAs can also diffuse into the extracellular space. One suggested implication of this is that FFAs may act as retrograde signalling molecules, modulating the presynaptic terminals of brain neurons and playing a role in synaptic plasticity (Bazan, 2005). Extracellular FFA signalling also regulates energy metabolism through their action on free fatty acid receptors (Hara et al., 2014); inflammation through their effects on Toll-like receptors (Glass and Olefsky, 2012); and gene expression through their activation of peroxisome proliferator-activated receptors, toll-like receptors and G protein-coupled receptors (Georgiadi and Kersten, 2012).

1.3 Aims and objectives

There were two major aims of this study. The first was to examine the firing features of SGNs from post-hearing onset animals. Systematic investigation of SGNs' firing features and membrane conductances have up to now been primarily carried out in pre-hearing animals. Given the significant maturation of the cochlea around the onset of hearing and after, characterisation of neurons from hearing animals is of great importance. The second aim was to investigate whether the firing features of functionally mature SGNs could be modulated. This study focused, in particular, on the effect of membrane lipids on SGN activity. Membrane lipids are ideally situated for modulating SGNs' firing behaviour and membrane conductances and this study aimed to examine the physiological effects of adjusting the levels of these membrane lipids.

Individual objectives working towards these aims were also pursued. The most important task was to develop a robust and stable tissue preparation that allowed whole cell patch clamp recordings to be obtained from the soma of the SGNs. Secondly, in the absence of genetic tools, pharmacological methods to adjust the levels of membrane bound PIP_2 were investigated. These involved complimentary experimental approaches, combining traditional strategies of PIP_2 reduction, such as inhibiting phosphoinositide synthesis, with recently developed strategies for PIP_2 sequestration and capture. Another important objective was to develop a heterologous expression system. This could be employed to correlate the effects of PIP_2 modulation on specific SGNs conductances with similar effects observed on the expressed Kv subunits in isolation. This would help provide the molecular basis for any observed modulatory effects. Furthermore, once this molecular basis had been established, a heterologous expression system would provide an ideal tool to screen other native and synthetic lipids for their potential modulatory effects in SGNs

Understanding the molecular basis of SGN firing could provide a better understanding of the heterogeneous firing patterns observed in ANFs in vivo. An analysis of the lipid modulation of SGN activity could provide two important outcomes. First, it could shed light on potential lipid-mediated regulatory pathways available to SGNs. Secondly, it could identify new targets for pharmacological intervention and provide a novel mechanism of adjusting the sensitivity and output of the auditory nerve.

Chapter 2

Materials and Methods

2.1 Materials

2.1.1 Reagents and solutions

All reagents and solutions were obtained from Sigma Aldrich unless otherwise stated

2.1.1.1 Neuronal cell culture solutions

Neuronal cell culture medium was made up of Dulbecco's Modified Eagle's Medium (DMEM) supplemented with foetal calf serum (FCS; 10%), 10 mM HEPES and 1% penicillin/streptomycin (Invitrogen). Brain-derived neurotrophic factor (BDNF; Insight Biotechnology LTD) was made up as a stock solution in DMEM to 500 ng/ml before being aliquoted and stored at -20^{0}C until use. Trypsin was made up as a solution of 0.25% w/v in PBS, aliquoted, frozen and stored until use. A stock solution of poly-L-lysine hydrobromide, (Molecular weight >70,000; M P Biomedicals UK) was made up as 1 mg/ml in cell culture H_20 (ccH_20), aliquoted and frozen until use. A working concentration of 50 µg/ml (1:20 dilution) poly-L-lysine in ccH_20 was made up on the day of use. 11 mm diameter glass coverslips (VWR International LTD) were incubated in the 50 µg/ml poly-L-lysine for 1 hr in 35 mm dishes (Corning) and washed three times with 2 ml of ccH_20 before use.

2.1.1.2 HEK293 cell culture solutions

HEK293 cell culture medium was composed of DMEM:F12-HAM 1:1 supplemented with 10% FCS, 2 mM L-glutamine, and penicillin/streptomycin (Invitrogen). Trypsin/EDTA (1x) was obtained as a solution (Sigma) and used directly. HEK293 cryopreservation medium was composed of DMEM F12: HAM 1:1 supplemented with 20% FCS, 2 mM L-glutamine and 10% dimethyl sulfoxide (DMSO).

2.1.1.3 Electrophysiology and pharmacology

The extracellular solution (ECS) was made up of (mM): NaCl, 145; KCl, 4; $MgCl_2$, 1; $CaCl_2$, 1.3; HEPES, 10; glucose, 5; pH adjusted to 7.3 with aq. NaOH. The intracellular pipette solution (ICS) was made up of (mM): K-gluconate, 130; KCl, 5; MgATP, 2; Na_2ATP, 2; Na_3GTP, 0.3; $Na_2Phosphocreatine$, 10; HEPES, 5; EGTA, 1; pH adjusted to 7.2 using aq. KOH.

Drug stocks: With the exception of wortmannin and LY294002, which were added to the neuronal culture medium prior to patch-clamp recording, and diC_8PIP_2, which was added to the intracellular pipette solution, all drugs were dissolved in AP and added through the bath perfusion system. Dendrotoxin-K (DTX-K) and tityustoxin-Kα (TsTx) were obtained from Alomone Labs and made up as a stock solution in ddH2O at 50 µM and 100 µM, respectively. Toxins were stored at -20°C before dilution in ECS (100 nM) for patch-clamp recordings. Wortmannin (Santa Cruz Biotechnology) was prepared as a 1 mM stock in ddH2O and stored at -20^0C before dilution to 100 nM or 10 µM in neuronal cell culture medium. LY294002 was prepared as 10 mM stock in ddH2O and stored at -20°C before added to neuronal cell culture medium (5 µM). Oxotremorine-M (Oxo-M) and m-3M3FBS were prepared as 10 mM stocks in $ddH_20$and stored at -20^0C before dilution to the appropriate concentration in ECS. XE991 (Tocris Bioscience) was prepared as 1 mM stock in ddH_2O stored at -20^0C and dilution to the appropriate concentration in ECS on the day of use. PIP_2 binding peptides and their analogues: PIP_2-PP, Fluoro-PP and PolyK-PP (generous gifts from Dr Jon Robbins, Kings College London), were obtained as a 10 mM stock solution, aliquoted into single use aliquots and stored at -20^0C until use. The Non-Pal PIP_2 Peptide and Neutral-PP analogues were obtained from Biomatik and made up as a stock solution in ddH2O at a concentration of 10 mM before being aliquoted and stored at -20^0C until use. Commercial fatty acids, obtained from Sigma Aldrich, were made up as a stock solution in DMSO at a concentration of 100 mM before being aliquoted, frozen and stored until use. Fatty acids were then diluted in bath solution as required. Aromatic fatty acids were synthesised as described below, made up as a stock solution in DMSO at a concentration of 100 mM before being aliquoted, frozen and stored until use.

2.1.2 Animals

The present study was carried out on Sprague Dawley rats (P2–P12) and C57BL6 mice (P4-P21) of either sex, reared at University College London. All procedures were carried out in accordance with the United Kingdom Animals (Scientific Procedures) Act of 1986, and were approved by the UCL Animal Ethics Committee. Animals were killed by inhalation of CO_2 and cervical dislocation.

2.2 Methods

2.2.1 Immunofluorescence of cochlear tissue

P2–P12 rats were killed by inhalation of CO_2. The rats were decapitated and the cochleae were exposed by hemisection of the cranium in ice cold artificial perilymph. They were fixed in a solution of 4% paraformaldehyde in PBS for 1-2 hrs at room temperature or left overnight at 4°C. P2 cochleae could be sliced directly but P6 and P12 were rat cochleae were decalcified in an EDTA solution for 24 hrs prior to being sliced on a vibrating blade microtome (*Vibratome* Series *1000 Plus, Intracel* Ltd). Block and permeabilisation of slices was achieved by incubation with 10% goat serum and 0.1% Triton in PBS for 40 mins at room temperature. The slices were labelled using primary antibodies: rabbit polyclonal anti-Kv1.1 antibodies and mouse monoclonal anti-acetylated tubulin antibodies obtained from Alomone and Sigma respectively. These were used at a 1:400 and a 1:1000 dilution respectively, in 0.1 M lysine and 0.1% Triton overnight at 4°C. Primary antibody labelling was visualised using Alexa Fluor-coupled secondary antibodies. Following washes in PBS, primary antibody labelled slices were incubated in secondary antibodies: goat-anti rabbit Alexa488 (Invitrogen) and goat anti-mouse Alexa555 (Invitrogen) antibodies were used to visualise the primary antibodies and phalloidin-Alexa633 was used to visualise actin. This was carried out in 0.1 M lysine and 0.1% Triton in PBS for 1 hr at room temperature. The slices were then washed 3 times in PBS before being mounted on glass slides with a ground cavity and overlaid with a coverslip in Vectashield with DAPI (Vector Labs, Peterborough, UK). Imaging was carried out using a laser scanning confocal microscope (LSM510; Carl

Zeiss MicroImaging). *Z*-stack confocal images were acquired at 2-3 µm intervals and 5-6 images were acquired per stack. Image processing and analysis were performed on images derived from each *Z*-stack series using Zeiss LSM Image Browser and ImageJ. Images were imported into Inkscape (Inkscape.org, Version 0.48) for optimal contrast and brightness. All images were oriented with the modiolus at the left hand side for comparison.

2.2.2 HEK293 cell handling and transfection

2.2.2.1 HEK293 cell maintenance

HEK293 cells, obtained from Sigma Aldrich, were cultured in a 25 cm^2 flask containing 5 ml of HEK293 cell culture medium. Cells were maintained in a humidified incubator at 37^0C and 5% CO_2. When cells reached ~90% confluence they were passaged into a new 25 cm^2 flask. To passage, cells were washed once with PBS and then incubated with ~0.5 ml trypsin/EDTA for 1-5 mins until cells fully detached from the flask. The enzymatic reaction was quenched by addition of 4 ml HEK293 cell culture medium and the cells were further dissociated by gentle trituration through a pipette. 0.5 ml of the re-suspended cells was added to 4.5 ml of fresh HEK293 cell culture medium in a new flask.

2.2.2.1 Transient transfection of HEK293 cells

Rat cDNAs of Kv1.1 and Kv1.2 (a generous gift from Dr Martin Stocker, UCL), were cloned into pcDNA3 (Invitrogen) by Dr. Katie Smith. Accession numbers: Kv1.1 (Kcna1), NM_173095; Kv1.2 (Kcna2), NM_012970. 1-2 days before transfection, cells were plated in 35 mm dishes to obtain a density of ~80%. A total of 2.5 µg of the DNA (see Table 1) was pre-incubated with the transfection reagent, Lipofectamine 2000 (Invitrogen) for 15 mins. The 2.5 µg DNA was made up to 1.2 µg of pcDNA3 containing either Kv1.1 (pcDNA-Kv1.1) or Kv1.2 (pcDNA-Kv1.2); 1.2 µg of the empty pcDNA3 or the alternate pcDNA-Kv1.1/ pcDNA-Kv1.2 and finally 0.14 µg of plasmid

DNA containing EGFP to visualise transfected cells. Table 1 show the possible permutations.

Table 2.1 Transient transfection of HEK293 cells with Kv1 DNA

Kv channel expression	Kv1.1 DNA (µg)	Kv1.2 DNA (µg)	pcDNA3 (µg)	EGFP (µg)
Homomeric Kv1.1	1.2	0	1.2	0.14
Homomeric Kv1.2	0	1.2	1.2	0.14
Heteromeric Kv1.1/1.2	1.2	1.2	0	0.14

After 4 hrs, the Opti-MEM media and transfection complex were replaced with normal growth medium. After 18 hrs, cells were trypsinised and re-plated onto 11 mm glass coverslips at low density. After a short recovery (~3 hrs), coverslips with transferred to a recording chamber for patch-clamp recordings.

2.2.2.2 Stable transfection of HEK293 cells with Kv1.2 DNA

In order to create a stable Kv1.2 expressing cell line, transiently transfected HEK293 cells were exposed to positive selection by the antibiotic G418 (Geneticin). Positive selection was possible because of the neomycin selection marker present in pcDNA3. In order to determine the optimal selection dose, G418 was titrated against untransfected HEK293 cells. HEK293 cells were plated in a 24 well plate and exposed to concentrations of G418 between 50 and 1000 mg/ml which exhibited effective cytotoxicity at concentrations above 500 mg/ml.

HEK293 cells transiently transfected with pcDNA-Kv1.2 as described above (but without empty pcDNA3 or EGFP) were trypsinised and re-plated into a 6 well plate (Corning), with one well containing untransfected HEK293 cells (Control). Cells were incubated in standard HEK293 cell culture medium supplemented with 500 mg/ml G418 until all cells in control well had died (~5 days) and visible colonies appeared in the transfected wells (~1-2 weeks). Small colonies (<100 cells) were isolated, trypsinised and re-plated into 24 well plates at a density of ~1-2 cells per well and

maintained in standard HEK293 cell culture medium. 24 well plates were monitored closely for the appearance of monoclonal colonies. Selected colonies were trypsinised and seeded to a 35 mm dish, where their electrophysiological properties were examined for Kv1.2 currents. Once the presence of Kv1.2 currents was confirmed, cells were seeded to a 25 cm^2 flask where they were maintained as above.

2.2.2.3 Cryopreservation of HEK cells

For freezing, cells were grown to near confluency in a 75 cm^2 flask. Cells were washed once with PBS and then incubated with ~1 ml trypsin/EDTA for 1-5 mins until cells fully detached from the flask. Cells were subsequently resuspended in 5 ml of HEK293 cell culture medium. To quantity the approximate total number of cells, 10 µl of the cell suspensions was removed, diluted 1/10 and enumerated in a counting chamber. Cells were centrifuged at 1000 rpm for 3 min and the pellet was resuspended in HEK293 cryopreservation medium to a concentration of $3x10^6$ cells/ml. Aliquots of 3 million cells were apportioned to individual cryo-vials and placed into a Nalgene cryo container containing propan-2-ol. Cryo-vials and propanol container were stored in a -80^0C freezer overnight then transferred into liquid N_2 for long term storage.

2.2.3 Dissociated spiral ganglion neuron preparation

Several preparations of dissociated neuronal cultures have been described previously (Whitlon et al., 2006, Chen, 1997, Santos-Sacchi, 1993) and our method is similar to those reported. Cultures were prepared from P12-P21 mice. Following decapitation, the cochleae were exposed by hemisection of the midsagittal plane of the cranium. The outer cochlear capsule was removed, followed by the peeling off of the lateral wall and the removal of the spiral limbus and the OC. The whole dissected ganglia were divided into thirds along the cochlear spiral to give apical, mid and basal derived tissues which were digested separately in 10 µl 0.25% Trypsin/PBS for 30 mins at 37^0C in a small falcon tube. Digestion was ceased by addition of neuronal cell culture medium. The

digested tissue was mechanically dissociated using a P1000 pipette, triturating the cellular suspension 10-12 times. The suspension was centrifuged at 2000 rpm for 10 mins, the supernatant removed, and the cells resuspended in neuronal cell culture medium. 30 µl of the cell suspension was administered onto each poly-L-lysine coated glass coverslip and placed inside 35 mm petri dishes. These were then incubated at 37°C and 5% CO_2 levels for 2 hrs to allow the cell suspension to settle and adhere to the coverslips. 2 ml of neuronal cell culture medium was then added to the 35 mm dish, supplemented with BDNF to a final concentration of 20 ng/ml. The cultures were subsequently incubated at 37°C and 5% CO_2 levels for 2-3 days during which time the neurons shed their myelin coating.

2.2.4 Electrophysiology

Recordings from SGNs and HEK293 cells were carried out in whole-cell configuration using a patch clamp amplifier (Axo-patch 200B; Axon Instruments) and a Digidata board (Axon Instruments) under the control of computer software (pClamp version 8; Axon Instruments). Cells were visualised using an upright microscope (E600FN, Nikon, Tokyo, Japan) equipped with a x40 water-immersion objective. Patch clamp recordings were performed under infrared differential interference contrast (IR-DIC) video-microscopy, using a CCD video camera and IR-DIC optics mounted on the microscope. Patch pipettes were fabricated on a vertical two-stage puller (Narishige, PC-10) from borosilicate capillary tubes (GC120TF-10; Harvard Apparatus), coated with molten ski wax and positioned using a piezoelectric micromanipulator (PCS-5000 Series, exfo-lifesciences). The pipette resistance was 2.5-4.6 MΩ when measured in the bath solution. All drugs were applied to the cell bath directly by perfusion using a Gilson MINIPULS® 3 peristaltic pump. Capacitance transients were cancelled online and series resistance was compensated 70% in order to limit the voltage error. Series resistance typically was around 3-10 MΩ, and recordings which exceeded series resistance of 15 MΩ were rejected. Leak currents were not subtracted for SGN recordings; leak subtraction using a P/4 method was routinely performed as part of whole cell recordings from HEK293 cells. Measurement of membrane voltage was carried out in the ‘fast’ current clamp mode of the amplifier. All experiments were carried out at room

temperature (20-25^{o}C). The liquid junction potential was measured using a KCl salt bridge filled with 3 M KCl. Liquid junction potential was measured at -13 mV and subtracted offline.

2.2.5 Data analysis and statistics

Analysis was performed using Clampfit (Axon Instruments), and Igor (WaveMetrics Inc.). The voltage dependence of activation was calculated by fitting conductance-voltage data with the Boltzmann function:

$$G_{norm} = G_{min} + (G_{max} - G_{min})/(1 - \exp((V_{1/2} + V_m)/k))$$

where G is conductance, $V_{1/2}$ is the half-maximal activation, V_m is the membrane potential, and k is the slope. Single exponential fitting, where used, took the form:

$$y = A\exp(-x/\tau)$$

where x is time and τ is the time constant. Statistics were performed on Origin software (version 9, Microcal Software Inc.) with a P-value less than 0.05 considered significant.

2.2.5 Chemistry

2.2.5.1 General

All starting materials were commercially available from Sigma Aldrich. Reactions were monitored by thin-layer chromatography (TLC) on silica gel plates (60 F254, Merck), visualizing with ultraviolet light and by liquid chromatography-mass spectrometer (LCMS). Nuclear magnetic resonance (NMR) spectra were recorded on a Bruker Avance III 600 Cryo (600 MHz). ^{1}H NMR chemical shifts are reported in parts per million downfield from tetramethylsilane. Accurate Mass was reported by UCL

Chemistry Mass Spectrometry Facility. All compounds were at least 95% pure as assayed by LCMS (electrospray +ve).

2.2.5.2 General synthesis for 1,2,3-triazole fatty acids

To a solution of the bromoalkane (1.1 eq., 0.4 mmol) in methanol (2 ml) was added the alkyne (1.0 eq., 0.36 mmol), sodium azide (2.0 eq., 0.8 mmol, 56 mg) and Copper oxide (0.1 eq., 0.04 mmol, 6 mg). The contents were reacted at 40^0C overnight before the methanol was removed under reduced pressure. The precipitate was redissolved in EtOAc, and the pH adjusted to ~3 using before the addition of ddH2O (10 ml). The mixture was extracted three times with EtOAc (5ml) and the combined organic phases were extracted further with brine (10 mL), dried over magnesium sulphate (1 g), filtered and concentrated under reduced pressure.

2.2.5.2.1 LPB-01 [4-(1-pentyl-1H-1,2,3-triazol-4-yl)butanoic acid]

Appearance: Waxy solid (yield 15%); δ_H (600 MHz, Acetone-d_6) 0.89 (t, 3H, CH_3), 1.29 (dt, 2H, CH_2), 1.35 (m, 2H, CH_2), 1.89 (m, 2H, CH_2), 1.95 (m, 2H, CH_2), 2.38 (t, 2H, CH_2), 2.74 (t, 2H, CH_2), 4.37 (t, 2H, CH_2N), 7.77 (s, 1H, aromatic); δ_C (75.5 MHz, Acetone-d_6) 173.529, 146.653, 121.353, 49.577, 33.038, 31.755, 29.956, 28.244, 24.566, 24.669, 14.349; Monoisotopic Mass (EI); Calculated ($C_{11}H_{19}N_3O_2$): 225.1477, Found: 224.5925 (M-1).

2.2.5.2.2 LPB-02 [3-(1-pentyl-1H-1,2,3-triazol-4-yl)propanoic acid]

Appearance: Waxy solid (yield 17%); δ_H (600 MHz, Acetone-d_6) 0.87 (t, 3H, CH_3), 1.28 (m, 2H, CH_2), 1.34 (m, 2H, CH_2), 1.87 (m, 2H, CH_2), 2.69 (t, 2H, CH_2), 2.95 (t, 2H, CH_2), 4.35 (t, 2H, CH_2N), 7.73 (s, 1H, aromatic); δ_C (75.5 MHz, Acetone-d_6) 174.137, 146.998, 122.362, 51.881, 34.202, 32.090, 29.995, 22.959, 21.688. Monoisotopic Mass (EI); Calculated ($C_{10}H_{17}N_3O_2$): 211.1321, Found: 212.1396 (M+1).

2.2.5.2.3 LPB-03 [10-(4-pentyl-1H-1,2,3-triazol-1-yl)decanoic acid]

Appearance: Waxy solid (yield 42%); δ_H (600 MHz, DMSO-d_6) 0.91 (t, 3H, CH_3) 1.25-1.50 (m, 16H, 8xCH_2), 1.65 (m, 2H, CH_2), 1.88 (m, 2H, CH_2), 2.66 (t, 3H, CH_2), 3.27 (t,

3H, CH_2), 4.34 (t, 3H, CH_2), 7.72 (s, 1H, aromatic); δ_C (75.5 MHz, Acetone-d_6) 179.929, 148.478, 120.583, 50.339, 34.489, 32.044, 31.083, 30.398, 29.892, 28.792, 28.236, 26.787, 25.635, 22.721, 22.667,19.473, 14.331. Monoisotopic Mass (EI); Calculated ($C_{17}H_{31}N_3O_2$): 309.2416, Found: 310.2480 (M+1).

2.2.5.2.4 LPB-04 [4-(1-tetradecyl-1H-1,2,3-triazol-4-yl)butanoic acid]

Appearance: Waxy solid (yield 37%); δ_H (600 MHz, DMSO-d_6) 0.88 (t, 3H, CH_3), 1.25-1.50 (m, 22H, 11xCH_2) 1.59 (m, 2H, CH_2), 1.85 (m, 2H, CH_2), 3.33 (t, 2H, CH_2), 3.47 (t, 2H, CH_2), 4.35 (t, 2H, CH_2N), 7.71 (s, 1H, aromatic); δ_C (75.5 MHz, DMSO-d_6) 179.053, 147.958, 123.632, 51.603, 34.226, 33.542, 33.080, 32.811, 32.156, 31.928, 31.075, 30.420, 29.610, 29.282, 29.127, 28.304, 26.506, 24.663, 18.125, 14.886. Monoisotopic Mass (EI); Calculated ($C_{20}H_{37}N_3O_2$): 379.3199, Found: 380.3271 (M+1)

2.2.5.2.5 LPB-05 [10-(4-decyl-1H-1,2,3-triazol-1-yl)decanoic acid]

Appearance: Waxy solid (yield 54%); δ_H (600 MHz, DMSO-d_6) 0.87 (t, 3H, CH3), 1.25-1.50 (m, 26H, 13xCH_2) 1.63 (m, 2H, CH_2), 1.86 (m, 2H, CH_2), 2.35 (m, 2H, CH_2), 2.65 (t, 2H, CH_2), 4.30 (t, 2H, CH_2N), 7.25 (s, 1H, aromatic); δ_C (75.5 MHz, DMSO-d_6) 174.837, 148.609, 121.883, 51.945, 34.816, 34.192, 33.613, 33.231, 32.644, 31.024, 30.728, 30.253, 30.033, 29.787, 29.081, 28.778, 28.022, 27.380, 26.650, 26.161, 23.124, 14.900. Monoisotopic Mass (EI); Calculated ($C_{22}H_{41}N_3O_2$): 379.3199, Found: 380.3271 (M+1)

2.2.5.2.6 LPB-06 [9-(1-tetradecyl-1H-1,2,3-triazol-4-yl)nonanoic acid]

Appearance: Waxy solid (yield 59%); 0.86 (t, 3H, CH_3), 1.25-1.50 (m, 30H, 15xCH_2) 1.67 (m, 4H, 2CH_2), 1.86 (m, 2H, CH_2), 2.29 (m, 2H, CH_2), 2.69 (t, 2H, CH_2), 4.29 (t, 2H, CH_2N), 7.24 (s, 1H, aromatic); δC (75.5 MHz, Acetone-d_6) 174.475, 147.403, 120.993, 50.977, 35.004, 34.232, 33.661, 33.737, 33.654, 31.534, 31.238, 30.980, 30.743, 30.549, 30.091, 29.872, 29.512, 29.101, 28.551, 27.110, 26.789, 26.589, 26.311, 23.131, 14.498. Monoisotopic Mass (EI); Calculated ($C_{25}H_{47}N_3O_2$): 421.3668, Found: 422.3730 (M+1)

Chapter 3

A molecular basis for the heterogeneous excitability of SGNs in post-hearing onset mice

3.1 Introduction

3.1.1 Investigating the heterogeneity of the auditory nerve

ANFs display significant heterogeneity in their activity and response to sound stimuli. Fibres differ in their frequency tuning, sound threshold of activation, spontaneous spike rate and dynamic range (Kiang et al., 1965, Evans, 1972, Liberman and Kiang, 1978, Heil and Peterson, 2015). This heterogeneity allows the cochlea to encode the full range of acoustic information in terms of frequency/pitch and loudness. The first successful *in vivo* recordings from individual ANFs were achieved by Tasaki in 1954 from anaesthetised guinea-pigs (Tasaki, 1954). This study and subsequent investigations into the activity of ANFs typically involved positioning a high resistance electrode close to the nerve exiting the cochlea, and recording their responses to sound stimuli (Borg et al., 1988, Evans, 1972, Kiang et al., 1965, Tasaki, 1954). Subsequently, recordings from IHC afferent synapses were also achieved by the opening of the otic capsule and insertion of the electrode close to the IHC synapse (Palmer and Russell, 1986, Siegel and Dallos, 1986, Siegel, 1992). These studies revealed important insights into the spontaneous and sound evoked activity of the AN *in vivo*. Nonetheless, a comprehensive understanding of the physiology of the AN also requires knowledge of the molecular electrophysiology and intrinsic membrane properties of the constituent SGNs. To this end, the structure and organisation of the cochlea has so far precluded *in vivo* patch clamp recordings from SGNs within the AN. However a wealth of information has been gleaned from *in vitro* studies, using a variety of tissue preparations to examine the properties of isolated neurons. These include mechanically isolated neuronal preparations (Santos-Sacchi, 1993), gangliotopic preparations (Mo and Davis, 1997) and preparations where the cochlea was sectioned and patched *in situ* (Jagger et al., 2000).

3.1.2 The intrinsic excitability of isolated spiral ganglion neurons

The first successful patch clamp recordings from SGNs were achieved in 1993 by Joe Santos-Sacchi. SGNs from adult guinea pigs were obtained non-enzymatically by crushing the cochlear modiolus and triturating in a nominally Ca^{2+} free medium. Neurons were plated on glass coverslips and incubated until they were observed to have lost their myelin sheath (~10 mins). Whole-cell patch clamp recordings showed the presence of fast inward tetrodotoxin (TTX)-sensitive Na^{+} currents and somewhat slower outward K^{+} currents. Brief current injections produced graded APs with an after hyperpolarisation that lasted several milliseconds (Santos-Sacchi, 1993). Subsequent work by Chu Chen in 1997, using the same preparation, identified a significant inward, non-inactivating current in response to hyperpolarizing voltage steps. Likewise, Chen demonstrated notable depolarising sag in the membrane voltage during hyperpolarizing current injections. This also resulted in an overshoot or a rebound firing upon termination of the current injection (Chen, 1997).

Consistent with the large diversity in responses from fibres within the AN *in vivo*, SGNs were also found to display intrinsic variability in their firing properties *in vitro*. The first reports of the heterogeneous nature of SGN membrane properties were published independently in studies by Xi Lin, and Mo and Davis. Whole-cell recordings from P0-1 gerbil (Lin, 1997) displayed either single APs or trains of actions potentials in response to sustained current injections. Mo and Davis reported similar findings in SGNs which had been explanted and cultured from P1-6 mice (Mo and Davis, 1997). The variation was classified broadly into two categories based on a neurons ability to "adapt" to the depolarising stimulus. Adaptation can be defined as a decline in neuron firing rate in response to constant current injection (Granit et al., 1963). Neurons were described as rapidly adapting (RA) or slowly adapting (SA) based on the number of APs fired over a period of depolarizing current injection. Further work from the same group also showed that SGNs from postnatal mice (P3-P8) displayed firing features which were related to their original position along the tonotopic axis (Adamson et al., 2002b). Interestingly, this heterogeneity could not be replicated in enzymatically isolated guinea pig SGNs which displayed only RA responses to current injection (Szabo et al., 2002).

Brain-Derived Neurotrophic Factor (BDNF) and Neurotrophin-3 (NT-3), two neurotrophins released during early development and expressed differentially in the cochlea, are also important determinants of firing behaviour (Adamson et al., 2002a). In early postnatal development (P3-P8) BDNF exposure favours an RA phenotype while NT-3 exposure produces cells with SA characteristics. This tonotopic dependence and neurotrophic influence on firing phenotype was correlated with differences in the densities of important ion channel such as K_{Ca}, Kv1.1, Kv4.2 and Kv3.1 (Adamson et al., 2002a, Adamson et al., 2002b). A vast array of ion channels are now known to contribute to the firing features observed in mammalian SGN, including many different Cav, Navs and hyperpolarisation-activated cyclic nucleotide-gated (HCN) channels, as well as Kv7, Kir and others (see Table 3.1 for a comprehensive list).

A significant technical advance has been the ability to make patch clamp recordings *in situ*. A technique for slicing the rat cochlea around the onset of hearing was developed by Jagger and Housley in 2000. This allowed whole-cell patch clamp recordings to be made from acutely prepared rat SGNs without the need for tissue explant or dissociation (Jagger et al., 2000). This helps maintain the SGN and their peripheral and central neurites that are typically lost during trituration and explant. Furthermore, this technique allowed Lucifer yellow labelling of SGNs and their peripheral projections to provide post-hoc identification of type I and type II fibres (Jagger and Housley, 2003).

Despite much characterisation of the electrophysiological properties of early postnatal SGNs (Adamson et al., 2002b, Jagger et al., 2000, Lin, 1997, Mo and Davis, 1997, Szabo et al., 2002), the characterisation of the firing properties of SGNs from animals post-onset of hearing has been somewhat ignored. Though the initial work from Santos-Sacchi and Chen did record from adult SGNs, little characterisation of the firing features was carried out. Apart from the notable exception of Lv et al. in 2010, which examined mice as old as 17 months, little investigation into the firing properties of SGNs from post-hearing onset animals has been conducted (Lv et al., 2010).

Table 3.1 Ion channels in the spiral ganglion. Abbreviations: BK, large-conductance calcium-activated potassium channel; HCN, hyperpolarisation-activated cyclic nucleotide-gated channel; SK, small conductance calcium-activated potassium channel; TASK, two-pore-domain channel; THIK, tandem pore domain halothane-inhibited K^+ channel; MAP, microtubule-associated protein channel; MBP, myelin basic protein; SGN, neuronal soma; Ax, axon; M, myelin; LM, loose myelin; SC, satellite cells; NSC, non-myelinating Schwann cells; MSC, myelinating Schwann cells; P, postnatal; A, adult; E, embryonic; EP electrophysiology; I, immunocytochemistry; ISH, in situ hybridisation; R, polymerase chain reaction of RNA; W, Western blot. (Adapted from (Davis and Crozier, 2015)

Ion channel	Location	Age/species	Method	Reference
BK	SGN	E, P, A/Mouse; A/Guinea pig	EP, I, ISH, R	(Chen and Davis, 2006, Hafidi et al., 1992, Langer et al., 2003, Skinner et al., 2003, Adamson et al., 2002a)
BKβ1	SGN	P/Rat	ISH, R	(Langer et al., 2003)
BKβ4	SGN	P/Rat	ISH, R	(Langer et al., 2003)
CaV1.2	SGN, NSC, MSC	P, A/Mouse; A/Chinchilla; A/Guinea pig	EP, I, R	(Chen et al., 2012, Chen et al., 2011, Layton et al., 2005, Lin, 1997, Xie et al., 2007, Zuccotti et al., 2013, Lopez et al., 2003)
CaV1.3	SGN	P, A/Mouse; P, A/Rat	EP, I, W, R	(Chen et al., 2012, Chen et al., 2011, Lv et al., 2014, Lv et al., 2012)
CaV2.1	SGN, NSC, MSC	P, A/Mouse; A/Chinchilla	EP, I, R	(Chen et al., 2011, Lopez et al., 2003, Lv et al., 2012)
CaV2.2	SGN	P, A/Mouse; A/Chinchilla	EP, I, R	(Chen et al., 2011, Lopez et al., 2003, Lv et al., 2012)
CaV2.3	SGN, NSC, MSC	P, A/Mouse; A/Chinchilla	E, I, R	(Chen et al., 2011, Lopez et al., 2003, Lv et al., 2012)
CaV3.1	SGN, NSC, MSC	P, A/Mouse	EP, I, R	(Chen et al., 2011, Lv et al., 2012)
CaV3.2	SGN	P, A/Mouse	EP, I, R	(Chen et al., 2011, Lv et al., 2012)

CaV.3.3	SGN	P, A/Mouse	EP, I, R	(Chen et al., 2011, Lv et al., 2012)
HCN1	SGN	P, A/Mouse; A/Guinea pig	EP, I, W	(Kim and Holt, 2013, Liu et al., 2014b, Yi et al., 2010, Bakondi et al., 2009)
HCN2	SGN	P, A/Mouse; A/Guinea pig	EP, I, R, W	(Bakondi et al., 2009, Kim and Holt, 2013, Yi et al., 2010)
HCN3	SGN	A/Guinea pig	I, W	(Bakondi et al., 2009)
HCN4	SGN	P, A/Mouse; A/Guinea pig	EP, I, R, W	(Bakondi et al., 2009, Kim and Holt, 2013, Liu et al., 2014a, Yi et al., 2010)
KV1.1	SGN, SC, Ax	P, A/Mouse; A/Guinea pig	EP, I, R,	(Adamson et al., 2002a, Chen and Davis, 2006, Liu et al., 2014a, Mo et al., 2002, Reid et al., 2004, Bakondi et al., 2008, Wang et al., 2013, Smith et al., 2015)
KV1.2	SGN, SC, Ax	P/Mouse; A/Guinea pig	EP, I	(Liu et al., 2014a, Bakondi et al., 2008, Wang et al., 2013, Smith et al., 2015)
KV3.1	SGN	P, A/Mouse; A/Guinea pig	I, R	(Chen and Davis, 2006, Adamson et al., 2002a, Bakondi et al., 2008, Smith et al., 2015)
KV3.3	SGN	P/Mouse	I, R	(Chen and Davis, 2006)
KV4.2	SGN	P, A/Mouse; A/Guinea pig	I, R	(Chen and Davis, 2006, Adamson et al., 2002a, Bakondi et al., 2008)
KV7	SGN	P, A/Mouse	EP, I, R	(Beisel et al., 2005, Lv et al., 2010)
Kir	SC, NSC	P, A/Rat	I, R	(Hibino et al., 1999)
NaV1.1	SGN	A/Rat	I, R	(Fryatt et al., 2009)
NaV1.6	SGN	A/Mouse & Rat	I, R	(Fryatt et al., 2009, Hossain et al., 2005)
NaV1.7	SGN	A/Rat	I, R	(Fryatt et al., 2009)
SK1	Absent or below detection	P, A/Rat	ISH	(Dulon et al., 1998)
SK2	SGN	P, A/Rat	ISH	(Dulon et al., 1998)
SK3	SGN	P, A/Rat	ISH	(Dulon et al., 1998)
TASK-1		P/Mouse	R	(Chen and Davis, 2006)
TASK-3		P/Mouse	R	(Chen and Davis, 2006)
THIK-2		P/Mouse	R	(Chen and Davis, 2006)

TRAAK		P/Mouse	R	(Chen and Davis, 2006)
TREK-1		P/Mouse	R	(Chen and Davis, 2006)
TWIK1	SGN	P/Mouse	I, R	(Chen and Davis, 2006)
MAP2	SGN	P/Mouse; A/Human; P, A/Rat	I	(Anniko et al., 1995, Chen et al., 2011, Hafidi et al., 1992)
MBP	MSC	P, A/Rat; A/Guinea pig	I	(Toesca, 1996, Liu et al., 2014c)

Characterisation of the mature neurons is essential to determine if the features observed in immature SGNs are relevant to the working ear, and not just a feature of development. For instance, in the mammalian cochlea before the onset of hearing, IHCs fire spontaneous APs that are believed to be vital for the development of the higher auditory system. However, these APs are not characteristic of IHCs in the mature sensory system (Johnson et al., 2011). Further, SGN electrophysiology is highly plastic. BDNF and NT-3 expression, which notably alter firing in SGNs (Davis, 2003), varies over the course of development with SGNs likely experiencing changing humoral cues up to and past the post-hearing onset (Fritzsch et al., 2004). In this chapter, the firing properties of post-hearing onset SGNs were investigated. Initial work focused on determining a practical neuronal preparation in order to facilitate robust and stable recordings. Proceeding work then investigated the firing properties of mature SGNs, and examined the ionic properties which underlie differences in firing. Ultimately, this chapter attempts to elucidate the molecular components underlying differences in firing behaviour between SGNs originating from common locations in the cochlea.

3.2 Results

3.2.1 Identifying SGN subtypes in a dissociated ganglion preparation

To investigate the electrophysiology of mature SGNs from post-hearing onset animals, isolated sections of the spiral ganglion derived from apical, mid and basal thirds of the

cochlea from mice around the age of hearing onset (P12-15) and one week post-onset (P20-21) were dissociated using enzymatic and mechanical treatment followed by cell culture. These "neuronal cultures" contained a variety of cell types derived from the cochlea. Morphologically, SGNs were identifiable by their large, round cell body, asymmetric nucleus and single large nucleolus (Figure 3.1A-C; *Neurons identified by* *). The neuronal identity of SGNs was confirmed by their ability to fire APs in response to depolarisation current injection. Consistent with reports from pre-hearing animals, voltage clamp recordings from mature SGNs showed large inward Na^+ transients, significant outward K^+ currents and a slowly activating hyperpolarisation-activated inward currents (Figure 3.1D) (Santos-Sacchi, 1993). The majority of these recordings are assumed to come from type I SGNs. Although type II SGNs cannot be unambiguously distinguished from type I SGN without post hoc labelling to ascertain their innervation patterns, a small minority of cells displayed morphology and ionic conductances consistent with the characterised electrophysiology of type II neurons (Jagger and Housley, 2003). Putative type II SGNs were physically smaller (Figure 3.1B, 5-9 pF, n = 3) than type I SGNs (Figure 3.1A, 5-43 pF n = 82). They also displayed lower K^+ current amplitudes, slower activation kinetics and more prominent inactivation of their outward K^+ currents (Figure 3.1E). As type I SGNs are the focus of this study putative type II SGNs, once identified, were excluded from further analysis. Within these cultures some neurons with very large somata and extensive processes were observed (Figure 3.1C, G). These neurons have been reported elsewhere (Mo and Davis, 1997, Jagger and Housley, 2003) and have variously been suggested to correspond to large cell type II neurons (Berglund and Ryugo, 1987) or to the speculative type III neurons reported in an ultrastuctural study by Romand and Romand (Romand and Romand, 1987). These neurons often possessed somata with a measured whole cell-capacitance (C_m) of 30 pF or higher, and shared common electrophysiological characteristics such as the activation of very large outward K^+ currents (often >20 nA) and the generation of spontaneous APs. Other cell types observed in the preparation were glial like cells (Hansen et al., 2001). These were morphologically distinct by their elliptical soma and bipolar morphology and can be seen on the right of Figure 3.1A.

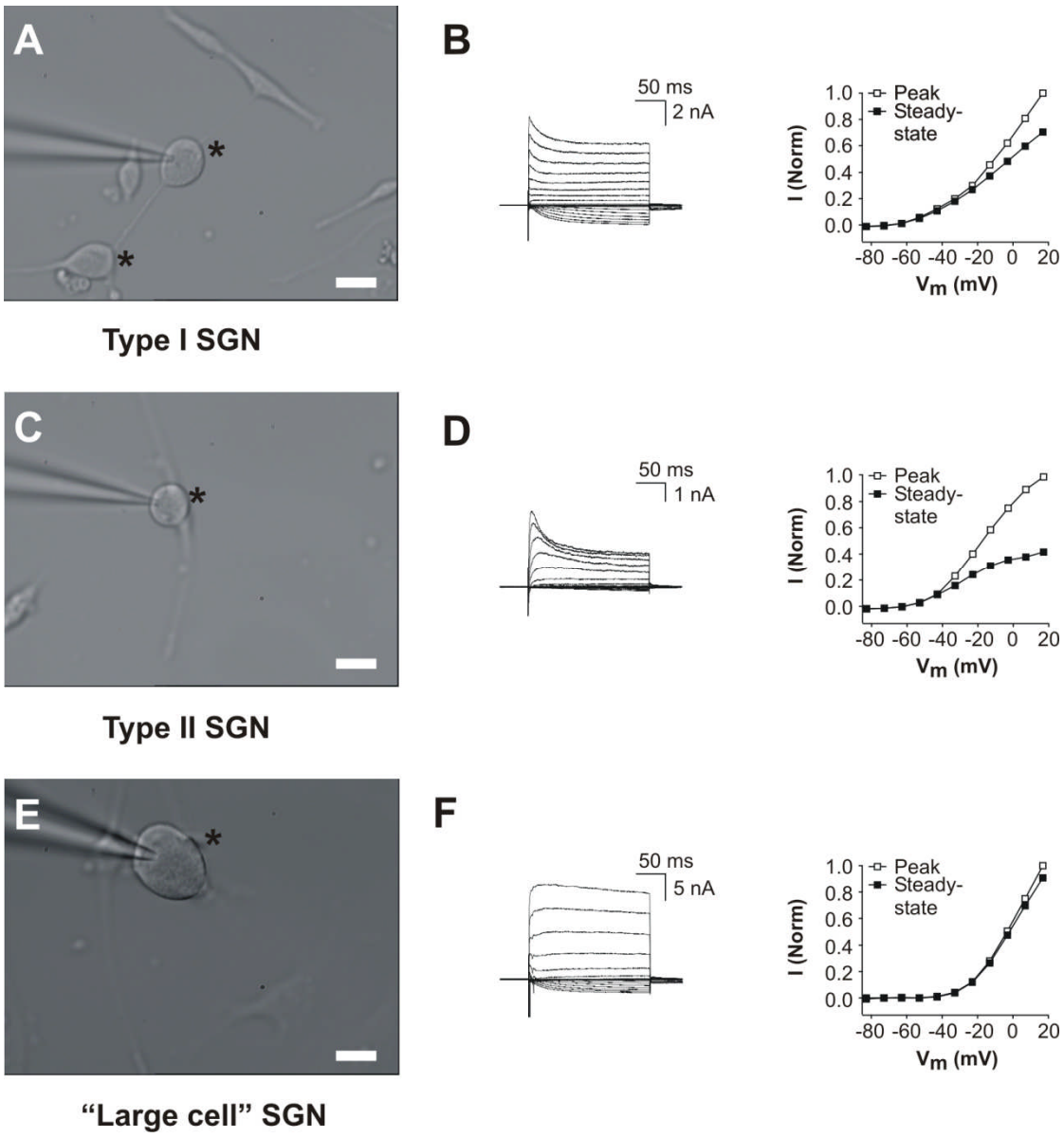

Figure 3.1 Voltage activated currents from cultured P12 SGNs. Enzymatically dissociated SGN cultures contained a variety of cell types derived from different tissues within the cochlea. SGNs, labelled here by *, have large, round cell bodies, asymmetric nuclei and single large nucleoli. **A** Type I SGNs, as expected, make up the majority of cultured neurons. Also visible are putative glial cells, characteristic by their small oval soma and bipolar morphology. **B** Type I SGNs display large inward Na+ transients, slowly or non-inactivating outward K^+ currents and hyperpolarisation-activated inward currents. **C** DIC image of a putative Type II SGN in culture. Type II SGN make up 5-10% of neurons in vivo and cannot be distinguished by morphology alone but were typically smaller than Type I SGNs. **D** Type II SGNs have distinctly lower current magnitudes, slower activation kinetics and increased inactivation of their outward K^+ currents. **E** Large cell SGNs were a subpopulation observed in neuronal cultures defined here as a cell with C_m >25pF. **F** "Large cell" SGNs exhibited large inward Na^+ transients and large non-inactivating outward K^+ currents (both often exceeding 20 nA). Scale bar: 10 µM for all images.

3.2.2 Heterogeneous firing properties of post-hearing onset SGNs

In order to investigate the firing properties of SGNs, whole-cell current clamp recordings were made from the soma of cultured SGNs. Neurons were held at a potential of -73mV and APs were evoked by depolarising current injection. In total, 85 recording of SGNs firing responses were successful obtained. Consistent with previous observations from pre-hearing SGNs (Mo and Davis, 1997), a broad range of firing properties were observed in response to injected depolarising current. Neurons either fired a single AP in response to the injected current i.e. adapting rapidly to the stimulus, or fired multiple APs i.e. adapting more slowly or not at all (Figure 3.2B). Spontaneous APs were also observed in a number of cells in the absence of a depolarising stimulus. Figure 3.2A shows the distribution of firing responses observed across all recordings for a single 200 ms current injection of +100 pA. SGNs from both age groups and all three tonotopic regions displayed these diverse firing properties, suggesting the tonotopic determination of firing type observed in early postnatal animals (Adamson et al., 2002b) is not maintained beyond the onset of hearing. In this chapter no distinction was made between neurons that adapted slowly and neurons that failed to adapt at all e.g. Figure 3.2B, lower trace; all neurons that fired >1 AP in response to +100 pA injection were classified as SA. This is in line with most studies (Mo and Davis, 1997, Adamson et al., 2002b). However, further demarcation of the SA classification into slowly and non-adapting phenotype is carried out in the next chapter.

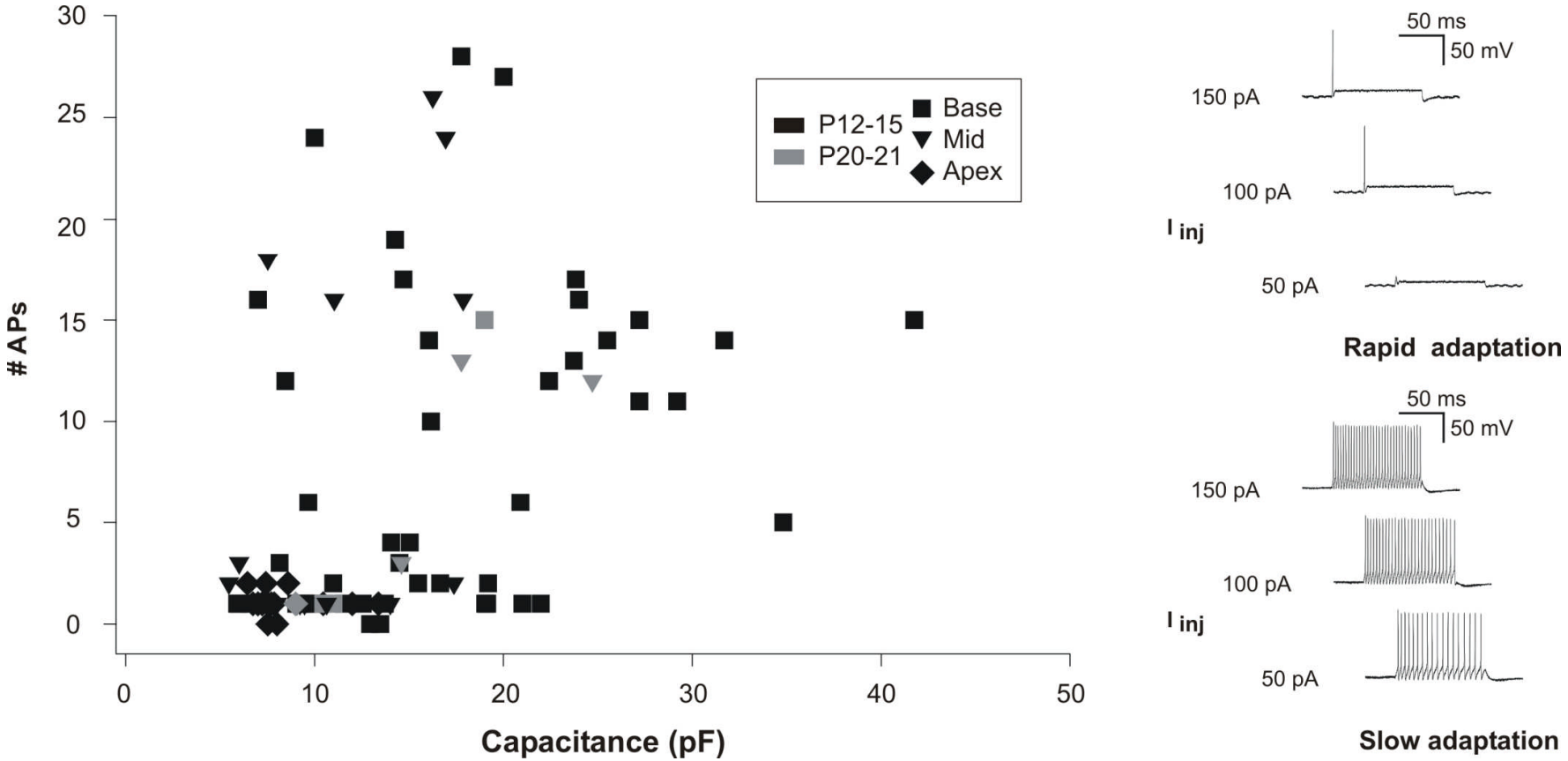

Figure 3.2 Heterogeneous excitability in populations of SGNs cultured from post-hearing onset mice. A Scatter-plot of the number of APs (#APs) in response to a depolarizing current injection versus the C_m. 200 ms current injections of +100 pA were applied from a holding potential of -73 mV (n = 85). **B** Firing responses of two neurons. Neurons display different responses to injected current, requiring different quantities of current to stimulate an AP and display varying ability to adapt to sustained current injections.

Subpopulations of RA and SA neurons exhibited other discernible differences in their excitability. Spontaneous activity, defined here as the observation of APs in the absence of injected current, was a common occurrence in SA cells (19/44 cells exhibited spontaneous activity, 42.2%). Examples of some of these kinds of activity are shown in Figure 3.3A. This activity included intense regular firing (12/19, *left panel*), sporadic or irregular firing (6/18, *middle panel*) and once as a burst-like firing (1/19, *right panel*). In contrast, no example of spontaneous activity was observed in RA cells (0/41, 0%, Figure 3.3B). RA and SA neurons also displayed different sensitivities to injected current. In SA neurons all but one neuron (43/44, 97.8%) fired an AP in response to the minimum current injection examined (+50 pA). In the RA population however, only 15/40 (37.5%) did so. The median current injection in order to evoke an AP was +100 pA, but many SGN needed as much as +200 pA in elicit firing (Figure 3.3C, $P<0.001$, unpaired Student's t-test).

The variability in sensitivity to depolarising stimuli led to comparison of the voltage-gated currents present in the two populations. Voltage clamp experiments obtained from the same neurons in Figure 3.4, revealed distinct differences in the voltage-activated currents between the two groups. RA and SA neurons both displayed prominent outward K^+ currents (I_k) in response to depolarising voltage steps, but the voltage at which I_k was first activated was shifted between the neuronal phenotypes (Figure 3.4B). In SA neurons a much greater depolarisation was required in order to evoke comparable levels of I_K. The current-voltage (I-V) plots in Figure 3.4B shows a prominent shift, ~20 mV in the low voltage region. Figure 3.4A shows current traces obtained from typical RA (left panel) and SA (right panel) neurons. RA neurons displayed characteristic low-threshold voltage-activated (LVA) K^+ currents which were largely absent from SA neurons. LVA K^+ currents are known to be important in setting the RMP of neurons, increasing the threshold for AP firing and reducing excitability (Johnston et al., 2010). These results are consistent with the observations in pre-hearing mice that LVA K^+ currents are an important determinant of rapid adaptation in SGN (Mo et al., 2002).

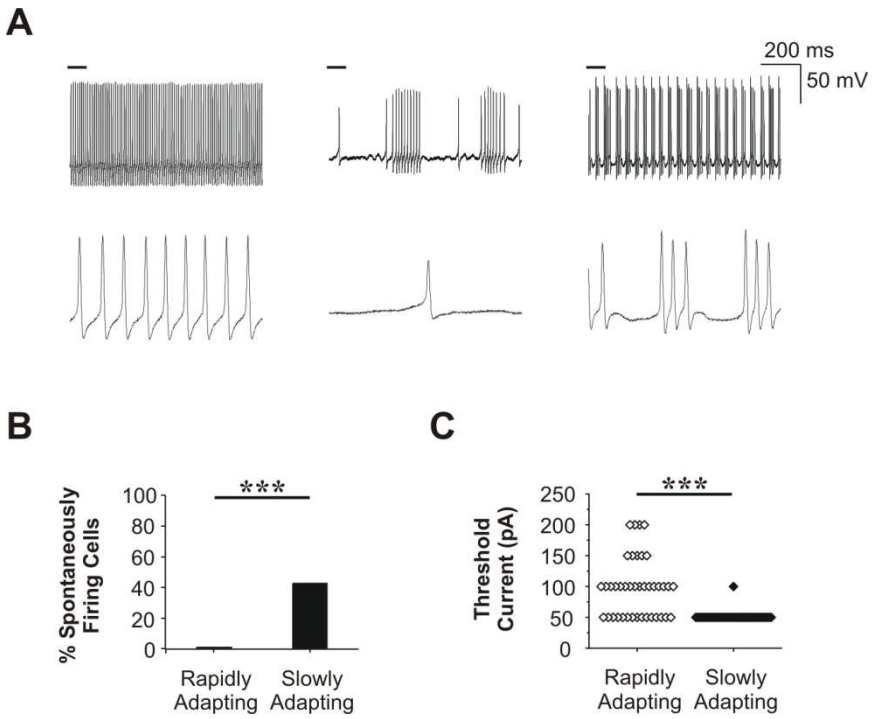

Figure 3.3 Adaptation is correlated with spontaneous activity and firing threshold. A Spontaneous firing i.e. AP firing in the absence of any current injection, was observed in a number of recordings. Spontaneous firing was usually observed as either a constant train of APs (left panel), a sporadic or irregular firing pattern (middle), or in consistent bursts (right). The lower panels correspond to an expanded 100 ms period denoted by a line in the upper panels. **B** Spontaneous firing is an exclusive property of slowly adapting (SA) cells. Spontaneous activity was observed in 0/41 (0%) cells in rapidly adapting (RA) neurons whilst occurring in 19/45 (42.2%) of slowly adapting cells. **C** Cells which display rapid adaptation to an injected current also required more current to evoke an AP. Under current clamp conditions slowly adapting cells almost exclusively fired APs in response to the lowest injected current stimulus of 50 pA (43/44, 97.8%). In cells which display rapid adaptation, this was considerably lower (15/40, 37.5%) with some cells requiring as much as 200 pA of current to elicit a response.

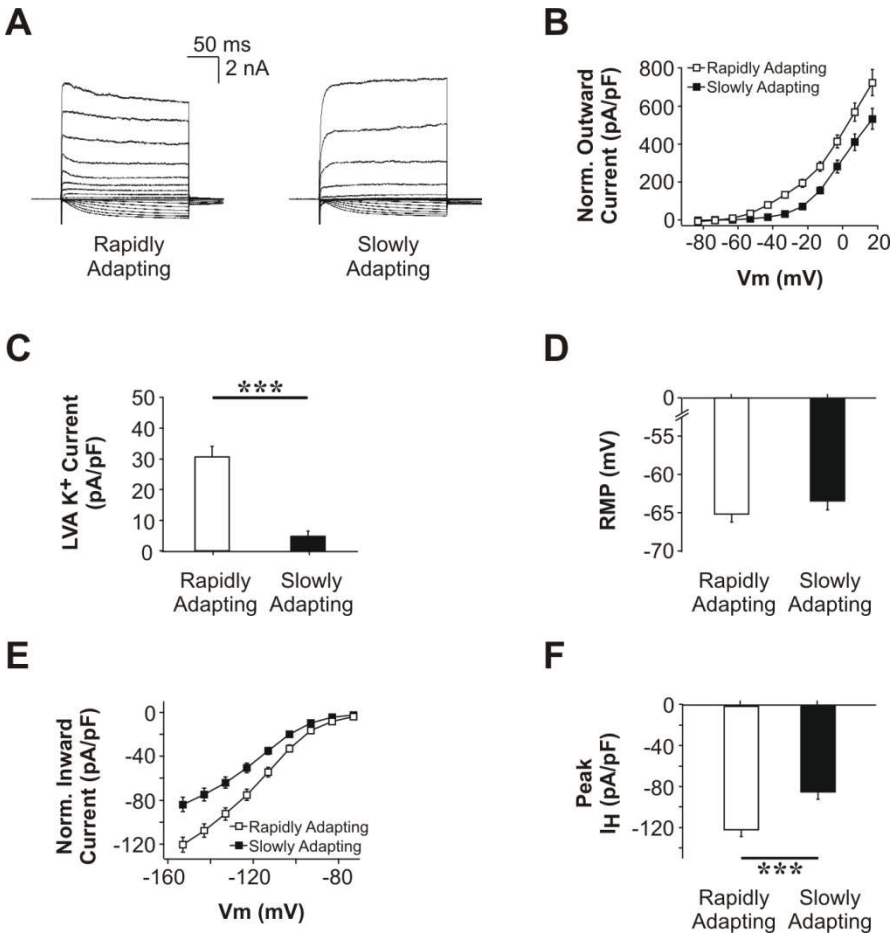

Figure 3.4 Rapid adaptation is correlated with the magnitudes of specfic ionic conducatances. A Representative voltage clamp traces for two cells which showed either rapid adaptation (left panel) or slow adaptation (right panel) previously under current clamp. Cells were held at a holding potential of -73 mV and stepped from -153 mV to +17 mV in 10 mV steps. Each step was held for 200 ms before returning to the holding potential. Inward sodium transients were cropped from current traces for expedience but could exceed 20 nA. **B** Mean normalised steady-state current-voltage (I-V) relationships for rapidly adapting (white squares) or slowly adapting (black squares) neurons. Steady-state currents were measured 10 ms from the end of the voltage steps described for A and normalised steady-state currents were obtained by divided the current by the measured whole-cell capacitance (Cm). **C** Calculated low threshold voltage-activated (LVA) K^+ currents for RA (white) or SA (black) cells. LVA K^+ currents were calculated by subtracting currents measured at -73 mV from those at -53 mV. **D** Measured RMP for RA (white) or SA (black) cells. **E** Mean normalised steady-state I-V plot showing hyperpolarisation-activated (I_h) inward currents. **F** Calculated Peak I_h currents for rapidly adapting (white) or slowly adapting (black) cells. Peak I_h currents were measured 5 to 15 ms before the end of a 200 ms step to -153 mV. *****P<0.05 ******P<0.01 *******P<0.001.

Due to the role of LVA K^+ current in setting the RMP of neurons (Johnston et al., 2010), RA and SA neurons were investigated to determine whether they displayed significant differences in their measured RMP. An estimate of the RMP was obtained by recording the potential at which there was absence of current flow (I = 0 mode of the amplifier). In both populations of SGNs, large variations in measured RMP were observed (RA: -51 to -73 mV, SA: -49 to -73mV), and the mean RMP did not vary significantly between the two populations (Figure 3.4C, RA: -64.9 ± 1 mV, SA: -63.2 ± 1.2 mV, P = 0.27, unpaired Student's t-test). This was surprising as in other studies blocking LVA K^+ current from adult guinea-pig SGNs caused a notable depolarisation in the RMP (Szabo et al., 2002). Multiple conductances contribute to setting the RMP of a neuron however, and the activity of other channels may help maintain a consistent RMP in the absence of hyperpolarising LVA K^+ current: constitutively active M-currents or hyperpolarising-activated cation currents (I_h) for example. For this reason we analysed the relative contributions of I_h in the two populations. HCN-mediated I_h is a prominent feature of both rapidly and slowly adapting SGNs *in vitro* (Liu et al., 2014b, Chen, 1997). There was a significant difference in the mean magnitudes of I_h displayed in RA and SA neurons. RA neurons displaying I_h current magnitudes of 1½ times that of the SA population (Figure 3.4E, P<0.001, paired Student's t-test, Figure 3.4F). This difference might help to explain the lack of variation in RMP between populations.

3.2.3 Dendrotoxin-K blocks LVA K^+ currents and increase excitability in post-hearing onset SGNs

In pre-hearing SGNs (P3-8) rapid adaption has been shown to be regulated by an α-dendrotoxin (α-DTX) sensitive conductance. Furthermore, dendrotoxin-K (DTX-K) demonstrated potent current inhibition and identified Kv1.1 subunits as an important contributor to the adaptive response (Mo et al., 2002). Accordingly, the effects of DTX-K were investigated here in post-hearing onset SGNs. 100 nM DTX-K was applied through the bath to RA neurons from P12-15 mice (Figure 3.5A, C). DTX-K typically enhanced the excitability of SGNs, as determined by the number of APs fired in response to a depolarising current injection. It also reduced the amplitude of the stimulus current required to first evoke an AP (Figure 3.5A, 2/5 cells). In the presence

of 100 nM DTX-K the number of APs was increased in 4/5 cells in response to a 100 pA depolarising current step (Figure 3.5B), with one cell displaying spontaneous firing as a result of DTX-K application (shown in Figure 3.5C). This was an important finding as spontaneous firing is a property normally only observed in SA neurons (Figure 3.3A, B). The increased excitability observed after DTX-K application confirmed that Kv1.1 subunits remain an important contributor to rapid adaptation in after hearing onset.

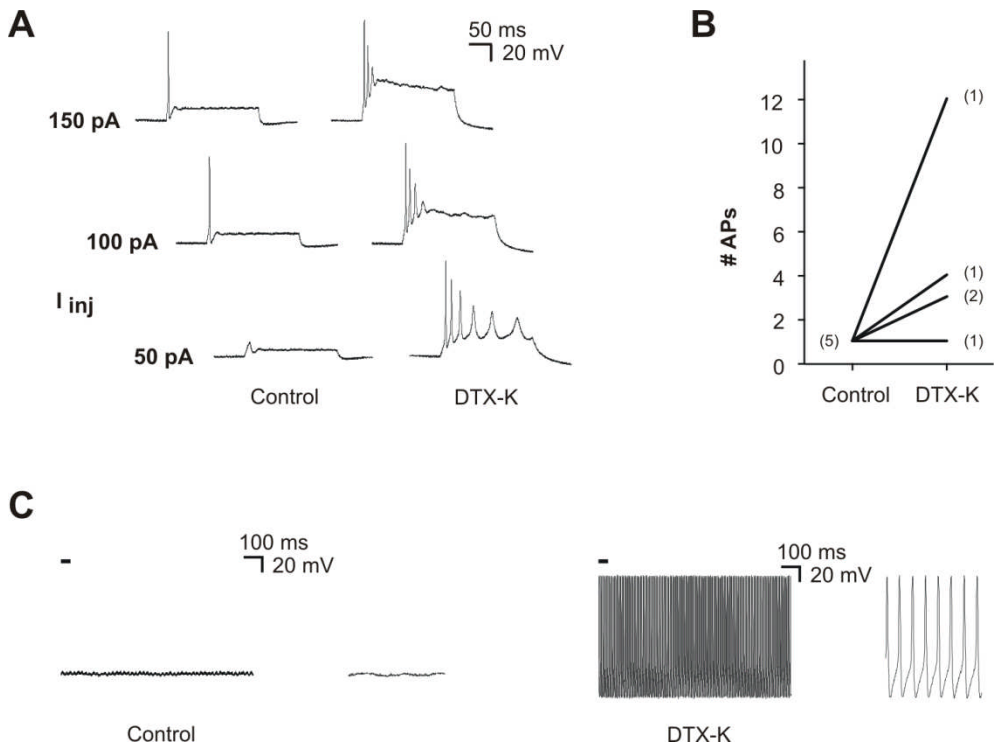

Figure 3.5 DTX-K increases the excitability of SGNs cultured from post-hearing onset mice. **A** Adaptation was slowed in RA neurons (P12-15) following bath application of dendrotoxin-K (DTX-K, 100 nM). From a holding potential of -73 mV, responses to 50 pA current injections are shown before (left) and after (right) the application of DTX-K. The required current to evoke AP firing was reduced following DTX-K application. **B** The number of APs elicited during a +100 pA current injection increased in 4/5 SGNs following application of DTX-K. Numbers of recorded cells are indicated in parentheses. **C** DTX-K evoked spontaneous firing in 1/5 cells, a feature normally observed exclusively in slowly adapting cells. The left hand traces of both Control and DTX-K panels correspond to a 1 second recording in the absence of any current clamp (I = 0). The right hand panels are 50 mS enlargement corresponding to the annotated line in the left traces.

The effect of DTX-K on the SGN voltage-gated currents was also examined (Figure 3.6). The application of 100 nM DTX-K resulted in a substantial reduction in LVA K^+ current amplitudes (Figure 3.6A, B) consistent with the observations from pre-hearing mice that Kv1.1 subunits are an important contributor to LVA K^+ currents (Mo et al., 2002). In order to quantify the amount of LVA current inhibition, currents activated by a 20 mV depolarising step from -73 mV were compared before and after DTX-K application. DTX-K reduced LVA current in 6/6 cells with a mean reduction of 82.2 ± 6.9% (Figure 3.6C, Control LVA: 146 ± 34 pA; DTX-K LVA: 16 ± 9 pA, P = 0.009, n = 6, paired Student's t-test). DTX-K block was rapid and irreversible, reaching maximum block ~2 minutes after bath perfusion began (Figure 3.6E).

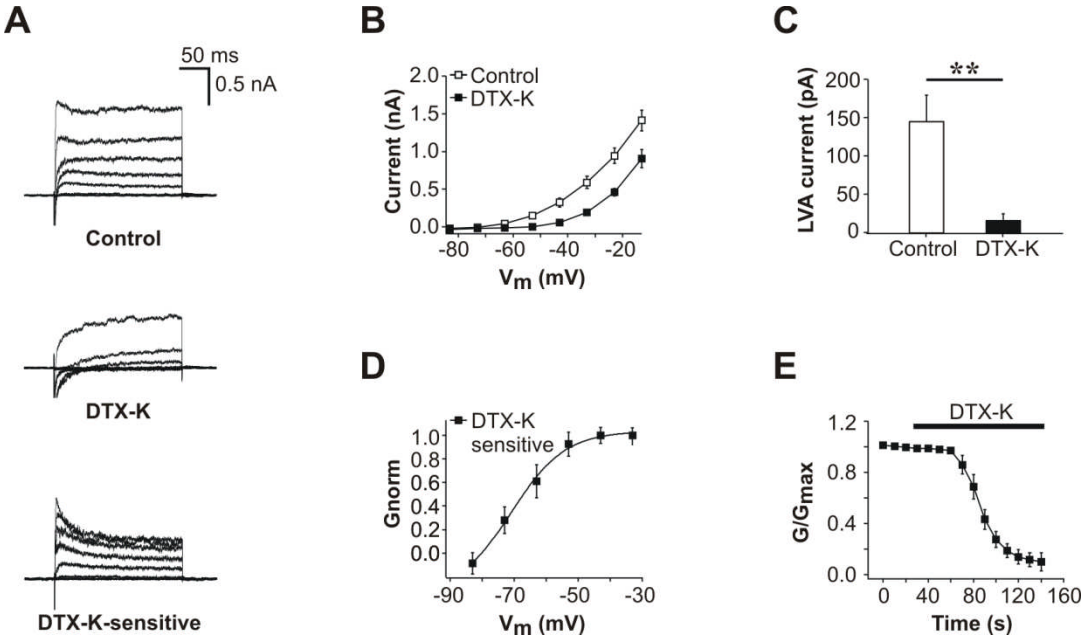

Figure 3.6 Rapid adaptation-associated LVA K^+ currents are blocked by the Kv1.1-subunit specific DTX-K. A Representative outward current responses during 200 ms voltage steps in 10 mV increments from a holding potential of -73 mV, before (Control, upper panel) and after (middle panel) bath application of 100 nM DTX-K. Subtracted DTX-K-sensitive currents are shown in the lower panel. **B** Mean steady-state current-voltage relationships before and after DTX-K application (n = 6). **C** Comparison of evoked LVA current from neurons in 5B. LVA current was calculated by subtracting any steady-state current present at the -73 mV holding potential from the evoked steady-state current measured at -53 mV. DTX-K application significantly reduced the measured LVA current. P<0.01. **D** Normalised G-V plot of the DTX-K-sensitive component. **E** The rate of DTX-K inhibition, as measured by reduction in normalised slope conductance between -63 mV and -53 mV.

3.2.4 Kv1.1 is expressed in SGNs around the onset of hearing

Following the pharmacological identification of functional Kv1.1-subunit containing channels in post-hearing onset animals, immunofluorescence experiments were performed in order to detail the distribution of Kv1.1 around the onset of hearing (Figure 3.7 & 3.8). Cochleae were fixed and sectioned along the modiolar plane, which exposed the individual spiral ganglion and cochlear nerve (Figure 3.7A, B). The cell bodies of SGNs reside in the spiral ganglion (SG), and their peripheral neurites (PN) extend from the sensory IHCs in the organ of Corti (OC). Their central neurites project towards the brainstem (Figure 3.7C, D). As predicted by the previous electrophysiological recordings, strong immunofluorescence was observed in the SGN somata; Kv1.1 labelling was also observed in the peripheral and central neurites (Figure 3.7E, F). There was no obvious difference in labelling intensity between apical and basal SGN as has been reported elsewhere (Adamson et al., 2002b, Liu and Davis, 2007) but no quantitative analysis was carried out. Kv1.1 labelling of the SGN and its neurites was not seen when the anti-Kv1.1 primary antibody was excluded from the staining process, nor if the secondary antibody was pre-incubated with a control Kv1.1 peptide (Figure 3.7G, H).

In order to examine the developmental expression of Kv1.1 around the onset of hearing, cochleae from P2, P6 and P12 animals were fixed and labelled for the Kv1.1 subunit. In order to avoid any potential tonotopic gradients in subunit expression the basal turn from each animal was compared. As shown before, P12 SGN displayed clear Kv1.1 labelling which could be localised to SGN somata and neurites (Figure 3.8G-I). In P6 sections, Kv1.1 staining was moderately weaker but still clearly present in both the somata and neurites of the SGNs (Figure 3.8D-F). In P2 animals however, staining was completely absent from neuronal structures (Figure 3.8A-C). This points to a clear developmental increase in Kv1.1 subunit expression in the early postnatal period, and suggests the appearance of Kv1.1-mediated LVA currents in SGN is important for the normal functioning of the mature cochlea.

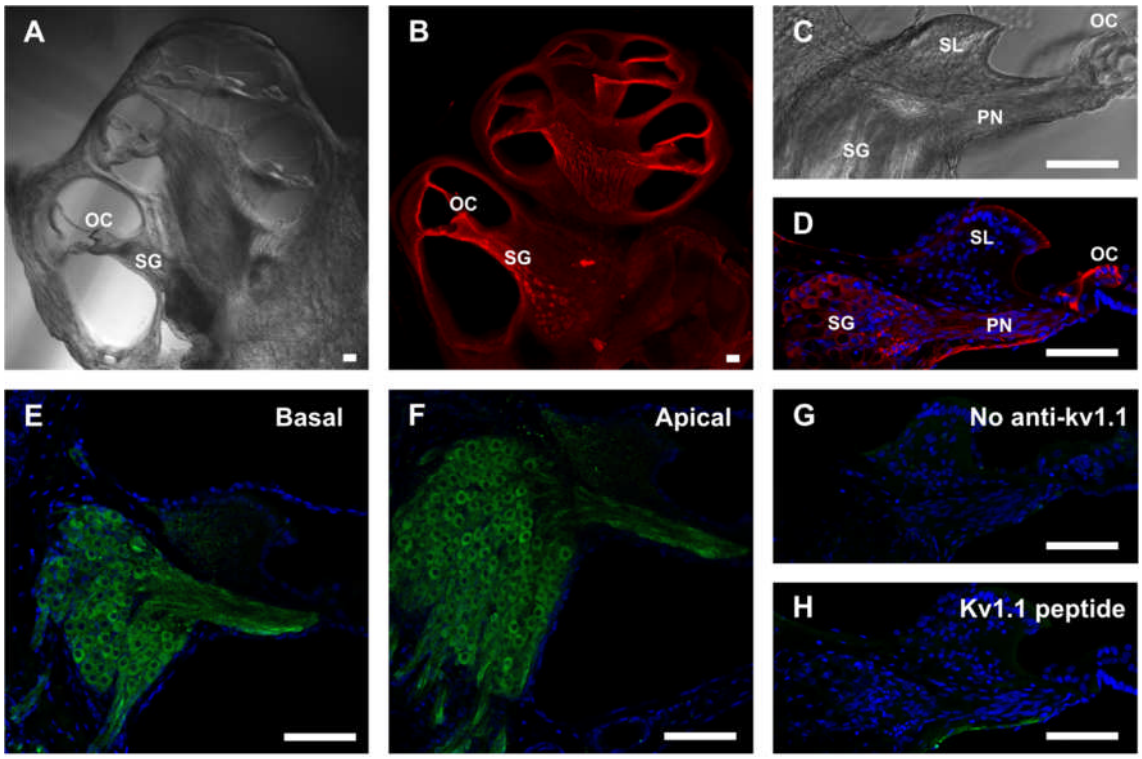

Figure 3.7 Kv1.1 subunit expression in the spiral ganglion. A DIC image of a cochear cross-section from a P12 cochlea. Individual regions of the spiral ganglion (SG) can be distinguished. **B** Confocal image of the same cross-section showing anti-acetylated tubulin (AcT) antibody labelling of microtubules (red). Anti-AcT labelled several cochlear tissues, but prominent labelling of axonal bundles was also observed (also see D) **C** DIC image of the P12 apical turn region of the SG and the peripheral neurites (PN) extending from the organ or Corti (OC). Also labelled is the bony spiral limbus (SL). **D** Confocal image of the apical SG region. SGN somata and their peripheral neurites were labelled by anti-AcT. Nuclei were stained with DAPI (Blue). **E, F**. P12 SGN were immunolabelled for the Kv1.1 subunit. Anti-Kv1.1 immunofluorescence (green) was detected in SGN somata and their neurites, in both basal and apical turns of the cochlea. **G** No Primary control: P12 basal turn SGN labelled as in E and F but excluding the primary anti-Kv1.1 antibody. No labelling of the SGN somata or PN was observed. **H** Kv1.1-Peptide control: P12 basal turn SGN labelled as in E and F but pre-incubating the primary antibody with a control Kv1.1 peptide. No labelling of the SGN somata or PN was observed. Scale bar: 50 µm for all panels.

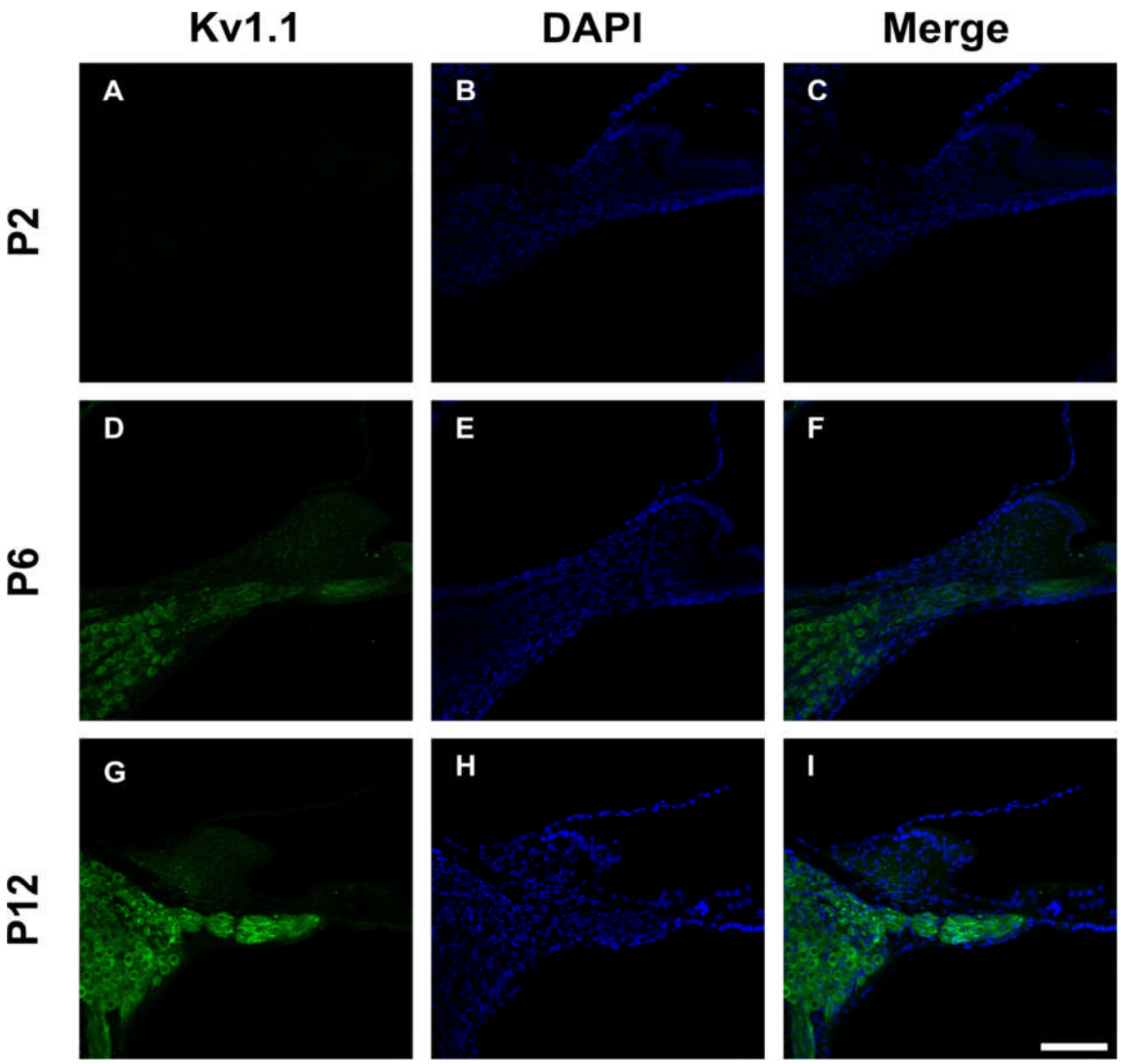

Figure 3.8 Developmental expression of the Kv1.1 subunit in SGN. A-C P2 basal turn SGN labelled for the Kv1.1 subunit. No anti-Kv1.1 immunofluorescence (green) was detected in SGN somata or neurites. Cell nuclei were labelled with DAPI (Blue). **D-F** P6 basal turn SGN labelled for the Kv1.1 subunit. Kv1.1 immunofluorescence (green) was detected in SGN somata and neurites. **G-I** P12 basal turn SGN labelled for the Kv1.1 subunit. Kv1.1 immunofluorescence is observed in SGN somata and neurites. Scale bar: 50 µm is the same for all panels.

3.2.5 Tityustoxin-Kα blocks LVA K+ currents in post-hearing onset SGNs

The Kv1.1 subunit can form functional channels by homomeric tetramerisation or by heteromerically tetramerising with other K^+ subunits. Kv1.1 is heteromerised with Kv1.2 subunits in neurons (Wang et al., 1994, Dodson et al., 2002). To examine the possibility of Kv1.2 subunit involvement in LVA K^+ current in SGNs, sensitivity to the Kv1.2-specific toxin tityustoxin-Kα (TsTx) was investigated (Werkman et al., 1993). Bath application of 100 nM TsTx resulted in a substantial reduction in the LVA K^+ current amplitude (Figure 3.9A, B) in RA neurons. In order to quantity the amount of LVA K^+ current inhibition, the currents from a 20 mV depolarising step were compared before and after 100 nM TsTx application. 100 nM TsTx reduced LVA current in 3/3 cells with an average reduction of 65.9 ± 7.5% (Figure 3.9C, Control LVA: 457 ± 153 pA; TsTx LVA: 141 ± 49 pA, n = 3,). TsTx block was rapid; reaching maximum block ~1.5 minutes after bath perfusion began (Figure 3.9E). In contrast to DTX-K however, the effects of TsTx could be washed off, albeit slowly. TsTx-sensitive current traces and I-V plots (Figure 3.9A, D) resembled those of DTX-K-sensitive currents, although maximal current block was more depolarised in the TsTx-sensitive current-voltage plot (-23 mV to -3 mV).

Table 3.2 Boltzmann parameters for toxin-sensitive SGN conductances.

Toxin	$V_{½}$ (mV)	*k* (mV)	n
DTX-K	-66.2 ± 3.5	6.4 ± 1.3	6
TsTx	-47.2 ± 5.1	10.2 ± 1.6	3

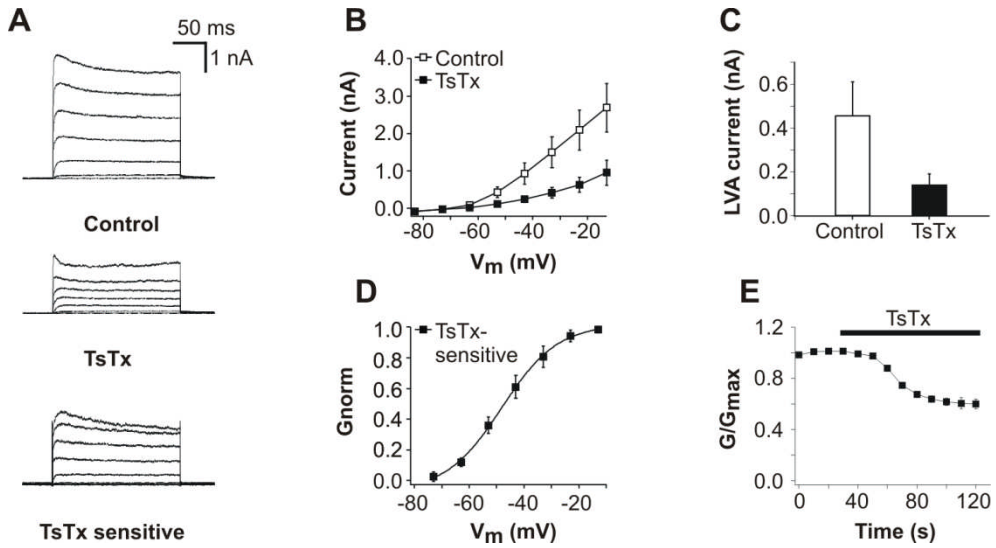

Figure 3.9 SGN LVA K^+ currents are sensitive to Kv1.2-subunit specific tityustoxin. A Representative outward current responses during a 200 ms voltage steps in 10 mV increments from a holding potential of -73 mV, before (Control, upper panel) and after (middle panel) bath application of 100 nM tityustoxin (TsTx). Subtracted TsTx-sensitive currents are shown in the lower panel. **B** Mean steady-state I-V relationships before and after TsTx application (n = 3). **C** Comparison of evoked LVA current from neurons in B. LVA K^+ current was calculated by subtracting any steady-state current present at the -73 mV holding potential from the evoked steady-state current measured at -53 mV. **D** Normalised G-V plot of the TsTx-sensitive component. **E** The rate of TsTx inhibition, as measured by reduction in slope conductance between -63 mV and -53 mV. TsTx inhibition reached maximum block after ~1.5 minutes.

3.3 Discussion

In this chapter, the membrane properties of SGNs, obtained from post-hearing onset mice, were investigated. Whole cell recordings from the somata of these neurons showed diverse heterogeneity in responses to depolarisation. This heterogeneity could be correlated with differences in ionic conductances such as I_h and LVA K^+ current. Rapidly adapting neurons displayed large LVA K^+ currents and smaller I_h than their slowly adapting counterparts. SGN LVA K^+ currents were found to be highly sensitive to both DTX-K and TsTx channel block, demonstrating that LVA K^+ currents must be mediated, at least in part, by Kv1.1 and Kv1.2 subunits. The developmental expression of Kv1.1 was also documented, demonstrating that Kv1.1 is not strongly expressed at 2 days after birth. However, by the onset of hearing, strong Kv1.1 expression is seen in

both the somata and neurites of SGNs suggesting LVA K^+ currents play an important role in the mature cochlea.

3.3.1 Whole cell recordings from post-hearing onset SGNs required dissociation and cell culture

Preliminary investigation in this project focused on the development of a robust preparation of adult SGNs for whole-cell patch clamp recordings. A search of the literature highlighted three well developed approaches: a dissociated cell culture preparation (Santos-Sacchi, 1993, Szabo et al., 2002), a gangliotypic or explant preparation (Liu and Davis, 2007, Mo and Davis, 1997) and a cochlear slice preparation (Jagger and Housley, 2003, Jagger et al., 2000). The cochlear slice preparation is the closest *ex vivo* representation of SGN in their native physiological state and was therefore assessed first. The gradual ossification of the cochlea in the days following birth made slicing of the mounted cochlea difficult however. Whole-cell access to neurons from P2 mice was attained but no further success could be achieved in older cochlea. Despite being the most physiologically representative model, the technical difficulties encountered at older ages resulted in other models being investigated. The gangliotypic or explant preparation (the former being distinguished from the latter by maintaining the entire ganglion in a single piece (Liu and Davis, 2007)) of SGN was subsequently assessed. Whole sections of spiral ganglion tissue were removed from the cochlea by careful dissection and cultured. The method was adapted from Adamson et al., 2002. Again however, electrophysiological recordings from P12-14 explanted tissue were largely unsuccessful; pipette access of cells was the largest hindering factor. Non-neuronal structures, such as unshed myelin and other glial cells, likely comprised the obstructing material. Removal of this material by positive pressure down a large access pipette or by mechanical abrasion using a second glass pipette proved fruitless. The lack of success employing this method in older animals was considered to be an age-related phenomenon. Until 2014, P8 murine SGN cultures were the oldest anyone had reported success from using this approach. During the progress of this study however successful recordings from mice as old at P14 were reported from explanted cultures (Davis and Crozier, 2015). Due to the practical difficulties encountered with the first two models

investigated, results obtained in this study were from cultures of enzymatic and mechanical isolated neurons. This was based upon the preparation described in (Whitlon et al., 2006). Robust and stable recordings from dissociated neurons up to one week after the onset of hearing (P20-21) were readily achievable by this approach. Success with mice as old as 17 months has been reported using a similar approach (Lv et al., 2010) further emphasising its utility in the examination of post-hearing onset SGN properties.

It is difficult to speculate on the effects of the different preparations on cell electrophysiology but it would be surprising if there were none. The use of neurotrophins to maintain SGNs in culture has already been shown to induce significant changes in firing phenotypes (Adamson et al., 2002a, Zhou et al., 2005). Further, neurotrophic maintenance of SGNs in culture may have a selective survival effect for subpopulations of neurons and therefore the distributions of phenotypes observed may not be representative of the real distribution in animals (Davis, 2003). For this reason, analysis of the distributions of firing phenotypes from cultures should be treated with caution and was largely avoided in this study except to note their variation (Figure 3.2). Some clear preparation-based differences have been documented; gangliotypic preparations of early post-natal murine SGNs (P3-8) were significantly less excitable than their enzymatically dissociated counterparts despite identical culture conditions. Similarly acutely prepared cochlear slice recordings show almost exclusively RA behaviour with little or no spontaneous or SA cells (Jagger and Housley, 2003, Jagger and Housley, 2002). Whether this represents a trend towards reduced excitability is uncertain, but future work should focus on validating the effects observed in neuronal cultures in more acutely dissected preparation to avoid variation due to neurotrophic effects. Before discussing the functional properties of SGNs it is important to note that along with the considerable difficulties discussed above, several other problems hinder the assessment of the their ionic currents and firing features. Amongst other difficulties, SGN currents and firing properties show considerable interspecies variability. *In vivo* studies and cochlear imaging also demonstrate a well-documented maturation of the SGNs in early post-natal development with spontaneous firing rates with ABR thresholds and ion channels expression changing markedly in this time (Rusznak and Szucs, 2009).

3.3.2 Heterogeneous excitability is a functional feature of SGNs

Spontaneous activity in the absence of sound is a feature of primary ANFs *in vivo.* Results from this study and from others have demonstrated that spontaneous APs can be generated in isolated SGNs somata (Lin and Chen, 2000, Lv et al., 2010). Spontaneous activity *in vivo* is thought to result from the spontaneous release of glutamate at the ribbon synapse of IHCs (Glowatzki and Fuchs, 2002). However, glutamate receptor antagonism only reduces spontaneous firing and fails to abolish it entirely (Cousillas et al., 1988, Puel et al., 1989). This suggests that a portion of the spontaneous activity observed is as a result of the intrinsic excitability of SGNs. In this study spontaneous activity was shown to be a feature exclusively of slowly adapting neurons and that spontaneous activity could be induced in previously non-spontaneous cells by inhibition of a DTX-K-sensitive LVA K^+ current. Spontaneous activity has also been reported as a feature of ~10% of SGNs around the onset of hearing (Wang et al., 2013). Interestingly, in the same study Kv1.2 null mutants were shown to have an increased tendency for spontaneous activity (~18% of total neurons) despite having a more hyperpolarised RMP, increased current thresholds to generate APs and larger LVA K^+ currents. This suggests LVA currents alone may not be predictive of spontaneous activity.

Each IHC receives multiple innervations from anything between 10 and 30 ANFs depending on the tonotopic location and species (Bohne et al., 1982, Stamataki et al., 2006). Despite being stimulated by a single IHC, these multiple ANFs display a heterogeneity in the spontaneous discharge rates (SR) and as well as in their thresholds of acoustic stimulation (See *Physiology of the auditory nerve*). The fibre population provides a gradient of firing properties, ranging from high-threshold low-spontaneous rate fibres, to low-threshold, high-spontaneous rate fibres. In this study two separable subpopulations of cells with distinct differences in their excitability and sensitivity to depolarisation were observed. In contrast to other studies (Adamson et al., 2002b, Lv et al., 2010) RA and SA neurons were identified in all tonotopic regions of the cochlea and at both age ranges investigated.

It is tempting to speculate about a possible connection between the heterogeneity observed in ANFs thresholds and SRs and the heterogeneity in firing features observed in SGNs in vitro. There is little direct evidence for this relationship however. Possible

evidence has been suggested to come from *in vivo* cat ANF responses to click stimuli (Adamson et al., 2002a). In these experiments, some neurons could be shown to fire repetitive APs at intervals corresponding to the period of the cell's characteristic frequency. But notably, other neurons were found only to fire singly in response to the click (Kiang et al., 1965, Ruggero et al., 1992). The current consensus however is that differential release of neurotransmitter between ribbon synapses gives rise to the observed heterogeneity. Nevertheless SGNs show significant intrinsic variation in their firing features and ionic currents.

Studies in pre-hearing cultured SGNs have typically suggested a base-to-apex gradient in excitability, with basally derived cells comprised exclusively of RA neurons and apical cells comprising of a mix of RA and SA neurons (Adamson et al., 2002a, Adamson et al., 2002b). Developmental changes within the cochlea make interpretation of these results difficult however. The development of the cochlea is not uniform either; rather it matures with a base to apex gradient with the basal region displaying mature adult characteristics earlier than the apex (Rubel, 1978, Romand, 1983). Furthermore, the presence of neurotrophins is graded in the developing cochlea: BDNF is localised primarily to the apex of the cochlea during development, whilst NT-3 localises in the base (Farinas et al., 2001). SGN firing shows a high sensitivity not just to the presence of NT-3 and BDNF, but also their concentrations (Zhou et al., 2005). Increasing levels of NT-3 exposure slows adaptation, up to a concentration 10 ng/ml. Subsequent increase in NT-3 however result in an increase in adaptation rate. This complex interaction between SGNs and neurotrophins casts further doubt on the reliability of using pre-hearing cultured SGNs as representative of the functionally mature cochlea.

Of the few studies examining the firing features of SGNs in post-hearing onset animals, the results have been inconsistent. As mentioned, this study reported the presence of both RA and SA neurons in all regions of the cochlea and at both the onset of hearing as well as one week after. In other studies, recordings from cultured mouse explants around the onset of hearing (P10-14) showed little heterogeneity in firing with RA neurons making up the majority (>75%) of all cells recorded (Davis and Crozier, 2015). The tonotopic variation observed by the same group in earlier studies was also markedly reduced, with a RA firing pattern dominating in both apical and basal cultures. However, the same study noted a large impact of holding potential upon the measured

excitability. RA was the dominant feature of SGNs when measured from a holding potential of -80 mV. However, RA neurons made up <30% of the total firing behaviours when the same cells were measured at -60 mV. This is an interesting finding as reported RMPs for SGNs vary considerable between -77 and -61 mV (Jagger and Housley, 2003, Jagger et al., 2000, Santos-Sacchi, 1993, Szabo et al., 2002). Here APs were stimulated from a holding potential of -73 mV. Contrary to these results, other studies from post-hearing onset animals have reported a strong tonotopic gradient in firing features (Lv et al., 2010, Lv et al., 2014). Surprisingly however, the gradient in excitability was in diametric opposition to that reported for pre-hearing mice; RA was an exclusive property of apical neurons whilst nearly all basal neurons displayed a SA phenotype (Lv et al., 2010, Lv et al., 2014). This firing pattern was consistent in mice as young as two weeks and up until the age of 17 months. However, there is little explanation that can be offered to account for these markedly different findings but to note their discrepancy with the results presented here and elsewhere.

The development of vestibular ganglion cells (VGCs) shares many commonalities with SGNs. VGCs, like SGN, are bipolar afferent neurons whose processes form synapses with sensory hair cells. These hair cells, however, are located in the utricle, saccule and semicircular canals. Instead of sound information they relay information relating to balance. Like SGNs they display an intrinsic heterogeneity in their firing properties (Iwasaki et al., 2008). Two prominent subpopulations of “tonic” or “phasic” phenotypes can be identified, with a small number of “intermediate” firing types also present. Consistent with the results here, the reported phasic firing cells (RA cells in our study) were also distinguishable for the presence of a prominent LVA K^+ current. This LVA K^+ current also displayed DTX-K and TsTx sensitivity and increased excitability was reported in neuronal firing upon exposure to the LVA K^+ current inhibiting toxins (Iwasaki et al., 2008). There were also significant developmental changes in the prevalence of different firing types; in early postnatal animals (P5-7) phasic firing predominated but at older ages and beyond (P12-22) tonic firing begins to dominate. This is interesting as this shift toward tonic firing is the opposite of what is observed in the spiral ganglion maturation (Davis and Crozier, 2015).

3.3.3 Rapid adaptation is dependent on LVA K^+ currents in murine SGNs

Rapid adaption in SGNs is determined by a LVA K^+ current (This study, Mo et al., 2002). In pre-hearing SGNs this current shows sensitivity to DTX-I, DTX-α, DTX-K and low doses of 4-aminopyridine (Mo et al., 2002, Szabo et al., 2002, Jagger and Housley, 2002). This study showed the LVA K^+ current in post-hearing onset animals was sensitive to both DTX-K and TsTx. This provides evidence that LVA K^+ current in SGNs is mediated by both Kv1.1 and Kv1.2 containing channels. Consistent with this, strong immunolabelling was observed for the Kv1.1 subunit as early as six days after birth. Kv1.1 expression was observed in the somata as well as in the peripheral and central neurites. This indicates a key role for Kv1.1 in the generation and maintenance of APs in acoustic coding. Interestingly, no Kv1.1 expression was observed in P2 SGN. Kv1.1 expression in SGNs only begins after the first few days postnatally, and expression then continues to increase up to the onset of hearing (~P12). This temporal expression pattern of Kv1.1 might be expected to lead to adaptation becoming more prominent as animals mature. Recent evidence has offered support to this idea. Recordings from explanted SGN tissue from P1-P2 mice revealed a very small prevalence of RA SGNs (1.5%). By P6–P8 however, RA SGNs made up more than half of all recordings and by P10-P14 RA SGNs accounted for >75% of neurons (Davis and Crozier, 2015). Allowing for differences in species variation, these results suggest that the SGN's LVA K^+ current is established in the early postnatal period (1-2 weeks) and that rapid adaptation is the predominant phenotype by the onset of hearing. Notwithstanding these results, some inter-species differences in the response of SGN to LVA K^+ current inhibition have cast doubt on the role of Kv1.1 in adaptation. Application of DTX-K to isolated guinea pig SGNs depolarised the RMP of the neuron but did not slow adaptation (Szabo et al., 2002). Despite this reported effect of DTX-K on RMP, the role of Kv1.1 in setting the RMP in SGN has not been the focus of much study. It was noted however that in acute cochlear slice preparations of rat SGNs there seemed a notable hyperpolarising of RMP during development. SGNs from P2–6 rats were reported as having a mean RMP of −61 mV (Jagger 2002) which dropped to −77 mV by P7-10 (Jagger 2003). This would be consistent with our observations that Kv1.1 expression increased significantly in the first week after birth and played an important role in setting the neuronal RMP.

Functional Kv1 channels are made up of four pore-forming subunits arranged together as homomeric or heteromeric complexes. In this work, it was demonstrated that the SGN LVA K^+ current was highly sensitive to the actions of both DTX-K and TsTx. The high levels of block (82.2% and 65.9% respectively) was suggestive that SGN LVA K^+ currents are made up of at least some Kv1.1 and Kv1.2 containing heteromers, rather than unique populations of Kv1.1 and Kv1.2 homomeric channels (Dodson 2002). Analysis of the voltage dependence of the DTX-K and TsTx-sensitive LVA components show that the DTX-K-sensitive component has more negative $V_{1/2}$ than the TsTx-sensitive components (-66 mV vs -47 mV; Table 3.2). In heteromeric expression systems, Kv1.1 homomeric channels display a significantly more negative $V_{1/2}$ that Kv1.2 homomer channels (Al-Sabi et al., 2013). The different voltage dependences of the toxin sensitive currents therefore also suggest the presence of homomeric populations of Kv1 channels.

Further work from our lab has since characterised the block of Kv1 mediate LVA K^+ currents further. Co-application experiments using sequential addition of Kv1.1 and Kv1.2 specific toxins have provided strong evidence that this current is indeed mediated by Kv1.1/Kv1.2-containing heteromers as opposed to discreet populations of Kv1.1 and Kv1.2 homomeric channels (Smith et al., 2015). Furthermore confocal immunofluorescence experiments localised both Kv1.1 and Kv1.2 subunits to specific neuronal microdomains. These include the somatic membranes of the SGNs, as well as the juxtaparanodes of the central and peripheral neurites. Kv1.1 and Kv1.2 subunits were also localised to the first heminode, which forms the spike initiation site of the AN (Smith et al., 2015). Taken together, these results suggest a key role for Kv1.1/Kv1.2-containing heteromeric channels in the initiation and propagation of APs in the AN.

3.3.4 The role of rapid adaptation in SGN coding

Rapid adaptation is a key feature of post-synaptic recordings from SGNs boutons (Glowatzki and Fuchs, 2002). SGNs fire single AMPA-receptor mediated AP spikes in response to large depolarizing stimuli. This phasic response ensures the high fidelity encoding of ribbon synapse neurotransmitter release (97% of excitatory post synaptic

currents result in successful APs) (Rutherford et al., 2012). The result is a system that is adapted for high temporal precision and phase synchronisation to acoustic signals (Johnston et al., 2010).

LVA currents have been reported in whole cell recordings from the terminal boutons of SGNs (Yi et al., 2010). Combined with findings from our lab that Kv1.1 and Kv1.2 subunits are expressed together at the first heminode near the proposed spike initiator site (Smith et al., 2015), this suggests an important role for Kv1-mediated LVA K^+ conductances in AP initiation. The notably large EPSCs and relatively low failure rate (97% of all EPSC events result in APs) suggest that LVA currents are not acting in a significant fashion to filter out subthreshold EPSC events. Rather, LVA K^+ currents most likely inhibit spiking in response to slow stimuli and prevent temporal summation of inputs ensuring a minimum rate of depolarisation is required (Rutherford et al., 2012). This reduces temporal variations that could arise from normal variation in the EPSC waveform. This dependency on the rate of rise of membrane voltage is mirrored in Octopus cells in the CN which require a minimal depolarisation rate of between 5 and 15 mV/ms. Firing in neighbouring T stellate cells, which lack strong dendrotoxin-sensitive LVA K^+ conductances, depends much less strongly on the rate of voltage rise (Ferragamo and Oertel, 2002).

This provides some interesting questions as the basis for future research. If rapid adaptation is a feature of all neurons, as is reported in SGN bouton recordings, why do neurons display such heterogeneity in their intrinsic firing properties? Do differences in LVA K^+ conductances between individual neurons contribute to the difference in spontaneous firing rates *in vivo*? What effect does modulating SGN LVA currents have on signalling *in vivo* and do SGN modulate their ionic conductances in response to external or internal signalling, such as in response to input from the Efferent System? Answers to these questions would significantly improve our understanding of how the AN encodes sound at the molecular level.

Chapter 4

PIP_2 regulation of SGN spike adaptation via Kv1 heteromeric channels

4.1 Introduction

The excitability and firing properties of a neuron is established by its electrophysiological architecture. The abundance, type and location of ion channels in the plasma membrane combine to give a neuron its characteristic electrical responses. In physiological situations however, neurons are more than the sum of their ion channels, adjusting and modifying the influences of different ion channels, allowing them to adapt and respond to changing external signals. Phosphoinositides (PI) are now recognised as key regulators of neuronal electrophysiology, coupling the external activation of membrane bound receptors to electrical changes in the cell and acting as important cofactors for the functioning of a variety of native ion channels.

In many experimental systems, neuronal excitability has been shown to be influenced by PI signalling. The most common mediator of phosphoinositide-based neuronal regulation is phosphatidylinositol 4,5-bisphosphate (PIP_2). PIP_2 regulates excitability by acting as a cofactor in the functioning of specific PIP_2-sensitive ion channels or via its hydrolysis into other potent signalling molecules which mediate downstream effects. The best studied example of PIP_2 control over excitability is through its regulation of the neuronal M-current. In hippocampal CA1 pyramidal neurons for instance, PIP_2-mediated M-currents 'clamp' the membrane potential to a hyperpolarised level and so reduce AP firing (Shah et al., 2002). Stimulating muscarinic acetylcholine receptors (mAChRs) with muscarinic agonists causes increased neuronal excitability through the activation of PLC and the resulting PIP_2 hydrolysis (Brown and Passmore, 2009).

Angiotensin II's ability to regulate neuronal excitability in superior cervical ganglion sympathetic also converges upon this mechanism of neuronal modulation. Activation of the AT1 receptor results in a PLC-dependent PIP_2 hydrolysis, leading to an increase in excitability (Zaika et al., 2006). M-current inhibition, however, is not the only example of PIP_2 determined excitability. Recently, PIP_2 and diacylglycerol (DAG) were shown to determine the excitability of thalamocortical relay (TC) neurons (Bista et al., 2015). TC neurons exhibit distinct excitatory states depending upon sleep and wakefulness behaviour, and fire APs either in high frequency bursts or slower tonic sequences respectively. PIP_2 and DAG determine these distinct excitatory states via their actions on the two-pore domain potassium channels TASK and TREK. Similarly, muscarinic

inhibition of K2P channels enhances the excitability of cerebellar granule neurons via the PIP_2 hydrolysis product DAG (Wilke et al., 2014). Another interesting case study of PIP_2 modulation is in thalamic intergeniculate leaflet neurons where PIs act to upregulate the function of hyperpolarisation-activated cyclic nucleotide-gated channels HCNs (Ying et al., 2011). The presence of PIP_2 results in low-threshold burst firing, whilst its depletion profoundly inhibits excitability. PI mediated excitability changes can also result from the production of their potent downstream effectors. For example, Dopamine D_2 receptor stimulation reduces excitability in medium spiny neurons by suppressing transmembrane Ca^{2+} currents (Hernandez-Lopez et al., 2000). In this instance, PI regulation is effected by PIP_2 hydrolysis yielding inositol 1,4,5-triphosphate (IP_3), and the subsequent release of intracellular pools of Ca^{2+} activating calcium-dependent phosphatase calcineurin.

Whilst PIP_2 is the principal PI regulator of neuronal excitability, PIP_3 also plays an important role. Whilst some short-term effects of PIP_3 signalling have been documented, the most notable effects of PIP_3 on neuronal excitability occur over longer timescales than the mechanisms discussed above. PIP_3 acts through the AKT/mTOR pathway to affect processes such as protein translation, cell proliferation and cell growth. In the CNS, knockout of the phosphatase and tensin homolog (PTEN) protein (a lipid phosphatase that dephosphorylates PIP_3, see Figure 1.11) affects somatic, dendritic and axonal growth, spine maturation, and results in reduced synaptic plasticity, and reduced intrinsic excitability (Garcia-Junco-Clemente and Golshani, 2014). Conversely, mTOR hyper-activation is associated with enhanced synaptic transmission and plasticity and epileptogenesis, highlighting its impact on neuronal excitability (Lasarge and Danzer, 2014).

4.1.1 Experimental methods of phosphoinositide modulation

In this chapter the effects of manipulating the levels of PI in SGNs, in particular the levels of PIP_2, were investigated to determine if this could modulate the firing properties of the neurons. Manipulating the levels of membrane-bound PIP_2 in an experimental setting presents many challenging aspects. The role of PIP_2 and its

metabolic products as signalling molecules, along with its potential for dynamic interconversion with other PI family members, introduces many potential mechanisms of action which may confound any simple explanation for a given effect. Additionally, many of the current methods of PIP_2 modulation are crude or represent exaggerated forms of PIP_2 addition or depletion and care must be taken in interpreting these results and placing them within a physiological context (Suh and Hille, 2008). The methods of PIP_2 depletion employed in this study are discussed here, with a brief discussion of other methods of PIP_2 modulation.

4.1.2 Inhibition of phosphoinositide synthesis

A metabolic focused approach to PI modulation is to interrupt synthesis of PIP_2 and PIP_3 by inhibiting the enzymes that synthesise them. In the case of PIP_2, this requires the inhibition of one of two lipid kinases: Phosphatidylinositol 4-kinase (PI4K) or Phosphatidylinositol 5-kinase (PI5K). PIP_3 synthesis requires the inhibition of Phosphatidylinositol 3-kinase (PI3K; Figure 1.11). Inhibition of PI synthesis is typically achieved by pharmacological agents such as wortmannin (Suh and Hille, 2005). Wortmannin, a fungal steroid metabolite, is one of the most widely used modulators of cellular PI synthesis. This is due to many favourable properties such as cell permeability, commercially availability, and the fact it is largely ineffective against other signalling molecules (Wymann et al., 1996). Another useful property is its difference in affinity for PI3Ks vs PI4Ks. Wortmannin is a potent inhibitor of PI3Ks at low nanomolar concentrations (Yano et al., 1993), whilst inhibiting PI4K with an affinity of an order of magnitude lower (Figure 4.1) (Fruman et al., 1998). This difference provides a diagnostic method of examining the relative contributions of PIP_2 and PIP_3 to biological processes. LY294002 is a synthetic inhibitor of PI3Ks, which like wortmannin binds to the ATP binding site of PI3K. It displays low micromolar affinity against PI3K enzymes in vitro (Walker et al., 2000) but unlike wortmannin however, it binds reversibly to the enzyme.

4.1.3 Genetic approaches to PIP_2 modulation

One area of investigation which will be briefly mentioned here is the recent development of a number of genetic based techniques for the modulation of PIs. Conventional cell biology approaches involving overexpression of important enzymes or knockdown and knockout using siRNA and gene deletion have long been seen as unsatisfactory due to the fact these methods alter PI levels over a period of hours or even days. More recent techniques have focused on rapid and inducible methods of PI perturbation. These methods, which act over a period of seconds rather than hours, typically act by recruiting transfected enzymes, such as lipid 5-phosphatase (which converts PIP_2 to PIP) to the cell membrane. Current methods involve a rapamycin-induced dimerisation, or light-induced optogenetic dimerisation which brings the phosphatase into proximity with the PIP_2 rich plasma membrane (Suh and Hille, 2008). Of most use to electrophysiological investigation has been the development of a voltage-sensing lipid phosphatase (VSP). The major advantage is that the enzyme itself can be activated by depolarizing voltage pulses in whole-cell patch clamp recordings, allowing both the PIP_2 modulation and current measurements to be carried out almost simultaneously (Suh and Hille, 2005). Although, these approaches provide a sensitive method of examining the effects of phosphoinositide modulation in cellular systems, the necessity for genetic manipulation makes their application to primary cell culture a considerable challenge.

4.1.4 PIP_2 sequestration

Certain strategies employed to deplete membrane bound PIP_2 levels involve some form of phosphoinositide capture or sequestration. The popularity of these techniques is explained by their obvious practicality. Patches of channel rich membrane can be excised with a patch pipette and PIP_2 sequestering agent (often polycations such as Mg^{2+}, neomycin, polylysine or spermine) directly applied to the exposed cytoplasmic surface (Suh and Hille, 2007). Specific PIP_2 antibodies can also be employed for this purpose (Suh and Hille, 2008). In fact, PIP_2 sequestration may not even be necessary; post-excision, PIP_2 synthesis may slow or even stop and PIP_2 becomes depleted over a

short period. Channel function may decrease in tandem in a process called “channel rundown”. Conversely PIP_2 or other lipids can also be applied to the surface to observe their effects on ion channel activity (Suh and Hille, 2005).

Recently, innovative new strategies for PIP_2 sequestration and capture have been pursued through the design of targeted peptides (Robbins et al., 2006). These molecules consist of a peptide with high affinity for PIP_2 and a long chain fatty acid group (palmitoylation) to target it to the plasma membrane (Figure 4.2). This PIP_2-binding palmitoylated peptide (PIP_2-PP) consists of a 10 amino acid polypeptide, palmitoylated on the terminal histidine (Pal-HRQKHFEKRR). This 10 amino acid chain is identical to the putative PIP_2 binding sequence of the Kv7.2-7.5 (Figure 4.2) (Zhang et al., 2003). The PIP_2-PP has some significant practical advantages over tradition polycationic PIP_2 sequestering agent. Most notable, PIP_2-PP can be applied externally during whole cell patch clamp recordings and sequester PIP_2 at the inner leaflet of the membrane.

4.2 Results

4.2.1 Inhibition of PIP_2 synthesis increases excitability in SGNs

To examine the effects of PIP_2 and PIP_3 modulation on the electrophysiology of SGN, the synthesis of these PIs were inhibited by pharmacological means. Accordingly, basal turn cultures were pre-treated for one hour with wortmannin at either a low dose (100 nM), targeting PI3Ks only (Yano et al., 1993), and thus reducing the pools of PIP_3 available to the cell, or a high dose (10 µM) to target both PI3Ks and PI4Ks, therefore also depleting PIP_2 levels in the membrane (Fruman et al., 1998). A simplified form of this pathway and its inhibition is shown in Figure 4.1B. After incubation with drug concentration or vehicle alone (0.1% DMSO), cells were transferred to the recording chamber and recordings were made using the current clamp mode of the amplifier to determine SGN responses to depolarising current injections. Cells were pooled by number of APs fired in response to a 200 ms depolarizing current injection of 100 pA: rapidly-adapting, 0-1 APs; slowly-adapting, 2-9 APs; non-adapting, ≥10 APs (Figure 4.1C).

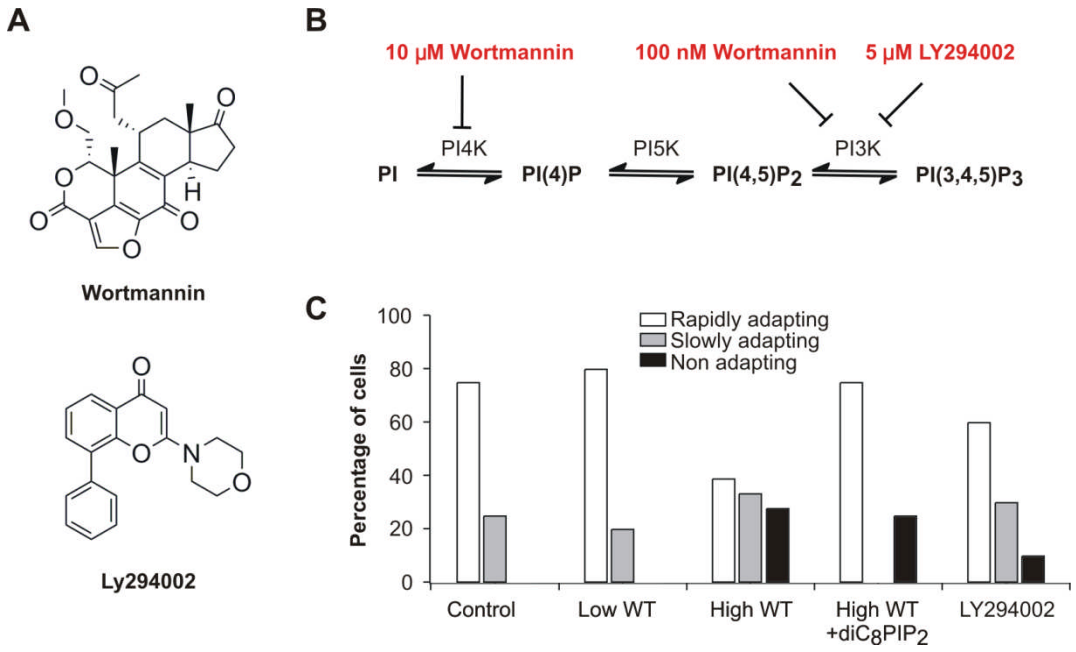

Figure 4.1 Excitability in cultured SGNs is dependent on availability of PIP_2. A Chemical structures of the phosphoinositide inhibitors, wortmannin and LY294002. **B** Simplified schematic of phosphoinositide metabolism showing the site of action of the various inhibitors. **C** The distribution of adaptation phenotypes within the population of cultured SGN exposed to varying conditions of phosphoinositide inhibition. SGN pre-incubated for 1 hour in 0.1% DMSO (Control, n = 12) display a predominance of rapidly-adapting phenotypes, as do SGN pre-incubated in 100 nM Wortmannin ('Low WT', n = 10). SGN pre-incubated in 10 µM wortmannin, ('High WT', n = 18) display an increase in excitable firing behaviour, with a reduced proportion of rapidly-adapting cells. When diC_8PIP_2 (100 µM) is included intracellularly during recordings from SGN pre-incubated in 10 µM Wortmannin ('High WT+diC_8PIP_2', n = 8), the proportion of rapidly-adapting cells returns to near control levels. SGN preincubated with the PI3K inhibitor LY294002 ('LY294002', n = 10) also resembles the control population.

Under control conditions, where cells were pre-incubated with vehicle alone, 75% (9/12) matched a rapidly-adapting phenotype, with the remaining 25% (3/12) exhibiting slow adaptation. Pre-incubation of SGN cultures with 100 nM wortmannin had little effect on the rapidly-adapting phenotype. However, pre-incubation with 10 µM wortmannin resulted in a substantially reduced proportion of rapidly-adapting neurons (39%; 7/18), and an increased proportion of non-adapting neurons (33%; 6/18), with the remaining neurons slowly-adapting (28%; 5/18). Broadly, pre-incubation with 10 µM wortmannin resulted in a significantly more excitable population of SGN neurons than

under control conditions. Accordingly, incubation with 10 µM wortmannin produced a small increase in the proportion of spontaneously active cells, i.e. cells which fired APs at rest in the absence of any depolarising injection, though this was not significant (28%; 5/18 in 10 µM wortmannin-treated cells compared to 17%; 2/12 in control). In a subset of cells pre-incubated with 10 µM wortmannin, a non-hydrolysable PIP_2 analogue diC_8-PIP_2 (100 µM) was added to the intracellular pipette solution. Under these conditions the proportion of rapidly-adapting cells was identical to the control (75%; 6/8).

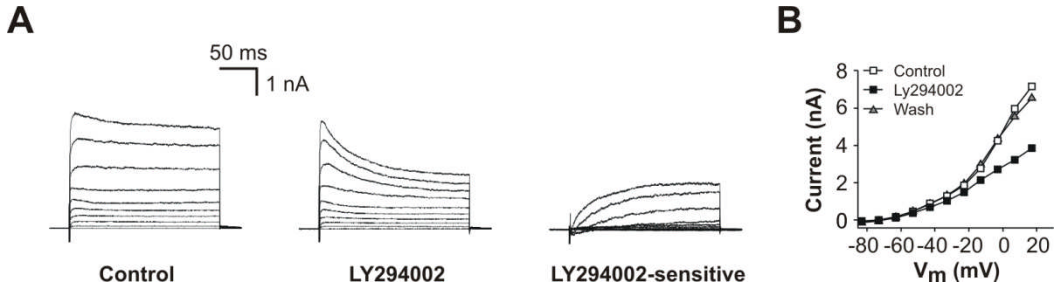

Figure 4.2 Transient application of LY294002 blocks Kv channels in SGNs. A Current traces evoked by depolarising voltage step protocol in the presence and absence of the PI3K inhibitor LY294002. Cell was held at -73 mV and stepped to +17 mV in 10 mV increments. Perfusion of 5 µM LY294002 across the cell caused significant inhibition of steady state IK. Peak I_k however showed little to no reduction. Upon washing the I_k quickly recovered. **B** I-V trace showing the steady state I_k in the presence and absence of the LY294002 as well as 3 mins after washing off.

In separate experiments, cultures were pre-treated for one hour with the reversible PI3K inhibitor LY294002 (5 µM). Pre-incubation with LY294002 resulted in a modest decline in the occurrence of rapid adaptation (60%; 6/10). Together these results suggested PIP_2 availability could be an important determinant in the rapid adaptation of cells but conversely that PIP_3 availability did not seem to influence SGN excitability. Interestingly, transient bath application of LY294002 resulted in a marked effect on the outward current which was not observed upon transient application of the other PI3K inhibitor, wortmannin. Figure 4.2A shows the effects of 5 µM LY294002 perfused over

a SGN for 3 mins. LY294002 increased the rate of inactivation of outward K^+ currents, an effect that was rapid and reversible, reaching maximum effect after 80 s and subsequently washing out in a similar period, to recover the initial current inactivation kinetics (Figure 4.2). It seems therefore, that the LY294002 pre-incubation experiment should be interpreted with caution due potential non-PI3K related effects.

4.2.2 Sequestration of PIP_2 increases excitability in SGN

To further explore the role of PIP_2 in the regulation of SGN excitability, other methods of altering PIP_2 availability were explored. To this end, a novel membrane-targeting palmitoylated peptide with high affinity for cellular PIP_2 was employed (Robbins et al., 2006). In current clamp mode, bath application of 3 µM PIP_2-PP enhanced the excitability of rapidly adapting SGNs (P12-15; Figure 4.3C, D). The extent of this enhancement was variable, however, with most SGNs becoming more slowly adapting, firing 2-5 APs instead of 1 (7/10), whilst others became non-adapting, continuing to fire as long as the current stimulus was applied (Figure 4.3C). In addition to increasing the number of APs, PIP_2-PP also reduced the amount of current required to fire an AP in 2/9 cases, and induced spontaneous firing in the absence of any injected current in those two cells. Furthermore, PIP_2-PP significantly increased the steady-state voltage in response to depolarising current injection steps ($n = 4$, $p<0.001$, two-way ANOVA; Figure 4.3E), indicating an increased membrane resistance.

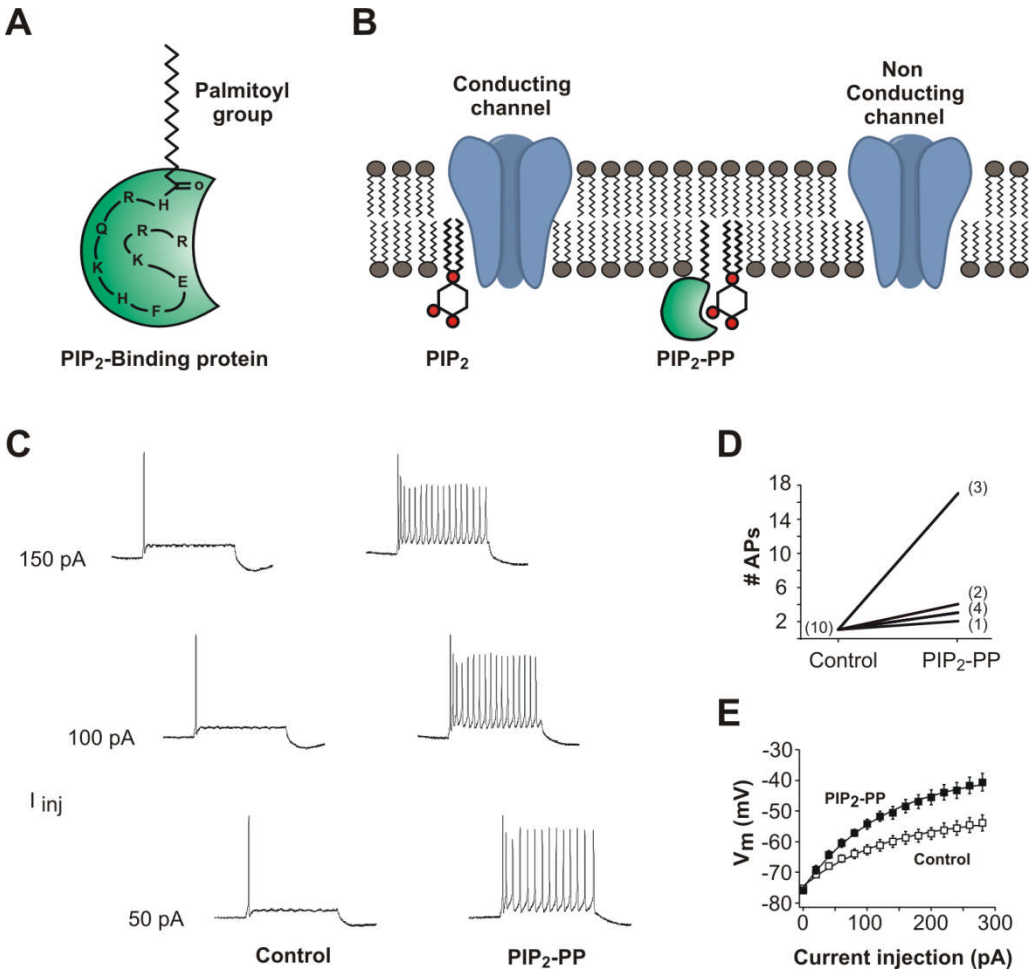

Figure 4.3 A PIP_2 sequestering peptide enhances the excitability of post-hearing onset SGNs. A Cartoon of the structure of the PIP_2-binding palmitoylated peptide (PIP_2-PP). **B** Putative mechanism of action of the PIP_2-PP. The PIP_2-PP is proposed to act by sequestering membrane bound PIP_2 and making it unavailable for interaction with membranous ion channels. **C** Voltage response from a P13 rapidly adapting SGN to depolarizing current injections, before (Control, left) and after the bath application of 3 μM PIP_2-PP (right). 200 ms current injections were applied in +50 pA increments from a holding potential of -73 mV. Typically, PIP_2-PP slowed the rate of adaptation or removed it entirely, and reduced the current required to elicit AP firing. **D** Summary of the effect of 3 μM PIP_2-PP on the number of APs (#APs) elicited in response to a +100 pA current step (number of cells is shown in parentheses). **E** Comparison of the mean voltage-current relationship before (Control) and after the bath application of 3 μM PIP_2-PP (n = 4). Steady-state voltage was measured 10 ms from the end of 600 ms current injections applied in +20 pA increments from a holding potential of -73 mV.

The increased membrane resistance following application of the PIP_2-PP possibly indicated a decreased activity of Kv channels, and so separate voltage clamp experiments were performed to further elucidate the effects of PIP_2 sequestration on SGNs. Bath application of 3 µM PIP_2-PP resulted in a prominent inhibition of outward K^+ currents. Furthermore, PIP_2-PP was found to have differential effects between HVA and LVA K^+ currents (Figure 4.4A, B). PIP_2-PP markedly reduced the outward current amplitude measured at -53 mV (74.2 ± 2.9%), but had less effect on currents at -13 mV (34.5 ± 4.6%; $P<0.001$, n = 15). Subtraction of the PIP_2-PP exposed trace from the control trace gave the PIP_2-PP-sensitive component (Figure 4.4A, lower trace), a LVA current with a $V_{1/2}$ of -51.1 ± 1.1 mV and slope of 6.7 ± 0.5 (Figure 4.4C). The effects of the peptide were rapid, with maximal inhibition obtained within ~2 mins of the onset of the application (Figure 4.4D, control). The effects of the peptide could not be washed out, either using extracellular solution or extracellular solution supplemented with FBS.

To further examine if PIP_2 depletion was the mechanism behind LVA inhibition, diC_8PIP_2 was included in the intracellular recording solution. Under control conditions LVA current inhibition by PIP_2-PP reached a maximum after about 2 mins of its application (Figure 4.4D, control), and this rate of current inhibition could be fitted using a standard single exponential decay function ($\tau_{control}$ = 28.4 ± 5.3 s). Inclusion of diC_8PIP_2 in the recording pipette was found to significantly slow the rate of LVA current inhibition by PIP_2-PP ($\tau_{diC8PIP2}$ = 115.5 ± 16.6 s, p = 0.002, paired Student's t-test, Figure 4.4D). Similarly, the mean% currents remaining after 2 mins of drug application was significantly higher in the presence of the diC_8PIP_2 intracellular solution (23.4 ± 3.9%, n = 5) than with the control solution (59.5 ± 5.4%, n = 5, p = 0.002, unpaired Student's t-test). These findings further support the hypothesis that the channels underlying the LVA current in SGNs are regulated via binding of PIP_2.

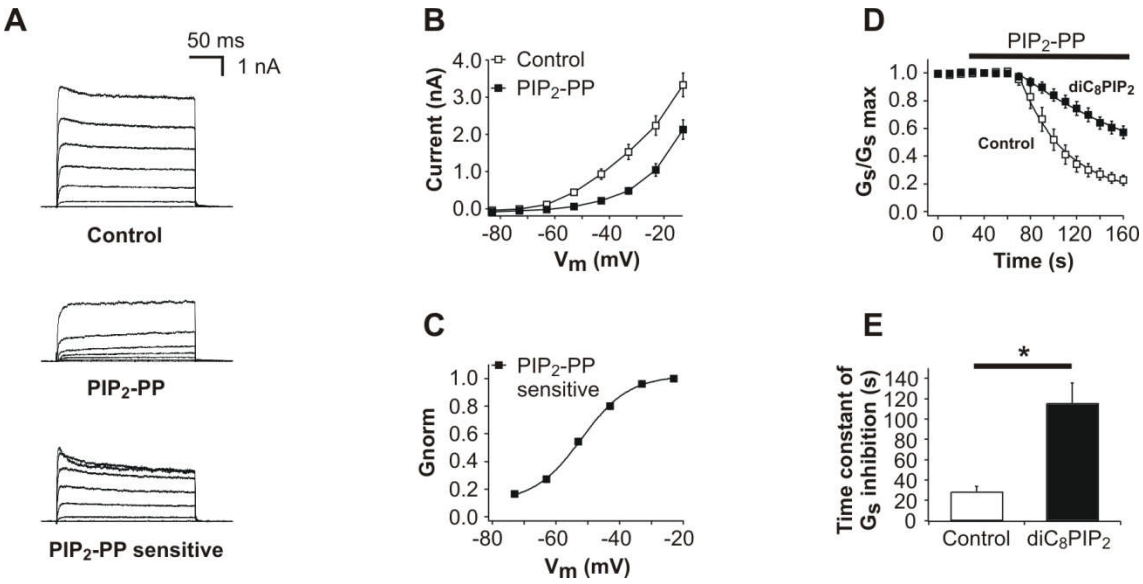

Figure 4.4 PIP_2 sequestration inhibits a Kv1-like, LVA current in SGNs. A Representative current responses to 200 ms voltage steps in 10 mV increments from a holding potential of -73 mV. Traces shown are before (Control, *upper panel*) and after (*middle panel*) bath application of 3 µM PIP_2-PP. PIP_2-PP-sensitive currents are shown in the lower panel and were obtained by subtraction of PIP_2-PP from control currents. **B** Mean steady-state current-voltage relationships before (Control, open squares), and after (PIP_2-PP, filled squared) PIP_2-PP application (3 µM; n = 15). Steady-state currents were measured between 15 ms and 5 ms from the end of the voltage steps described. **C** Normalised G-V plot of the PIP_2-PP-sensitive component. **D** Effects of PIP_2-PP application on normalised slope conductance (G_s), calculated from a voltage ramp protocol applied every 10 s (G_s; measured between -63 mV to -53 mV). G_s decreases during the bath application of PIP_2-PP (Control; 1 µM; n = 5) reaching near maximal inhibition ~2 mins post application. Inclusion of diC_8PIP_2 (200 µM) in the intracellular solution significantly slows the effect of PIP_2-PP (diC_8PIP_2; n = 7). **E** Comparison of the rates of G_s inhibition in the absence (Control; n = 5) and presence of diC_8PIP_2 (200 µM) in the intracellular solution (diC_8PIP_2; n = 7). The time constant of G_s inhibition was calculated by fitting mono-exponential functions to the data in *D*. *P<0.05.

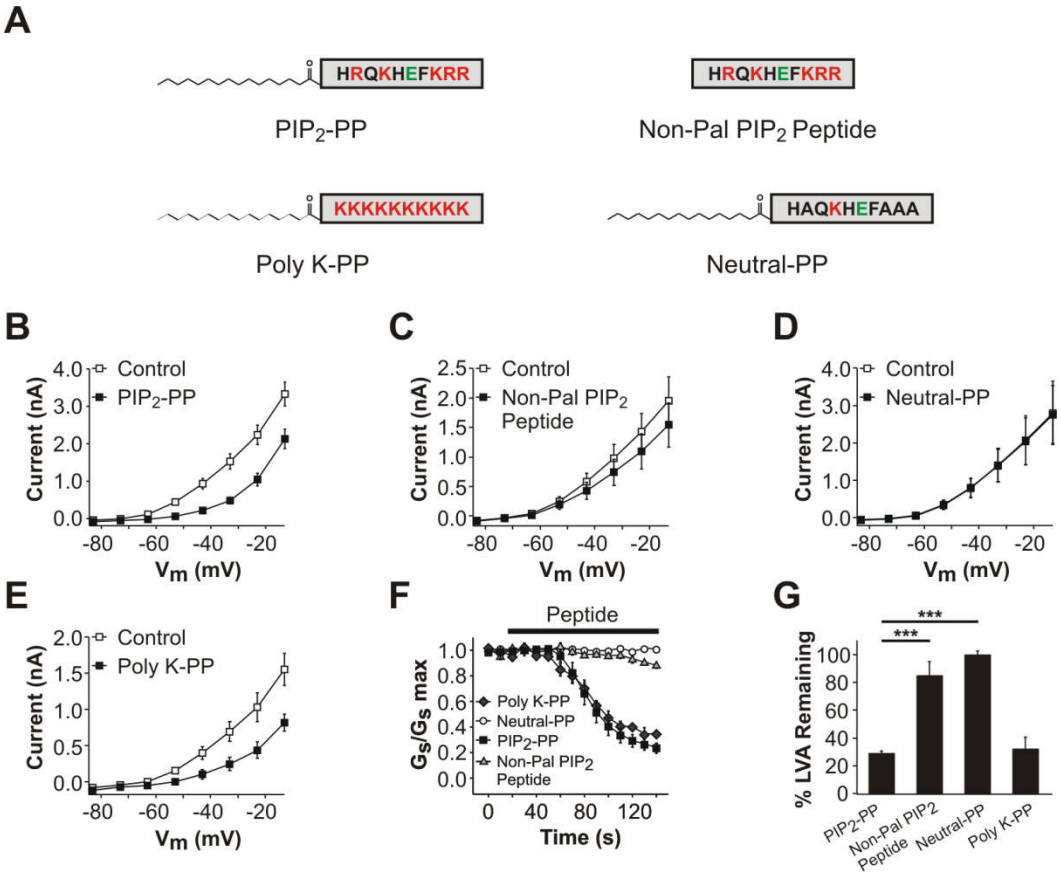

Figure 4.5 The effect of PIP_2-PP analogues on SGN LVA currents. A Design of the various PIP_2-PP analogues. These analogues were designed to examine the important structural features which gave rise to ability to sequester PIP_2. The Grey filled box indicates the peptide structure with positively charged residues in red, negatively charge residues in green and neutral residues in black. **B** (Replicated from Figure 4.4B) Mean steady-state current-voltage relationships before (Control, open squares), and after (PIP_2-PP, filled squared) PIP_2-PP application (3 μM; n = 15). **C** Mean current-voltage relationships before and after application of an unpalmitoylated analogue of PIP_2-PP (Non-Pal PIP_2 Peptide, 3 μM; n = 7). **D** Mean current-voltage relationships before and after application of a neutrally charged analogue of PIP_2-PP (Neutral-PP, 3 μM; n = 5). **E** Mean current-voltage relationships before and after application of a Poly K-palpeptide, a poly-cationic analog of PIP_2-PP. (Poly K-PP, 3 μM; n = 5). **F** Timecourse of the effect of PIP_2-PP application and its various analogues as measured by normalised slope conductance (G_s). **G** The effects of PIP_2-PP and its analogues on SGN LVA steady-state K^+ currents (measured at -53 mv). *P<0.05 .

In order to better characterise the mechanism of action of PIP_2-PP and identify the important structural features which give rise to its pharmacological properties, a set of

PIP_2-PP analogues was designed and tested. These peptides explored the importance of palmitoylation as well as both the presence and position of cationic peptide residues within palmitoylated peptide (Figure 4.5A). The importance of the lipid modification was tested with a non-palmitoylated analogue of PIP_2-PP ("Non-Pal PIP_2 Peptide") which was identical in sequence to the PIP_2-PP but was missing the membrane-targeting acyl group. Robbins and co-workers originally characterised this Non-Pal PIP_2 Peptide as an inactive analogue of PIP_2-PP (Robbins et al., 2006). Although a small current reduction was observed in 2/7 cells, there was no significant effect of the Non-Pal PIP_2 Peptide on LVA currents (Figure 4.5B, C, G). The average current remaining after 2 mins of Non-Pal PIP_2 Peptide application was 84.6 ± 10.3%, significantly higher than that of the PIP_2-PP (pre- vs post-application: P = 0.187, n = 7, paired Student's t-test; PIP_2-PP vs Non-Pal PIP_2 Peptide application, P<0.001, n = 15 vs n = 7, unpaired Student's t-test, Figure 4.5C,G).

The second modification of the PIP_2-PP examined was the importance of cationic residues using a neutrally charged peptide ("Neutral-PP") where the four positively charged residues were substituted for uncharged alanine residues in the manner R2AK8AR9AR10A, to yield an overall neutrally charged, albeit zwitterionic, peptide (Figure 4.5A). In this case the peptide contained the membrane-targeting palmitoyl group and only the peptide sequence differed from PIP_2-PP. This peptide was not described in the initial *Robbins et al*., study but since then other groups have reported the Neutral-PP to be an inactive analogue and successfully employed it as a negative control for the PIP_2-PP (Buchmayer et al., 2013, Hamilton et al., 2014). The Neutral-PP showed no activity against LVA current in SGNs. The average current remaining after Neutral-PP application was 99.6 ± 2.8% (pre- vs post-application: P = 0.5, n = 5, paired Student's t-test; PIP_2-PP vs Neutral-PP application, P<0.001, n = 15/5, unpaired Student's t-test, Figure 4.5D, G).

In order to examine if this cationic charge was the determining factor for PIP_2 binding or whether the specific peptide sequence was also important, a poly cationic analogue of PIP_2-PP ("Poly K-PP") was tested. In Poly K-PP all the residues in the peptide sequence were replaced with positively charged lysine residues (Figure 4.5A). The Poly K-PP mirrored the effect of the original PIP_2-PP, inhibiting the LVA current in all of the cells tested. The average current remaining after Poly K-PP application was 32.1 ± 8.3%

(pre- vs post-application: P = 0.004, n = 5, paired Student's t-test; PIP_2-PP vs Poly K-PP: Peptide application, P = 0.36, n = 15/5, unpaired Student's t-test, Figure 4.5E, G). It also exhibited a very similar time course of action; a maximal steady-state inhibition was reached after about 2 mins of perfusion into the bath (Figure 4.5F). This is consistent with the findings of *Robbins et al.*, that observed that Poly K-PP could induce similar levels of Kv7 inhibition as PIP_2-PP. Additionally, this suggests that it is not the specific peptide sequence that is required for activity but rather the strong cationic character which helps it interact with the PIP_2 (and most likely other) anionic phospholipids. Finally, we examined the localisation of a Fluorescein-tagged analogue of Pal-PIP_2 (Fluoro PIP_2-PP) under confocal microscopy. 2 mins before examination, 10 µM Fluoro PIP_2-PP was added to cultured HEK293 cells. Fluoro PIP_2-PP was observed to localise to the plasma membranes of the cells (Figure 4.6A-C). Very little fluorescence was observed within the cell cytoplasm suggesting the peptide exerts its effect by interaction with plasma membrane bound lipids rather than other intracellular candidates.

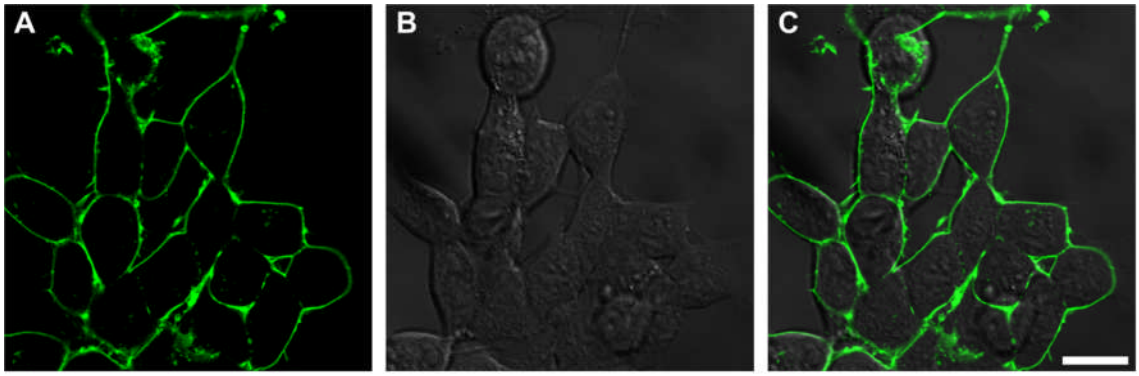

Figure 4.6 Fluorescein-tagged PIP_2 palpeptide (Fluoro PIP_2-PP) localises to the plasma membrane of HEK293 cells. A Confocal image of cultured HEK293 cells with 10 µM Fluoro PIP_2-PP in the bathing solution. Fluoro PIP_2-PP localises strongly to the plasma membrane. Excitation wavelength, 488 nm; emission, 543 nm. **B** DIC image of the same cells. **C** Combined confocal and DIC image. Scale bar: 20 µm.

In summary, these control experiments demonstrated that PIP_2-PP targets the neuronal plasma membranes and highlighted the importance of palmitoylation and cationic residues to the efficacy of PIP_2-PP in inhibiting SGN LVA currents. Furthermore, the similarity in the structure-activity relationship between this work and the previous characterisations provide evidence that the PIP_2-PP is acting via PIP_2 depletion and not through an alternate mechanism e.g. direct interaction with the Kv channels.

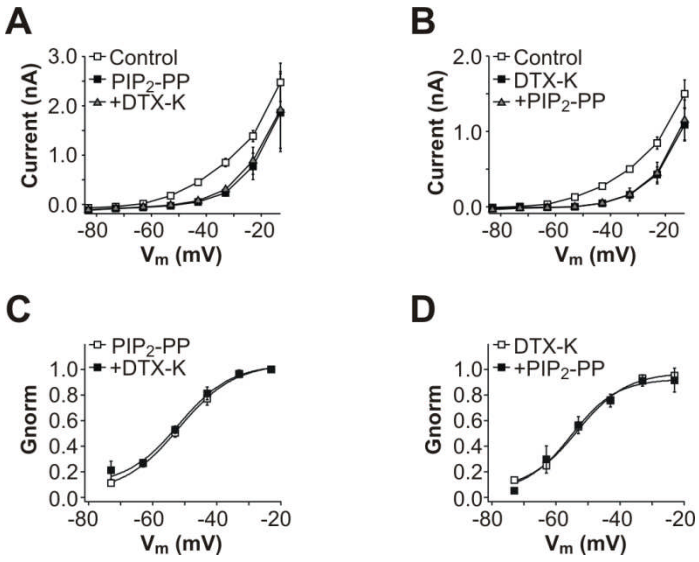

Figure 4.7 PIP_2-PP and DTX-K block the same LVA K^+ current componant in SGNs. **A** Mean current-voltage relationships of SGNs before (Control, open squares), and after sequential application of PIP_2-PP (PIP_2-PP; 3 μM, black squares), and subsequent application of PIP_2-PP with DTX-K (+DTX-K; 100 nM; n = 3, grey triangles). Application of PIP_2-PP blocks an LVA current as discussed but there is no additive effect observed upon the addition of DTX-K to the bath. **B** There was no additive effect when the drugs were applied in reverse order (n = 3). **C** Normalised G-V plots showing a comparison of the PIP_2-PP-sensitive component (open squares) and PIP_2-PP+DTX-K-sensitive component (black squares) obtained from the SGN currents in A. **D** Similar comparison of the currents obtained from B.

To confirm whether PIP_2-PP was inhibiting Kv1-mediated currents, co-application experiments using both channel toxins and peptide were performed. Following initial application of 3 μM PIP_2-PP, addition of 100 nM extracellular DTX-K failed to further reduce the LVA current amplitude (Figure 4.7A). A reversal of the order of application

of the PIP_2-PP and DTX-K similarly did not show any enhancement of inhibition after application of the latter agent (Figure 4.7B). Overlaying the conductance-voltage relationship of the two groups in both cases show comparable plots (Figure 4.7C, D). This suggests that the PIP_2-mediated LVA currents in SGNs are mediated by Kv1.1-containing channels.

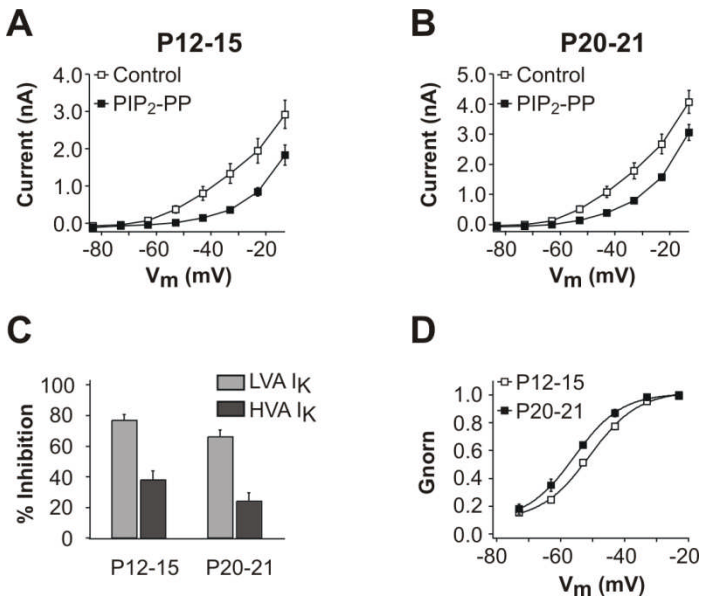

Figure 4.8 Inhibition of low-threshold voltage-activated current in SGNs is consistent one week after the onset of hearing. A Mean steady-state current-voltage relationships, from P12-P15 mice, before (Control, open squares), and after (PIP_2-PP, filled squared) PIP_2-PP application (3 μM; n = 11). Steady-state currents were measured at the end of the voltage steps described for *Figure 4.4A*. **B** Mean steady-state current-voltage relationships, from P20-P21 mice. (n = 4). **C** The % current inhibition after application of 3 μM PIP_2-PP was not significantly different between the two ages for either LVA currents (measured at -53 mV) or HVA currents (measured at +17 mV). **D** Normalised G-V plots showing the PIP_2-PP-sensitive components of P12-P15 and P20-P21 mouse SGN currents.

The inhibitory effect of PIP_2-PP was analysed in mice of different developmental ages. Of the 15 SGN exposed to PIP_2-PP in this study, they could be divided into roughly 2 groups by their age - animals at the onset of hearing (P12-15) and animals one week after the onset of hearing (P20-21). PIP_2-PP showed little difference in its inhibitory

effect on SGN from P12-15 and P20-21 mice (Figure 4.8A, B). In SGN from P12-15 mice the current remaining at -53 mV after PIP_2-PP application (77.2 ± 3.3%, n = 11) was not significantly different to that in SGN from P20-21 mice (66.2 ± 4.2%, n = 4, P = 0.094, unpaired Student's t-test). Analysis of the voltage dependence of the PIP_2-PP-sensitive components showed a small but significant difference in the $V_{1/2}$ (P12-15: -49.4 ± 0.9 mV, n = 11; P20-21: -55.7 ± 1.6 mV; P = 0.004, unpaired Student's t-test; Table 4.1). This suggests the PIP_2-PP-sensitive LVA current established by the onset of hearing may continue to mature at least one week after hearing onset.

Table 4.1 Boltzmann parameters for PIP_2-PP sensitive SGN conductances

Age	$V_{½}$ (mV)	*k* (mV)	n
P12-15	-49.4 ± 0.9	6.35 ± 0.44	11
P20-21	-55.6 ± 1.6	7.71 ± 1.4	4

4.2.3 Inhibition of Kv7 mediated current does not increase excitability

Kv7 subunits are encoded by the KCNQ family of genes and form low-threshold voltage-gated K^+ channels when expressed in cell membranes. The Kv7 family are composed of five members: Kv7.1-Kv7.5, of which four, Kv7.2–Kv7.5, have been identifies in the neurons (Brown and Passmore, 2009, Robbins, 2001). Kv7 channels have relatively slow activation times, but do not inactivate and thus typically generate a steady outward current. They activate at subthreshold potentials and stabilise the membrane potential in the presence of depolarizing stimuli (Brown and Passmore, 2009). Kv7-mediated currents are highly PIP_2 dependent and have been shown to be important regulators of excitability in neuronal models (Brown et al., 2007). The contribution of Kv7-mediated currents to SGN excitability was therefore investigated. To this end, we examined the effedcts the Kv7 blocker, XE991, had on SGN membrane physiology.

Under current clamp mode, bath application of 3 µM XE991 failed to increase AP firing in five rapidly or slowly adapting SGNs (P12-15) (Figure 4.9A, B). Voltage clamp recordings were also obtained from the same cells in order to determine if XE991 had any effect on the native currents. Cells were depolarised from a holding potential of -73 mV in 10 mV steps for 1 second before returning to the holding potential. The extended step length of 1 s was used to examine the effect of XE991 on the slower activating Kv7 channels (Figure 4.9C, D).

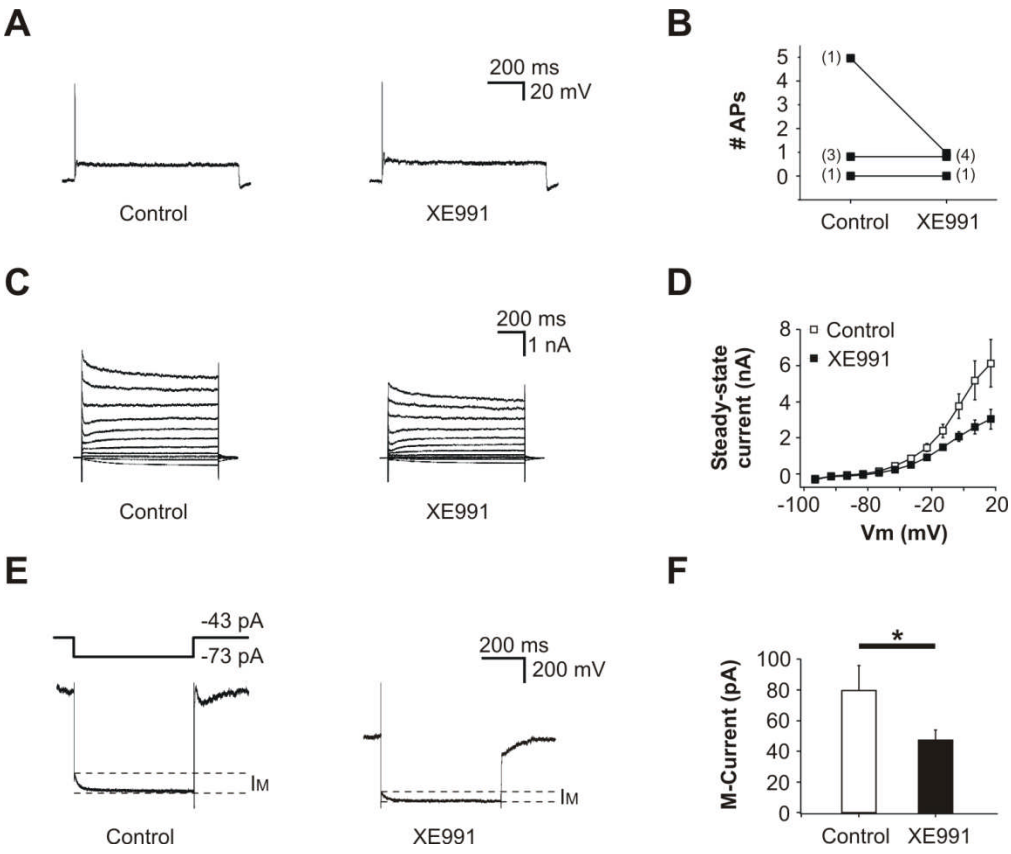

Figure 4.9 Effects of the Kv7 blocker, XE991, on SGN in vitro. A Representative voltage response from a rapidly adapting SGN to 100 pA depolarizing current injections, before (Control, left) and after the bath application of 3 µM XE991 (XE991; right). **B** In 5/5 cells, bath application of 3 µM XE991 failed to increase or resulted in a decrease in the number of APs fired. **C** Representative evoked current responses before (Control, left) and after the bath application of 3 µM XE991 (XE991; right). Cells were held at a holding potential of -73 mV and stepped from -93 mV to +17 mV in 10 mV increments. Voltage steps were held for 1 s before returning to the holding potential. **D** Mean steady-state current-voltage relationships, from P12-

P15 mice, before (Control, open squares), and after (XE991, filled squared) XE991 application (1 mM; n = 5). Steady-state currents were measured between 900 ms and 1 s at the end of the voltage steps described in C. **E** Current responses from mouse SGN using an "M-current protocol" (Hernandez et al., 2008) before (Control, left) and after the bath application of 3 μM XE991 (XE991; right). SGN, held at a potential of -73 mV and were depolarised to -43 mV for 1 s in order to activate neuronal Kv7 currents before being returned to a holding potential of -73 mV for 500 ms. M-current was calculated by measuring the peak amplitude of the tail currents and subtracting it from the steady state currents at -73 mV (dotted lines). **F** Mean M-current amplitudes as calculated from E. Bath application of 3 μM XE991 reduced neuronal M-currents in 5/5 cells. *p<0.05.

3 μM XE991 blocked an outward I_k in a manner that was not reversible after 5 mins wash. The effect of 3 μM XE991 on cellular M-currents was also examined. Recordings were made using an "M-current protocol" (Hernandez et al., 2008) and the M-current amplitude was calculated as described in Figure 4.9E. In 5/5 cells M-current amplitude was reduced, with a mean current reduction of 40.7% (79.98 ± 16.06 pA; control vs 47.4 ± 6.5 pA; p = 0.041, paired Student's t-test, Figure 4.9F) In light of these results, despite substantial XE991-sensitive currents in SGNs, they do not seem likely to play a major role in determining the excitability of SGN *in vitro*.

4.2.4 PLC activation does not inhibit SGN LVA currents

To test whether available PIP_2 in SGN could be reduced via native physiological mechanisms, we employed activators of normal metabolic pathways which may deplete membrane bound PIP_2. The initial approach was to target activation of the Gq/11 G-protein-coupled receptor (GPCRs) pathway, which subsequently activates PLCβ and results in PIP_2 hydrolysis. M1, M3 and M5 muscarinic receptors are metabotropic GPCRs preferentially coupled to Gq/11 and activate PLCβ (Ishii and Kurachi, 2006), and so we examined the effects of Oxotremorine-M (Oxo-M), a broad muscarinic agonist (Birdsall et al., 1978) on outward evoked I_k in SGNs. Under voltage clamp mode, recordings were made in the absence and presence of 1-10 μM bath applied Oxo-M. Oxo-M showed little effect upon outward evoked I_k between -73mV to -3mV

(Figure 4.10A). LVA currents, measured at -53 mV, showed little inhibition at either 1 or 10 μM Oxo-M (1 μM, 93.5 ± 2.9% current remaining, n = 5, p = 0.08; 10 μM, 91.8 ± 2.6% current remaining, n = 5, p = 0.054, paired Student's t-test, Figure 4.10B).

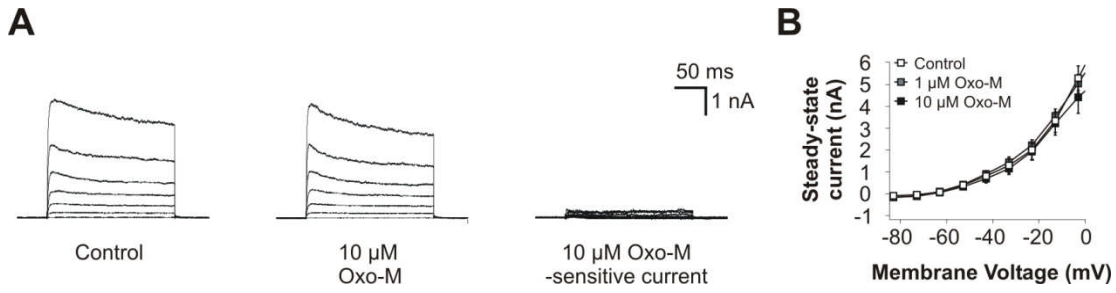

Figure 4.10 Effects of muscarinic receptor agonism on the SGN LVA current. A Representative evoked outward current responses to 200 ms voltage steps in 10 mV increments from a holding potential of -73 mV. Traces shown are before (Control, Left) and after (middle panel) bath application of 10 μM Oxo-M. Oxo-M-sensitive currents are shown in the right panel and were obtained by subtraction of 10 μM Oxo-M treated currents from control currents. **B** Mean steady-state current-voltage relationships before (Control, open squares), and after 1 μM (grey squares) and 10 μM Oxo-M (Black squares, n = 5).

The potential contribution of PLC was also examined using the PLC activator m-3M3FBS. At doses of 10-50 μM, m-3M3FBS has been shown to increase the hydrolytic activity of PLC against membrane bound PIs (Bae et al., 2003). Recordings from SGNs were made in voltage-clamp mode, and 10 μM m-3M3FBS was applied for a period of at least 10 mins to observe the effects. Application of 10 μM m-3M3FBS showed variable effects between different SGN currents. There was an inhibitory effect upon hyperpolarising I_H currents (not shown) as well as on the outward I_K, an effect most obvious at higher voltages (Figure 4.11A). Interestingly, in different cells the LVA K^+ currents displayed variously, both inhibition and activation in response to 10 μM m-3M3FBS. This variable drug response is demonstrated in Figure 4.11C by the comparison of two individual SGNs isolated from a P21 mouse. The current responses were obtained from single voltage step applied from -73 mV to -53 mV, showing both an inhibitory (Figure 4.11C, left panel) or stimulatory response (Figure 4.11C, right

panel). In total, 6/8 neurons showed a decrease in current at -53 mV, whilst 2/8 neurons displayed increased current at this test voltage. The mean current remaining after 10 mins of 10 µM m-3M3FBS application was 88.2 ± 8.2% (P = 0.93, paired Student's t-test, n = 8, Figure 4.11A, B).

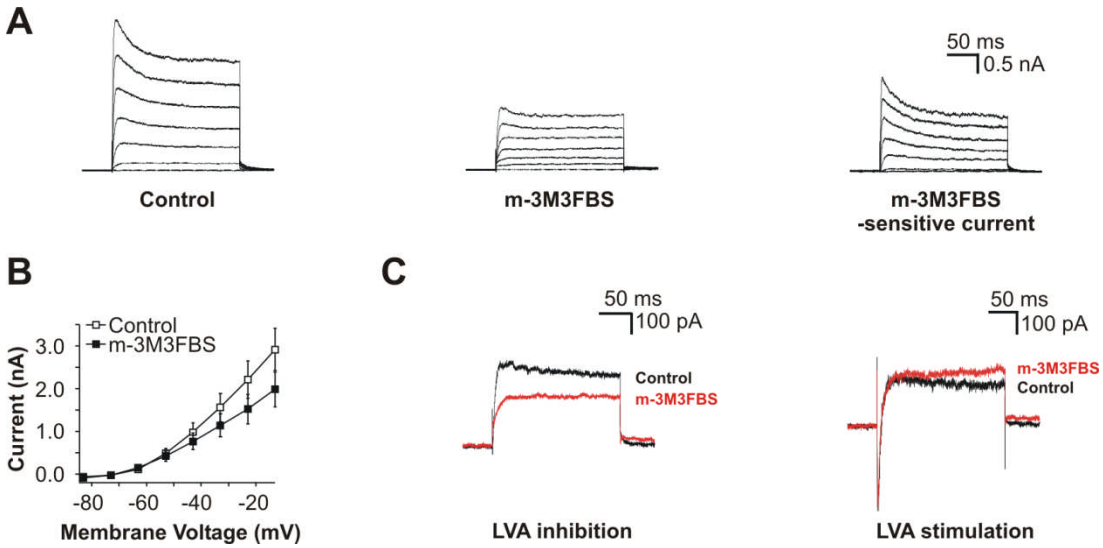

Figure 4.11 Effects of the PLC activator, m-3M3FBS, on the SGN LVA K+ current. A Representative evoked outward current responses to 200 ms voltage steps in 10 mV increments from a holding potential of -73 mV. Traces shown are before (Control, Left) and after (middle panel) bath application of 10 µM m-3M3FBS. m-3M3FBS-sensitive currents are shown in the right panel and were obtained by subtraction of m-3M3FBS from control currents. **B** Mean steady-state current-voltage relationships before (Control, open squares), and after 10 µM m-3M3FBS application (Black squares, n = 8). **C** Current responces to a single voltage step, from -73 mV to -53 mV, showing SGN currents before (black trace), and after 10 mins of 10 µM m-3M3FBS application (red trace). m-3M3FBS application shows a variable effect on SGN LVA currents. Inwards sodium transients can be observed in the "LVA stimulation" trace.

4.2.5 PIP_2 sequestration inhibits Kv1.1/Kv1.2 heteromeric channel currents

This work along with other studies has implicated both Kv1.1 and Kv1.2 as contributing to the LVA current in SGN (Smith et al., 2015, Mo et al., 2002). Previous

electrophysiological examination the Kv1 family of channels (Kv1.1/β1.1, Kv1.3, Kv1.4 and Kv1.5) expressed homomerically in heterologous systems has revealed an apparent lack of sensitivity to PIP_2 (Kruse et al., 2012). Kv1.2 homomeric channels however, do display sensitivity to PIP_2, with an approximate 20-30% reduction in current amplitude upon PIP_2 depletion, as well as an apparent leftward shift of the voltage dependence (Kruse and Hille, 2013, Rodriguez-Menchaca et al., 2012). However, there has been no investigation to date as to the effects of PIP_2 modulation on Kv1heteromeric channels expressed in heterologous systems.

In order to re-examine the effects of PIP_2 depletion on Kv1.2 homomeric channels, the Kv1.2 channel subunits were expressed transiently in HEK293 cells. In line with previous findings, we observed that Kv1.2 currents were significantly decreased following application of PIP_2-PP (18.6 ± 5.5% at +57 mV, n = 6; Figure 4.12A, B). Unlike previous findings however, no leftward shift in the $V_{1/2}$ of activation was observed (control: $V_{1/2}$ = -11.7 ± 2.2 mV; PIP_2-PP: $V_{1/2}$ = -11.3 ± 2.2 mV, n = 6, p = 0.64, paired Student's t-test). The notably greater reduction of the LVA current in SGNs by PIP_2-PP application and the proposal that Kv1.1/Kv1.2 heteromeric channels likely mediate this LVA current (Smith et al., 2015), led to the investigation of the effects of PIP_2-PP application on Kv1.1/Kv1.2 heteromeric channels. Application of PIP_2-PP to Kv1.1/Kv1.2 channel currents resulted in larger inhibition (77.7 ± 5.1% at +57 mV, n = 5; Figure 4.12A, C) compared to the Kv1.2 homomers ($p<0.001$, unpaired Student's t-test). Once again, there was no significant shift in the $V_{1/2}$ of activation (control: $V_{1/2}$ = -21 ± 3.7 mV; PIP_2-PP: $V_{1/2}$ = -19.7 ± 6 mV, n = 4, p = 0.63, paired Student's t-test). Intracellular dialysis with diC_8PIP_2-containing ICS produced a marked decrease in the extent and slowing of the rate of inhibition by PIP_2-PP (Figure 4.12C, D). This confirmed that the effect of PIP_2-PP on Kv1.1/Kv1.2 channels was caused by PIP_2 sequestration rather than a direct action on the channel. It was noted that the reduction of heterologous Kv1.1/Kv1.2 currents using PIP_2-PP resembled the effect observed on the LVA current in SGNs, further supporting the proposal that the LVA current is mediated by Kv1.1/Kv1.2 heteromers.

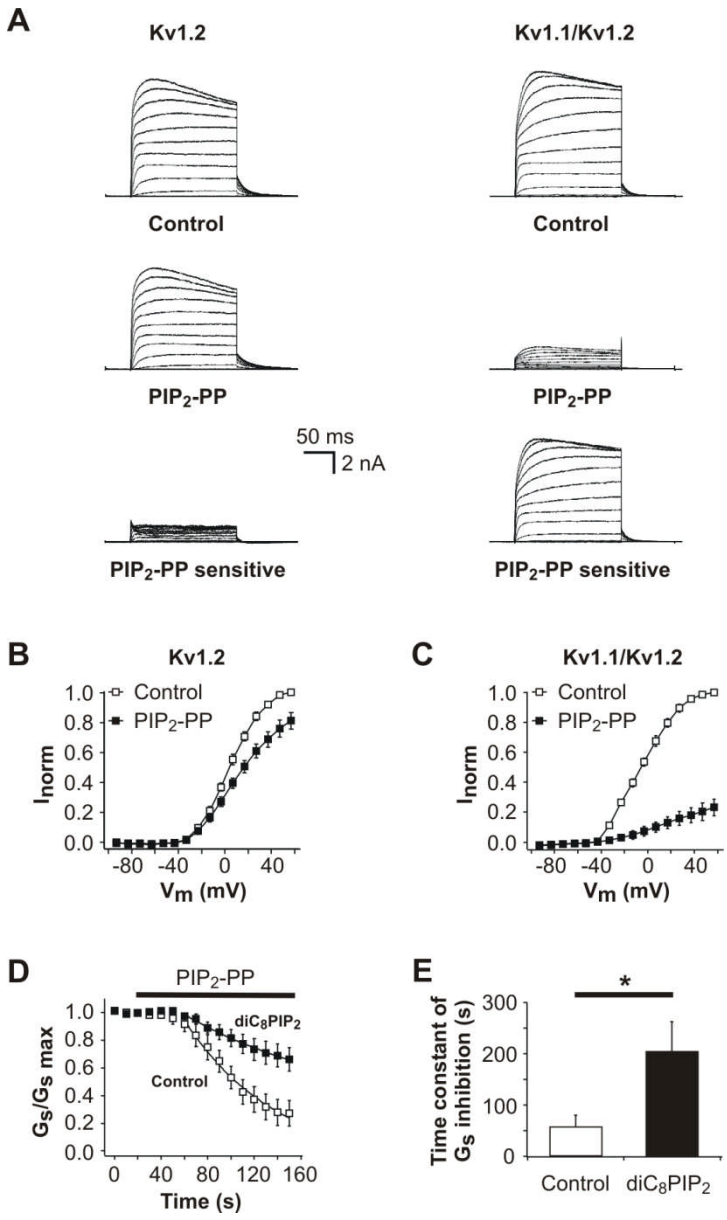

Figure 4.12 PIP_2 sequestration preferentially inhibits Kv1.1/1.2 heteromeric channels expressed in HEK293 cells. A Representative outward evoked current traces from Kv1.2 homomeric channels (left) and heteromeric Kv1.1/1.2 channels (right), before (top) and after 1 μM PIP_2-PP application (middle). PIP_2-PP-sensitive currents are shown (bottom) and were obtained by subtracting PIP_2-PP application traces from control traces. **B** Normalised steady-state current-voltage plots for Kv1.2 homomeric channels before (control) and after the application of PIP_2-PP (PIP_2-PP; 1 μM; n = 6). **C** Normalised steady-state current-voltage plots for Kv1.1/Kv1.2 channels before (control) and after the application of PIP_2-PP (PIP_2-PP; 1 μM; n = 5). In *B* and *C*, steady-state currents were measured at the end of 200 ms voltage steps applied in 10 mV increments from a holding potential of -73 mV. **D** Normalised slope conductance (G_S) of Kv1.1/Kv1.2, calculated from a voltage ramp protocol applied every 10 s (G_s; measured between -63 mV to -53 mV) decreases during application of PIP_2-PP (Control; 1 μM; n = 7). The addition of diC_8PIP_2 (200 μM) to the intracellular solution, reduces the effect of

PIP_2-PP (diC_8PIP_2; n = 5). *E*, Comparison of the rate of Kv1.1/Kv1.2 G_s inhibition by PIP_2-PP in the absence (control; n = 7) and presence of diC_8PIP_2 (200 μM) in the intracellular solution (diC_8PIP_2; n = 5). The time constant of G_s inhibition was calculated by fitting mono-exponential functions to the G_s data in D.

4.3 Discussion

This chapter presents evidence for a dependence of rapid adaptation in murine, post hearing-onset SGNs on endogenous PIP_2 levels. This was demonstrated by depleting membrane bound PIP_2 levels via two separate methods; inhibition of PIP_2 synthesis and PIP_2 sequestration. These experiments revealed that the effect of PIP_2 on spike adaptation was via Kv1.1/1.2 heteromeric channels. This work presents a new mechanism of action for PIP_2 in the regulation of neuronal excitability which merits further investigation.

4.3.1 Experimental depletion of cellular PIP_2

Initial work in this chapter focused on the effects of the inhibition of PIP_2 synthesis on SGN membrane electrophysiology. Here, three conditions of PI depletion were induced - two focusing on PI3K inhibition and one on PI4K inhibition. Only the PI4K inhibition produced marked reductions in rapid adaptation. A limitation to this approach is the inability to make pre and post- incubation recordings from SGNs. Because of the high degree of heterogeneity inherent in SGN, it is impossible to discern what changes in SGN membrane properties might be giving rise to the observed differences in population firing phenotypes. Another potential caveat to this approach is that wortmannin affects other PI pathways. Though wortmannin discriminates between PI3Ks and PI4K it shows little discrimination between subtypes of PI3Ks, or the reactions they catalyse. In practice this means that whilst PI3K inhibition results in reduced levels of PIP_3, it also results in reduced pools of PI(3)P (and consequently $PI(3,5)P_2$), as well as reduced pools of $PI(3,4)P_2$ (see Figure 1.11). This fact is often neglected in discussions of wortmannin induced effects, probably because of a paucity

of knowledge about the biological roles of these other PIs, but also because $PI(4,5)P_2$ makes up 99%, by weight, of all the possible PIP_2 molecules in the cell (Lemmon, 2008). Despite these concerns, the fact that PI3K does not substantially affect excitability and the observation that the inclusion of diC_8PIP_2 in the patch pipette rescued the effects of PI4K inhibition suggets that PIP_2 is the best candidate as the regulator of SGN excitability.

One substantial concern was the observed inhibition of outward I_k upon addition of LY294002 to the bath. Due to rapid onset and wash off of this effect (~1 minute), this was not believed to be a result of PI3K inhibition. Consistent with this idea, other labs have noted similar effects of this drug. The first possible non-PI3K electrophysiological involvement of LY294002 was a reported block of Kv currents in a MIN6 β cell line via direct action on the channel (El-Kholy et al., 2003). A detailed study of the effects of LY294002 on the human Kv1.5 channel determined that it appears to act as an open channel blocker, independently of its effects on PI3K activity, and provided evidence for a putative binding site within the pore region of the channel (Wu et al., 2009). This provides a substantial concern about the use of LY294002 when investigating the role of PIP_3 on ion channels and highlights the need for more specific, electrophysiologically inert PI3K and PI4K inhibitors for the examination of PIP_2 on membrane ion channels.

To overcome some of these potential limitations an alternative method of PIP_2 sequestration was attempted. PIP_2-PP provides a simple, efficient and rapid method of PIP_2 capture which had been characterised initially to inhibit the activity of the highly PIP_2 dependent Kv7.2/Kv7.3 channels in both heterologous expression systems as well as rat superior cervical ganglion cells (Robbins et al., 2006). When this work began, only the initial characterisation of the peptide had been published but since its initial documentation it has now been employed successfully in a two different studies to examine the effects of PIP_2 on the human dopamine transporter and serotonin transporter (Hamilton et al., 2014, Buchmayer et al., 2013). PIP_2-PP takes advantage of the known affinity of Kv7 channels for PIP_2, and is comprised of a peptide sequence known to be important in the interaction between PIP_2 and Kv7.2/3 (Zhang et al., 2003). PIP_2-PP most likely acts by embedding within the plasma membrane and interacting with PIs at the intracellular leaflet of the membrane. This is evidenced by the ineffectiveness of the non-palmitoylated PIP_2-PP analogue in our study and experiments

from Robbins et al. that report inhibition of M-current in response to intracellular application of a non-palmitoylated PIP_2-PP analogue. Interestingly, a concentration of at least 10-fold higher of the non-palmitoylated peptide was required to produce an equivalent inhibition to that of the externally applied PIP_2-PP (Robbins et al., 2006). This indicates that the palmitoyl group is not just essential in allowing access of the PIP_2-binding peptide to the inner leaflet of the membrane, but it also markedly increased its ability to sequester PIP_2, most likely by ensuring a high membrane partitioning of the PIP_2-binding peptide. This is consistent with experiments here and from Robbins et al., that show strong targeting of a fluorescent PIP_2-PP analogue the plasma membrane.

The results here also demonstrated that although the palmitoylated peptide sequence, Pal-HRQKHFEKRR, is sufficient to sequester PIP_2, it is not obligatory for the peptide to function. Rather, the evidence points to both palmitoylation and the strong cationic nature of the peptide as the important features for activity. This is consistent with findings from the original characterisation which also demonstrated the efficacy of "poly K-PP" to inhibit M-current (Robbins et al., 2006). In the same work it was shown that up to 2 positive residues in the PIP_2-PP could be mutated to neutral alanine (net peptide charge, +2) without losing considerable potency. Conversely they also showed that a poly-aspartate or non-palmitoylated analogue of PIP_2-PP did not sequester PIP_2. This suggests that PIP_2-PP is not acting in the manner of classic protein-substrate recognition but rather interactions are most likely driven by electrostatics. Consequently, this also means that PIP_2-PP most likely binds a range of anionic phospholipids present in the plasma membrane. Interestingly, results from Thomas et al. have shown that the C-terminus peptide from Kv7.1 pulls down a range of different PIs in various abundances from cell lysates (Thomas et al., 2011). The homologous amino acid sequence in Kv7.1 varies somewhat from the Kv7.2/7.3 sequence. Nonetheless, the results from Thomas et al. suggest similar broad electrostatic interactions underlie the Peptide-PIP_2 affinity.

The excitatory effects of the PIP_2 depletion were attributed primarily to its ability to modulate SGN Kv1-mediated LVA currents, as opposed to other ionic conductances. Other mechanisms cannot be completely ruled out, but some observations lead us to believe it acts via modulation of Kv1-mediated current. Firstly, PIP_2-PP has a negligible

effect on cells which were previously treated with a Kv1 channel blocker (Figure 4.7), or which had negligible LVA currents (not shown). Secondly, PIP_2-PP recapitulates the increased excitability observed by other KV1 blockers such as DTX-K (Figure 4.3B). Finally, the contribution of the other major PIP_2 sensitive conductance, Kv7, does not seem to regulate spike firing (Figure 4.9) (Lv et al., 2010).

4.3.2 Physiological mechanisms of PIP_2 depletion in SGN

The question of whether SGNs employ PIP_2 modulation of LVA currents in a physiological context remains open. The advent of recent genetic manipulations has allowed highly responsive methods of PIP_2 depletion; techniques such as voltage-gated phosphatase activation or drug induced-membrane translocation of specific phosphatases allow the experimenter to rapidly reduce membrane bound PIP_2 levels in a precise manner. However these techniques, along with the methods of PIP_2 sequestration described here, do not fully address the question of whether the effects observed can be induced by physiological means alone i.e. whether a cell can achieve the same effects via endogenous methods of PIP_2 depletion. Evidence in this direction would support the hypothesis that PIP_2 regulates SGN signalling *in vivo*. To this end we employed two alternate methods of PIP_2 reduction. The first method involved the attempted activation of muscarinic G-protein-coupled receptors (GPCRs) to stimulate PLC activation to hydrolyse PIP_2, and the second method involved the use of a PLC activator.

Based on the results observed in the PIP_2 depletion experiments, muscarinic activation was investigated as a possible mechanism of LVA current modulation. Muscarinic receptors (mAChRs) respond to the presence of acetylcholine (ACh) and other muscarinic agonists. They can be classified into 5 subtypes (M1-M5), which are distinguished by their different G protein-receptor complexes, pharmacological responses and differential distribution and expression. M1, M3 and M5 receptors act via the Gq/11 GPCR pathway which signals through the Gα complex and resulting PIP_2 hydrolysis. M2 and M4 act via the Gi/o pathway which signals via Gβγ (Brown, 2010). This work attempted to take advantage of the M1, M3 and M5 Gq/11 pathway as a

means to reduce cellular PIP_2, a pathway responsible for the muscarinic inhibition of Kv7-mediated M-currents in neurons (Brown et al., 2007).

Evidence supports a function for Gq/11-linked muscarinic receptors in normal hearing. Isolated SGNs from post hearing-onset animals showed increased intracellular [Ca^{2+}] in response to ACh and muscarine (Rome et al., 1999), and muscarinic agonists activate transient nonselective cation currents in isolated rat SGNs (Ito and Dulon, 2002). The recordings here did not show the transient cation conductance reported previously, but slower, rather than transient effects, were the focus of this study. Oxo-M did produce a small but non-significant reduction in SGN LVA current. The inability of Oxo-M to produce significant inhibition of the LVA current could have many explanations. Muscarinic receptor activation may simply not reduce PIP_2 levels sufficiently to induce PIP_2 dissociation from the Kv1 channels. For example, the highly PIP_2-dependent channel Kir2.1 was shown to be insensitive to muscarinic activation, but it could be inhibited by other forms of PIP_2 depletion such as VSP activation (Kruse et al., 2012). Other possible explanations are that mAChRs and PLC exist in spatially distinct patterns to SGN Kv channels and are thus quite poor at modulation their activity. PLC has been shown to exist in discrete microdomains within neurons and may act to exert local control over proximate ion channels (Delmas et al., 2004).

We still have only an incomplete knowledge of the role of mAChRs in the cochlea. The location and function of the various muscarinic receptors and subtypes in the cochlea are still under investigation. Immunohistochemistry of the cochlea showed the presence of moderate levels of M3 and M5 receptor subtypes in the rat SGNs and weak staining observed for M1 receptor (Khan et al., 2002, Safieddine et al., 1996). These results are consistent with RT-PCR findings. However, mice lacking the Gq-coupled mAChRs (M1, M3, or M5) have been shown to display normal cochlear function, as measured by auditory brainstem response and distortion product otoacoustic emission recordings, casting doubt on a functional role for Gq-coupled mAChRs (Maison et al., 2010). The function of such muscarinic signalling is still speculative. ACh represents the primary neurotransmitter of the olivocochlear efferent system, which provides feedback to cochlear hair cells and SGNs. Feedback from the lateral olivocochlear (LOC) nerves therefore may modulate SGN excitability via mAChRs (Maison et al., 2010). The depolarisation associated with mAChRs activation has been hypothesised to increase

cochlear nerve fibres' excitability *in vivo*, based on observations that cochlear nerve fibres increase in excitability during ACh perfusion of the inner ear (Felix and Ehrenberger, 1992). One final caveat to note when interpreting this result is to consider the limits of the preparation used for these recording. Our cultured SGN preparations are typically missing both peripheral and central neurites due to the mechanical and enzymatic treatment of the ganglion prior to recording. In other neuronal systems, such as the sciatic and vegus nerve, considerable levels of functional M1 and M3 are localised to the nerve fibres (Day et al., 1991, Sierro et al., 1992). Our system is necessarily limited to isolated somatic recordings. Repeating the experiment in a more intact preparation, such as a cochlear slice model (Jagger et al., 2000) where the neurites are left intact, could circumvent this limitation.

For these reasons, PLC activation was attempted directly, using m-3M3FBS (Bae et al., 2003). m-3M3FBS considerably inhibited outward I_k in SGNs, but it produced inconsistent and contradictory effects. One concerning issue was that m-3M3FBS might be having a direct effect on the outward I_K. Much of the (particularly HVA) current inhibition seemed to occur through a PIP_2 independent manner. Inhibition of the HVA current was observed in cells with no LVA current and in cells with LVA, strong inhibition of outward I_k persisted even when PIP_2-PP had been added beforehand (not shown). PLC independent effects have been noted for m-3M3FBS; m-3M3FBS has been shown to increase intracellular [Ca^{2+}] in a PLC-independent manner (Krjukova et al., 2004), but it is also reported to block outward currents in murine colon cells (Dwyer et al., 2010). Unfortunately m-3M3FBS is the only well-characterised PLC activator available commercially, highlighting the need for more specific PLC activators for electrophysiological investigation. Notwithstanding the above-mentioned caveats, the lack of an effect Oxo-M and m-3M3FBS on excitability suggests PIP_2 depletion via PLC activation is insufficient for inhibiting SGN LVA *in vitro*.

4.3.3 Mechanism of PIP_2 modulation

Despite the importance of PIP_2 modulation across a range of K^+ ion channels, the molecular mechanisms of its actions remain elusive. What is understood, from the

functional and structural study of K^+ channels such as TRP, KCNQ, hERG, Kir and HCN is that PIP_2 seems to play an important role in the stabilisation of the open state conformation of these channels (Brauchi et al., 2007, Hansen et al., 2011, Zaydman et al., 2013, Rodriguez et al., 2010) despite its relatively low concentration within cells: ~1% total lipid content (Hilgemann et al., 2001). Whilst investigations into the action of PIP_2 on Kv1.1 and Kv1.2 regulation have been only very recent, the findings from those studies will be the subject of the following discourse - with mention of the important finding from both studies on Shaker and KCNQ channels where these may provide mechanistic insights into the regulation of Kv1.1 and Kv1.2.

An array of biological lipids composes the physical and chemical environment of Kv channels. They affect membrane channel function primarily in one of two ways. Global or bulk effects are related to the structure and composition of the cell membrane and how the channels embed and interact within it. For instance the activation of the Shaker channel is markedly suppressed if it is reconstituted in a positively charged bilayer (Schmidt et al., 2006). Changes in the lipid composition have also been suggested to induce mechanosensory effects in ion channels related to changes in membrane lateral tension (Combs et al., 2013). However these effects are to be unlikely to account for PIP_2 activity. The primary criticism has been that the levels of PIP_2 within cells are simply too low (~1%) to significantly impact the membrane biophysics in these ways (Kasimova et al., 2014). Specific or cofactor lipid interactions, in contrast, involve interactions between particular parts of the ion channel and the lipid (usually the charged headgroup) which act to promote or restrict channel activity.

One notable effect is the ability of PIP_2 to relieve the N-type inactivation that is a characteristic of particular voltage-gated K+ channels, e.g. Kv1.4 and Kv3.4. These channels display strong and rapid inactivation of their currents due to the presence of an N terminus “ball domain” located on one of their α pore-forming subunits. But this form of PIP_2 modulation and its mechanism will not be the focus here (Decher et al., 2008, Oliver et al., 2004) but to note that Kv1.1 can show this N-type inactivation property when it is co-expressed with the ball domain-containing accessory subunit, Kvβ1.1 and that the application of exogenous PIP_2 in this context removes this N-type inactivation (Oliver et al., 2004).

The first direct evidence for PIP_2 regulation of Kv channels was the discovery that PIP_2 hydrolysis underlay the receptor-mediated inhibition observed in Kv7 channels (Zhang et al., 2003, Suh and Hille, 2002). Kv7 channels show exquisite sensitivity to the presence of PIP_2 which has made them a useful tool in studying the PIP_2 regulation of ion channels. A series of experiments has now the determined that the long chain C-terminus to be the most likely site of action for PIP_2 on Kv7 channels. This was elegantly demonstrated by Hernandez and co-workers who looked at the apparent sensitivities of the Kv7.3 and Kv7.4 homomeric channels (the latter being ~100 fold less sensitive to PIP_2 than the former); by exchanging the long chain C-termini, they could effectively reverse the apparent phosphoinositide sensitivity (Hernandez et al., 2008). Mutational analysis of the Kv7 channel subunits lead to the identification of key residues that bestow PIP_2 sensitivity upon the functional channels. These were often, but not exclusively, basic residues. At least two prospective binding sites for PIP_2 have now been proposed based on clusters of such key residues in close proximity within the amino acid sequence (Hernandez et al., 2008, Telezhkin et al., 2013, Thomas et al., 2011). Reduced interactions of the long chain flexible C-termini with the anionic headgroups of membrane bound PIP_2 was proposed to account for the reduced probability of opening and reduced maximal opening observed in the mutant channels. Interestingly, much of the same work has revealed that these so-called PIP_2 sensitive Kv7 channels show an affinity for many other phosphoinositides; the C-terminus peptide effectively pulling down a range of PIs in vitro (Thomas et al., 2011). Furthermore, PI(4)P, PI(3,4,5) and even some non-PI lipid phosphates have been shown to be able to stimulate M-type channel activity when expressed in mammalian cells lines (Telezhkin et al., 2012).

Unfortunately, a lack of homology between C-termini of Kv1 and Kv7 channels, and the absence of a clear analogous PIP_2 binding site, has made inferring information about the activity of PIP_2 on Kv1 channels difficult. In fact little was known about the PIP_2 sensitivity of the greater Kv family of channels until 2012, when initial findings suggested Kv channels may have little or no sensitivity to PIP_2 (Kruse et al., 2012). The Hille laboratory examined the effects of PIP_2 depletion on, amongst others, Kv1.1/Kvβ1.1, Kv1.3, Kv1.4 and Kv1.5 channels expressed in tsA-201 cells. They employed 3 distinct mechanisms of PIP_2 depletion and found that apart from Kv7 channels, Kv channels were, in general, insensitive to PIP_2 (Kruse et al., 2012). In 2012,

Rodriguez-Menchaca et al., reported the first observed sensitivity of the Kv1.2 channel to PIP_2 in Xenopus oocyte excised patches (Rodriguez-Menchaca et al., 2012). This was somewhat surprising given the previous findings that many other close members of the Kv1 family were insensitive to the phosphoinositide. They reported that the presence of PIP_2 stabilised the voltage sensor of Kv channels, decreasing its sensitivity to changes in membrane voltage (observed as a right-shifted I-V relationship) whilst simultaneously promoting the stability of the open state of the channel (demonstrated by an increase in open probability during single channel recording).

Through these experiments Rodriguez-Menchaca et al., also began to make the first mechanistic insights into the possible mode of action of PIP_2. Mutational analysis of a number of positively charged residues in the N terminus and S4–S5 linker region of Kv1.2 – a region which acts to couple changes at the voltage-sensor domain (VSD) to the pore domain (PD) of the Kv channels – along with docking and molecular dynamic simulations suggested key interaction of PIP_2 with polybasic domains in these channels. These interactions, they suggested, lead to the observed dual regulation of Kv1.2. These results were soon replicated in the Shaker channel (Abderemane-Ali et al., 2012) which observed similar decreases in currents and $V_{1/2}$ shifts. Modelling of the Kv1.2 channel found a similar site of action (S4–S5 linker region) but expanded the mechanism of action to include positive residues from the S5 gate region. This model of PIP_2 interaction has been leant credibility by its similar pattern of binding interactions to that of PIP_2 with Kir2.2 (Rodriguez-Menchaca et al., 2012, Hansen et al., 2011). The interactions of PIP_2 with positively charged residues in the S4–S5 linker region act to constrain the movement of the VSD, resulting in desensitisation of the channel to changes in membrane voltage, and also to stabilise and maintain the channel once it is in its open state. In their 2012 paper, Abderemane-Ali et al. summarised these effects - "PIP_2 stabilises the gate in the open state and the voltage sensor in the resting state" (Abderemane-Ali et al., 2012).

Interestingly, the two components of this dual regulation seem to be distinct and separable phenomenon, distinguishable by differences in kinetics, PIP_2 sensitivities and molecular components i.e. mutation of protein residues could be shown to discriminate between effects. This insight into the nature of these effects, and the hypothesis that they may rely on distinct and separable interactions between PIP_2 and specific cationic

residues in Kv1.2, provide a plausible explanation for the difference in responses seen across a range of experiments, including our own. Differences in the method of PIP_2 depletion has been shown to be able to selectively affect the voltage dependence of activation without reducing overall current amplitude (Rodriguez-Menchaca et al., 2012). Further example comes from the effects of PIP_2 depletion were examined in a mammalian expression system. Although the effects on the evoked current amplitude are reproduced (20-30% reduction depending on the method of depletion used), the effects upon the voltage dependence vary considerably (only -3.5 mV shift in HEK293 cells, compared to -14 mV in oocytes (Kruse and Hille, 2013)). This study reports a mean reduction of Kv1.2 current by ~20%, in line with others, but there was no observed change in the $V_{1/2}$ of activation in either Kv1.2 homomeric channels or Kv1.1/1.2 heteromers. Without a comprehensive mechanistic understanding of how PIP_2 interacts with Kv1.2 at a molecular level it is impossible to offer a satisfying explanation as to the variation in results across experiments. But it is conceivable that differences in experimental conditions, expression systems, or membrane architecture may differentially affect some PIP_2 interactions over others and give rise to the variations observed.

More in-depth molecular dynamics simulations have borne out the view that PIP_2 modulation arises out of electrostatic interactions with the channel at the inner leaflet of the membrane but has questioned if open-state stabilisation alone accounts for the gain-of-function effects observed by PIP_2. Kasimova et al., in agreement with the previous work from Rodriguez-Menchaca et al., found that PIP_2 made multiple robust salt bridge interactions with positively charged residues in both the S4 VSD as well as the S4-S5 linker region (Kasimova et al., 2014). They suggested that the proximity of a number of cationic residues from the S4–S5 linker with positive charges from the bottom of the S4 VSD lead to a pocket of excess positive charge at the inner membrane forming a sort of "PIP_2-binding pocket" for the highly negatively charged PIP_2 molecules. Interestingly however, they found that when the channel is in the activated state, the S4 helix is in a conformational different position and embedded further in the membrane and none of its positive residues are involved in electrostatic interactions with PIP_2. However there were still robust interactions between PIP_2 and positive residues in the S4–S5 linker, as well as new interactions made with the distal positive residues of S6 pore forming helix.

In summary, the modulatory effects of PIP_2 on Kv channels can be interpreted in two ways. One view is that PIP_2 stabilises the open configuration of the channel by making energetically favourable interactions with positive residues when the channel is in its open state, particularly those in the S5 or S6 gate region. In this model, in the absence of PIP_2, a depolarizing voltage activates the VSD, which is weakly couple to the channel pore, and results in fluctuations of the channel between an open and closed state, thus producing a small current. When PIP_2 is present however, it interacts with the channel to stabilise the open conformation, resulting in larger currents. This hypothesis might suggest that channels lacking a VSD could also avail of this mechanism. This has, incidentally, proved to be the best current understanding of how the Kir family of channels are modulated by PIP_2 (Huang et al., 1998). This is also consistent with results from single channel recordings of voltage-independent potassium K_{ATP} channels, and simulations of Kv7.1 and Kv11.1 currents that implicate PIP_2 in stabilizing the open state, by acting on the final concerted opening transition (Loussouarn et al., 2003, Shyng and Nichols, 1998). It also explains the observations that mutations in the positive residues which are involved in these putative open-state stabilising interaction (such as those in the in the distal S6 helix region), significantly reduce the channels sensitivity to PIP_2 (Thomas et al., 2011).

A second interpretation is to reframe the view of PIP_2 sensitivity in terms of a Kv channel's ability to effectively couple, in the absence of anionic lipids, changes in membrane potential to changes in channel activity (Kasimova et al., 2014). Kv channels such as Kv1.3 or Kv1.4 which show no sensitivity to reductions in endogenous levels of PIP_2 (Kruse et al., 2012), can be imagined to produce effective communication between the VSD and the PD. Therefore, conformational changes in the channel can occur without needing additional stabilisation from membrane-bound phospholipid. However, in highly PIP_2-dependent channels in the absence of PIP_2, although a depolarizing voltage may activate the VSD, the channel itself will remain closed as a result of weakened interactions between the S4-S5 region and S6 region. As recent experiments on the PIP_2-dependent Kv7.1 channel have demonstrated, open state stabilisation is not sufficient to explain PIP_2 dependence but rather, this coupling of VSD-PD is not possible without the stabilisation of anionic lipids (Zaydman et al., 2013). It is obvious that these two mechanisms of action are, at least in theory, distinguishable with their modes of action dependent on distinct and separable interactions. Future work should

focus on identifying which mechanism, if either, best explains PIP_2 activity. One key difference is that the former interpretation requires only that PIP_2 make contact with residues which stabilise the open state of the channel, whilst the latter relies on the PIP_2 binding site being at least partly formed by the S4–S5 linker (Kasimova et al., 2014). Also noteworthy is the fact that this mode of action is distinguishable from that of negatively charged lipids other than PIP_2 that are known to regulate Kv channel activity such as polyunsaturated fatty acids and ceramide-1-phosphate. In these cases the negatively charged lipids are proposed to interact with channel at the external leaflet of the membrane (Combs et al., 2013, Borjesson and Elinder, 2011).

An important finding in this study has been the higher sensitivity of heteromeric Kv1.1/1.2 channels compared to that of homomeric Kv1.2 channels when expressed in HEK293 cells. In light of the discussed mechanisms of PIP_2 regulation of Kv1.2, there may be a number of possible explanations for this effect. A simple explanation is that the Kv1.1 subunit is highly PIP_2-dependent and confers a strong PIP_2-dependance upon the heteromer. This is a somewhat naïve hypothesis and there is, of course, no guarantee that even should Kv1.1 show high PIP_2 sensitivity that the heteromer should, as Kv1.1/Kv1.2 heteromers are known to show quite different pharmacological properties than the sum of their constituent subunits would predict and even show different pharmacological sensitivities depending arrangement of the subunits within the heteromers (Al-Sabi et al., 2013). Notwithstanding these caveats, in order to examine this possibility, recordings from HEK293 cells transiently transfected with the Kv1.1 subunit were attempted but were largely unsuccessful. The preponderance of transfected cells displayed no voltage-evoked current responses and the few cells which displayed voltage-evoked currents were too unstable to obtain meaningful recordings from. This difficulty most likely arises from the poor protein trafficking ability and low cell surface expression of the Kv1.1 homomer (Manganas and Trimmer, 2000). Experiments using cDNA to express the Kv1.1 subunit in HEK293 cells show that although strong Kv1.1 subunit accumulation is seen at the Endoplasmic Reticulum less than 4% of transfected cells show any Kv1.1 surface expression (Manganas and Trimmer, 2000). This is a result of an ER retention motif in the Kv1.1 peptide (see *Kv channel biogenesis*). Kv1.2 homomers in contrast show much higher levels of cell surface expression (~20%). As a result, Kv1.1 sensitivity to PIP_2 has only previously been examined when co-expressed with auxillary subunits, such as the Kvβ1.1 auxiliary subunit, where it seems to act via

different mechanism (Oliver et al., 2004). It would be instructive to learn if Kv1.1 could confer sensitivity to PIP_2 if coexpressed with other PIP_2 insensitive subunits such as Kv1.4, which have been shown to produce surface expressed heteromeric channels in HEK293 (Manganas and Trimmer, 2000).

Another suggestion is that Kv1.1/Kv1.2 heteromeric channels may have a lower affinity for PIP_2 compared to the Kv1.2 homomer. As a result PIP_2-PP may be able to compete more effectively for channel-bound PIP_2. A similar rational was employed to explain the surprising ineffectiveness of PIP_2-PP in inhibiting the highly PIP_2-dependent Kir2.1 channel (Robbins et al., 2006). This distinction between "affinity" and "sensitivity" is an interesting and important one. A channel may be highly PIP_2 sensitive and almost completely unable to function in its absence, but have such a high affinity for the PI that PIP_2 levels have to be reduced very low before PIP_2 can reasonably be expected to become dissociated. This has important experimental and physiological implications. Channels highly sensitive to, and highly dependent on, changes in membrane bound PIP_2 levels will be best suited to responding to signalling cascades which result in PIP_2 hydrolysis. For instance, the strong inhibition of M-current observed upon muscarinic receptor agonism (Zhang et al., 2003). At a molecular level, it is easy to understand how these effects arise out of distinct chemical interaction of PIP_2 with the channel. The sensitivity of a channel to the presence of PIP_2 arises, as discussed above, from the activity of PIP_2 in stabilising the open configuration of the channel, or alternately, in the coupling of the VSD with the PD. The affinity of PIP_2 for a channel however is a reflection of the strength of the interactions between PIP_2 and the channel. These interactions are primarily electrostatic interactions between the strongly negatively charged headgroup of PIP_2 and densities of positive charge located at the inner leaflet of the channel. This distinction is an important consideration when interpreting results which used PIP_2 depletion or addition to modulate channel function.

From what is known about the binding site and putative mechanism of action of PIP_2, explanations of the observed effects based on sequence comparisons alone are difficult to justify. Figure 4.13 shows the sequence of the putative Kv1.2-PIP_2 interacting region as predicted by mutagenesis and computational studies (Rodriguez-Menchaca et al., 2012, Kasimova et al., 2014) aligned with mouse Kv1.1 and the Shaker channel (*Drosophila melanogaster*). The alignment highlights important interacting residues that

have been determined by molecular dynamics and docking simulations (yellow) as well as residues that have been shown empirically to have a role in the channels sensitivity to PIP_2 (boxed). The primary sequences of the two proteins share a high sequence homology and are identical within the putative PIP_2 interacting region. There was no difference between residues known, by mutagenesis experiments, to be important in mediating PIP_2 sensitivity. Neither, were there were any differences between residues which have been implicated, by molecular dynamics and docking studies, to interact with PIP_2 at the channel (Figure 4.13). Changes in the molecular interactions which occur at the putative PIP_2 binding site, if responsible for the differences in PIP_2 sensitivities between the Kv1.2 homomeric channel and Kv1.1/Kv1.2 heteromeric channel, must arise out of more long distance residue effects. Finally, despite the high similarity between Kv1.1 and Kv1.2 subunits within the putative PIP_2 binding site, the global effects of incorporating different subunits into a functioning channel are unknown. Whether or not the heteromer resembles closely the binding site as projected onto the crystal structure of the Kv1.2 homomer is not yet clear. Homology modelling of the heteromer or, more ideally, a crystal structure is needed to speculate further on the mechanisms that underlie these differences.

```
                    ________S4_____ _    ___S4-S5_ _  _______S5_________
Shaker      KSSNQAMSLAILRVIRLVRVFRIFKLSRHSKGLQILGRTLKASMRELGLLIFFLFIGVVL
mKv1.1      QKGEQATSLAILRVIRLVRVFRIFKLSRHSKGLQILGQTLKASMRELGLLIFFLFIGVIL
mKv1.2      QQGQQAMSLAILRVIRLVRVFRIFKLSRHSKGLQILGQTLKASMRELGLLIFFLFIGVIL
            :..:** ****************************:*********************:*
                    _________          Pore Helix_          ________S6________
Shaker      FSSAVYFAEAGSENSFFKSIPDAFWWAVVTMTTVGYGDMTPVGVWGKIVGSLCAIAGVLT
mKv1.1      FSSAVYFAEAEEAESHFSSIPDAFWWAVVSMTTVGYGDMYPVTIGGKIVGSLCAIAGVLT
mKv1.2      FSSAVYFAEADERDSQFPSIPDAFWWAVVSMTTVGYGDMVPTTIGGKIVGSLCAIAGVLT
            ********** . :* * ***********:********* *. : ***************
                        ___________________
Shaker      IALPVPVIVSNFNYFYHRETDQEEMQSQNFNHVTSCPYLPGTLGQHMKKSSLSESSSDMM
mKv1.1      IALPVPVIVSNFNYFYHRETEGEEQ--AQLLHVSS-PNLASDSDLS-RRSSSTISKSEYM
mKv1.2      IALPVPVIVSNFNYFYHRETEGEEQ--AQYLQVTSCPKIPSSPDLKKSRSASTISKSDYM
            ********************: **    :  :*:* * : .       :*: : *.*: *
```

Figure 4.13 Sequence alignment of the voltage-sensor domain and pore domains of the Shaker, Kv1.1 and Kv1.2 channels. In bold are the important channel structures. In the Kv1.2 sequence, residues which are thought to be important to PIP_2 modulation are highlighted. Boxed: Mutations in these residues affect PIP_2 modulation of the channel. Yellow: Interactions observed by molecular dynamics and docking simulations. Data on important residues obtained from Rodriguez-Menchaca 2012, Kasimova 2012, Abderemane-Ali 2012.

Chapter 5

Investigating the effects of free fatty acids on Kv1.2-mediated currents

5.1 Introduction

5.1.1 Free fatty acids are modulators of neuronal electrophysiology

In the preceding chapter, Kv1.1 and Kv1.2-mediated LVA K^+ currents were shown to be highly dependent on the presence of the membrane phospholipid PIP_2. For this reason, further investigation of the effects of native membrane lipids on the constituent LVA K^+ channel, Kv1.2, was carried out. In this chapter the functional effects of biological fatty acids were investigated for their activity against the heterologously expressed Kv1.2 channel.

Fatty acids are biological lipids that are usually present as part of triglycerides or phospholipids, where they play important roles in energy storage and as the structural basis for the plasma membrane. Free fatty acids (FFAs), uncoupled to any such structures, have distinct biological roles in energy metabolism, inflammation and synaptic plasticity (Bazan, 2005, Hara et al., 2014, Tassoni et al., 2008). Alongside diverse roles in metabolism and signalling, FFAs also influence the activity of membrane-bound ion channels directly. Voltage-gated ion channels are ideally positioned for modulation by FFAs. The TM domain of the channel is embedded within a mass of FFAs and fatty acid precursors and channel gating involves movement of the protein within this hydrophobic environment. External signalling molecules such as neurotrophic factors and cytokines stimulate the production of the FFA signalling molecules by activating their cleavage from the plasma membrane (Papackova and Cahova, 2015). Combined with other long term changes in membrane fatty acid levels due to dietary effects, disease etc. this allows short and long term regulation of membrane ionic conductances. In neurons and cardiac muscle, fatty acids add further diversity to the mechanisms of fine-tuning the electrical properties of the cell (Boland and Drzewiecki, 2008).

The first recognised ion channel sensitivity to fatty acids was reported in 1992. Arachidonic acid (AA) and other long-chain fatty acids modified the activity of voltage dependent Ca^{2+} channels in heart and smooth muscle cells (Hallaq et al., 1992, Shimada and Somlyo, 1992). This was shortly followed by the discovery that Nav channels and Kv channels are also major targets for fatty acid modulation (Boland and Drzewiecki,

2008). Fatty acid modification of Kv channel is common across a range of different K^+ currents and tissue types. Fatty acids modulate Kv channel activity in cells and tissues as diverse as glia (Visentin and Levi, 1998), myocytes (Smirnov and Aaronson, 1996), pinealocytes (Poling et al., 1995), pancreatic islet beta cells (Jacobson et al., 2007), hippocampal neurons (Keros and McBain, 1997) and IHCs (Sokolowski et al., 2004). However, modelling how these changes might impact neuronal features has been difficult. Dietary consumption of unsaturated fatty acids has been shown to change the lipid composition of neurons in the brain and result in concomitant changes in firing properties and behaviour (Arsenault et al., 2012, Yang et al., 2012). But the diversity of potential neuronal targets has resisted any simple mechanistic explanation for the role of fatty acids in determining this firing behaviour.

Experiments on Kv channels in recombinant expression systems have recapitulated many of the observed effects of fatty acids on K^+ currents in biological tissues. Interestingly, fatty acids demonstrate clear trends in activity across tissues and channel types. Typically, externally applied fatty acids (usually arachidonic acid (AA)) affect the voltage sensitivity of the activation and inactivation, as well accelerating the inactivation of the channel and/or inducing inactivation in previously non-inactivating channels (Honore et al., 1994, Oliver et al., 2004, Poling et al., 1995). Table 5.1 catalogues these experiments, the types of fatty acid used, the expression systems and range of effects observed. These findings point to a key role for fatty acids in determining the activity of Kv channels.

5.1.2 The structural diversity of free fatty acids

In chemical terms a fatty acids fatty is a carboxylic acid connected to a long aliphatic carbon chain or “tail”, which is typically unbranched and usually contains an even-numbered of carbon atoms (McNaught et al., 1997). Figure 5.1 shows the structure of the common mammalian fatty acid, arachidonic acid. It also highlights the important structural motifs within the fatty acid structure, variation upon which gives rise to the large families of fatty acids recognised today. Despite the surprising reproducibility of effects caused by AA and docosahexaenoic acid (DHA) across diverse K^+ channels and

tissue types, individual fatty acid members can differ markedly in their efficacy and type of effect produced upon a single channel (see Table 5.1).

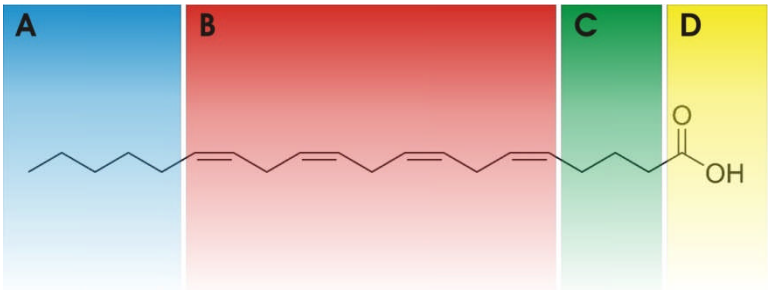

Figure 5.1 The chemical structure of a fatty acid. A fatty acid is a carboxylic acid combined with an aliphatic carbon tail, which is either saturated or unsaturated. Fatty acid family members primarily differ in the length and organisation of the fatty acid tail and in the degree of saturation. **A** The length of the terminal carbon chain is an important classification of fatty acids. In this example molecule, arachidonic acid has its final carbon-carbon double bond six atoms from the terminal atom (in the ω-6 position). In this way it is designated a ω-6 fatty acid. **B** One of the most important descriptors of fatty acids is the presence or absence or double bonds. Unsaturated fatty acids vary in the position, number and type (cis/trans) of double bonds present along the fatty acid tail. **C** Similar to A the distance between the initial acid group and first double bond varies between fatty acids. **D** The carboxylic head group is essential in order to be a fatty acid. Functionalisation of this acid headgroup is a common metabolic pathway for fatty acids.

A notable structural feature of fatty acids is the number of carbon atoms that make up the length between the final carbon double bond and the terminal carbon in the fatty acid chain (see Figure 5.1A). Counting from the terminal carbon, these acids are thus classified ω-n fatty acids, where n is the number of carbon atoms. ω-n fatty acids are clustered into important groups of dietary fatty acids, most notably ω-3 and ω-6 fatty acids. The relative intake of these fatty acids (i.e the ω-3/ω-6 ratio) had been implicated as an important contributory factor in cardiac disease and other chronic conditions (Simopoulos, 2008a, Simopoulos, 2008b). The presence (unsaturated) or absence (saturated) of double bonds within the fatty acid tail is also an important structural feature (Figure 5.1B). The number, position and type (cis/trans) of double bonds within

the fatty acid chain all contribute to the variety of available fatty acids. Mammals have the capacity to synthesise saturated fatty acid (SFAs) and to a limited extent fatty acids with a single double bond in its tail (monounsaturated, MUFAs) (Boland and Drzewiecki, 2008). However, mammals lack the capacity to synthesise fatty acids with multiple double bonds (polyunsaturated) fatty acids and therefore ω-3 and ω-6 polyunsaturated fatty acids (PUFAs) are often referred to as essential fatty acids since they must be obtained from dietary sources or synthesised from precursor molecules (Jakobsson et al., 2006). The presence and degree of unsaturation has been shown to be important in the interaction of fatty acids with Kv channels (Honore et al., 1994, Poling et al., 1996b, Borjesson et al., 2008).

Although not strictly fatty acids themselves, analogues of fatty acids based on esters of the free carboxylic acid have also been shown to be able to mimic the effects of PUFAs on Kv channels. For instance, N-arachidonoylethanolamine (AEA, commonly known as anandamide) and methandamide have been shown to be able to recapitulate the effects of AA independent of their activity on cannabinoid receptors (Oliver et al., 2004, Sade et al., 2006). Although the subject of much research the precise relationship between the structure and activity of fatty acids against various Kv channels is still unclear. The ubiquitous nature of fatty acids within mammalian cells and their known interactions with Kv channels however make them an ideal candidate for neuronal ion channel modulation (Boland and Drzewiecki, 2008). This chapter examines the modulatory effects of FFAs against the Kv1.2 subunits, which mediate the LVA K^+ currents in SGNs.

Table 5.1 Fatty acid modulation of recombinant Kv channels. Abbreviations: DHA – Docosahexaenoic acid; EPA - Eicosapentaenoic acid; AA - Arachidonic Acid; LnA - Linolenic Acid; HA - Hexadecatrienoic acid; LA - Linoleic acid; αLA - α-Linolenic acid; OA - Oleic Acid; ArA - Arachidic Acid; LaA - Lauric acid; AEA - Anandamide; mAEA - Methandamide; VDM11 - (N-(4-hydroxy-2-methylphenyl) arachidonylamide); SA - Stearic acid; PaA - Palmitic acid; CA - Caprylic acid.

Recombinant Kv channels	Expression system	Fatty acid	Effect on current	References
Kv1-type Shaker	Xenopus oocytes	DHA, EPA, AA, LnA, HA, LA, OA, ArA,	DHA, EPA, AA, LnA, HA, LA: left-shifted activation curve. DHA speeds up the on-gating current. OA, ArA: No effect	(Borjesson et al., 2008)
Kv1.1	Sf9 cells	AA	Concomitant acceleration of the activation and inactivation kinetics (possibly via Ca2+-independent phospholipase A2)	(Gubitosi-Klug et al., 1995)
Kv1.1 and Kv3.4	Xenopus oocytes	AA, DHA, AEA, ETYA, VDM11	No inhibition of peak current magnitude, acceleration of the inactivation kinetics.	(Decher et al., 2010)
Kv1.2 and Kv3.1a	Mammalian fibroblasts	DHA, AEA	Inhibition + increased inactivation.	(Poling et al., 1996a, Poling et al., 1996b)
Kv3.4 and Kv1.1/β1.1	Xenopus oocytes	AA, AEA	Inhibition + increased inactivation of currents when N-type inactivation had been removed by PIP_2	(Oliver et al., 2004)
Kv1.5	CHO cells	AA, DHA, ETYA, OA	AA, DHA, ETYA: Inhibition + increased inactivation. Left-shifted inactivation curve. OA: no effect	(Honore et al., 1994)
Kv1.5	Stably transfected fibroblast cell line	EPA, DHA, αLA	EPA and DHA reduced steady-state currents. ALA left-shifted activation curve + accelerated activation kinetics and slowed deactivation.	(Guizy et al., 2008)

Kv1.5	HEK 293	AEA	Reduced the magnitude of the peak and steady-state currents and + accelerated the rate of current decay	(Moreno-Galindo et al., 2010)
Kv1.5 and Kv2.1	CHO cells	αLA	Inhibition + Increased rate of activation and left-shifted activation curve.	(McKay and Worley, 2001)
Kv2.1	HEK 293	AA	Inhibition + increased inactivation	(Jacobson et al., 2007)
Kv 4	Xenopus oocytes	AA, ETYA	Inhibition + Increased in rate of recovery from inactivation. Kv1, Kv2 & Kv3 family unaffected	(Villarroel and Schwarz, 1996)
Kv4.2	Xenopus oocytes	AA, ETYA, ETI	Inhibition + accelerated inactivation when co-expressed with KChIP.	(Holmqvist et al., 2001)
Kv4.2/ KChIPs	Xenopus oocytes	AA, DHA	Inhibition + increased inactivation of currents.	(Boland et al., 2009)
Kv4.3/ KChIPs	Xenopus oocytes	AA, DHA	Inhibition + increased inactivation of currents.	(Boland et al., 2009)
Kv4.3	CHO cells	DHA	Inhibition	(Singleton et al., 1999)
Kv7.1 and KCNE1-Kv7.1	Xenopus oocytes	DHA	Left-shifted activation curve	(Liin et al., 2015)
Kv7.1/mink	Xenopus oocytes	DHA, OA, LaA	Increased currents	(Doolan et al., 2002)
BK	HEK 293	AEA, mAEA	Increased activity independent of cannabinoid receptors or G-protein activation	(Sade et al., 2006)
BK	Xenopus oocytes	AA, DHA, OA, SA, PaA, CA	AA, DHA, OA: Increased current; SA, PA, CA: No effect	(Sun et al., 2007)

5.2 Results

5.2.1 Arachidonic Acid inhibits Kv1.2 channels in a concentration dependent manner

To examine the effects of fatty acids upon the Kv1.2 channel, a stable expression line was first developed, in order to reduce variability between cells and increase throughput. The construction of the Kv1.2-transfected HEK293 cell line was performed as described in *Material and Methods*. Figure 5.2 shows the properties of the cell line as determined by whole-cell patch clamp recordings. Due to the ability of HEK293 to electrically couple to adjacent cells via gap junction, transfected cells were plated at a low density and recordings were made from spatially isolated cells (Figure 5.2C). Consistent with recordings from transiently transfected cells (see Chapter 4), stably Kv1.2-transfected cells displayed outward currents upon depolarisation which activated more rapidly with increasing depolarisation. Inactivation was largely absent during small depolarisations, but some inactivation was observed for test potentials exceeding +30 mV (Figure 5.2B, C). Comparable currents were not present in untransfected cells, where only small outward currents were noted (not exceeding 200 pA at large depolarisations). 100 nM TsTx inhibited 84.1 ± 3.1% of the current (Figure 5.2 D, E; n = 3 cells). Residual TsTx-insensitive currents were comparable to native HEK293 cell currents.

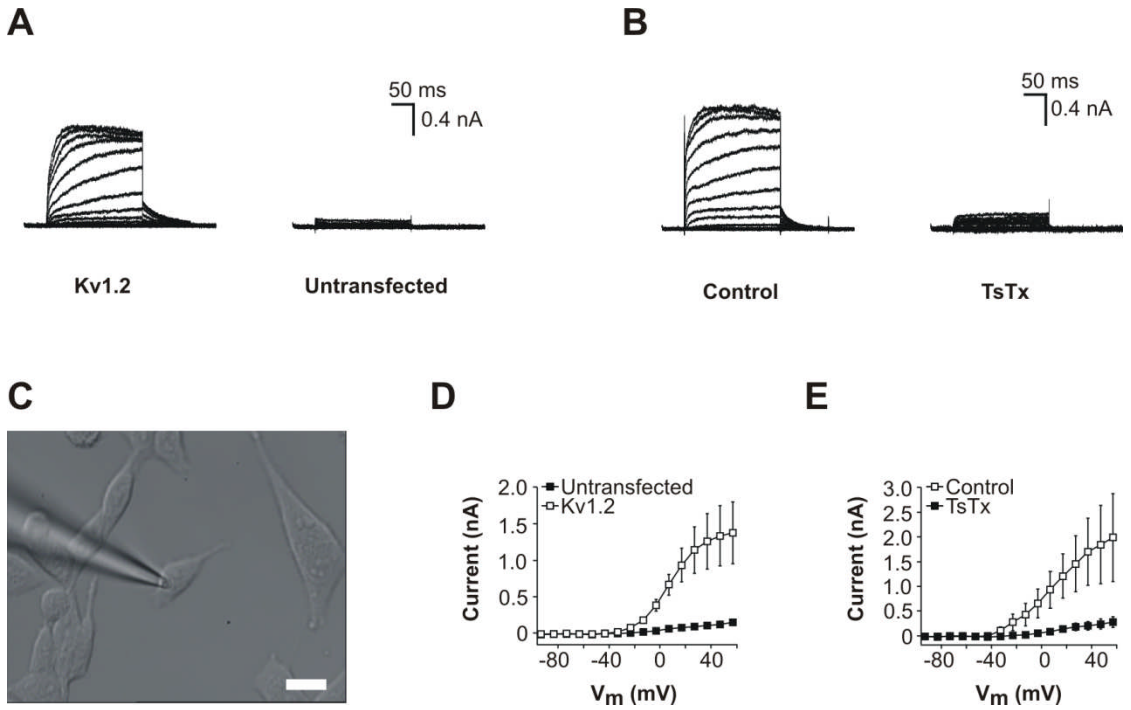

Figure 5.2 Characterisation of a stably Kv1.2-transfected HEK293 cell line. A Representative traces from a Kv1.2-transfected HEK293 cell (left) and untransfected HEK293 cell (right) in response to the same voltage step protocol. Cells were stepped from a holding potential of -73 mV to voltages of between -93 and +57 mV in 10 mV steps. **B** Current traces showing inhibitory effects of TsTx on outward K^+ currents. Currents were obtained as in A. **C** Transfected HEK293 cells were plated at low density and recordings were made from isolated cells to avoid gap-junction coupling with other cells. Scale bar: 10 µM **D** I-V plot of Kv1.2-transfected HEK293 (closed squares) and untransfected HEK293 cells (open squares). Currents were measured 50 ms from the end of the voltage protocol described in A. **E** I-V plot of Kv1.2 currents before (open squares) and after 100 nM TsTx (closed squares) application of TsTx to Kv1.2 expressing cells. Currents were measured 50 ms from the end of the voltage protocol described in A.

Figure 5.3 shows the effects of increasing concentrations of arachidonic acid (AA) on the Kv1.2 currents characterised above. Addition of 1 µM, 10 µM or 100 µM AA was found to inhibit Kv1.2 currents in a dose dependent manner. Addition of 1 µM or 10 µM AA accelerated activation, whilst reducing peak currents and increasing inactivation. 100 µM produced rapid inactivation and 96% block of steady state currents (Figure 3A, C). AA is a major substrate for the biosynthesis of the lipid messenger molecule prostaglandin H_2. Therefore, in subset of experiments, 10 µM indomethacin (a

nonselective inhibitor of cyclooxygenase 1 and 2) was added to the culture medium 1 hr prior to recording (Cuendet et al., 2006). Indomethacin did not prevent the inhibitory effects of 100 µM AA in the experiments. Figure 5.3D shows the time course of activity and reversibility of AA application. 100 µM AA reached a steady-state inhibition after 3-4 minutes bath application. Inhibition could be reversed by perfusion with bath solution over a period of 12 minutes.

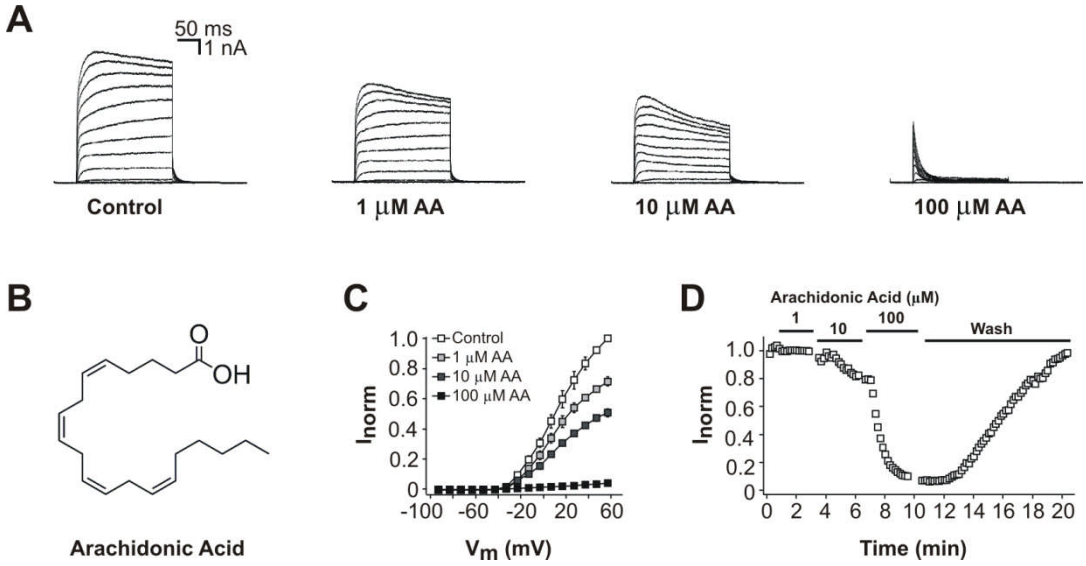

Figure 5.3 Effects of increasing concentration of arachidonic acid (AA) on Kv1.2 currents. **A** Current traces from a Kv1.2-transfected HEK293 cell in the absence (control) and presence of 1 µM, 10 µM and 100 µM AA. Cells were stepped, for 200 ms, from a holding potential of -73 mV to voltages of between -93 and +57 mV in 10 mV steps. **B** Chemical structure of AA. **C** I-V plot of the steady-state Kv1.2 currents in the absence (control, open squares) and presence of 1 µM (light grey squares), 10 µM (dark grey squares), and 100 µM (black squares) AA. Currents were measured from the end of the voltage protocol described in A. **D** Time course of Kv1.2 current inhibition by AA. AA inhibition was monitored by a voltage protocol applied every 10 s. Currents were measured 20 ms before the end of the 400 ms ramp from -153 to +47 mV. I_{norm} was calculated as the proportion of current remaining compared to the control Kv1.2 currents. Wash off was carried out using bath solution alone.

The AA-induced, rapid inactivating of Kv1.2 currents was subsequently characterised. Figure 5.4A shows the AA treated Kv1.2 outward currents in response to a series of voltage steps. The voltage dependence of activation AA-treated Kv1.2 current was determined by plotting the normalised peak conductance against the membrane potential; the derived GV plot (Figure 5.4C filled squares) could be fitted with a Boltzmann function. There was no significant effect of the AA on the voltage of half-maximal activation, $V_{1/2}$, or slope values respectively. (AA treated $V_{1/2}$: -16.6 ± 1.7 mV vs. Control $V_{1/2}$: -13 ± 2.2 mV, p = 0.08, n = 6, paired Student's t-test; AA treated slope: 12.1 ± 1.6 vs. Control slope: 11.5 ± 1.2 mV, p = 0.31, n = 6, paired Student's t-test). The voltage dependence of steady-state inactivation was also determined using a two-step voltage-clamp protocol outlined in Figure 5.4B. Briefly, AA-treated, Kv1.2-transfected cells were exposed to a series of preconditioning voltage steps (-93 mV to +17 mV) before being stepped to a test potential of +27 mV (corresponding to maximal activation of Kv1.2, Figure 5.4C), Figure 5.4B shows typical currents obtained from using this experimental protocol. The voltage dependence of AA treated Kv1.2 inactivation was described by a Boltzmann equation (Figure 5.4D), in which the $V_{1/2}$ of inactivation was -50.5 ± 1.1 mV (slope factor 3.9 ± 0.3; n = 7).

To explore the kinetics of recovery of the AA-induced inactivation, a two-step protocol was employed (Figure 5.4E). A 200 ms depolarising pre-pulse was followed by a 200 ms test pulse after an interval of a variable duration (16 to 8192 ms). The relative peak magnitudes from the two stimulus pulses could be compared to get a measure of recovery. Plotting this recovery against the interstimulus interval yielded a single exponential relationship (Figure 4E, F). Figure 5.4F shows the mean recovery from inactivation kinetics expressed as normalised peak amplitude against interpulse interval and fitted with a mono-exponential function, as in D. The time mean constant for the recovery from inactivation (τ) was 1.11 ± 0.3 s (n = 6).

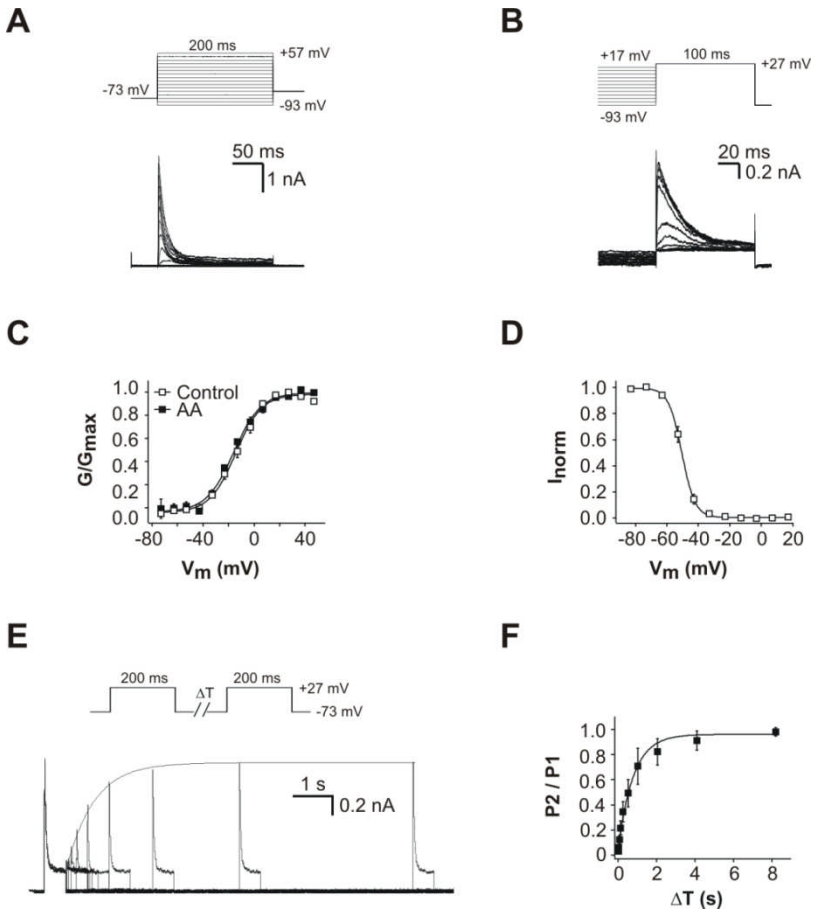

Figure 5.4 Biophysical properties of AA treated Kv1.2 currents. A Representative currents obtained from AA treated Kv1.2 transfected cells in response to voltage steps from −73 mV to potentials between −93 and +57 mV in 10 mV increments. **B** Steady-state inactivation of AA treated Kv1.2 currents. Currents were obtained with a double pulse protocol: 200 ms conditioning pulses to potentials between -93 and +17 mV were applied from a holding potential of −73 mV and the steady-state inactivation was assessed from the peak outward current during the subsequent step to +27 mV. **C** Normalised GV plot showing the steady-state activation obtained from peak outward K^+ currents before (open symbols) and after 100 µM AA (closed symbols). Data was fitted with a Boltzmann function. **D** Normalised current plot of steady-state inactivation as obtained from the double pulse protocol described in B. Data was fitted with a Boltzmann function. **E** The kinetics of recovery from AA induced inactivation was analysed with a double pulse protocol shown above: A 200 ms prepulse from −73 mV to +27 mV was followed by a second 200 ms test pulse to +27 mV after an interstimulus interval of variable duration (16 to 8192 ms) at −73 mV. Recovery of peak amplitude could be fit with a single exponential function. The solid line show a superimposed fit for the normalised peak amplitude against interpulse interval (τ = 1.91 s) **F** Mean recovery from inactivation kinetics expressed as normalised peak amplitude against interpulse interval. Normalised peak amplitudes were fit with a monoexponetial function as in D (τ = 1.11 ± 0.3 s; n = 6).

5.2.2 PUFAs inhibit Kv1.2 currents

Ion channels modulation is rarely a property of a single fatty acid family member but rather fatty acids displays trends in activity across series of chemical analogues (Borjesson et al., 2008, Guizy et al., 2008, Sun et al., 2007). Because of this, structurally related fatty acids were also examined for potency against stably expressed Kv1.2 currents. Figure 5.5 shows the effects of a series of PUFAs against Kv1.2-mediated currents: linoleic acid (LA), DHA, and linolenic (LnA) acid. These molecules are PUFAs which vary in the length of their fatty acid tail and the position and number of double bonds within their structure and are important biological lipids present in significant quantities within mammalian cell membranes (Abbott 2012).

LA is an essential fatty acid in humans and used in the biosynthesis of AA. Like AA it is a member of ω-6 fatty acid family, and it had comparable effects to AA on Kv1.2-mediated currents (Figure 5A, C). Like AA, the effects were dose-dependent and partially reversible upon wash off. However LA did not inhibit peak outward currents or increase the rate of inactivation to the same degree. 100 μM LA resulted in a reduction of steady-state current by 58.9 ± 9.5% (measured at +27 mV, n = 4). Of the series of PUFAs tested, the ω-3 fatty acid DHA at 100 μM showed the most comparable effect to AA, inhibiting a mean 78.5 ± 6.8% of the steady-state current (Figure 5A, C). DHA is a highly unsaturated molecule containing two additional carbon atoms and two additional double bonds, compared to AA. The increased activity of AA and DHA over ALA is consistent with findings from other channels that the degree of saturation is important for the effects on ion channels (Borjesson et al., 2008, Sun et al., 2007). Somewhat surprisingly therefore were the findings that the ω-3 PUFA LnA was largely inactive against Kv1.2-mediated currents (<5% block after 100 μM LnA application, n = 3) despite the high degree of unsaturation in its tail.

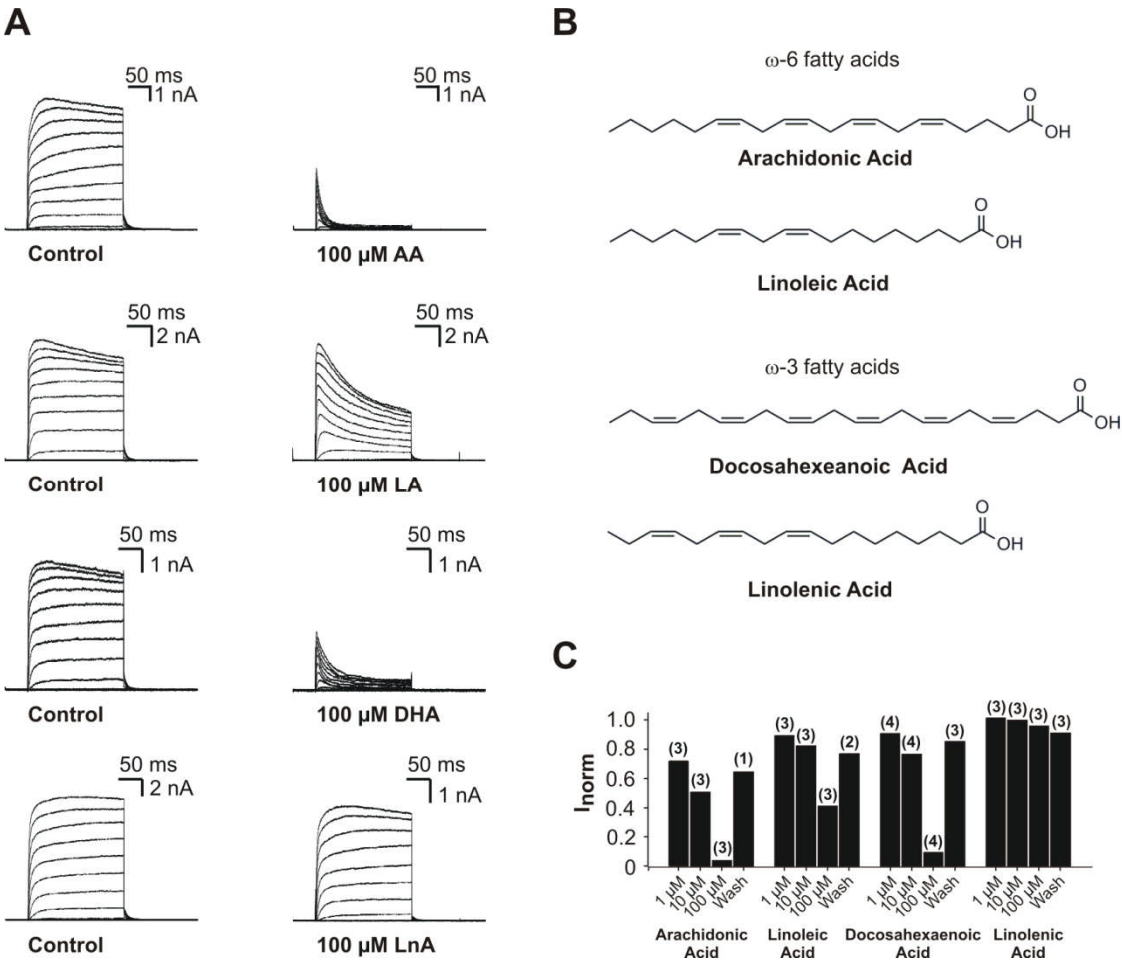

Figure 5.5 The effects of PUFAs on Kv1.2 currents. A Current traces from Kv1.2-transfected HEK293 cells in the absence (control) and presence of various PUFAs (100 µM). **B** Chemical structures of the PUFAs examined in A **C** Graph showing the normalised steady-state current remaining after application of various concentrations of PUFAs. Steady-state currents were measured at 10 ms from the end of a +27 mV voltage step shown in A. Currents were normalised to the current magnitude as measured in normal bath solution. The number of successful measurements is shown in parenthesises. Current measurements for "Wash" represent 10 minutes of perfusion in normal bath solution post PUFA application.

5.2.3 MUFAs show little activity against Kv1.2 currents

Alongside these PUFAs, a range of MUFAs were also examined for activity. A series of naturally occurring dietary fatty acids of different lengths and double bond position were chosen for investigation: palmitoleic acid (PA), oleic acid (OA), elaidic acid (EA), nervonic acid (NA), erucic acid (ErA) and petroselinic acid (PSA) (Figure 5.6). As a series, MUFAs caused considerably less inhibition and induced less inactivation than PUFAs. The measured steady-state currents were reduced 0-23% across the series. 100 µM PA displayed the greatest inhibition (22.4 ± 3.6%, n = 3; Figure 5.6C). Three MUFAs; EA, ErA and PSA showed no inhibition at any of the concentrations tested. The general lack of activity of MUFAs as a series prevented any significant analysis of the structure-activity relationship except to note that the relative inactivity of the MUFAs is consistent with reports that SFAs and MUFAs are less active than their polyunsaturated counterparts against some Kv channel members (Borjesson et al., 2008).

In line with the analysis of the important structural features of fatty acids for their activity against Kv1.2, the relative contribution of the fatty acid head group was assessed (Figure 5.7). For that reason, the effects of externally applied ethyl arachidonate (EtA) and AEA were assessed for activity. AEA, or anadamide is the ethanolamine ester of AA, and has been the focus of considerable interest due to its activity against the CB1 and CB2 cannabinoid receptors (Vemuri and Makriyannis, 2015). AEA was found here to have considerable inhibitory effects against Kv1.2-mediated currents, blocking 16.2 ± 8.9% of the steady-state current at 10 µM and 77.9 ± 4.6% at 100 µM (Figure 5.7B, C; n = 3). This inhibition was slightly less than that observed for the free AA and was comparable to DHA in the extent of its effect. EtA also displayed a notable inhibition of Kv1.2 currents. Interestingly however this inhibition was less than that of AEA (49.7 ± 8.5% at 100 µM; n = 3). These results suggest that the free acid head group is not as important to the inhibitory effects of the fatty acid as the presence and organisation of double bonds within the fatty acid tail.

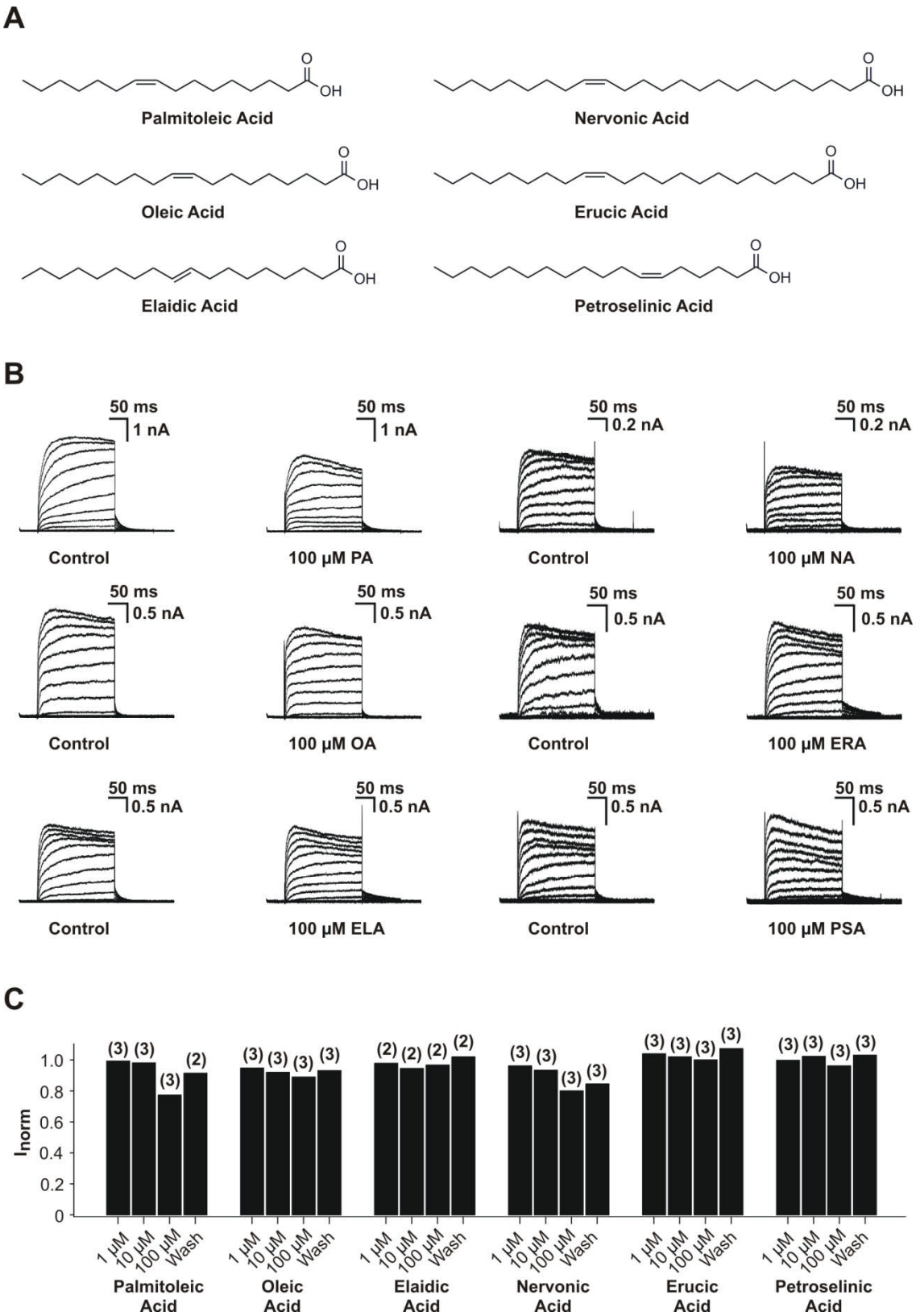

Figure 5.6 The effects of MUFAs on Kv1.2 currents. A Chemical structures of the MUFAs examined. **B** Kv1.2 current traces in the absence (control) and presence of various PUFAs (100 µM). **C** Graph showing the normalised steady-state current remaining after application of various concentrations of MUFAs. Steady-state currents were measured as in Figure 5.5C.

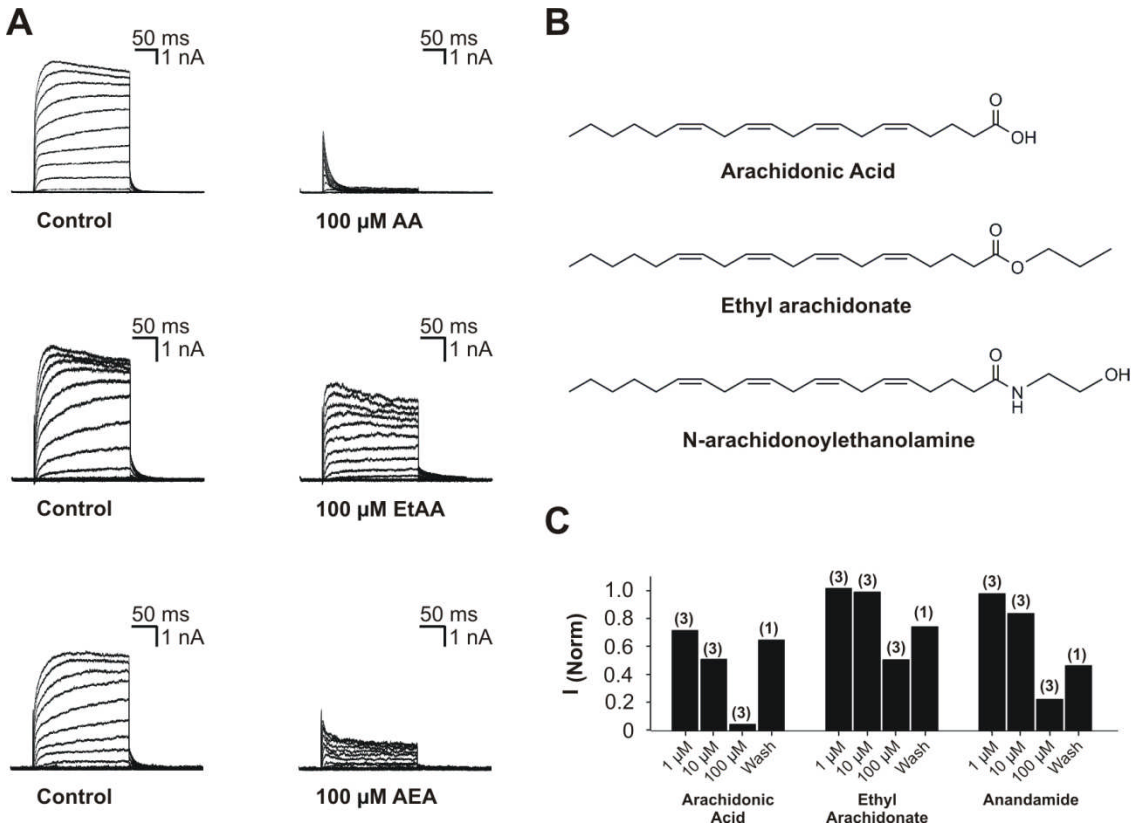

Figure 5.7 The effects of carboxylic acid-functionalised fatty acids on Kv1.2 currents. A Kv1.2 current traces in the absence (control) and presence of various AA, EtAA and AEA (100 µM). **B** Chemical structures of the carboxylic acid-functionalised fatty acids examined. **C** Graph showing the normalised steady-state current remaining after application of various concentrations of functionalised fatty acids. Steady-state currents were determined as in Figure 5.5C.

5.2.4 Synthesis of conformationally restricted fatty acid analogues

Fatty acids are highly flexible molecules. They are capable of the participating in highly ordered structures, e.g. plasma membranes (Feller, 2008), but studies have shown that even unsaturated fatty acids retain significantly flexibility within their molecule, and are capable of occupying several distinct low energy conformations (Shaikh, 2012). The role of polyunsaturation in determining the conformation and topology of fatty acids was examined through a chemical biology approach. Chemical strategies were employed to develop fatty acid molecules with inherent conformational restrictions within their molecule.

Conformational restriction (sometimes called “rigidification”) is a strategy aimed at reducing a molecules inherent flexibility. This can help ligands obtain the “best” conformation for binding and minimise the entropic loss in taking up the bioactive conformation, thus enhancing the potency and selectivity of a drug (Fang et al., 2014). This can be achieved by introducing unsaturated double or triple bonds to prevent rotational movement around carbon-carbon bonds or by the introduction of steric or chemical moieties which help favour particular conformational states over others. Additionally, intramolecular interactions through the use of covalent and non-covalent interactions can significantly alter and restrict the free movement of a molecule (Figure 5.8). Here, the incorporation of ring systems or cycles into saturated or unsaturated fatty acids was examined to determine its effect on Kv1.2 inhibition. Ring systems can be either aliphatic or aromatic. Aromatic ring systems were chosen due to their increased rigidity over aliphatic ring systems and for their better chemical tractability (synthesis feasibility). Aromatic rings can be comprised of exclusively hydrocarbons, or Alternatively, contain heteroatoms in their ring system, known as heteroaromatic systems.

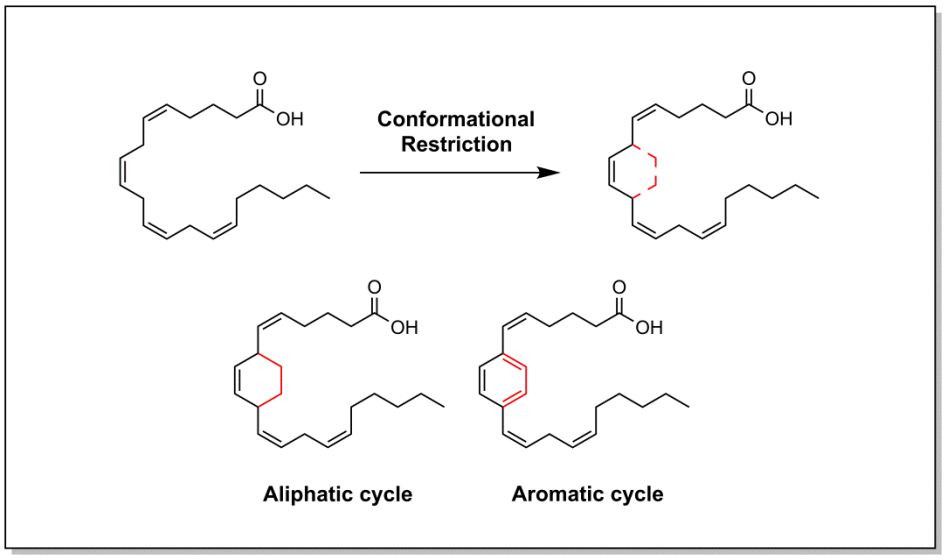

Figure 5.8 Design of conformationally restricted fatty acid analogues. An example of how conformational restriction can be achieved in AA by creating intramolecular cheminal rings or cycles. The example cycle comprises 6 atoms, linking atom N and N+3, but could be expanded to link more distant atoms. These cycles can either be aliphatic or aromatic.

Incorporation of a phenyl moiety within the aliphatic "tail" of the fatty acid (Scheme 5.1) required the alkylation of a benzene core with the requisite alkyl and acid groups. The approach adopted here used palladium-catalysed cross-coupling alkynylation to form the important carbon-carbon bonds. This approach had the advantage of making fatty acids which, alongside the desired aromatic group, contained multiple alkyne features. These could be reduced partially and in a stereoselective manner to give access to the polyunsaturated series of analogues (Scheme 1). Or alternatively they could be reduced completely to yield saturated aromatic fatty acids. Scheme 5.1A and B shows the synthetic route to obtain both the 1,4- and 1,3- functionalised aromatic fatty acid analogue of AA.

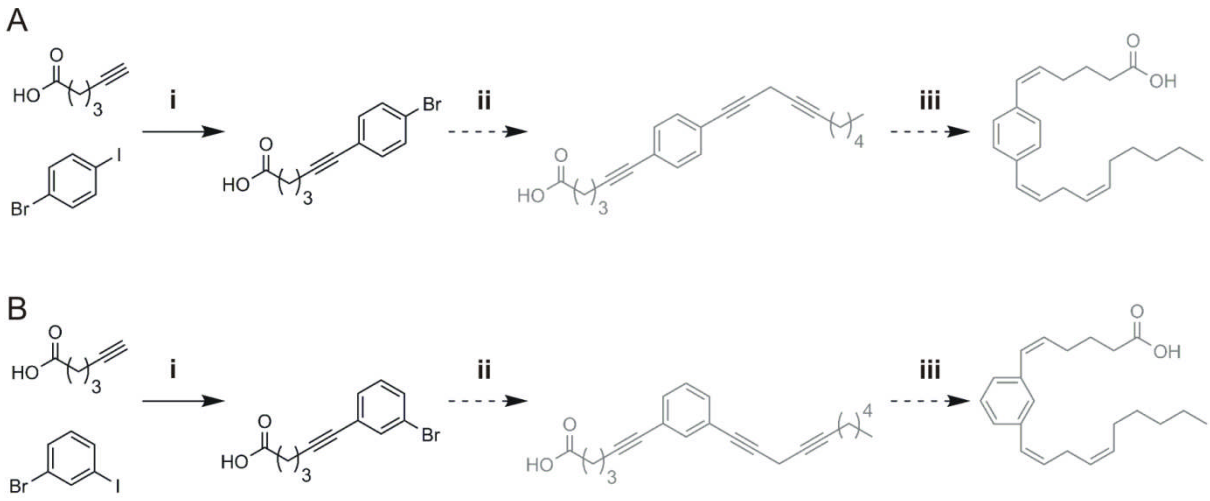

Scheme 5.1 Synthesis of aromatic analogues of AA. (i) $Pd(PPh_3)_4$, CuI, DIPEA, THF, 40^0C, 24hr (ii) 1,5-Decadiyne (For condition See Table 5.2) (iii) H_2, Lindlar catalyst. Dotted arrows and grey structures show unsuccessful steps.

The initial synthetic step (Scheme 5.1(i)) involved the cross-coupling of the carboxylic acid chain with the aromatic core via palladium coupled sonogashira reaction. The reaction proceeded with good yields (40-70%), under mild temperatures and reacted selectively with the iodo-functionality. However the 2nd cross-coupling alkynylation

step proved very difficult and was ultimately the limiting step in this synthesis (Scheme 5.1(ii)). Reaction of the bromophenyl-hexynoic acid product with 1,5-Decadiyne under thermal conditions showed no appearance of the bi-functionalised benzene, as monitored by LCMS. Increased temperature, reaction times and catalyst loading (2-10 mol%) also failed to facilitate the alkynylation. Similarly, modifying the amine base used in the reaction (Et_3N/DIPEA/Piperidine) made no impact. Table 5.2 shows the extensive reaction conditions examined in this study.

A recent advance in transition-metal catalysed reactions has been the use of designer amphiphiles or surfactant molecules to considerably increase the rate and efficiency of reactions (Klumphu and Lipshutz, 2014). These surfactant molecules form nanomicelles in water which are proposed to serve as nanoreactors for transition-metal chemistry. To this end we examined the effects of performing the alkynylation step in nanoparticles composed of the surfactant DL-α-Tocopherol methoxypolyethylene glycol succinate (TPGS). Accordingly the reaction was carried out in the presence of 2% TPGS in water at room temperature. After 24 hours agitation, no product could be observed by LCMS.

As an alternative synthetic strategy, microwave-assisted sonogashira chemistry was explored. Microwave chemistry involves using microwave irradiation to promote chemical reactions instead of the conventional externally applied thermal heating. Microwave-assisted reactions have many advantages over traditional thermal heating and can be associated with increased chemical reaction rates and higher chemical yields than thermal heating alone (de la Hoz et al., 2005). Microwave-assisted sonogashira chemistry has been employed successfully in a number of studies and has been shown, in some cases, to radically improve reaction times and efficiencies (Erdelyi and Gogoll, 2001, Mehta and Van der Eycken, 2011). Because of the higher throughput, a range of conditions and catalysts were tested. Three different Pd catalysts were examined: $Pd(PPh_3)_4$, $Pd((o\text{-tolyl})_3P)_2Cl_2$ and $Pd(PPh_3)_2Cl_2$ along with two other pre-catalyst Pd(II) complexes: $Pd(acac)_2$ and $Pd(OAc)_2$ which were reduced to their active complexes *in situ* by addition of PPh_3. Further, Cu(I)I (10 mol%) was either added or left absent from the reaction mix. These various permutations gave rise to 12 unique reactions (detailed in Table 5.2). Although trace amounts of the bi-functionalised aryl could be identified by LCMS, no successful product was yielded by this approach.

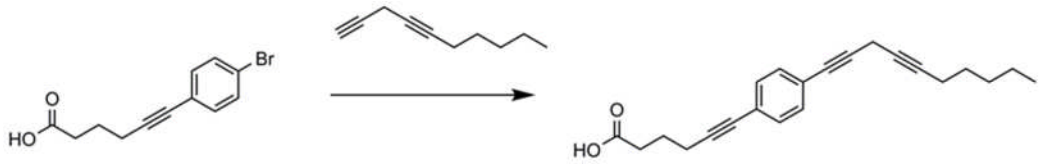

Table 5.2 Reaction conditions examined for the 2nd cross-coupling alkynylation step. As detailed in Scheme 5.1(ii). Abbreviation: TPGS - DL-α-Tocopherol methoxypolyethylene glycol succinate DIPEA - Diisopropylethylamine; Solv. - Solvent; DMF - Dimethylformamide.

Catalyst	mol %	CuI	PPh_3	Base	Solv.	Therm /µW	Temp	Time
$Pd(PPh_3)_4$	2	●		DIPEA	THF	Therm	66^0C	24 hr
$Pd(PPh_3)_4$	2	●		DIPEA	DMF	Therm	80^0C	24 hr
$Pd(PPh_3)_4$	5	●		DIPEA	DMF	Therm	80^0C	24 hr
$Pd(PPh_3)_4$	10	●		DIPEA	DMF	Therm	80^0C	24 hr
$Pd(PPh_3)_4$	5	●		Et_3N	DMF	Therm	80^0C	24 hr
$Pd(PPh_3)_4$	5	●		DIPEA	DMF	Therm	120^0C	24 hr
$Pd((PPh_3)_2Cl_2$	6	●		Piperidine	DMF	Therm	116^0C	24 hr
$Pd(PPh_3)_4$	2			Et_3N	H_20, TPGS	NA	RT	24 hr
$Pd(PPh_3)_4$	5			Et_3N	DMF	µW	100^0C	5 min
$Pd((o\text{-}tol)_3P)_2Cl_2$	5			Et_3N	DMF	µW	100^0C	5 min
$Pd(acac)_2$	5			Et_3N	DMF	µW	100^0C	5 min
$Pd(PPh_3)_4$	5	●		Et_3N	DMF	µW	100^0C	5 min
$Pd((o\text{-}tol)_3P)_2Cl_2$	5	●		Et_3N	DMF	µW	100^0C	5 min
$Pd(acac)_2$	5	●		Et_3N	DMF	µW	100^0C	5 min
$Pd(PPh_3)_2Cl_2$	5		●	Et_3N	DMF	µW	100^0C	5 min
$Pd(OAc)_2$	5		●	Et_3N	DMF	µW	100^0C	5 min
$Pd(PPh_3)_4$	5	●	●	Et_3N	DMF	µW	100^0C	5 min
$Pd((o\text{-}tol)_3P)_2Cl_2$	5	●	●	Et_3N	DMF	µW	100^0C	5 min
$Pd(OAc)_2$	5	●	●	Et_3N	DMF	µW	100^0C	5 min
$Pd(PPh_3)_2Cl_2$	5	●	●	Et_3N	DMF	µW	100^0C	5 min

Finally, the order in which the reactants were attached to the benzene scaffold was also reversed. Monitoring with LCMS showed the formation of the 1,5-Decadiyne aryl product which could be purified out and isolated, but subsequent reaction with the alkyne carboxylic acid resulted in the same non-reactivity. Additional modification of the synthesis replaced the 1,5-decadiyne reactant in the original synthetic pathway with potentially more reactive alkyne reagents. Accordingly, the bromophenylhexynoic acid intermediate was reacted with other terminal alkynes such as Heptyne, Pentyne and Propargyl alcohol. This failed to improve reactivity however.

For this reason an alternate synthetic approach was pursued. The incorporation of a heteroaromatic rings into the fatty acid tail provided a much wider scope for chemical synthesis due to the availability of reactive nitrogen-containing starting reagents and the ability to form the aromatic structure *in situ*. To this end, a synthetic approach utilizing 1,3-dipolar cycloaddition was developed. This approach, often referred to as "click chemistry" was chosen due to its reported effectiveness and versatility. "Click chemistry" refers to a subset of chemical reactions which are particularly high yielding; generating products quickly and reliably, usually under relatively mild conditions (Kolb et al., 2001). This also had the advantage of allowing access to aromatic fatty acid structures in a single step.

Scheme 5.2A-F shows the synthetic route used to obtain a series of heteroaromatic fatty acid analogue of varying length. Note that the orientation of the triazole group could be altered depending on arrangement of the functional groups on the starting materials. The alkyl azide intermediate was formed *in situ* and further reaction with the alkyne was done without isolation of the azide. This effectively allowed heteroaromatic fatty acids to be formed in a single chemical step. Reactions proceeded rapidly under mild conditions with total conversion of materials to product after 24 hours. Adjustment of the resulting reaction mixture to pH3 followed by filtration and extraction yielded pure product without the need for further purification. Yields varied widely (15-59%) and correlated with the tail length of the fatty acid being synthesised. The longer chained fatty acids were isolated in significantly higher yields. This was proposed to result from the poorer organic solubility of short fatty acids at the extraction step. To examine the

effect of differences in fatty acid length two acids from each of the medium-chain fatty acids (MCFAs, 6-12 carbon atoms), long-chain fatty acids (LCFAs, 13-21 carbon atoms) and very long-chain fatty acids (VLCFAs, 22< carbon atoms) (Lemarie et al., 2015) were designed and tested for their inhibitory potential against Kv1.2.

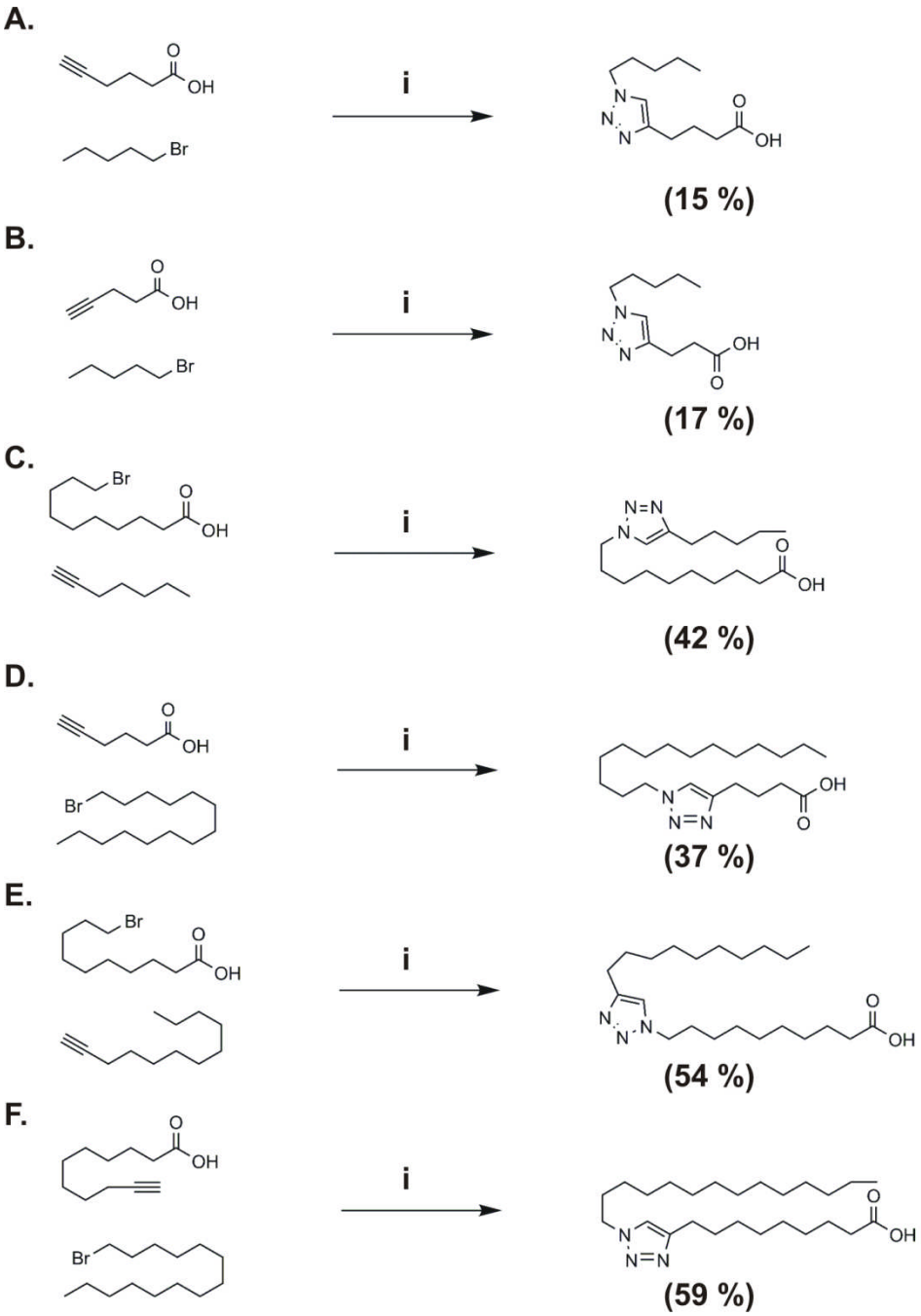

Scheme 5.2 Synthesis of heteroaromatic fatty acids. (i) NaN_3, Cu(I)O, MeOH, 40^0C, 24hr. Yields are shown in parenthesises.

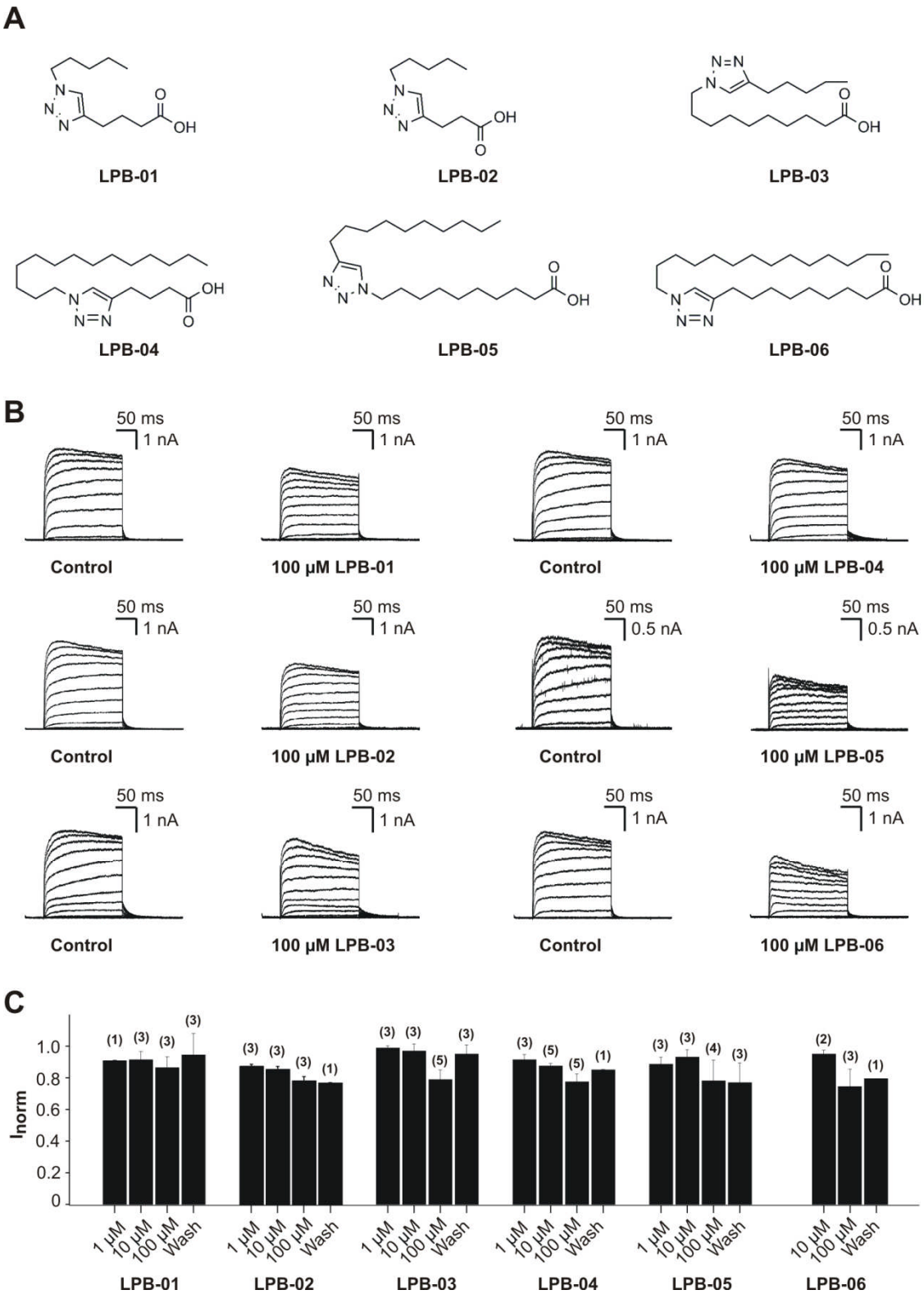

Figure 5.9 The effect of heteroaromatic fatty acids on Kv1.2 currents. **A** Chemical structures of the aromatic fatty acids examined. **B** Kv1.2 current traces in the absence (control) and presence of various aromatic fatty acids (100 µM). **C** Graph showing the normalised steady-state current remaining after application of various concentrations of aromatic fatty acids fatty acids. Steady-state currents were measured as in Figure 5.5C.

Figure 5.9 shows the effects of the six aromatic fatty acid analogues tested against Kv1.2 currents. The two MCFAs, LPB-01 and LPB-02, displayed a modest inhibitory effect against Kv1.2. At 100 µM, LPB-01 and LPB-02 reduced the steady-state current magnitude by 12.3 ± 6.6% (n = 3) and 21.8 ± 2.8% (n = 3) respectively. This effect was dose dependent and reversible upon washing out. LCFA analogues, LPB-03 and LPB-04, showed a similar inhibitory potency against Kv1.2. At 100 µM, LPB-03 and LPB-04 reduced the steady-state current magnitude by 20.8 ± 5.9% (n = 5) and 22.3 ± 4.9% (n = 5) respectively. This was equivalent to the effects of the most potent MUFAs such as nervonic acid or palmitoleic acids (Figure 5.6) but considerably less effective than the PUFAs. The VLCFAs, LPB-05 and LPB-06, produced a current inhibition of 21.7 ± 12.9% (n = 4) and 15.4 ± 11.1% (n = 3) respectively, at 100 µM. At the maximal VLCFA dose tested however (100 µM), a precipitate was observed. Therefore, the tested concentration of LPB-05 and LPB-06 were probably less than the desired 100 µM.

5.3 Discussion

Kv1.2-containing channels are important mediators of SGN LVA K^+ currents. In this chapter the effect of native and synthetic fatty acids against the Kv1.2 channel were investigated. PUFAs, exemplified by AA, were found to be strong inhibitors of stably expressed Kv1.2 currents, markedly increasing the inactivation rate of the channel. These effects were also seen in PUFA analogues modified at the carboxylic head group, such as AEA. The inhibitory effect of fatty acids, however, declined sharply with increasing saturation of the fatty acid tail, pointing to a key role of the fatty acid chain in the activity of FFAs. A chemical biology approach was pursued, focusing on conformational restriction of the free fatty acid carbon tail. Accordingly, a simple and efficient synthesis was developed to access a range of novel aromatic fatty acid structures in a single step. Although low activity was noted in the initial series of analogues, chemically modified fatty acids could provide a useful approach to adjust the activity and biophysical properties of FFAs against Kv1.2.

5.3.1 Physiological functions for FFA modulation of voltage-gated ion channels

Alongside its myriad roles in cellular signalling pathways, FFAs exert important effects upon membrane bound ion channels directly (Boland and Drzewiecki, 2008). The modulation of various ion channels has been implicated as an important determinants in neuronal transmission, synaptic plasticity, cardiac and ischemic disease and aging (Lee et al., 2008, Horrocks and Farooqui, 2004, Michael-Titus and Priestley, 2014, Boland and Drzewiecki, 2008).

Evidence of a physiological role for fatty acid modulation in neuronal signalling comes from the action of PUFAs on ion channels and synaptic plasticity. Kv4 channels are highly localised to post-synaptic membranes in the hippocampal CA1 region and regulate long-term potentiation (LTP) through their role in the integration of high frequency trains of synaptic activity (Tkatch et al., 2000, Andrasfalvy et al., 2008). Application of DHA or AA to Kv4 currents results in marked inhibition and increase inactivation (Boland et al., 2009). Inhibition of phospholipase A2 (an enzyme that produces free fatty acids from a precursor glycerol molecule) blocked LTP in a manner that could be reversed by direct application of DHA or AA (Fujita et al., 2001, Wolf et al., 1995). In this way FFAs have been proposed as signalling molecules in synaptic plasticity.

FFAs have also been proposed as important ameliorators of hyper-excitability in neurons. Under conditions of ischemic-reperfusion injury and seizure, neurons release high quantities of AA into the surrounding media (Lipton, 1999). AA has been postulated to have a neuroprotective effect by dampening the pathological excitability that may arise under these conditions (Bazan et al., 2002). This effect is achieved primarily through its inhibitory actions on Na^+ and Ca^{2+} channels. This is of particular importance in injured neurons where structural degradation of the axolemmal bilayer can lead to chronically left-shifted or “leaky” Nav channels (Morris et al., 2012). There is now considerable evidence to suggest that fatty acids, and in particular ω-3 fatty acids, can act as neuroprotective molecules in disease and aging (Michael-Titus and Priestley, 2014, Lin and Perez-Pinzon, 2013, Denis et al., 2015).

However, PUFA inhibition of K^+ channels might also be expected to oppose these protective effects. It has been suggested that local differences in the FFA concentration might lead to preferential inhibition some channels over others (Boland and Drzewiecki, 2008). A simpler and more satisfying explanation is that the neuroprotection observed in studies of disease and aging arise from the pleiotropic effects of FFA *in vivo,* including vasodilation of brain arteries, and neuroplasticity (Blondeau et al., 2015).

An alternative hypothesis suggests that PUFAs can act to reduce the excitability of neurons by left-shifting the voltage-sensitivity of certain Kv channels in neurons. Specifically, PUFAs were demonstrated to left-shift the voltage dependence of activation of the Shaker Kv channel (Borjesson et al., 2008, Borjesson and Elinder, 2011). More recently these effects were recapitulated in the Kv7.1 and KCNE1/Kv7.1 mammalian channel (Liin et al., 2015). These results have not been validated in brain tissue however so the extent of this effect on neuronal firing is unknown. Together, these results suggest that FFAs may have heterogeneous effects across different tissue and channel types.

As shown in this this study, an important factor in determining whether channel function will be affected is the concentration at which various FFAs are present in the ion channel environment. In the blood plasma, free fatty acid concentration is heavily buffered by the presence of fatty acid binding proteins and albumin. On average, two FFA molecules are bound to each albumin molecule under normal physiological conditions. Accordingly, serum concentrations of unbound FFAs can regularly be less than 20 nM (Oliveira et al., 2015). Whilst the relative composition of FFAs within tissues is routinely reported, considerably less is reported about the absolute concentrations of these various FFAs. For free AA, the levels are typically described as “low”. Resting leukocytes reportedly contain around 0.5–1 µM free AA (Chilton et al., 1996) whilst isolated islets of Langerhans cells, by comparison, have resting level of AA of about 15 µM, as measured by mass spectrometry (Ramanadham et al., 1992). Nonetheless, free AA is disproportionately low compared with the vast quantities of the esterified AA motif contained within the cells’ plasma membrane. This has been calculated as corresponding to approximately 5 mM in platelets (but in specific subcellular compartments such as membranes, this may be substantially higher) (Brash, 2001). The low level of AA detected in the cytosol likely reflects the activity of

enzymes, such as cyclooxygenases and acyl transferases which use AA as a substrate (Irvine, 1982). This low concentration of free AA would suggest relatively little K^+ channel modulation under non-pathological, resting conditions. However, the vast reservoirs of esterified arachidonate contained in the plasma membrane means receptor-mediated liberation of as little as 1% of this reserve could give up to 50 µM local concentration of FFA. In fact, in platelets, the percentage of esterified arachidonate liberated upon activation is around 10% (Neufeld and Majerus, 1983). Ion channels in tissues under pathological conditions may also experience abnormally high levels of FFAs. In samples of inflamed skin tissue from psoriasis patients, free AA is abundant, with approximately 30 µg/g of free AA detected. This represents an effective cellular concentration of 100 µM free AA; equivalent to the highest dose tested in our study (Hammarstrom et al., 1975). This suggests a role for FFA K^+ channel modulation in tissues under conditions of receptor-mediated activation or under conditions of pathological dysregulation.

Subsequent experiments, building on work in this chapter, should focus on the effects of FFAs on the membrane properties of SGNs. AA has already been shown to affect the electrophysiology of SGNs in neonatal rats (Ruel et al., 2008), potentiating the excitatory effects of NMDA signalling. Further experiments should examine whether AA inhibits Kv1.2-mediated LVA currents in isolated SGNs and whether AA and other FFAs can change their firing properties as observed under the influence of other agents elsewhere in this thesis.

5.3.2 How do fatty acids modulate the activity of Kv1.2?

The fatty acid motif is ubiquitous in the plasma cell membrane, comprising an important component of both structural phospholipids and triglycerides. The presence of free FFAs is dynamic and tightly regulated however. These FFAs may modulate the function of membrane embedded ion channels in a number of ways (Moreno et al., 2012). First, they may change the biophysical properties of the membrane, changing the mechanical forces upon the channel or how the membrane conducts charge. Secondly, they can modify the hydrophobic interactions between the ion channel and the lipid

bilayer. Finally, they can interact directly with specific amino acids in the ion channel, altering gating or affecting the conduction of ions through the pore.

One caveat anticipated here is the heterologous nature of the Kv1.2 expression system and the differences the Kv1 channels in SGNs. Expressed in HEK293 cells, the Kv1.2 gene produces functional Kv1.2 homomers with an expression profile determined by the translation and trafficking properties of the cell line as well as the copy number of the gene. These channels may differ from those in SGNs in a myriad of ways, not least because they represent a purely homomeric population of Kv channel. Heterologous channels are also absent co-expression with any auxillary subunits, which can radically alter the functional and expression characteristics of the Kv channel. Heterologous channels may also experience different post translation modifications compared to SGNs. The differences in physical properties of the membrane and the lipid species which are present can also alter the gating and conductive properties of the channel (Combs et al., 2013). Finally, the relative proportions and concentrations of FFA most likely differ in HEK293 cells from those experienced by SGNs *in vivo*. Nonetheless, Kv1.2 channels, stably expressed in HEK293 cells, offer a practical and efficient way to examine the effects of FFAs on LVA K^+ channels, which can be subsequently validated in the isolated SGN preparation. This allows for a much higher throughput than would be possible in an isolated SGN preparation.

In this study, stably expressed Kv1.2 currents showed a marked sensitivity to externally applied PUFAs. AA provided the greatest inhibition; 10 µM AA reduced the steady state current by approximately half. The inhibitory activity of AA at low µM concentrations is in line with the values reported for plasma concentrations of free, unesterified AA (1–15 µM) (Burtis et al., 1999). Because of the dynamic interconversion of fatty acids products near plasma membrane and the potential for receptor mediated liberation of AA, it is very conceivable that local concentrations of AA are, at times, much higher (Boland and Drzewiecki, 2008). The induction of rapid inactivation observed in this study is notable effect of PUFAs across various Kv channels (Table 5.1). The molecular basis for this effect is still controversial. Nonetheless, the general effect of PUFAs on the fluidity and mechanics of the lipid environment has been disfavoured as an “imprecise” explanation for their effects since not all ion channels are targets for PUFA modulation (Boland and Drzewiecki, 2008).

There is now a strong body of work suggesting PUFAs make important direct intermolecular interactions with residues within the Kv channel.

The site of action of PUFAs is also controversial. The current consensus is that PUFAs act at the cytoplasmic side of the membrane. Evidence for this arrives from multiple independent observations. TEA reduces the fractional block of AEA against Kv1.5 when applied intracellularly but not when TEA is applied externally (Moreno-Galindo 2010). Similarly, mutation in key pore residues at the intracellular side of the membrane abolish the inhibitory effects of applied AA against Kv1.1 (Decher et al., 2010). Finally, external application of the membrane impermeant arachidonoyl-coenzyme A failed to replicate the inhibition and inactivation displayed by AA against Kv4/KChIP expressed in Xenopus oocytes (Boland 2009). However, some reports have shown evidence for a preferential effect of PUFAs on the external leaflet of the membrane and have suggested they exert their effect by interaction with an external binding site on the channel (Honore et al., 1994, Guizy et al., 2008). These reports are complicated by the fact that FFAs can cross the plasma membrane easily to access both sides of the channel.

The exact binding site of FFAs to the Kv channel has also been the focus of some investigation. Currently the most likely hypothesis has come from Decher and colleagues, who carried out a systematic mutational analysis of the important intracellular residues for AA binding to the inner cavity of Kv1.5. This study is particularly relevant for the analysing AA binding as the inner cavity of Kv1.5 is identical in sequence to all Kv1.x channels (Decher et al., 2010). They identified a number of key hydrophobic residues which, when mutated, abolished the effects of AA current inhibition (Figure 5.10). These residues, representing a “binding site” for AA, were all in close proximity to the central conducting pore region. Virtual simulations of AA interaction with these residues suggested a physical occlusion of the central pore via hydrophobic interactions between the aliphatic tail of the FFA and the pore. Interestingly the proposed binding overlaps considerably with the binding site for the Kvβ1.1- and Kvβ1.3- peptide binding site (Decher et al., 2005, Decher et al., 2008, Zhou et al., 2001a). AA acid inhibition superficially resembles the N-type inactivation induced by Kvβ1.1- and Kvβ1.3 action in Kv channels. In fact, when the Kv1.1 channels are co-expressed with Kvβ1.1, the fractional block of AA was significantly reduced. This provides appealing evidence that AA and the Kvβ1.1 ball peptide are

competing for the same binding site at the inner pore of the channel (Decher et al., 2010). The molecular mechanism of AA acid induced inactivation of Kv channels can be seen as analogous to the N-type inactivation imparted by Kvβ1 auxiliary subunits.

This proposed mechanism of action is by no means shared across Kv channel subtypes, or in other voltage-gated ion channels in general. In certain cases such as Kv7.1 and BK channels, where currents are *enhanced* by FFA application, this is almost certainly not the case. But there is some experimental evidence to support the idea of an open channel block across channel subtypes, and further speculation that implies that this may in fact be the case. The strongest evidence for a shared mechanism comes from the common etiology of the fatty acid effect. The inhibition of I_k magnitudes and increased rates of inactivation are observed in both non-inactivating and inactivating currents alike (Table 5.1). Similar changes in the voltage sensitivity are also observed. Furthermore, these effects are commonly observed in both Nav and Cav channels (Bendahhou et al., 1997, Xiao et al., 2006, Chemin et al., 2001, Talavera et al., 2004). Empirical evidence for this shared mechanism is also provided by evidence that FFA modulation is sensitive to analogous mutations across different ion channels. Mutation of a key isoleucine residue which is located in the inner cavity of the pore of the potassium channel Kv1.1 (I400V) abolishes the modulatory effects of externally applied AA and AEA. This insensitivity to FFAs can be introduced into other Kv channels such as Kv3.1 channels by making mutations to the analogous isoleucine residue in the inner cavity (I428). Molecular dynamics and docking simulations have also reached similar conclusion about the sites of action of FFAs across different ion channels (Decher et al., 2010).

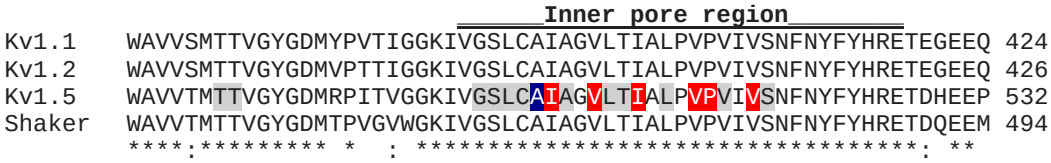

Figure 5.10 A putative binding site for AA at the inner pore region of Kv1 channels. Sequence alignment showing the inner pore region of the Kv1.1, Kv1.2 and Kv1.5 channels along with the Kv1-like Shaker channel. Highlighted residues are sites that were mutated in the Kv1.5 channel to examine their effect on AA binding. Each residue was mutated to an alanine to examine its effect on binding, except for A501, A503, and A509 which were mutated to valines and L510 which was mutated to a methionine. Red: Mutations which resulted in a loss of channel block in response to AA. Blue: Mutation which enhanced the channels sensitivity to AA. Grey: residues which made no impact on AA block when mutated. Results from Decher at al., 2010.

5.3.3 The structure-activity relationship of fatty acids and voltage-gated ion channels

Despite the activity of certain PUFAs such as AA and DHA against a wide range of channels, there is surprisingly little room to accommodate changes in the fatty acid structure itself. Any variation on the structure of AA was found to reduce the activity of FFA against Kv1.2 or abolish it completely. The most significant effects occurred with changes to the structure of the fatty acid tail. This is consistent with experiments which suggest open channel block is achieved through interactions between hydrophobic residues in the pore region and the hydrocarbon tail of the fatty acid (Decher et al., 2010).

The effect of FFAs on Kv1.2 showed a sharp drop off in activity between FFAs that contained multiple double bonds and those that contained just one. In fact, apart from the notable exception of linolenic Acid, all PUFAs displayed notable Kv1.2 modulation at 100 µM. In contrast MUFAs displayed little or no effect at the same concentration. This trend has been replicated in other Kv channels (Borjesson et al., 2008, Honore et al., 1994) and Nav channels (Xiao et al., 1995). Against the Cav3.1, Cav3.2, and Cav3.3 channels, Chemin et al., starting with the fully saturated arachidic acid, showed a linear increase in potency with the addition of 1, 2, 3, 4 and 5 double bonds to the molecule

(Chemin et al., 2007). Some MUFAs, in particular oleic acid, do modulate the activity of a subset of Kv channels which were positively modulated by PUFAs, i.e Kv7.1 and BK channels (Sun et al., 2007, Liin et al., 2015).

The relative inactivity of SFAs and MUFAs across voltage-gated ion channels is difficult to explain in terms of molecular interaction alone. In fact, virtual docking simulations based on the interaction of AA and the 'open channel' Kv1.2 crystal structure found multiple docking solutions that differed in the orientation of the AA tail. This suggests that some considerable flexibility is allowed within the proposed binding site. So why is there such a cliff in activity as FFAs move towards a single double bond in their chain? One suggestion, which was pursued here, draws on an idea from medicinal chemistry that a drug-like molecule has a bioactive conformation they must adopt before it will bind to a target. Double bonds or unsaturation restricts the movement of the molecule by preventing the free rotation of its atoms. Decreasing the number of double bonds increases the flexibility of a molecule and greatly increased the number of conformations it can adopt. In theory, molecules which are hindered in their movement or have the range of possible conformations restricted are more effective binders as they do not have to overcome the a entropic loss it requires to adopt a specific pose (Fang et al., 2014). By synthetically restricting the free movement of FFAs it was hoped the potency and selectivity of these molecules could be tailored to the channel.

5.3.4 Click chemistry yields access to aromatic fatty acids in a single step

The introduction of aromatic rings into the chemistry of fatty acids stretches back more than 120 years when the introduction of phenyl groups into various length fatty acids was shown to improve their antimicrobial effects (Laws, 1894). Since then, the incorporation of aromatic groups into fatty acids employed for many different ends. For instance, novel photo-optic surfactant molecules can produced by the incorporation of 4,4'-substituted stilbenes into the tail of long chain fatty acids (Brown and Whitten, 1985).

Here the incorporation of aromatic cycles into the fatty acid structure was used to reduce the flexible movement and free rotation in at least some of the molecule. Traditional approaches to introducing phenyl rings into the fatty acid tail have focused on electrophilic addition, i.e Friedel Crafts acylation, to achieve this (Wan et al., 1983). This is a useful approach but it is limited by the type of starting materials than can be used for addition to the aromatic ring (reactive carbonyls with no other electrophilic substituents). The initial approach used here involved a multistep synthetic pathway involving the bi-functionalisation of a central benzene scaffold with two alkyne substituents. This had the advantage of allowing access to both saturated and unsaturated aryl fatty acids by subsequent reduction. In this study the alkyne functionalisation of the 1,4-halobenzene scaffold could only be partially accomplished (scheme 5.1) with the second functionalisation step proving to be insuperable. This was unexpected as the bi- and tri-functionalisation of benzene with alkyne substituents has been successfully reported using Pd-catalysed sonogashira reactions (Chanteau and Tour, 2003).

The construction of a central aromatic core was achieved instead by forming a heteroaromatic 1,2,3-triazole structure *in situ.* The simple and effective construction of 1,2,3-triazole structures has become a vital tool in the production of a range of biomolecules and bio-conjugates (Nwe and Brechbiel, 2009). 1,2,3-triazole are important functionalities across a range of important drugs including anti-cancer drugs (Soltis et al., 1996) and anti-biotics (Sheng et al., 2011), as well as in the design of drug delivery nano-structures such as polymeric nanocarriers and “designer micelles” (Avti et al., 2013).

Cu catalysed 1,3-Dipolar cycloaddition allows access to aromatic fatty acid of any length and triazole position by simply varying the lengths and functionalisation of the starting material. Aromatic fatty acids of chain length 12 – 25 atoms were synthesised successfully by this method. Here, the construction of the 1,2,3-triazole core was achieved in a one-pot synthesis without the need to isolate the alkyl azide intermediate. The alkyl azide intermediate was a stable compound and its production and consumption could be monitored by LCMS during the reaction. Initial reaction conditions involved reducing $Cu(II)SO_4$ to catalytic Cu(I) *in situ* using sodium ascorbate as a co-catalyst within the reaction. The resulting reaction mix could be

purified by column chromatography to obtain the desired acid. However, replacing Cu(II)SO_4/sodium ascorbate with the catalytic Cu(I)O allowed the final product to be isolated with in purity without the need for column chromatography. The heterogeneous nature of the Cu catalyst as well as the production of ionic salts as the only bi-products allowed the isolation of the fatty acid by filtration and extraction alone. This synthesis yields access a wide range of aromatic fatty acids in a single step and without the need for further purification. In order to reproduce the high inhibitory effects of PUFAs on Kv1.2, future work should focus on modifying the structures of the reactants to incorporate double bonds within the alkyl chain of the aromatic fatty acid.

Chapter 6

Final Discussion

6.1 Summary

The aim of this study was to examine intrinsic firing properties of SGNs and probe their regulation by native and synthetic lipid molecules. In Chapter 3, the intrinsic firing properties of SGNs were examined and found to correlate with the magnitudes of particular ionic currents, notably LVA K^+ current and I_h. These LVA K^+ currents were DTX-K- and TsTx-sensitive, implicating Kv1.1 and Kv1.2 as contributing to the subunit composition of the LVA channels. The elucidation of some of the molecular subunits of SGN LVA led to an examination of their potential regulation. Chapter 4 detailed an investigation into the phosphoinositide sensitivity of SGN LVA K^+ currents. Depletion of PIP_2 by wortmannin or PIP_2-PP had a significant effect on SGN adaptation rates via the inhibition of Kv1.1- and Kv1.2-mediated LVA K^+ current. Finally, in Chapter 5 the effects of native and synthetic free fatty acid molecules were examined on Kv1.2 currents stably expressed in a HEK293 cell line and a series of polyunsaturated fatty acids were shown to provide strong inhibition of Kv1.2 currents.

Understanding the molecular basis of SGN excitability is essential for a complete understanding how the auditory nerve encodes sound. Understanding the difference in membrane electrophysiology in the distinct SGN subpopulations may also shed light on the heterogeneous firing patterns observed in ANFs *in vivo*. Furthermore, identifying biological targets that alter SGN firing provides a potential mechanism to adjust the output of the AN. This is of particular interest for improving the functioning of cochlear implants to aid "electrical hearing" or for modifying inputs to the central auditory pathway in cases of aberrant neural signalling i.e. tinnitus. The wider utility of LVA K^+ currents in the auditory system are now discussed and some of the important questions that remain unanswered are addressed. Finally, the potential therapeutic implications of SGN modulation are discussed along with a discussion of the practical limitations to pharmacologically treating SGNs in humans.

6.1.1 The wider role of LVA K^+ currents in the auditory system

LVA currents are a prominent feature of neurons throughout the auditory system (Schwarz and Puil, 1997, Brew and Forsythe, 1995, Smith, 1995, Barnes-Davies et al., 2004, Bal and Oertel, 2001). This is consistent with findings from Grigg et al., which reported heavy Kv1.1 subunit expression in the auditory brainstem, in particularly in octopus and bushy cells of the VCN, the MNTB, the MSO and LSO (Grigg et al., 2000). Strong Kv1.1 and Kv1.2 channel expression has also been reported in regions of the VCN (Rusznak et al., 2008) and the MNTB (Tong et al., 2010). Kv1.1/Kv1.2 heteromeric channels therefore, have been proposed as likely mediators of LVA currents throughout the auditory system (Brew et al., 2007, Dodson et al., 2002), with the Kv1.6 subunit also implicated in some tissues. Functional examination of these current indicate that the exact composition and stoichiometry of these channels may differ between tissues, most likely to accommodate the diverse functional roles of their tissues in signal propagation and integration. Notable interspecies variation in LVA composition and stoichiometry is also apparent, perhaps contributing to the variation in auditory characteristics observed across species (Dodson et al., 2002).

Behavioural studies on *Kcna1* (Kv1.1) knockout mice report significant deficits in the animals ability to localise sound (Allen et al., 2008, Allen and Ison, 2012, Brew et al., 2003). *In vivo* single-unit recordings from the VCN and MNTB cells of *Kcna1*-null (-/-) mice and littermate control (+/+) mice show that whilst the thresholds and spontaneous firing rates of these neurons may remain unchanged between genotypes, the evoked firing rates of these neurons were significantly lower in -/- mice at higher sound stimulus (Kopp-Scheinpflug et al., 2003). Further deficits were observed at high rates of sinusoidal amplitude modulation, where MNTB neurons from *Kcna1*-/- mice discharged on significantly fewer cycles of the stimulus than their *Kcna1*+/+ littermates. The observed cognitive deficits are likely a result of increased temporal variability in the onset response of neurons, known as jitter. This increased jitter reduces a neuron's ability to code acoustic information at the required millisecond or even sub-millisecond accuracy (Brew et al., 2007).

These behavioural and single-unit experiments are correlated with results from *in vitro* experiments that show a significant reduction in the LVA K^+ currents of brainstem

nuclei that mediate binaural processing (Kopp-Scheinpflug et al., 2003). Neurons in the MSO process sound localisation cues via a process known as binaural coincidence detection. This process uses excitatory synaptic inputs from each ear and separates them onto different branches of a bipolar dendritic structure. These inputs are then summed at the soma and axon of the neuron with submillisecond timings. LVA K^+ channels have been shown to accelerate membrane repolarisation improve the temporal resolution of synaptic integration (Mathews et al., 2010).

LVA K^+ current also contributes to synaptic integration in the cochlear nucleus. Octopus cells in the VCN receive inputs from ~50 ANFs across the tonotopic axis; APs are only evoked robustly and consistently when these inputs are synchronised to millisecond accuracy. Octopus cells have a low input resistance and membrane time constant, ensuring the amplitude of voltage changes associated with a synaptic input is small. LVA K^+ currents prevent the slow temporal summation of inputs and ensure that octopus cells fire only when they are depolarised quickly by multiple synchronous inputs. Blockage of Kv1-mediated LVA currents with α-dendrotoxin results in a significant loss of this synchronisation (Ferragamo and Oertel, 2002).

LVA K^+ currents are also present in presynaptic terminals such as at the Calyx of held where their presence prevents the occurrence of aberrant spikes following an incoming AP (Dodson et al., 2003). LVA K^+ currents have been shown to enhance the signal-to-noise ratio of MSO neurons *in vitro* by filtering out weak synaptic conductance transients (Svirskis et al., 2002).

6.1.2 Implications for cochlear implants and "electrical" hearing

Many forms of sensorineural hearing loss are characterised by the loss of the mechanosensory hair cells and their afferents. The loss of the SGN peripheral processes can precede SGN cell death by some considerable period however. As a result many individuals with sensorineural hearing loss retain considerable numbers of SGN bodies within their modiulos capable of sending signals to the brain. This is the basis for auditory prostheses. Cochlear implants (CIs) are a series of electrodes positioned along

the spiral of the cochlea close to the cell bodies of the SGNs (Yawn et al., 2015). An external component positioned outside the head detects acoustic inputs which are translated into evoked current along the internal electrode array. Auditory prostheses have helped restore functional hearing to many deaf individuals. CI can enable good speech understanding in ideal listening conditions. However CIs are suboptimal in more challenging listening conditions i.e, understanding speech in noisy environments, discerning multiple competing speeches, listening to music, etc.

In electrical hearing acoustic information is limited to signalling from the CI down different electrodes or "channels". The most significant difficulty arises from the poor spectral resolution provided by implants. CI studies have revealed that basic speech recognition in quiet listening conditions requires as few as 4 spectral channels (Shannon et al., 1995). However for the more challenging task of speech recognition in noise (10 dB signal-to-noise ratio or less) 8 spectral channels are needed (Fu et al., 1998, Friesen et al., 2001). For more complex tasks, such as perceiving music or discerning competing speeches, even more channels are required (Shannon et al., 2004). The limitations in spectral resolution are not on the CI side; commercial CI signal processing devises provide up to 22 channels. Despite this, current CIs have exhibited a notable upper limit in their efficacy with CI recipients rarely performing better than as if they had 8-10 effective channels (Landsberger et al., 2012).

The major limitation to CI improvement is the phenomenon of current spread in the cochlea. Channel electrodes provide stimulation to the cochlea by charging the SGN bodies with current. This current is most effective in proximity to the electrode but current spread from the electrode source can also charge more distant neurons. As a result CI users are often able to discriminate between channel activation when compared in isolation. However stimulation of adjacent channel electrodes is often perceived as a single intermediate pitch (McDermott and McKay 1994). Thus, the spectral resolution of CI users is significantly limited by channel interactions. This has been proposed as the primary limiting faction for CI performance (Fu and Nogaki, 2005). Bingabr et al. showed that a reduction in the spread of current excitation improved performance during speech discrimination tasks in patients with only a few spectral channels. However this reduced overall performance, suggesting both strong excitation of SGNs and narrow current spread are needed for good CI performance (Bingabr et al., 2008).

To overcome the limitations imposed by current spread in the cochlea, many strategies have been proposed, such as experimenting with different methods of current application to reduce the spread of excitation, e.g. (Landsberger et al., 2012) and (Srinivasan et al., 2013). Other studies have suggested reducing the neural gap by stimulating the regrowth of SGN neurites towards the stimulus electrode with neurotrophins such as BDNF (Pinyon et al., 2014). The advent of new optogenetic techniques has also opened the door to the promising new idea of optical cochlear implants. Incorporation and stimulation of light sensitive proteins into the membranes of SGNs would allow considerable greater stimulus precision and sidestep the limitations imposed by current spread. For a discussion of the possible application for optogenetic stimulation for cochlear implants see (Jeschke and Moser, 2015).

A complementary approach could be to adjust the excitability of SGNs via pharmacological manipulation of neuronal LVA K^+ currents. Whilst LVA K^+ currents play an important role under normal physiological conditions, they may hinder the activity of CIs in providing electrical hearing to the damaged ear. LVA K^+ currents reduce the membrane resistance of SGNs, requiring significantly more current to charge the membrane. Indeed, maintaining a strong current stimulus is necessary to maintain a fixed loudness in CI, but as current increases so does the spread of excitation along the cochlear axis (Landsberger et al., 2012). Minimizing the necessary input energy to elicit the same loudness precept would reduce the current spread and area of excitation. In theory this would increase the number of perceptual channels available to CI users. Methods of LVA K^+ currents modulation could provide a new and complementary approach to optimising CI technologies.

6.1.3 Localised drug delivery to the inner ear

Attempts to medicate neuronal tissue in the inner ear face some significant challenges. Conventional routes of drug bioavailability such as injection or oral administration are not effective because of the presence of the blood-perilymph barrier (BPLB) that separates the inner ear from the blood (El Kechai et al., 2015). The BPLB is a continuous capillary endothelium which lines the blood vessels of the cochlea. The

BPLB acts to protect the cochlea and maintain the homeostasis of the inner ear fluids (Juhn et al., 2001). Importantly it acts as a barrier to undesirable chemicals and contains efflux pump systems such as P-glycoprotein and multidrug resistance-related protein-1 (Saito et al., 2001a, Saito et al., 2001b). Like the blood-brain barrier, the BPLB is only permeable to highly lipophilic molecules, excluding other molecules based on size, charge and water-solubility (Swan et al., 2008). The absence of a viable systemic drug route has led to the development of strategies for localised drug delivery to the inner ear (Staecker and Rodgers, 2013, Pararas et al., 2012, McCall et al., 2010). There are primarily two approaches for local drug delivery; administration into the middle ear (intratympanic) or directly into the cochlea itself (intracochlear). Both have shown effectiveness in delivering drugs to cochlear tissues (Pararas et al., 2012).

Intratympanic administration is achieved by the direct application of drugs to the round window of the cochlea. This can be achieved by direct injection of the drug solution into the middle ear cavity and subsequent diffusion across the round window. Though still used for some drugs such as corticosteroids, the reliance on passive diffusion along the cochlea results in a longitudinal drug gradient from base to apex (Salt and Plontke, 2009). In reality this means drugs often do not reach the apical regions (Mynatt et al., 2006). Combined with rapid elimination via the Eustachian tube other methods of prolonged intratympanic drug administration have been developed. Implantable medical devices such as microcatheters and osmotic pumps have been shown effective in humans for sustained drug application for anything up to 6 weeks (El Kechai et al., 2015). Intracochlear administration avoids these diffusion based problems but encounters the considerable task of accessing the interior of the cochlea. Furthermore any drug that is introduced must be careful to maintain a relatively constant fluid volume, ion composition and osmolality. Intracochlear injection has been achieved (Stover et al., 1999) but is technically difficult and not viable for continued drug administration (Pararas et al., 2012).

Once present in the perilymph, drugs access the tissues of the cochlea by diffusion. Access to the SG has now been demonstrated in numerous studies (Zhang et al., 2012, Buckiova et al., 2012, Warnecke et al., 2012). Typically, these studies have used the neurotrophic agent BDNF as their drug and measured SGN neuroprotection as an assessment of the efficacy of their drug delivery. Typically, delivery of the drug to the

round window or directly into the perilymph is sufficient to provide neuroprotection to the SGNs. This provides an important proof of concept that SGNs are in practice druggable, with delivery of the drug to the cochlear perilymph the primary practical limitation.

Finally, the nature of CI implant technology may provide an intriguing opportunity for drug delivery to the SGN. By design, CI electrodes are inserted along the cochlear spiral, in proximity to the SGN cell bodies. Combined CI/drug delivery systems have drawn considerable interest as a means of reducing local tissue trauma during CI surgery and for delivering neurotrophins and growth factors to promote sensorineural cell growth (Quesnel et al., 2011a, Quesnel et al., 2011b, El Kechai et al., 2015). Biodegradable polymeric coatings on the surface of cochlear implant electrodes have been proposed as a means to deliver drug along with the implant. Embedding the cochlear implant in a polymeric matrix has already been shown to be effective in delivering drugs to the scala tympani of guinea pig (Kikkawa et al., 2014). Drug release can be sustained for up to several months using this method depending on the polymer and drug under investigation (Astolfi et al., 2014, Kikkawa et al., 2014, Wrzeszcz et al., 2015), although the long term effects of this approach have yet to be tested. The development of novel neuromodulatory agents in combination with improving drug delivery strategies for the inner ear could provide a powerful new approach to adjusting the output of the AN, particularly in the deafened ear.

References

ABBOTT, G. W., BUTLER, M. H., BENDAHHOU, S., DALAKAS, M. C., PTACEK, L. J. & GOLDSTEIN, S. A. 2001. MiRP2 forms potassium channels in skeletal muscle with Kv3.4 and is associated with periodic paralysis. *Cell,* 104**,** 217-31.

ABDEREMANE-ALI, F., ES-SALAH-LAMOUREUX, Z., DELEMOTTE, L., KASIMOVA, M. A., LABRO, A. J., SNYDERS, D. J., FEDIDA, D., TAREK, M., BARO, I. & LOUSSOUARN, G. 2012. Dual effect of phosphatidylinositol (4,5)-bisphosphate PIP(2) on Shaker K(+) [corrected] channels. *J Biol Chem,* 287**,** 36158-67.

ABRAMSON, S. B., LESZCZYNSKA-PIZIAK, J. & WEISSMANN, G. 1991. Arachidonic acid as a second messenger. Interactions with a GTP-binding protein of human neutrophils. *J Immunol,* 147**,** 231-6.

ACCILI, E. A., KIEHN, J., WIBLE, B. A. & BROWN, A. M. 1997. Interactions among inactivating and noninactivating Kvbeta subunits, and Kvalpha1.2, produce potassium currents with intermediate inactivation. *J Biol Chem,* 272**,** 28232-6.

ADAMSON, C. L., REID, M. A. & DAVIS, R. L. 2002a. Opposite actions of brain-derived neurotrophic factor and neurotrophin-3 on firing features and ion channel composition of murine spiral ganglion neurons. *J Neurosci,* 22**,** 1385-96.

ADAMSON, C. L., REID, M. A., MO, Z. L., BOWNE-ENGLISH, J. & DAVIS, R. L. 2002b. Firing features and potassium channel content of murine spiral ganglion neurons vary with cochlear location. *J Comp Neurol,* 447**,** 331-50.

ADELMAN, J. P., BOND, C. T., PESSIA, M. & MAYLIE, J. 1995. Episodic ataxia results from voltage-dependent potassium channels with altered functions. *Neuron,* 15**,** 1449-54.

AHERN, C. A. & HORN, R. 2005. Focused electric field across the voltage sensor of potassium channels. *Neuron,* 48**,** 25-9.

AL-SABI, A., KAZA, S. K., DOLLY, J. O. & WANG, J. 2013. Pharmacological characteristics of Kv1.1- and Kv1.2-containing channels are influenced by the stoichiometry and positioning of their alpha subunits. *Biochem J,* 454**,** 101-8.

ALLEN, P. D. & ISON, J. R. 2012. Kcna1 gene deletion lowers the behavioral sensitivity of mice to small changes in sound location and increases asynchronous brainstem auditory evoked potentials but does not affect hearing thresholds. *J Neurosci,* 32**,** 2538-43.

ALLEN, P. D., SCHMUCK, N., ISON, J. R. & WALTON, J. P. 2008. Kv1.1 channel subunits are not necessary for high temporal acuity in behavioral and electrophysiological gap detection. *Hear Res,* 246**,** 52-8.

AN, W. F., BOWLBY, M. R., BETTY, M., CAO, J., LING, H. P., MENDOZA, G., HINSON, J. W., MATTSSON, K. I., STRASSLE, B. W., TRIMMER, J. S. & RHODES, K. J. 2000. Modulation of A-type potassium channels by a family of calcium sensors. *Nature,* 403**,** 553-6.

ANDRASFALVY, B. K., MAKARA, J. K., JOHNSTON, D. & MAGEE, J. C. 2008. Altered synaptic and non-synaptic properties of CA1 pyramidal neurons in Kv4.2 knockout mice. *J Physiol,* 586**,** 3881-92.

ANNIKO, M., ARNOLD, W., STIGBRAND, T. & STROM, A. 1995. The human spiral ganglion. *ORL J Otorhinolaryngol Relat Spec,* 57**,** 68-77.

ARSENAULT, D., JULIEN, C., CHEN, C. T., BAZINET, R. P. & CALON, F. 2012. Dietary intake of unsaturated fatty acids modulates physiological properties of entorhinal cortex neurons in mice. *J Neurochem,* 122**,** 427-43.

ASTOLFI, L., GUARAN, V., MARCHETTI, N., OLIVETTO, E., SIMONI, E., CAVAZZINI, A., JOLLY, C. & MARTINI, A. 2014. Cochlear implants and drug delivery: In vitro evaluation of dexamethasone release. *J Biomed Mater Res B Appl Biomater,* 102**,** 267-73.

AVTI, P. K., MAYSINGER, D. & KAKKAR, A. 2013. Alkyne-azide "click" chemistry in designing nanocarriers for applications in biology. *Molecules,* 18**,** 9531-49.

BAE, Y. S., LEE, T. G., PARK, J. C., HUR, J. H., KIM, Y., HEO, K., KWAK, J. Y., SUH, P. G. & RYU, S. H. 2003. Identification of a compound that directly stimulates phospholipase C activity. *Mol Pharmacol,* 63**,** 1043-50.

BAKONDI, G., POR, A., KOVACS, I., SZUCS, G. & RUSZNAK, Z. 2008. Voltage-gated K+ channel (Kv) subunit expression of the guinea pig spiral ganglion cells studied in a newly developed cochlear free-floating preparation. *Brain Res,* 1210**,** 148-62.

BAKONDI, G., POR, A., KOVACS, I., SZUCS, G. & RUSZNAK, Z. 2009. Hyperpolarization-activated, cyclic nucleotide-gated, cation non-selective channel subunit expression pattern of guinea-pig spiral ganglion cells. *Neuroscience,* 158**,** 1469-77.

BAL, R. & OERTEL, D. 2001. Potassium currents in octopus cells of the mammalian cochlear nucleus. *J Neurophysiol,* 86**,** 2299-311.

BALLA, T. 2013. Phosphoinositides: tiny lipids with giant impact on cell regulation. *Physiol Rev,* 93**,** 1019-137.

BALSINDE, J., WINSTEAD, M. V. & DENNIS, E. A. 2002. Phospholipase A(2) regulation of arachidonic acid mobilization. *FEBS Lett,* 531**,** 2-6.

BARHANIN, J., LESAGE, F., GUILLEMARE, E., FINK, M., LAZDUNSKI, M. & ROMEY, G. 1996. K(V)LQT1 and lsK (minK) proteins associate to form the I(Ks) cardiac potassium current. *Nature,* 384**,** 78-80.

BARLOW, C. A., LAISHRAM, R. S. & ANDERSON, R. A. 2010. Nuclear phosphoinositides: a signaling enigma wrapped in a compartmental conundrum. *Trends Cell Biol,* 20**,** 25-35.

BARNES-DAVIES, M., BARKER, M. C., OSMANI, F. & FORSYTHE, I. D. 2004. Kv1 currents mediate a gradient of principal neuron excitability across the tonotopic axis in the rat lateral superior olive. *Eur J Neurosci,* 19**,** 325-33.

BAZAN, N. G. 2005. Lipid signaling in neural plasticity, brain repair, and neuroprotection. *Mol Neurobiol,* 32**,** 89-103.

BAZAN, N. G., TU, B. & RODRIGUEZ DE TURCO, E. B. 2002. What synaptic lipid signaling tells us about seizure-induced damage and epileptogenesis. *Prog Brain Res,* 135**,** 175-85.

BEISEL, K. W., ROCHA-SANCHEZ, S. M., MORRIS, K. A., NIE, L., FENG, F., KACHAR, B., YAMOAH, E. N. & FRITZSCH, B. 2005. Differential expression of KCNQ4 in inner hair cells and sensory neurons is the basis of progressive high-frequency hearing loss. *J Neurosci,* 25**,** 9285-93.

BEKESY, G. V. 1960. Neural inhibitory units of the eye and skin. Quantitative description of contrast phenomena. *J Opt Soc Am,* 50**,** 1060-70.

BENDAHHOU, S., CUMMINS, T. R. & AGNEW, W. S. 1997. Mechanism of modulation of the voltage-gated skeletal and cardiac muscle sodium channels by fatty acids. *Am J Physiol,* 272**,** C592-600.

BERGEVIN, C. & OLSON, E. S. 2014. External and middle ear sound pressure distribution and acoustic coupling to the tympanic membrane. *J Acoust Soc Am,* 135**,** 1294-312.

BERGLUND, A. M. & BROWN, M. C. 1994. Central trajectories of type II spiral ganglion cells from various cochlear regions in mice. *Hear Res,* 75**,** 121-30.

BERGLUND, A. M. & RYUGO, D. K. 1987. Hair cell innervation by spiral ganglion neurons in the mouse. *J Comp Neurol,* 255**,** 560-70.

BERNARD, P. A. & SPOENDLIN, H. 1973. Unmyelinated fibers in the cochlea. *JFORL J Fr Otorhinolaryngol Audiophonol Chir Maxillofac,* 22**,** 39-42.

BEZANILLA, F. & ARMSTRONG, C. M. 1972. Negative conductance caused by entry of sodium and cesium ions into the potassium channels of squid axons. *J Gen Physiol,* 60**,** 588-608.

BINGABR, M., ESPINOZA-VARAS, B. & LOIZOU, P. C. 2008. Simulating the effect of spread of excitation in cochlear implants. *Hear Res,* 241**,** 73-9.

BIRDSALL, N. J., BURGEN, A. S. & HULME, E. C. 1978. The binding of agonists to brain muscarinic receptors. *Mol Pharmacol,* 14**,** 723-36.

BISTA, P., PAWLOWSKI, M., CERINA, M., EHLING, P., LEIST, M., MEUTH, P., AISSAOUI, A., BORSOTTO, M., HEURTEAUX, C., DECHER, N., PAPE, H. C., OLIVER, D., MEUTH, S. G. & BUDDE, T. 2015. Differential phospholipase C-dependent modulation of TASK and TREK two-pore domain K+ channels in rat thalamocortical relay neurons. *J Physiol,* 593**,** 127-44.

BLONDEAU, N., LIPSKY, R. H., BOUROUROU, M., DUNCAN, M. W., GORELICK, P. B. & MARINI, A. M. 2015. Alpha-linolenic acid: an omega-3 fatty acid with neuroprotective properties-ready for use in the stroke clinic? *Biomed Res Int,* 2015**,** 519830.

BLUNCK, R. & BATULAN, Z. 2012. Mechanism of electromechanical coupling in voltage-gated potassium channels. *Front Pharmacol,* 3**,** 166.

BOHNE, B. A., KENWORTHY, A. & CARR, C. D. 1982. Density of myelinated nerve fibers in the chinchilla cochlea. *J Acoust Soc Am,* 72**,** 102-7.

BOLAND, L. M. & DRZEWIECKI, M. M. 2008. Polyunsaturated fatty acid modulation of voltage-gated ion channels. *Cell Biochem Biophys,* 52**,** 59-84.

BOLAND, L. M., DRZEWIECKI, M. M., TIMONEY, G. & CASEY, E. 2009. Inhibitory effects of polyunsaturated fatty acids on Kv4/KChIP potassium channels. *Am J Physiol Cell Physiol,* 296**,** C1003-14.

BORG, E., ENGSTROM, B., LINDE, G. & MARKLUND, K. 1988. Eighth nerve fiber firing features in normal-hearing rabbits. *Hear Res,* 36**,** 191-201.

BORJESSON, S. I. & ELINDER, F. 2011. An electrostatic potassium channel opener targeting the final voltage sensor transition. *J Gen Physiol,* 137**,** 563-77.

BORJESSON, S. I., HAMMARSTROM, S. & ELINDER, F. 2008. Lipoelectric modification of ion channel voltage gating by polyunsaturated fatty acids. *Biophys J,* 95**,** 2242-53.

BRAAKMAN, I. & BULLEID, N. J. 2011. Protein folding and modification in the mammalian endoplasmic reticulum. *Annu Rev Biochem,* 80**,** 71-99.

BRASH, A. R. 2001. Arachidonic acid as a bioactive molecule. *J Clin Invest,* 107**,** 1339-45.

BRAUCHI, S., ORTA, G., MASCAYANO, C., SALAZAR, M., RADDATZ, N., URBINA, H., ROSENMANN, E., GONZALEZ-NILO, F. & LATORRE, R. 2007. Dissection of the components for PIP2 activation and thermosensation in TRP channels. *Proc Natl Acad Sci U S A,* 104**,** 10246-51.

BREDBERG, G. 1968. Cellular pattern and nerve supply of the human organ of Corti. *Acta Otolaryngol,* Suppl 236:1+.

BRENNER, R., PEREZ, G. J., BONEV, A. D., ECKMAN, D. M., KOSEK, J. C., WILER, S. W., PATTERSON, A. J., NELSON, M. T. & ALDRICH, R. W. 2000. Vasoregulation by the beta1 subunit of the calcium-activated potassium channel. *Nature,* 407**,** 870-6.

BREW, H. M. & FORSYTHE, I. D. 1995. Two voltage-dependent K+ conductances with complementary functions in postsynaptic integration at a central auditory synapse. *J Neurosci,* 15**,** 8011-22.

BREW, H. M., GITTELMAN, J. X., SILVERSTEIN, R. S., HANKS, T. D., DEMAS, V. P., ROBINSON, L. C., ROBBINS, C. A., MCKEE-JOHNSON, J., CHIU, S. Y., MESSING, A. & TEMPEL, B. L. 2007. Seizures and reduced life span in mice lacking the potassium channel subunit Kv1.2, but hypoexcitability and enlarged Kv1 currents in auditory neurons. *J Neurophysiol,* 98**,** 1501-25.

BREW, H. M., HALLOWS, J. L. & TEMPEL, B. L. 2003. Hyperexcitability and reduced low threshold potassium currents in auditory neurons of mice lacking the channel subunit Kv1.1. *J Physiol,* 548**,** 1-20.

BROWN, D. A. 2010. Muscarinic acetylcholine receptors (mAChRs) in the nervous system: some functions and mechanisms. *J Mol Neurosci,* 41**,** 340-6.

BROWN, D. A., HUGHES, S. A., MARSH, S. J. & TINKER, A. 2007. Regulation of M(Kv7.2/7.3) channels in neurons by PIP(2) and products of PIP(2) hydrolysis: significance for receptor-mediated inhibition. *J Physiol,* 582**,** 917-25.

BROWN, D. A. & PASSMORE, G. M. 2009. Neural KCNQ (Kv7) channels. *Br J Pharmacol,* 156**,** 1185-95.

BROWN, M. C., BERGLUND, A. M., KIANG, N. Y. & RYUGO, D. K. 1988. Central trajectories of type II spiral ganglion neurons. *J Comp Neurol,* 278**,** 581-90.

BROWN, P. E. & WHITTEN, D. G. 1985. Photoisomerization and fluorescence of surfactant and hydrophobic 4- and 4,4'-substituted stilbenes in homogeneous solution. Observation of strong fluorescence enhancement by dialkyl substitution. *J Phys Chem,* 89**,** 1217–1220.

BUCHMAYER, F., SCHICKER, K., STEINKELLNER, T., GEIER, P., STUBIGER, G., HAMILTON, P. J., JURIK, A., STOCKNER, T., YANG, J. W., MONTGOMERY, T., HOLY, M., HOFMAIER, T., KUDLACEK, O., MATTHIES, H. J., ECKER, G. F., BOCHKOV, V., GALLI, A., BOEHM, S. & SITTE, H. H. 2013. Amphetamine actions at the serotonin transporter rely on the availability of phosphatidylinositol-4,5-bisphosphate. *Proc Natl Acad Sci U S A,* 110**,** 11642-7.

BUCKIOVA, D., RANJAN, S., NEWMAN, T. A., JOHNSTON, A. H., SOOD, R., KINNUNEN, P. K., POPELAR, J., CHUMAK, T. & SYKA, J. 2012. Minimally invasive drug delivery to the cochlea through application of nanoparticles to the round window membrane. *Nanomedicine (Lond),* 7**,** 1339-54.

BURTIS, C. A., ASHWOOD, E. R. & TIETZ, N. W. 1999. *Tietz textbook of clinical chemistry,* Philadelphia, W.B. Saunders.

BUTLER, A., WEI, A. G., BAKER, K. & SALKOFF, L. 1989. A family of putative potassium channel genes in Drosophila. *Science,* 243**,** 943-7.

CAMPOMANES, C. R., CARROLL, K. I., MANGANAS, L. N., HERSHBERGER, M. E., GONG, B., ANTONUCCI, D. E., RHODES, K. J. & TRIMMER, J. S. 2002. Kv beta subunit oxidoreductase activity and Kv1 potassium channel trafficking. *J Biol Chem,* 277**,** 8298-305.

CHANTEAU, S. H. & TOUR, J. M. 2003. Synthesis of anthropomorphic molecules: the NanoPutians. *J Org Chem,* 68**,** 8750-66.

CHEMIN, J., MONTEIL, A., PEREZ-REYES, E., NARGEOT, J. & LORY, P. 2001. Direct inhibition of T-type calcium channels by the endogenous cannabinoid anandamide. *EMBO J,* 20**,** 7033-40.

CHEMIN, J., NARGEOT, J. & LORY, P. 2007. Chemical determinants involved in anandamide-induced inhibition of T-type calcium channels. *J Biol Chem,* 282**,** 2314-23.

CHEN, C. 1997. Hyperpolarization-activated current (Ih) in primary auditory neurons. *Hear Res,* 110**,** 179-90.

CHEN, I., LIMB, C. J. & RYUGO, D. K. 2010. The effect of cochlear-implant-mediated electrical stimulation on spiral ganglion cells in congenitally deaf white cats. *J Assoc Res Otolaryngol,* 11**,** 587-603.

CHEN, J., CHU, H., XIONG, H., CHEN, Q., ZHOU, L., BING, D., LIU, Y., GAO, Y., WANG, S., HUANG, X. & CUI, Y. 2012. Expression patterns of Ca(V)1.3 channels in the rat cochlea. *Acta Biochim Biophys Sin (Shanghai),* 44**,** 513-8.

CHEN, W. C. & DAVIS, R. L. 2006. Voltage-gated and two-pore-domain potassium channels in murine spiral ganglion neurons. *Hear Res,* 222**,** 89-99.

CHEN, W. C., XUE, H. Z., HSU, Y. L., LIU, Q., PATEL, S. & DAVIS, R. L. 2011. Complex distribution patterns of voltage-gated calcium channel alpha-subunits in the spiral ganglion. *Hear Res,* 278**,** 52-68.

CHILTON, F. H., FONTEH, A. N., SURETTE, M. E., TRIGGIANI, M. & WINKLER, J. D. 1996. Control of arachidonate levels within inflammatory cells. *Biochim Biophys Acta,* 1299**,** 1-15.

CHOE, S. 2002. Potassium channel structures. *Nat Rev Neurosci,* 3**,** 115-21.

CHUNG, H. J., JAN, Y. N. & JAN, L. Y. 2006. Polarized axonal surface expression of neuronal KCNQ channels is mediated by multiple signals in the KCNQ2 and KCNQ3 C-terminal domains. *Proc Natl Acad Sci U S A,* 103**,** 8870-5.

COETZEE, W. A., AMARILLO, Y., CHIU, J., CHOW, A., LAU, D., MCCORMACK, T., MORENO, H., NADAL, M. S., OZAITA, A., POUNTNEY, D., SAGANICH, M., VEGA-SAENZ DE MIERA, E. & RUDY, B. 1999. Molecular diversity of K+ channels. *Ann N Y Acad Sci,* 868**,** 233-85.

COLEMAN, S. K., NEWCOMBE, J., PRYKE, J. & DOLLY, J. O. 1999. Subunit composition of Kv1 channels in human CNS. *J Neurochem,* 73**,** 849-58.

COMBS, D. J., SHIN, H. G., XU, Y., RAMU, Y. & LU, Z. 2013. Tuning voltage-gated channel activity and cellular excitability with a sphingomyelinase. *J Gen Physiol,* 142**,** 367-80.

CONNOR, J. X., MCCORMACK, K., PLETSCH, A., GAETA, S., GANETZKY, B., CHIU, S. Y. & MESSING, A. 2005. Genetic modifiers of the Kv beta2-null phenotype in mice. *Genes Brain Behav,* 4**,** 77-88.

COUSILLAS, H., COLE, K. S. & JOHNSTONE, B. M. 1988. Effect of spider venom on cochlear nerve activity consistent with glutamatergic transmission at hair cell-afferent dendrite synapse. *Hear Res,* 36**,** 213-20.

COVARRUBIAS, M., WEI, A. A. & SALKOFF, L. 1991. Shaker, Shal, Shab, and Shaw express independent K+ current systems. *Neuron,* 7**,** 763-73.

CROWLEY, K. S., LIAO, S., WORRELL, V. E., REINHART, G. D. & JOHNSON, A. E. 1994. Secretory proteins move through the endoplasmic reticulum membrane via an aqueous, gated pore. *Cell,* 78**,** 461-71.

CUELLO, L. G., JOGINI, V., CORTES, D. M. & PEROZO, E. 2010. Structural mechanism of C-type inactivation in K(+) channels. *Nature,* 466**,** 203-8.

CUENDET, M., MESECAR, A. D., DEWITT, D. L. & PEZZUTO, J. M. 2006. An ELISA method to measure inhibition of the COX enzymes. *Nat Protoc,* 1**,** 1915-21.

DARIOS, F., CONNELL, E. & DAVLETOV, B. 2007. Phospholipases and fatty acid signalling in exocytosis. *J Physiol,* 585**,** 699-704.

DAS SARMA, J., WANG, F. & KOVAL, M. 2002. Targeted gap junction protein constructs reveal connexin-specific differences in oligomerization. *J Biol Chem,* 277**,** 20911-8.

DAVIS, R. L. 2003. Gradients of neurotrophins, ion channels, and tuning in the cochlea. *Neuroscientist,* 9**,** 311-6.

DAVIS, R. L. & CROZIER, R. A. 2015. Dynamic firing properties of type I spiral ganglion neurons. *Cell Tissue Res,* 361**,** 115-27.

DAY, N. S., BERTI-MATTERA, L. N. & EICHBERG, J. 1991. Muscarinic cholinergic receptor-mediated phosphoinositide metabolism in peripheral nerve. *J Neurochem,* 56**,** 1905-13.

DE BOER, E. 1996. *Mechanics of the Cochlea: Modeling Efforts*, Springer publishing.

DE LA HOZ, A., DIAZ-ORTIZ, A. & MORENO, A. 2005. Microwaves in organic synthesis. Thermal and non-thermal microwave effects. *Chem Soc Rev,* 34**,** 164-78.

DE PALMA, A. & PARETI, G. 2011. Bernstein's long path to membrane theory: radical change and conservation in nineteenth-century German electrophysiology. *J Hist Neurosci,* 20**,** 306-37.

DE ROBERTIS, E. & FRANCHI, C. M. 1956. Electron microscope observations on synaptic vesicles in synapses of the retinal rods and cones. *J Biophys Biochem Cytol,* 2**,** 307-18.

DECHER, N., GONZALEZ, T., STREIT, A. K., SACHSE, F. B., RENIGUNTA, V., SOOM, M., HEINEMANN, S. H., DAUT, J. & SANGUINETTI, M. C. 2008. Structural determinants of Kvbeta1.3-induced channel inactivation: a hairpin modulated by PIP2. *EMBO J,* 27**,** 3164-74.

DECHER, N., KUMAR, P., GONZALEZ, T., RENIGUNTA, V. & SANGUINETTI, M. C. 2005. Structural basis for competition between drug binding and Kvbeta 1.3 accessory subunit-induced N-type inactivation of Kv1.5 channels. *Mol Pharmacol,* 68**,** 995-1005.

DECHER, N., STREIT, A. K., RAPEDIUS, M., NETTER, M. F., MARZIAN, S., EHLING, P., SCHLICHTHORL, G., CRAAN, T., RENIGUNTA, V., KOHLER, A., DODEL, R. C., NAVARRO-POLANCO, R. A., PREISIG-MULLER, R., KLEBE, G., BUDDE, T., BAUKROWITZ, T. & DAUT, J. 2010. RNA editing modulates the binding of drugs and highly unsaturated fatty acids to the open pore of Kv potassium channels. *EMBO J,* 29**,** 2101-13.

DELMAS, P., CREST, M. & BROWN, D. A. 2004. Functional organization of PLC signaling microdomains in neurons. *Trends Neurosci,* 27**,** 41-7.

DENIS, I., POTIER, B., HEBERDEN, C. & VANCASSEL, S. 2015. Omega-3 polyunsaturated fatty acids and brain aging. *Curr Opin Clin Nutr Metab Care,* 18**,** 139-46.

DEUTSCH, C. 2002. Potassium channel ontogeny. *Annu Rev Physiol,* 64**,** 19-46.

DEUTSCH, C. 2003. The birth of a channel. *Neuron,* 40**,** 265-76.

DODSON, P. D., BARKER, M. C. & FORSYTHE, I. D. 2002. Two heteromeric Kv1 potassium channels differentially regulate action potential firing. *J Neurosci,* 22**,** 6953-61.

DODSON, P. D., BILLUPS, B., RUSZNAK, Z., SZUCS, G., BARKER, M. C. & FORSYTHE, I. D. 2003. Presynaptic rat Kv1.2 channels suppress synaptic terminal hyperexcitability following action potential invasion. *J Physiol,* 550**,** 27-33.

DOOLAN, G. K., PANCHAL, R. G., FONNES, E. L., CLARKE, A. L., WILLIAMS, D. A. & PETROU, S. 2002. Fatty acid augmentation of the cardiac slowly activating delayed rectifier current (IKs) is conferred by hminK. *FASEB J,* 16**,** 1662-4.

DOYLE, A., MCGARRY, M. P., LEE, N. A. & LEE, J. J. 2012. The construction of transgenic and gene knockout/knockin mouse models of human disease. *Transgenic Res,* 21**,** 327-49.

DOYLE, D. A., MORAIS CABRAL, J., PFUETZNER, R. A., KUO, A., GULBIS, J. M., COHEN, S. L., CHAIT, B. T. & MACKINNON, R. 1998. The structure of the potassium channel: molecular basis of K+ conduction and selectivity. *Science,* 280**,** 69-77.

DULON, D., LUO, L., ZHANG, C. & RYAN, A. F. 1998. Expression of small-conductance calcium-activated potassium channels (SK) in outer hair cells of the rat cochlea. *Eur J Neurosci,* 10**,** 907-15.

DUNN, R. A. & MOREST, D. K. 1975. Receptor synapses without synaptic ribbons in the cochlea of the cat. *Proc Natl Acad Sci U S A,* 72**,** 3599-603.

DWYER, L., KIM, H. J., KOH, B. H. & KOH, S. D. 2010. Phospholipase C-independent effects of 3M3FBS in murine colon. *Eur J Pharmacol,* 628**,** 187-94.

EL-KHOLY, W., MACDONALD, P. E., LIN, J. H., WANG, J., FOX, J. M., LIGHT, P. E., WANG, Q., TSUSHIMA, R. G. & WHEELER, M. B. 2003. The phosphatidylinositol 3-kinase inhibitor LY294002 potently blocks K(V) currents via a direct mechanism. *FASEB J,* 17**,** 720-2.

EL KECHAI, N., AGNELY, F., MAMELLE, E., NGUYEN, Y., FERRARY, E. & BOCHOT, A. 2015. Recent advances in local drug delivery to the inner ear. *Int J Pharm,* 494**,** 83-101.

ENYEDI, P. & CZIRJAK, G. 2010. Molecular background of leak K+ currents: two-pore domain potassium channels. *Physiol Rev,* 90**,** 559-605.

ERDELYI, M. & GOGOLL, A. 2001. Rapid homogeneous-phase Sonogashira coupling reactions using controlled microwave heating. *J Org Chem,* 66**,** 4165-9.

EVANS, E. F. 1972. The frequency response and other properties of single fibres in the guinea-pig cochlear nerve. *J Physiol,* 226**,** 263-87.

FAHY, E., SUBRAMANIAM, S., MURPHY, R. C., NISHIJIMA, M., RAETZ, C. R., SHIMIZU, T., SPENER, F., VAN MEER, G., WAKELAM, M. J. & DENNIS, E. A. 2009. Update of the LIPID MAPS comprehensive classification system for lipids. *J Lipid Res,* 50 Suppl**,** S9-14.

FAN, Z., JI, X., FU, M., ZHANG, W., ZHANG, D. & XIAO, Z. 2012. Electrostatic interaction between inactivation ball and T1-S1 linker region of Kv1.4 channel. *Biochim Biophys Acta,* 1818**,** 55-63.

FANG, Z., SONG, Y., ZHAN, P., ZHANG, Q. & LIU, X. 2014. Conformational restriction: an effective tactic in 'follow-on'-based drug discovery. *Future Med Chem,* 6**,** 885-901.

FARINAS, I., JONES, K. R., TESSAROLLO, L., VIGERS, A. J., HUANG, E., KIRSTEIN, M., DE CAPRONA, D. C., COPPOLA, V., BACKUS, C., REICHARDT, L. F. & FRITZSCH, B. 2001. Spatial shaping of cochlear innervation by temporally regulated neurotrophin expression. *J Neurosci,* 21**,** 6170-80.

FAROOQUI, A. A. & HORROCKS, L. A. 2004. Brain phospholipases A2: a perspective on the history. *Prostaglandins Leukot Essent Fatty Acids,* 71**,** 161-9.

FEKETE, D. M., ROUILLER, E. M., LIBERMAN, M. C. & RYUGO, D. K. 1984. The central projections of intracellularly labeled auditory nerve fibers in cats. *J Comp Neurol,* 229**,** 432-50.

FELIX, D. & EHRENBERGER, K. 1992. The efferent modulation of mammalian inner hair cell afferents. *Hear Res,* 64**,** 1-5.

FELLER, S. E. 2008. Acyl chain conformations in phospholipid bilayers: a comparative study of docosahexaenoic acid and saturated fatty acids. *Chem Phys Lipids,* 153**,** 76-80.

FERRAGAMO, M. J. & OERTEL, D. 2002. Octopus cells of the mammalian ventral cochlear nucleus sense the rate of depolarization. *J Neurophysiol,* 87**,** 2262-70.

FETTIPLACE, R. & KIM, K. X. 2014. The physiology of mechanoelectrical transduction channels in hearing. *Physiol Rev,* 94**,** 951-86.

FRANK, T., KHIMICH, D., NEEF, A. & MOSER, T. 2009. Mechanisms contributing to synaptic Ca2+ signals and their heterogeneity in hair cells. *Proc Natl Acad Sci U S A,* 106**,** 4483-8.

FRIESEN, L. M., SHANNON, R. V., BASKENT, D. & WANG, X. 2001. Speech recognition in noise as a function of the number of spectral channels: comparison of acoustic hearing and cochlear implants. *J Acoust Soc Am,* 110**,** 1150-63.

FRITZSCH, B., TESSAROLLO, L., COPPOLA, E. & REICHARDT, L. F. 2004. Neurotrophins in the ear: their roles in sensory neuron survival and fiber guidance. *Prog Brain Res,* 146**,** 265-78.

FRUMAN, D. A., MEYERS, R. E. & CANTLEY, L. C. 1998. Phosphoinositide kinases. *Annu Rev Biochem,* 67**,** 481-507.

FRYATT, A. G., VIAL, C., MULHERAN, M., GUNTHORPE, M. J. & GRUBB, B. D. 2009. Voltage-gated sodium channel expression in rat spiral ganglion neurons. *Mol Cell Neurosci,* 42**,** 399-407.

FU, Q. J. & NOGAKI, G. 2005. Noise susceptibility of cochlear implant users: the role of spectral resolution and smearing. *J Assoc Res Otolaryngol,* 6**,** 19-27.

FU, Q. J., SHANNON, R. V. & WANG, X. 1998. Effects of noise and spectral resolution on vowel and consonant recognition: acoustic and electric hearing. *J Acoust Soc Am,* 104**,** 3586-96.

FUJITA, S., IKEGAYA, Y., NISHIKAWA, M., NISHIYAMA, N. & MATSUKI, N. 2001. Docosahexaenoic acid improves long-term potentiation attenuated by phospholipase A(2) inhibitor in rat hippocampal slices. *Br J Pharmacol,* 132**,** 1417-22.

FURMAN, A. C., KUJAWA, S. G. & LIBERMAN, M. C. 2013. Noise-induced cochlear neuropathy is selective for fibers with low spontaneous rates. *J Neurophysiol,* 110**,** 577-86.

GARCIA-JUNCO-CLEMENTE, P. & GOLSHANI, P. 2014. PTEN: A master regulator of neuronal structure, function, and plasticity. *Commun Integr Biol,* 7**,** e28358.

GEORGIADI, A. & KERSTEN, S. 2012. Mechanisms of gene regulation by fatty acids. *Adv Nutr,* 3**,** 127-34.

GLASS, C. K. & OLEFSKY, J. M. 2012. Inflammation and lipid signaling in the etiology of insulin resistance. *Cell Metab,* 15**,** 635-45.

GLOWATZKI, E. & FUCHS, P. A. 2002. Transmitter release at the hair cell ribbon synapse. *Nat Neurosci,* 5**,** 147-54.

GONZALEZ, T., NAVARRO-POLANCO, R., ARIAS, C., CABALLERO, R., MORENO, I., DELPON, E., TAMARGO, J., TAMKUN, M. M. & VALENZUELA, C. 2002. Assembly with the Kvbeta1.3 subunit modulates drug block of hKv1.5 channels. *Mol Pharmacol,* 62**,** 1456-63.

GRANIT, R., KERNELL, D. & SHORTESS, G. K. 1963. The Behaviour of Mammalian Motoneurones during Long-Lasting Orthodromic, Antidromic and Trans-Membrane Stimulation. *J Physiol,* 169**,** 743-54.

GREENWOOD, D. D. 1996. Comparing octaves, frequency ranges, and cochlear-map curvature across species. *Hear Res,* 94**,** 157-62.

GRIGG, J. J., BREW, H. M. & TEMPEL, B. L. 2000. Differential expression of voltage-gated potassium channel genes in auditory nuclei of the mouse brainstem. *Hear Res,* 140**,** 77-90.

GROTHE, B. & PECKA, M. 2014. The natural history of sound localization in mammals--a story of neuronal inhibition. *Front Neural Circuits,* 8**,** 116.

GU, C., ZHOU, W., PUTHENVEEDU, M. A., XU, M., JAN, Y. N. & JAN, L. Y. 2006. The microtubule plus-end tracking protein EB1 is required for Kv1 voltage-gated K+ channel axonal targeting. *Neuron,* 52**,** 803-16.

GUBITOSI-KLUG, R. A., YU, S. P., CHOI, D. W. & GROSS, R. W. 1995. Concomitant acceleration of the activation and inactivation kinetics of the human delayed rectifier K+ channel (Kv1.1) by Ca(2+)-independent phospholipase A2. *J Biol Chem,* 270**,** 2885-8.

GUIZY, M., DAVID, M., ARIAS, C., ZHANG, L., COFAN, M., RUIZ-GUTIERREZ, V., ROS, E., LILLO, M. P., MARTENS, J. R. & VALENZUELA, C. 2008. Modulation of the atrial specific Kv1.5 channel by the n-3 polyunsaturated fatty acid, alpha-linolenic acid. *J Mol Cell Cardiol,* 44**,** 323-35.

GULBIS, J. M., MANN, S. & MACKINNON, R. 1999. Structure of a voltage-dependent K+ channel beta subunit. *Cell,* 97**,** 943-52.

GULBIS, J. M., ZHOU, M., MANN, S. & MACKINNON, R. 2000. Structure of the cytoplasmic beta subunit-T1 assembly of voltage-dependent K+ channels. *Science,* 289**,** 123-7.

GUTMAN, G. A., CHANDY, K. G., GRISSMER, S., LAZDUNSKI, M., MCKINNON, D., PARDO, L., ROBERTSON, G. A., RUDY, B., SANGUINETTI, M. C., STÜHMER, W. & WANG, X. 2005. International Union of Pharmacology. LIII. Nomenclature and molecular relationships of voltage-gated potassium channels. *Pharmacol Rev,* 57**,** 473-508.

HAFIDI, A., FELLOUS, A., FERHAT, L., ROMAND, M. R. & ROMAND, R. 1992. Developmental differentiation of MAP2 expression in the central versus the peripheral and efferent projections of the inner ear. *J Comp Neurol,* 323**,** 423-31.

HALLAQ, H., SMITH, T. W. & LEAF, A. 1992. Modulation of dihydropyridine-sensitive calcium channels in heart cells by fish oil fatty acids. *Proc Natl Acad Sci U S A,* 89**,** 1760-4.

HAMILTON, P. J., BELOVICH, A. N., KHELASHVILI, G., SAUNDERS, C., ERREGER, K., JAVITCH, J. A., SITTE, H. H., WEINSTEIN, H., MATTHIES, H. J. & GALLI, A. 2014. PIP2 regulates psychostimulant behaviors through its interaction with a membrane protein. *Nat Chem Biol,* 10**,** 582-9.

HAMMARSTROM, S., HAMBERG, M., SAMUELSSON, B., DUELL, E. A., STAWISKI, M. & VOORHEES, J. J. 1975. Increased concentrations of nonesterified arachidonic acid, 12L-hydroxy-5,8,10,14-eicosatetraenoic acid, prostaglandin E2, and prostaglandin F2alpha in epidermis of psoriasis. *Proc Natl Acad Sci U S A,* 72**,** 5130-4.

HANSEN, M. R., VIJAPURKAR, U., KOLAND, J. G. & GREEN, S. H. 2001. Reciprocal signaling between spiral ganglion neurons and Schwann cells involves neuregulin and neurotrophins. *Hear Res,* 161**,** 87-98.

HANSEN, S. B., TAO, X. & MACKINNON, R. 2011. Structural basis of PIP2 activation of the classical inward rectifier K+ channel Kir2.2. *Nature,* 477**,** 495-8.

HARA, T., KASHIHARA, D., ICHIMURA, A., KIMURA, I., TSUJIMOTO, G. & HIRASAWA, A. 2014. Role of free fatty acid receptors in the regulation of energy metabolism. *Biochim Biophys Acta,* 1841**,** 1292-300.

HEGINBOTHAM, L., LU, Z., ABRAMSON, T. & MACKINNON, R. 1994. Mutations in the K+ channel signature sequence. *Biophys J,* 66**,** 1061-7.

HEIL, P. & PETERSON, A. J. 2015. Basic response properties of auditory nerve fibers: a review. *Cell Tissue Res,* 361**,** 129-58.

HEINEMANN, S. H., RETTIG, J., GRAACK, H. R. & PONGS, O. 1996. Functional characterization of Kv channel beta-subunits from rat brain. *J Physiol,* 493 (Pt 3)**,** 625-33.

HEINEMANN, S. H., RETTIG, J., WUNDER, F. & PONGS, O. 1995. Molecular and functional characterization of a rat brain Kv beta 3 potassium channel subunit. *FEBS Lett,* 377**,** 383-9.

HEITZMANN, D. & WARTH, R. 2008. Physiology and pathophysiology of potassium channels in gastrointestinal epithelia. *Physiol Rev,* 88**,** 1119-82.

HERNANDEZ-LOPEZ, S., TKATCH, T., PEREZ-GARCI, E., GALARRAGA, E., BARGAS, J., HAMM, H. & SURMEIER, D. J. 2000. D2 dopamine receptors in striatal medium spiny neurons reduce L-type Ca2+ currents and excitability via a novel PLC[beta]1-IP3-calcineurin-signaling cascade. *J Neurosci,* 20**,** 8987-95.

HERNANDEZ, C. C., ZAIKA, O. & SHAPIRO, M. S. 2008. A carboxy-terminal inter-helix linker as the site of phosphatidylinositol 4,5-bisphosphate action on Kv7 (M-type) K+ channels. *J Gen Physiol,* 132**,** 361-81.

HIBINO, H., HORIO, Y., FUJITA, A., INANOBE, A., DOI, K., GOTOW, T., UCHIYAMA, Y., KUBO, T. & KURACHI, Y. 1999. Expression of an inwardly rectifying K(+) channel, Kir4.1, in satellite cells of rat cochlear ganglia. *Am J Physiol,* 277**,** C638-44.

HIBINO, H., INANOBE, A., FURUTANI, K., MURAKAMI, S., FINDLAY, I. & KURACHI, Y. 2010. Inwardly rectifying potassium channels: their structure, function, and physiological roles. *Physiol Rev,* 90**,** 291-366.

HILGEMANN, D. W. & BALL, R. 1996. Regulation of cardiac Na+,Ca2+ exchange and KATP potassium channels by PIP2. *Science,* 273**,** 956-9.

HILGEMANN, D. W., FENG, S. & NASUHOGLU, C. 2001. The complex and intriguing lives of PIP2 with ion channels and transporters. *Sci STKE,* 2001**,** re19.

HOLMQVIST, M. H., CAO, J., KNOPPERS, M. H., JURMAN, M. E., DISTEFANO, P. S., RHODES, K. J., XIE, Y. & AN, W. F. 2001. Kinetic modulation of Kv4-mediated A-current by arachidonic acid is dependent on potassium channel interacting proteins. *J Neurosci,* 21**,** 4154-61.

HONORE, E., BARHANIN, J., ATTALI, B., LESAGE, F. & LAZDUNSKI, M. 1994. External blockade of the major cardiac delayed-rectifier K+ channel (Kv1.5) by polyunsaturated fatty acids. *Proc Natl Acad Sci U S A,* 91**,** 1937-41.

HORROCKS, L. A. & FAROOQUI, A. A. 2004. Docosahexaenoic acid in the diet: its importance in maintenance and restoration of neural membrane function. *Prostaglandins Leukot Essent Fatty Acids,* 70**,** 361-72.

HOSHI, T., ZAGOTTA, W. N. & ALDRICH, R. W. 1990. Biophysical and molecular mechanisms of Shaker potassium channel inactivation. *Science,* 250**,** 533-8.

HOSSAIN, W. A., ANTIC, S. D., YANG, Y., RASBAND, M. N. & MOREST, D. K. 2005. Where is the spike generator of the cochlear nerve? Voltage-gated sodium channels in the mouse cochlea. *J Neurosci,* 25**,** 6857-68.

HUANG, C. L., FENG, S. & HILGEMANN, D. W. 1998. Direct activation of inward rectifier potassium channels by PIP2 and its stabilization by Gbetagamma. *Nature,* 391**,** 803-6.

IMBRICI, P., D'ADAMO, M. C., KULLMANN, D. M. & PESSIA, M. 2006. Episodic ataxia type 1 mutations in the KCNA1 gene impair the fast inactivation properties of the human potassium channels Kv1.4-1.1/Kvbeta1.1 and Kv1.4-1.1/Kvbeta1.2. *Eur J Neurosci,* 24**,** 3073-83.

IRVINE, R. F. 1982. How is the level of free arachidonic acid controlled in mammalian cells? *Biochem J,* 204**,** 3-16.

ISHII, M. & KURACHI, Y. 2006. Muscarinic acetylcholine receptors. *Curr Pharm Des,* 12**,** 3573-81.

ISHIKAWA, T., NAKAMURA, Y., SAITOH, N., LI, W. B., IWASAKI, S. & TAKAHASHI, T. 2003. Distinct roles of Kv1 and Kv3 potassium channels at the calyx of Held presynaptic terminal. *J Neurosci,* 23**,** 10445-53.

ITO, K. & DULON, D. 2002. Nonselective cation conductance activated by muscarinic and purinergic receptors in rat spiral ganglion neurons. *Am J Physiol Cell Physiol,* 282**,** C1121-35.

IWASAKI, S., CHIHARA, Y., KOMUTA, Y., ITO, K. & SAHARA, Y. 2008. Low-voltage-activated potassium channels underlie the regulation of intrinsic firing properties of rat vestibular ganglion cells. *J Neurophysiol,* 100**,** 2192-204.

JACOBSON, D. A., WEBER, C. R., BAO, S., TURK, J. & PHILIPSON, L. H. 2007. Modulation of the pancreatic islet beta-cell-delayed rectifier potassium channel Kv2.1 by the polyunsaturated fatty acid arachidonate. *J Biol Chem,* 282**,** 7442-9.

JAGGER, D. J. & HOUSLEY, G. D. 2002. A-type potassium currents dominate repolarisation of neonatal rat primary auditory neurones in situ. *Neuroscience,* 109**,** 169-82.

JAGGER, D. J. & HOUSLEY, G. D. 2003. Membrane properties of type II spiral ganglion neurones identified in a neonatal rat cochlear slice. *J Physiol,* 552**,** 525-33.

JAGGER, D. J., ROBERTSON, D. & HOUSLEY, G. D. 2000. A technique for slicing the rat cochlea around the onset of hearing. *J Neurosci Methods,* 104**,** 77-86.

JAKOBSSON, A., WESTERBERG, R. & JACOBSSON, A. 2006. Fatty acid elongases in mammals: their regulation and roles in metabolism. *Prog Lipid Res,* 45**,** 237-49.

JENSEN, C. S., RASMUSSEN, H. B. & MISONOU, H. 2011. Neuronal trafficking of voltage-gated potassium channels. *Mol Cell Neurosci,* 48**,** 288-97.

JENSEN, M. O., JOGINI, V., BORHANI, D. W., LEFFLER, A. E., DROR, R. O. & SHAW, D. E. 2012. Mechanism of voltage gating in potassium channels. *Science,* 336**,** 229-33.

JENTSCH, T. J. 2000. Neuronal KCNQ potassium channels: physiology and role in disease. *Nat Rev Neurosci,* 1**,** 21-30.

JESCHKE, M. & MOSER, T. 2015. Considering optogenetic stimulation for cochlear implants. *Hear Res,* 322**,** 224-34.

JIANG, Y., LEE, A., CHEN, J., RUTA, V., CADENE, M., CHAIT, B. T. & MACKINNON, R. 2003. X-ray structure of a voltage-dependent K+ channel. *Nature,* 423**,** 33-41.

JOHNSON, A. E. & VAN WAES, M. A. 1999. The translocon: a dynamic gateway at the ER membrane. *Annu Rev Cell Dev Biol,* 15**,** 799-842.

JOHNSON, S. L., ECKRICH, T., KUHN, S., ZAMPINI, V., FRANZ, C., RANATUNGA, K. M., ROBERTS, T. P., MASETTO, S., KNIPPER, M., KROS, C. J. & MARCOTTI, W. 2011. Position-dependent patterning of spontaneous action potentials in immature cochlear inner hair cells. *Nat Neurosci,* 14**,** 711-7.

JOHNSTON, J., FORSYTHE, I. D. & KOPP-SCHEINPFLUG, C. 2010. Going native: voltage-gated potassium channels controlling neuronal excitability. *J Physiol,* 588**,** 3187-200.

JUHN, S. K., HUNTER, B. A. & ODLAND, R. M. 2001. Blood-labyrinth barrier and fluid dynamics of the inner ear. *Int Tinnitus J,* 7**,** 72-83.

KASIMOVA, M. A., TAREK, M., SHAYTAN, A. K., SHAITAN, K. V. & DELEMOTTE, L. 2014. Voltage-gated ion channel modulation by lipids: insights from molecular dynamics simulations. *Biochim Biophys Acta,* 1838**,** 1322-31.

KEITHLEY, E. M. & FELDMAN, M. L. 1979. Spiral ganglion cell counts in an age-graded series of rat cochleas. *J Comp Neurol,* 188**,** 429-442.

KEITHLEY, E. M. & FELDMAN, M. L. 1982. Hair cell counts in an age-graded series of rat cochleas. *Hear Res,* 8**,** 249-62.

KEROS, S. & MCBAIN, C. J. 1997. Arachidonic acid inhibits transient potassium currents and broadens action potentials during electrographic seizures in hippocampal pyramidal and inhibitory interneurons. *J Neurosci,* 17**,** 3476-87.

KHAN, K. M., DRESCHER, M. J., HATFIELD, J. S., KHAN, A. M. & DRESCHER, D. G. 2002. Muscarinic receptor subtypes are differentially distributed in the rat cochlea. *Neuroscience,* 111**,** 291-302.

KHAN, W. A., BLOBE, G. C. & HANNUN, Y. A. 1995. Arachidonic acid and free fatty acids as second messengers and the role of protein kinase C. *Cell Signal,* 7**,** 171-84.

KIANG, N. Y., PFEIFFER, R. R., WARR, W. B. & BACKUS, A. S. 1965. Stimulus coding in the cochlear nucleus. *Trans Am Otol Soc,* 53**,** 35-58.

KIANG, N. Y., RHO, J. M., NORTHROP, C. C., LIBERMAN, M. C. & RYUGO, D. K. 1982. Hair-cell innervation by spiral ganglion cells in adult cats. *Science,* 217**,** 175-7.

KIKKAWA, Y. S., NAKAGAWA, T., YING, L., TABATA, Y., TSUBOUCHI, H., IDO, A. & ITO, J. 2014. Growth factor-eluting cochlear implant electrode: impact on residual auditory function, insertional trauma, and fibrosis. *J Transl Med,* 12**,** 280.

KIM, Y. H. & HOLT, J. R. 2013. Functional contributions of HCN channels in the primary auditory neurons of the mouse inner ear. *J Gen Physiol,* 142**,** 207-23.

KLUMPHU, P. & LIPSHUTZ, B. H. 2014. "Nok": a phytosterol-based amphiphile enabling transition-metal-catalyzed couplings in water at room temperature. *J Org Chem,* 79**,** 888-900.

KOLB, H. C., FINN, M. G. & SHARPLESS, K. B. 2001. Click Chemistry: Diverse Chemical Function from a Few Good Reactions. *Angew Chem Int Ed Engl,* 40**,** 2004-2021.

KOPP-SCHEINPFLUG, C., FUCHS, K., LIPPE, W. R., TEMPEL, B. L. & RUBSAMEN, R. 2003. Decreased temporal precision of auditory signaling in Kcna1-null mice: an electrophysiological study in vivo. *J Neurosci,* 23**,** 9199-207.

KRJUKOVA, J., HOLMQVIST, T., DANIS, A. S., AKERMAN, K. E. & KUKKONEN, J. P. 2004. Phospholipase C activator m-3M3FBS affects Ca2+ homeostasis independently of phospholipase C activation. *Br J Pharmacol,* 143**,** 3-7.

KRUSE, M., HAMMOND, G. R. & HILLE, B. 2012. Regulation of voltage-gated potassium channels by PI(4,5)P2. *J Gen Physiol,* 140**,** 189-205.

KRUSE, M. & HILLE, B. 2013. The phosphoinositide sensitivity of the K(v) channel family. *Channels (Austin),* 7**,** 530-6.

KUANG, Q., PURHONEN, P. & HEBERT, H. 2015. Structure of potassium channels. *Cell Mol Life Sci,* 72**,** 3677-93.

KUBO, Y., ADELMAN, J. P., CLAPHAM, D. E., JAN, L. Y., KARSCHIN, A., KURACHI, Y., LAZDUNSKI, M., NICHOLS, C. G., SEINO, S. &

VANDENBERG, C. A. 2005. International Union of Pharmacology. LIV. Nomenclature and molecular relationships of inwardly rectifying potassium channels. *Pharmacol Rev,* 57**,** 509-26.

KUO, A., GULBIS, J. M., ANTCLIFF, J. F., RAHMAN, T., LOWE, E. D., ZIMMER, J., CUTHBERTSON, J., ASHCROFT, F. M., EZAKI, T. & DOYLE, D. A. 2003. Crystal structure of the potassium channel KirBac1.1 in the closed state. *Science,* 300**,** 1922-1926.

KURACHI, Y. & NORTH, A. 2004. Ion channels: their structure, function and control – an overview. *J Physiol,* 554**,** 245-247.

LAI, H. C. & JAN, L. Y. 2006. The distribution and targeting of neuronal voltage-gated ion channels. *Nat Rev Neurosci,* 7**,** 548-62.

LAMBE, E. K. & AGHAJANIAN, G. K. 2001. The role of Kv1.2-containing potassium channels in serotonin-induced glutamate release from thalamocortical terminals in rat frontal cortex. *J Neurosci,* 21**,** 9955-63.

LANDSBERGER, D. M., PADILLA, M. & SRINIVASAN, A. G. 2012. Reducing current spread using current focusing in cochlear implant users. *Hear Res,* 284**,** 16-24.

LANGER, P., GRUNDER, S. & RUSCH, A. 2003. Expression of Ca2+-activated BK channel mRNA and its splice variants in the rat cochlea. *J Comp Neurol,* 455**,** 198-209.

LARSSON, H. P., BAKER, O. S., DHILLON, D. S. & ISACOFF, E. Y. 1996. Transmembrane movement of the shaker K+ channel S4. *Neuron,* 16**,** 387-97.

LASARGE, C. L. & DANZER, S. C. 2014. Mechanisms regulating neuronal excitability and seizure development following mTOR pathway hyperactivation. *Front Mol Neurosci,* 7**,** 18.

LAWS, J. P. 1894. Note on the Comparative Antiseptic Action of the Phenyl-substituted Fatty Acids. *J Physiol,* 17**,** 360-3.

LAYTON, M. G., ROBERTSON, D., EVERETT, A. W., MULDERS, W. H. & YATES, G. K. 2005. Cellular localization of voltage-gated calcium channels and synaptic vesicle-associated proteins in the guinea pig cochlea. *J Mol Neurosci,* 27**,** 225-44.

LEE, A. G. 2004. How lipids affect the activities of integral membrane proteins. *Biochim Biophys Acta,* 1666**,** 62-87.

LEE, J. H., O'KEEFE, J. H., LAVIE, C. J., MARCHIOLI, R. & HARRIS, W. S. 2008. Omega-3 fatty acids for cardioprotection. *Mayo Clin Proc,* 83**,** 324-32.

LEE, T. E., PHILIPSON, L. H., KUZNETSOV, A. & NELSON, D. J. 1994. Structural determinant for assembly of mammalian K+ channels. *Biophys J,* 66**,** 667-73.

LEICHER, T., ROEPER, J., WEBER, K., WANG, X. & PONGS, O. 1996. Structural and functional characterization of human potassium channel subunit beta 1 (KCNA1B). *Neuropharmacology,* 35**,** 787-95.

LEMARIE, F., BEAUCHAMP, E., LEGRAND, P. & RIOUX, V. 2015. Revisiting the metabolism and physiological functions of caprylic acid (C8:0) with special focus on ghrelin octanoylation. *Biochimie*.

LEMMON, M. A. 2008. Membrane recognition by phospholipid-binding domains. *Nat Rev Mol Cell Biol,* 9**,** 99-111.

LI, M., JAN, Y. N. & JAN, L. Y. 1992. Specification of subunit assembly by the hydrophilic amino-terminal domain of the Shaker potassium channel. *Science,* 257**,** 1225-30.

LIBERMAN, M. C. 1978. Auditory-nerve response from cats raised in a low-noise chamber. *J Acoust Soc Am,* 63**,** 442-55.

LIBERMAN, M. C. 1980. Morphological differences among radial afferent fibers in the cat cochlea: an electron-microscopic study of serial sections. *Hear Res.,* 3**,** 45-63.

LIBERMAN, M. C. & KIANG, N. Y. 1978. Acoustic trauma in cats. Cochlear pathology and auditory-nerve activity. *Acta Otolaryngol Suppl,* 358**,** 1-63.

LIBERMAN, M. C. & KIANG, N. Y. 1984. Single-neuron labeling and chronic cochlear pathology. IV. Stereocilia damage and alterations in rate- and phase-level functions. *Hear Res,* 16**,** 75-90.

LIIN, S. I., SILVERA EJNEBY, M., BARRO-SORIA, R., SKARSFELDT, M. A., LARSSON, J. E., STARCK HARLIN, F., PARKKARI, T., BENTZEN, B. H., SCHMITT, N., LARSSON, H. P. & ELINDER, F. 2015. Polyunsaturated fatty acid analogs act antiarrhythmically on the cardiac IKs channel. *Proc Natl Acad Sci U S A,* 112**,** 5714-9.

LIM, D. J. 1986. Functional structure of the organ of Corti: a review. *Hear Res,* 22**,** 117-46.

LIM, S. T., ANTONUCCI, D. E., SCANNEVIN, R. H. & TRIMMER, J. S. 2000. A novel targeting signal for proximal clustering of the Kv2.1 K+ channel in hippocampal neurons. *Neuron,* 25**,** 385-97.

LIN, H. W. & PEREZ-PINZON, M. 2013. The role of fatty acids in the regulation of cerebral vascular function and neuroprotection in ischemia. *CNS Neurol Disord Drug Targets,* 12**,** 316-24.

LIN, X. 1997. Action potentials and underlying voltage-dependent currents studied in cultured spiral ganglion neurons of the postnatal gerbil. *Hear Res,* 108**,** 157-79.

LIN, X. & CHEN, S. 2000. Endogenously generated spontaneous spiking activities recorded from postnatal spiral ganglion neurons in vitro. *Brain Res Dev Brain Res,* 119**,** 297-305.

LIPTON, P. 1999. Ischemic cell death in brain neurons. *Physiol Rev,* 79**,** 1431-568.

LIU, Q. & DAVIS, R. L. 2007. Regional specification of threshold sensitivity and response time in CBA/CaJ mouse spiral ganglion neurons. *J Neurophysiol,* 98**,** 2215-22.

LIU, Q., LEE, E. & DAVIS, R. L. 2014a. Heterogeneous intrinsic excitability of murine spiral ganglion neurons is determined by Kv1 and HCN channels. *Neuroscience,* 257**,** 96-110.

LIU, Q., MANIS, P. B. & DAVIS, R. L. 2014b. I h and HCN channels in murine spiral ganglion neurons: tonotopic variation, local heterogeneity, and kinetic model. *J Assoc Res Otolaryngol,* 15**,** 585-99.

LIU, T. I., LEBARIC, Z. N., ROSENTHAL, J. J. & GILLY, W. F. 2001. Natural substitutions at highly conserved T1-domain residues perturb processing and functional expression of squid Kv1 channels. *J Neurophysiol,* 85**,** 61-71.

LIU, W., GLUECKERT, R., LINTHICUM, F. H., RIEGER, G., BLUMER, M., BITSCHE, M., PECHRIGGL, E., RASK-ANDERSEN, H. & SCHROTT-FISCHER, A. 2014c. Possible role of gap junction intercellular channels and connexin 43 in satellite glial cells (SGCs) for preservation of human spiral ganglion neurons : A comparative study with clinical implications. *Cell Tissue Res,* 355**,** 267-78.

LOGOTHETIS, D. E., PETROU, V. I., ADNEY, S. K. & MAHAJAN, R. 2010. Channelopathies linked to plasma membrane phosphoinositides. *Pflugers Arch,* 460**,** 321-41.

LONG, S. B., CAMPBELL, E. B. & MACKINNON, R. 2005. Voltage sensor of Kv1.2: structural basis of electromechanical coupling. *Science,* 309**,** 903-8.

LOPEZ-BARNEO, J., HOSHI, T., HEINEMANN, S. H. & ALDRICH, R. W. 1993. Effects of external cations and mutations in the pore region on C-type inactivation of Shaker potassium channels. *Receptors Channels,* 1**,** 61-71.

LOPEZ, I., ISHIYAMA, G., ACUNA, D., ISHIYAMA, A. & BALOH, R. W. 2003. Immunolocalization of voltage-gated calcium channel alpha1 subunits in the chinchilla cochlea. *Cell Tissue Res,* 313**,** 177-86.

LOUSSOUARN, G., PARK, K. H., BELLOCQ, C., BARO, I., CHARPENTIER, F. & ESCANDE, D. 2003. Phosphatidylinositol-4,5-bisphosphate, PIP2, controls KCNQ1/KCNE1 voltage-gated potassium channels: a functional homology between voltage-gated and inward rectifier K+ channels. *EMBO J,* 22**,** 5412-21.

LV, P., KIM, H. J., LEE, J. H., SIHN, C. R., FATHABAD GHARAIE, S., MOUSAVI-NIK, A., WANG, W., WANG, H. G., GRATTON, M. A., DOYLE, K. J., ZHANG, X. D., CHIAMVIMONVAT, N. & YAMOAH, E. N. 2014. Genetic, cellular, and functional evidence for Ca2+ inflow through Cav1.2 and Cav1.3 channels in murine spiral ganglion neurons. *J Neurosci,* 34**,** 7383-93.

LV, P., SIHN, C. R., WANG, W., SHEN, H., KIM, H. J., ROCHA-SANCHEZ, S. M. & YAMOAH, E. N. 2012. Posthearing Ca(2+) currents and their roles in shaping the different modes of firing of spiral ganglion neurons. *J Neurosci,* 32**,** 16314-30.

LV, P., WEI, D. & YAMOAH, E. N. 2010. Kv7-type channel currents in spiral ganglion neurons: involvement in sensorineural hearing loss. *J Biol Chem,* 285**,** 34699-707.

MAFFIE, J. & RUDY, B. 2008. Weighing the evidence for a ternary protein complex mediating A-type K+ currents in neurons. *J Physiol,* 586**,** 5609-23.

MAISON, S. F., LIU, X. P., VETTER, D. E., EATOCK, R. A., NATHANSON, N. M., WESS, J. & LIBERMAN, M. C. 2010. Muscarinic signaling in the cochlea: presynaptic and postsynaptic effects on efferent feedback and afferent excitability. *J Neurosci,* 30**,** 6751-62.

MANGANAS, L. N. & TRIMMER, J. S. 2000. Subunit composition determines Kv1 potassium channel surface expression. *J Biol Chem,* 275**,** 29685-93.

MANGANAS, L. N., WANG, Q., SCANNEVIN, R. H., ANTONUCCI, D. E., RHODES, K. J. & TRIMMER, J. S. 2001. Identification of a trafficking determinant localized to the Kv1 potassium channel pore. *Proc Natl Acad Sci U S A,* 98**,** 14055-9.

MATHEWS, P. J., JERCOG, P. E., RINZEL, J., SCOTT, L. L. & GOLDING, N. L. 2010. Control of submillisecond synaptic timing in binaural coincidence detectors by K(v)1 channels. *Nat Neurosci,* 13**,** 601-9.

MCCALL, A. A., SWAN, E. E., BORENSTEIN, J. T., SEWELL, W. F., KUJAWA, S. G. & MCKENNA, M. J. 2010. Drug delivery for treatment of inner ear disease: current state of knowledge. *Ear Hear,* 31**,** 156-65.

MCCORMACK, K., CONNOR, J. X., ZHOU, L., HO, L. L., GANETZKY, B., CHIU, S. Y. & MESSING, A. 2002. Genetic analysis of the mammalian K+ channel beta subunit Kvbeta 2 (Kcnab2). *J Biol Chem,* 277**,** 13219-28.

MCKAY, M. C. & WORLEY, J. F., 3RD 2001. Linoleic acid both enhances activation and blocks Kv1.5 and Kv2.1 channels by two separate mechanisms. *Am J Physiol Cell Physiol,* 281**,** C1277-84.

MCLAUGHLIN, S., WANG, J., GAMBHIR, A. & MURRAY, D. 2002. PIP(2) and proteins: interactions, organization, and information flow. *Annu Rev Biophys Biomol Struct,* 31**,** 151-75.

MCNAUGHT, A. D., WILKINSON, A. & INTERNATIONAL UNION OF PURE AND APPLIED CHEMISTRY. 1997. *Compendium of chemical terminology : IUPAC recommendations,* Oxford England ; Malden, MA, USA, Blackwell Science.

MEHTA, V. P. & VAN DER EYCKEN, E. V. 2011. Microwave-assisted C-C bond forming cross-coupling reactions: an overview. *Chem Soc Rev,* 40**,** 4925-36.

MICHAEL-TITUS, A. T. & PRIESTLEY, J. V. 2014. Omega-3 fatty acids and traumatic neurological injury: from neuroprotection to neuroplasticity? *Trends Neurosci,* 37**,** 30-8.

MO, Z. L., ADAMSON, C. L. & DAVIS, R. L. 2002. Dendrotoxin-sensitive K(+) currents contribute to accommodation in murine spiral ganglion neurons. *J Physiol,* 542**,** 763-78.

MO, Z. L. & DAVIS, R. L. 1997. Endogenous firing patterns of murine spiral ganglion neurons. *J Neurophysiol,* 77**,** 1294-305.

MORAIS-CABRAL, J. H., ZHOU, Y. & MACKINNON, R. 2001. Energetic optimization of ion conduction rate by the K+ selectivity filter. *Nature,* 414**,** 37-42.

MORENO-GALINDO, E. G., BARRIO-ECHAVARRIA, G. F., VASQUEZ, J. C., DECHER, N., SACHSE, F. B., TRISTANI-FIROUZI, M., SANCHEZ-CHAPULA, J. A. & NAVARRO-POLANCO, R. A. 2010. Molecular basis for a high-potency open-channel block of Kv1.5 channel by the endocannabinoid anandamide. *Mol Pharmacol,* 77**,** 751-8.

MORENO, C., MACIAS, A., PRIETO, A., DE LA CRUZ, A. & VALENZUELA, C. 2012. Polyunsaturated Fatty acids modify the gating of kv channels. *Front Pharmacol,* 3**,** 163.

MORRIS, C. E., BOUCHER, P. A. & JOOS, B. 2012. Left-shifted nav channels in injured bilayer: primary targets for neuroprotective nav antagonists? *Front Pharmacol,* 3**,** 19.

MURPHY, M. G. 1985. Membrane fatty acids, lipid peroxidation and adenylate cyclase activity in cultured neural cells. *Biochem Biophys Res Commun,* 132**,** 757-63.

MYNATT, R., HALE, S. A., GILL, R. M., PLONTKE, S. K. & SALT, A. N. 2006. Demonstration of a longitudinal concentration gradient along scala tympani by sequential sampling of perilymph from the cochlear apex. *J Assoc Res Otolaryngol,* 7**,** 182-93.

NADOL, J. B., JR. 1988a. Comparative anatomy of the cochlea and auditory nerve in mammals. *Hear Res,* 34**,** 253-66.

NADOL, J. B., JR. 1988b. Quantification of human spiral ganglion cells by serial section reconstruction and segmental density estimates. *Am J Otolaryngol,* 9**,** 47-51.

NAGAYA, N. & PAPAZIAN, D. M. 1997. Potassium channel alpha and beta subunits assemble in the endoplasmic reticulum. *J Biol Chem,* 272**,** 3022-7.

NAYAGAM, B. A., MUNIAK, M. A. & RYUGO, D. K. 2011. The spiral ganglion: connecting the peripheral and central auditory systems. *Hear Res,* 278**,** 2-20.

NEELY, S. T. & KIM, D. O. 1986. A model for active elements in cochlear biomechanics. *J Acoust Soc Am,* 79**,** 1472-80.

NEILSON, G. W. & SKIPPER, N. 1985. K+ coordination in aqueous solution. *Chem Phys Lett,* 114**,** 35–38.

NEUFELD, E. J. & MAJERUS, P. W. 1983. Arachidonate release and phosphatidic acid turnover in stimulated human platelets. *J Biol Chem,* 258**,** 2461-7.

NEYROUD, N., TESSON, F., DENJOY, I., LEIBOVICI, M., DONGER, C., BARHANIN, J., FAURE, S., GARY, F., COUMEL, P., PETIT, C., SCHWARTZ, K. & GUICHENEY, P. 1997. A novel mutation in the potassium channel gene KVLQT1 causes the Jervell and Lange-Nielsen cardioauditory syndrome. *Nat Genet,* 15**,** 186-9.

NIMIGEAN, C. M. & ALLEN, T. W. 2011. Origins of ion selectivity in potassium channels from the perspective of channel block. *J Gen Physiol,* 137**,** 405-13.

NWE, K. & BRECHBIEL, M. W. 2009. Growing applications of "click chemistry" for bioconjugation in contemporary biomedical research. *Cancer Biother Radiopharm,* 24**,** 289-302.

OGAWA, Y., HORRESH, I., TRIMMER, J. S., BREDT, D. S., PELES, E. & RASBAND, M. N. 2008. Postsynaptic density-93 clusters Kv1 channels at axon initial segments independently of Caspr2. *J Neurosci,* 28**,** 5731-9.

OLIVEIRA, A. F., CUNHA, D. A., LADRIERE, L., IGOILLO-ESTEVE, M., BUGLIANI, M., MARCHETTI, P. & CNOP, M. 2015. In vitro use of free fatty acids bound to albumin: A comparison of protocols. *Biotechniques,* 58**,** 228-33.

OLIVER, D., LIEN, C. C., SOOM, M., BAUKROWITZ, T., JONAS, P. & FAKLER, B. 2004. Functional conversion between A-type and delayed rectifier K+ channels by membrane lipids. *Science,* 304**,** 265-70.

OLSON, E. S., DUIFHUIS, H. & STEELE, C. R. 2012. Von Bekesy and cochlear mechanics. *Hear Res,* 293**,** 31-43.

ORIO, P., TORRES, Y., ROJAS, P., CARVACHO, I., GARCIA, M. L., TORO, L., VALVERDE, M. A. & LATORRE, R. 2006. Structural determinants for functional coupling between the beta and alpha subunits in the Ca2+-activated K+ (BK) channel. *J Gen Physiol,* 127**,** 191-204.

OTA, C. Y. & KIMURA, R. S. 1980. Ultrastructural study of the human spiral ganglion. *Acta Otolaryngol,* 89**,** 53-62.

PALMER, A. R. & RUSSELL, I. J. 1986. Phase-locking in the cochlear nerve of the guinea-pig and its relation to the receptor potential of inner hair-cells. *Hear Res,* 24**,** 1-15.

PAN, Z., KAO, T., HORVATH, Z., LEMOS, J., SUL, J. Y., CRANSTOUN, S. D., BENNETT, V., SCHERER, S. S. & COOPER, E. C. 2006. A common ankyrin-G-based mechanism retains KCNQ and NaV channels at electrically active domains of the axon. *J Neurosci,* 26**,** 2599-613.

PANYI, G. & DEUTSCH, C. 1996. Assembly and suppression of endogenous Kv1.3 channels in human T cells. *J Gen Physiol,* 107**,** 409-20.

PAPACKOVA, Z. & CAHOVA, M. 2015. Fatty acid signaling: the new function of intracellular lipases. *Int J Mol Sci,* 16**,** 3831-55.

PAPAZIAN, D. M., SCHWARZ, T. L., TEMPEL, B. L., JAN, Y. N. & JAN, L. Y. 1987. Cloning of genomic and complementary DNA from Shaker, a putative potassium channel gene from Drosophila. *Science,* 237**,** 749-53.

PARARAS, E. E., BORKHOLDER, D. A. & BORENSTEIN, J. T. 2012. Microsystems technologies for drug delivery to the inner ear. *Adv Drug Deliv Rev,* 64**,** 1650-60.

PATUZZI, R. 2011. Ion flow in stria vascularis and the production and regulation of cochlear endolymph and the endolymphatic potential. *Hear Res,* 277**,** 4-19.

PICKLES, O. 2008. *An Introduction to the Physiology of Hearing, 3rd edition*, Academic Press.

PICKLES, O. 2012. *An Introduction to the Physiology of Hearing, 4th edition,*, Academic Press.

PINYON, J. L., TADROS, S. F., FROUD, K. E., AC, Y. W., TOMPSON, I. T., CRAWFORD, E. N., KO, M., MORRIS, R., KLUGMANN, M. & HOUSLEY, G. D. 2014. Close-field electroporation gene delivery using the cochlear implant electrode array enhances the bionic ear. *Sci Transl Med,* 6**,** 233ra54.

POLING, J. S., KARANIAN, J. W., SALEM, N., JR. & VICINI, S. 1995. Time- and voltage-dependent block of delayed rectifier potassium channels by docosahexaenoic acid. *Mol Pharmacol,* 47**,** 381-90.

POLING, J. S., ROGAWSKI, M. A., SALEM, N., JR. & VICINI, S. 1996a. Anandamide, an endogenous cannabinoid, inhibits Shaker-related voltage-gated K+ channels. *Neuropharmacology,* 35**,** 983-91.

POLING, J. S., VICINI, S., ROGAWSKI, M. A. & SALEM, N., JR. 1996b. Docosahexaenoic acid block of neuronal voltage-gated K+ channels: subunit selective antagonism by zinc. *Neuropharmacology,* 35**,** 969-82.

PONGS, O., LEICHER, T., BERGER, M., ROEPER, J., BAHRING, R., WRAY, D., GIESE, K. P., SILVA, A. J. & STORM, J. F. 1999. Functional and molecular aspects of voltage-gated K+ channel beta subunits. *Ann N Y Acad Sci,* 868**,** 344-55.

PONGS, O. & SCHWARZ, J. R. 2010. Ancillary subunits associated with voltage-dependent K+ channels. *Physiol Rev,* 90**,** 755-96.

PUEL, J. L., BOBBIN, R. P. & FALLON, M. 1989. Suppression of auditory nerve activity in the guinea pig cochlea by 1-(p-bromobenzoyl)-piperazine-2,3-dicarboxylic acid. *Brain Res,* 487**,** 9-15.

QUESNEL, S., NGUYEN, Y., CAMPO, P., HERMINE, O., RIBEIL, J. A., ELMALEH, M., GRAYELI, A. B., FERRARY, E., STERKERS, O. & COULOIGNER, V. 2011a. Protective effect of systemic administration of erythropoietin on auditory brain stem response and compound action potential thresholds in an animal model of cochlear implantation. *Ann Otol Rhinol Laryngol,* 120**,** 737-47.

QUESNEL, S., NGUYEN, Y., ELMALEH, M., GRAYELI, A. B., FERRARY, E., STERKERS, O. & COULOIGNER, V. 2011b. Effects of systemic administration of methylprednisolone on residual hearing in an animal model of cochlear implantation. *Acta Otolaryngol,* 131**,** 579-84.

RAMANADHAM, S., GROSS, R. & TURK, J. 1992. Arachidonic acid induces an increase in the cytosolic calcium concentration in single pancreatic islet beta cells. *Biochem Biophys Res Commun,* 184**,** 647-53.

RASMUSSEN, H. B., FROKJAER-JENSEN, C., JENSEN, C. S., JENSEN, H. S., JORGENSEN, N. K., MISONOU, H., TRIMMER, J. S., OLESEN, S. P. & SCHMITT, N. 2007. Requirement of subunit co-assembly and ankyrin-G for M-channel localization at the axon initial segment. *J Cell Sci,* 120**,** 953-63.

REID, M. A., FLORES-OTERO, J. & DAVIS, R. L. 2004. Firing patterns of type II spiral ganglion neurons in vitro. *J Neurosci,* 24**,** 733-42.

RELKIN, E. M. & DOUCET, J. R. 1991. Recovery from prior stimulation. I: Relationship to spontaneous firing rates of primary auditory neurons. *Hear Res,* 55**,** 215-22.

RETTIG, J., HEINEMANN, S. H., WUNDER, F., LORRA, C., PARCEJ, D. N., DOLLY, J. O. & PONGS, O. 1994. Inactivation properties of voltage-gated K+ channels altered by presence of beta-subunit. *Nature,* 369**,** 289-94.

REVEST, P. & LONGSTAFF, A. 1998. *Molecular Neuroscience,* Oxford, UK, BIOS Scientific Publishers Ltd.

RIVERA, J. F., AHMAD, S., QUICK, M. W., LIMAN, E. R. & ARNOLD, D. B. 2003. An evolutionarily conserved dileucine motif in Shal K+ channels mediates dendritic targeting. *Nat Neurosci,* 6**,** 243-50.

ROBBINS, J. 2001. KCNQ potassium channels: physiology, pathophysiology, and pharmacology. *Pharmacol Ther,* 90**,** 1-19.

ROBBINS, J., MARSH, S. J. & BROWN, D. A. 2006. Probing the regulation of M (Kv7) potassium channels in intact neurons with membrane-targeted peptides. *J Neurosci,* 26**,** 7950-61.

ROBERTSON, D. 1984. Horseradish peroxidase injection of physiologically characterized afferent and efferent neurones in the guinea pig spiral ganglion. *Hear Res,* 15**,** 113-21.

RODRIGUEZ-MENCHACA, A. A., ADNEY, S. K., ZHOU, L. & LOGOTHETIS, D. E. 2012. Dual Regulation of Voltage-Sensitive Ion Channels by PIP(2). *Front Pharmacol,* 3**,** 170.

RODRIGUEZ, N., AMAROUCH, M. Y., MONTNACH, J., PIRON, J., LABRO, A. J., CHARPENTIER, F., MEROT, J., BARO, I. & LOUSSOUARN, G. 2010. Phosphatidylinositol-4,5-bisphosphate (PIP(2)) stabilizes the open pore conformation of the Kv11.1 (hERG) channel. *Biophys J,* 99**,** 1110-8.

ROMAND, M. R. & ROMAND, R. 1987. The ultrastructure of spiral ganglion cells in the mouse. *Acta Otolaryngol,* 104**,** 29-39.

ROMAND, R. 1983. Development in the frequency selectivity of auditory nerve fibers in the kitten. *Neurosci Lett,* 35**,** 271-6.

ROME, C., LUO, D. & DULON, D. 1999. Muscarinic receptor-mediated calcium signaling in spiral ganglion neurons of the mammalian cochlea. *Brain Res,* 846**,** 196-203.

ROSENBLUTH, J. 1962. The fine structure of acoustic ganglia in the rat. *J Cell Biol,* 12**,** 329-59.

RUBEL, E. W. 1978. *Ontogeny of Structure and Function in the Vertebrate Auditory System: Handbook of Sensory Physiology,* SpringerVerlag.

RUEL, J., CHABBERT, C., NOUVIAN, R., BENDRIS, R., EYBALIN, M., LEGER, C. L., BOURIEN, J., MERSEL, M. & PUEL, J. L. 2008. Salicylate enables cochlear arachidonic-acid-sensitive NMDA receptor responses. *J Neurosci,* 28**,** 7313-23.

RUGGERO, M. A., ROBLES, L. & RICH, N. C. 1992. Two-tone suppression in the basilar membrane of the cochlea: mechanical basis of auditory-nerve rate suppression. *J Neurophysiol,* 68**,** 1087-99.

RUSSELL, I. J. & SELLICK, P. M. 1978. Intracellular studies of hair cells in the mammalian cochlea. *J Physiol,* 284**,** 261-90.

RUSZNAK, Z., BAKONDI, G., POCSAI, K., POR, A., KOSZTKA, L., PAL, B., NAGY, D. & SZUCS, G. 2008. Voltage-gated potassium channel (Kv) subunits expressed in the rat cochlear nucleus. *J Histochem Cytochem,* 56**,** 443-65.

RUSZNAK, Z. & SZUCS, G. 2009. Spiral ganglion neurones: an overview of morphology, firing behaviour, ionic channels and function. *Pflugers Arch,* 457**,** 1303-25.

RUTHERFORD, M. A., CHAPOCHNIKOV, N. M. & MOSER, T. 2012. Spike encoding of neurotransmitter release timing by spiral ganglion neurons of the cochlea. *J Neurosci,* 32**,** 4773-89.

RYUGO, D. K. 2008. Projections of low spontaneous rate, high threshold auditory nerve fibers to the small cell cap of the cochlear nucleus in cats. *Neuroscience,* 154**,** 114-26.

RYUGO, D. K. & FEKETE, D. M. 1982. Morphology of primary axosomatic endings in the anteroventral cochlear nucleus of the cat: a study of the endbulbs of Held. *J Comp Neurol,* 210**,** 239-57.

RYUGO, D. K., WU, M. M. & PONGSTAPORN, T. 1996. Activity-related features of synapse morphology: a study of endbulbs of held. *J Comp Neurol,* 365**,** 141-58.

SADE, H., MURAKI, K., OHYA, S., HATANO, N. & IMAIZUMI, Y. 2006. Activation of large-conductance, Ca2+-activated K+ channels by cannabinoids. *Am J Physiol Cell Physiol,* 290**,** C77-86.

SAFIEDDINE, S., BARTOLAMI, S., WENTHOLD, R. J. & EYBALIN, M. 1996. Pre- and postsynaptic M3 muscarinic receptor mRNAs in the rodent peripheral auditory system. *Brain Res Mol Brain Res,* 40**,** 127-35.

SAFIEDDINE, S., EL-AMRAOUI, A. & PETIT, C. 2012. The auditory hair cell ribbon synapse: from assembly to function. *Annu Rev Neurosci,* 35**,** 509-28.

SAITO, T., ZHANG, Z. J., TOKURIKI, M., OHTSUBO, T., NODA, I., SHIBAMORI, Y., YAMAMOTO, T. & SAITO, H. 2001a. Expression of multidrug resistance protein 1 (MRP1) in the rat cochlea with special reference to the blood-inner ear barrier. *Brain Res,* 895**,** 253-7.

SAITO, T., ZHANG, Z. J., TOKURIKI, M., OHTSUBO, T., NODA, I., SHIBAMORI, Y., YAMAMOTO, T. & SAITO, H. 2001b. Expression of p-glycoprotein is associated with that of multidrug resistance protein 1 (MRP1) in the vestibular labyrinth and endolymphatic sac of the guinea pig. *Neurosci Lett,* 303**,** 189-92.

SALT, A. N. & PLONTKE, S. K. 2009. Principles of local drug delivery to the inner ear. *Audiol Neurootol,* 14**,** 350-60.

SANSOM, M. S., SHRIVASTAVA, I. H., BRIGHT, J. N., TATE, J., CAPENER, C. E. & BIGGIN, P. C. 2002. Potassium channels: structures, models, simulations. *Biochim Biophys Acta,* 1565**,** 294-307.

SANTOS-SACCHI, J. 1993. Voltage-dependent ionic conductances of type I spiral ganglion cells from the guinea pig inner ear. *J Neurosci,* 13**,** 3599-611.

SCHMIDT, D., JIANG, Q. X. & MACKINNON, R. 2006. Phospholipids and the origin of cationic gating charges in voltage sensors. *Nature,* 444**,** 775-9.

SCHULTE, U., THUMFART, J. O., KLOCKER, N., SAILER, C. A., BILDL, W., BINIOSSEK, M., DEHN, D., DELLER, T., EBLE, S., ABBASS, K., WANGLER, T., KNAUS, H. G. & FAKLER, B. 2006. The epilepsy-linked Lgi1 protein assembles into presynaptic Kv1 channels and inhibits inactivation by Kvbeta1. *Neuron,* 49**,** 697-706.

SCHULTZ, D., LITT, M., SMITH, L., THAYER, M. & MCCORMACK, K. 1996. Localization of two potassium channel beta subunit genes, KCNA1B and KCNA2B. *Genomics,* 31**,** 389-91.

SCHWAKE, M., PUSCH, M., KHARKOVETS, T. & JENTSCH, T. J. 2000. Surface expression and single channel properties of KCNQ2/KCNQ3, M-type K+ channels involved in epilepsy. *J Biol Chem,* 275**,** 13343-8.

SCHWARZ, D. W. & PUIL, E. 1997. Firing properties of spherical bushy cells in the anteroventral cochlear nucleus of the gerbil. *Hear Res,* 114**,** 127-38.

SHAH, M., MISTRY, M., MARSH, S. J., BROWN, D. A. & DELMAS, P. 2002. Molecular correlates of the M-current in cultured rat hippocampal neurons. *J Physiol,* 544**,** 29-37.

SHAIKH, S. R. 2012. Biophysical and biochemical mechanisms by which dietary N-3 polyunsaturated fatty acids from fish oil disrupt membrane lipid rafts. *J Nutr Biochem,* 23**,** 101-5.

SHANNON, R. V., FU, Q. J. & GALVIN, J., 3RD 2004. The number of spectral channels required for speech recognition depends on the difficulty of the listening situation. *Acta Otolaryngol Suppl***,** 50-4.

SHANNON, R. V., ZENG, F. G., KAMATH, V., WYGONSKI, J. & EKELID, M. 1995. Speech recognition with primarily temporal cues. *Science,* 270**,** 303-4.

SHENG, C., CHE, X., WANG, W., WANG, S., CAO, Y., MIAO, Z., YAO, J. & ZHANG, W. 2011. Design and synthesis of novel triazole antifungal derivatives by structure-based bioisosterism. *Eur J Med Chem,* 46**,** 5276-82.

SHIMADA, T. & SOMLYO, A. P. 1992. Modulation of voltage-dependent Ca channel current by arachidonic acid and other long-chain fatty acids in rabbit intestinal smooth muscle. *J Gen Physiol,* 100**,** 27-44.

SHYNG, S. L. & NICHOLS, C. G. 1998. Membrane phospholipid control of nucleotide sensitivity of KATP channels. *Science,* 282**,** 1138-41.

SIEGEL, J. H. 1992. Spontaneous synaptic potentials from afferent terminals in the guinea pig cochlea. *Hear Res,* 59**,** 85-92.

SIEGEL, J. H. & DALLOS, P. 1986. Spike activity recorded from the organ of Corti. *Hear Res,* 22**,** 245-8.

SIERRO, C. D., VITUS, J. & DUNANT, Y. 1992. Effects of muscarinic agonists and depolarizing agents on inositol monophosphate accumulation in the rabbit vagus nerve. *J Neurochem,* 59**,** 456-66.

SIMMONS, D. D., BERTOLOTTO, C., KIM, J., RAJI-KUBBA, J. & MANSDORF, N. 1998. Choline acetyltransferase expression during a putative developmental waiting period. *J Comp Neurol,* 397**,** 281-95.

SIMOPOULOS, A. P. 2008a. The importance of the omega-6/omega-3 fatty acid ratio in cardiovascular disease and other chronic diseases. *Exp Biol Med (Maywood),* 233**,** 674-88.

SIMOPOULOS, A. P. 2008b. The omega-6/omega-3 fatty acid ratio, genetic variation, and cardiovascular disease. *Asia Pac J Clin Nutr,* 17 Suppl 1**,** 131-4.

SINGLETON, C. B., VALENZUELA, S. M., WALKER, B. D., TIE, H., WYSE, K. R., BURSILL, J. A., QIU, M. R., BREIT, S. N. & CAMPBELL, T. J. 1999. Blockade by N-3 polyunsaturated fatty acid of the Kv4.3 current stably expressed in Chinese hamster ovary cells. *Br J Pharmacol,* 127**,** 941-8.

SKINNER, L. J., ENEE, V., BEURG, M., JUNG, H. H., RYAN, A. F., HAFIDI, A., ARAN, J. M. & DULON, D. 2003. Contribution of BK Ca2+-activated K+ channels to auditory neurotransmission in the Guinea pig cochlea. *J Neurophysiol,* 90**,** 320-32.

SMIRNOV, S. V. & AARONSON, P. I. 1996. Modulatory effects of arachidonic acid on the delayed rectifier K+ current in rat pulmonary arterial myocytes. Structural aspects and involvement of protein kinase C. *Circ Res,* 79**,** 20-31.

SMITH, K. E., BROWNE, L., SELWOOD, D. L., MCALPINE, D. & JAGGER, D. J. 2015. Phosphoinositide Modulation of Heteromeric Kv1 Channels Adjusts Output of Spiral Ganglion Neurons from Hearing Mice. *J Neurosci,* 35**,** 11221-32.

SMITH, P. H. 1995. Structural and functional differences distinguish principal from nonprincipal cells in the guinea pig MSO slice. *J Neurophysiol,* 73**,** 1653-67.

SMITH, P. H., JORIS, P. X. & YIN, T. C. 1993. Projections of physiologically characterized spherical bushy cell axons from the cochlear nucleus of the cat: evidence for delay lines to the medial superior olive. *J Comp Neurol,* 331**,** 245-60.

SOHMER, H. 2015. Reflections on the role of a traveling wave along the basilar membrane in view of clinical and experimental findings. *Eur Arch Otorhinolaryngol,* 272**,** 531-5.

SOKOLOV, M. V., SHAMOTIENKO, O., DHOCHARTAIGH, S. N., SACK, J. T. & DOLLY, J. O. 2007. Concatemers of brain Kv1 channel alpha subunits that give similar K+ currents yield pharmacologically distinguishable heteromers. *Neuropharmacology,* 53**,** 272-82.

SOKOLOWSKI, B. H., SAKAI, Y., HARVEY, M. C. & DUZHYY, D. E. 2004. Identification and localization of an arachidonic acid-sensitive potassium channel in the cochlea. *J Neurosci,* 24**,** 6265-76.

SOLTIS, M. J., YEH, H. J., COLE, K. A., WHITTAKER, N., WERSTO, R. P. & KOHN, E. C. 1996. Identification and characterization of human metabolites of CAI [5-amino-1-1(4'-chlorobenzoyl-3,5-dichlorobenzyl)-1,2,3-triazole- 4-carboxamide). *Drug Metab Dispos,* 24**,** 799-806.

SPOENDLIN, H. 1971. Degeneration behaviour of the cochlear nerve. *Arch Klin Exp Ohren Nasen Kehlkopfheilkd,* 200**,** 275-91.

SPOENDLIN, H. 1979. Sensory neural organization of the cochlea. *J Laryngol Otol,* 93**,** 853-77.

SPOENDLIN, H. 1981. Differentiation of cochlear afferent neurons. *Acta Otolaryngol,* 91**,** 451-6.

SRINIVASAN, A. G., PADILLA, M., SHANNON, R. V. & LANDSBERGER, D. M. 2013. Improving speech perception in noise with current focusing in cochlear implant users. *Hear Res,* 299**,** 29-36.

STAECKER, H. & RODGERS, B. 2013. Developments in delivery of medications for inner ear disease. *Expert Opin Drug Deliv,* 10**,** 639-50.

STAMATAKI, S., FRANCIS, H. W., LEHAR, M., MAY, B. J. & RYUGO, D. K. 2006. Synaptic alterations at inner hair cells precede spiral ganglion cell loss in aging C57BL/6J mice. *Hear Res,* 221**,** 104-18.

STOJANOVSKI, D., BOHNERT, M., PFANNER, N. & VAN DER LAAN, M. 2012. Mechanisms of protein sorting in mitochondria. *Cold Spring Harb Perspect Biol,* 4.

STOVER, T., YAGI, M. & RAPHAEL, Y. 1999. Cochlear gene transfer: round window versus cochleostomy inoculation. *Hear Res,* 136**,** 124-30.

SUH, B. C. & HILLE, B. 2002. Recovery from muscarinic modulation of M current channels requires phosphatidylinositol 4,5-bisphosphate synthesis. *Neuron,* 35**,** 507-20.

SUH, B. C. & HILLE, B. 2005. Regulation of ion channels by phosphatidylinositol 4,5-bisphosphate. *Curr Opin Neurobiol,* 15**,** 370-8.

SUH, B. C. & HILLE, B. 2007. Electrostatic interaction of internal Mg2+ with membrane PIP2 Seen with KCNQ K+ channels. *J Gen Physiol,* 130**,** 241-56.

SUH, B. C. & HILLE, B. 2008. PIP2 is a necessary cofactor for ion channel function: how and why? *Annu Rev Biophys,* 37**,** 175-95.

SUMNER, C. J. & PALMER, A. R. 2012. Auditory nerve fibre responses in the ferret. *Eur J Neurosci,* 36**,** 2428-39.

SUN, X., ZHOU, D., ZHANG, P., MOCZYDLOWSKI, E. G. & HADDAD, G. G. 2007. Beta-subunit-dependent modulation of hSlo BK current by arachidonic acid. *J Neurophysiol,* 97**,** 62-9.

SVIRSKIS, G., KOTAK, V., SANES, D. H. & RINZEL, J. 2002. Enhancement of signal-to-noise ratio and phase locking for small inputs by a low-threshold outward current in auditory neurons. *J Neurosci,* 22**,** 11019-25.

SWARTZ, K. J. 2008. Sensing voltage across lipid membranes. *Nature,* 456**,** 891-7.

SZABO, Z. S., HARASZTOSI, C. S., SZIKLAI, I., SZUCS, G. & RUSZNAK, Z. 2002. Ionic currents determining the membrane characteristics of type I spiral ganglion neurons of the guinea pig. *Eur J Neurosci,* 16**,** 1887-95.

TALAVERA, K., STAES, M., JANSSENS, A., DROOGMANS, G. & NILIUS, B. 2004. Mechanism of arachidonic acid modulation of the T-type Ca2+ channel alpha1G. *J Gen Physiol,* 124**,** 225-38.

TASAKI, I. 1954. Nerve impulses in individual auditory nerve fibers of guinea pig. *J Neurophysiol,* 17**,** 97-122.

TASSONI, D., KAUR, G., WEISINGER, R. S. & SINCLAIR, A. J. 2008. The role of eicosanoids in the brain. *Asia Pac J Clin Nutr,* 17 Suppl 1**,** 220-8.

TELEZHKIN, V., REILLY, J. M., THOMAS, A. M., TINKER, A. & BROWN, D. A. 2012. Structural requirements of membrane phospholipids for M-type potassium channel activation and binding. *J Biol Chem,* 287**,** 10001-12.

TELEZHKIN, V., THOMAS, A. M., HARMER, S. C., TINKER, A. & BROWN, D. A. 2013. A basic residue in the proximal C-terminus is necessary for efficient activation of the M-channel subunit Kv7.2 by PI(4,5)P(2). *Pflugers Arch,* 465**,** 945-53.

THIERS, F. A., BURGESS, B. J. & NADOL, J. B., JR. 2000. Prevalence and ultrastructural morphology of axosomatic synapses on spiral ganglion cells in humans of different ages. *Hear Res,* 150**,** 119-31.

THIERS, F. A., NADOL, J. B., JR. & LIBERMAN, M. C. 2008. Reciprocal synapses between outer hair cells and their afferent terminals: evidence for a local neural network in the mammalian cochlea. *J Assoc Res Otolaryngol,* 9**,** 477-89.

THOMAS, A. M., HARMER, S. C., KHAMBRA, T. & TINKER, A. 2011. Characterization of a binding site for anionic phospholipids on KCNQ1. *J Biol Chem,* 286**,** 2088-100.

THOMPSON, A. N., KIM, I., PANOSIAN, T. D., IVERSON, T. M., ALLEN, T. W. & NIMIGEAN, C. M. 2009. Mechanism of potassium-channel selectivity revealed by Na(+) and Li(+) binding sites within the KcsA pore. *Nat Struct Mol Biol,* 16**,** 1317-24.

THOMSEN, E. 1966. The ultrastructure of the spiral ganglion in the guinea pig. *Acta Otolaryngol***,** Suppl 224:442+.

TKATCH, T., BARANAUSKAS, G. & SURMEIER, D. J. 2000. Kv4.2 mRNA abundance and A-type K(+) current amplitude are linearly related in basal ganglia and basal forebrain neurons. *J Neurosci,* 20**,** 579-88.

TOESCA, A. 1996. Central and peripheral myelin in the rat cochlear and vestibular nerves. *Neurosci Lett,* 221**,** 21-4.

TONG, H., STEINERT, J. R., ROBINSON, S. W., CHERNOVA, T., READ, D. J., OLIVER, D. L. & FORSYTHE, I. D. 2010. Regulation of Kv channel expression and neuronal excitability in rat medial nucleus of the trapezoid body maintained in organotypic culture. *J Physiol,* 588**,** 1451-68.

TRIMMER, J. S. & RHODES, K. J. 2004. Localization of voltage-gated ion channels in mammalian brain. *Annu Rev Physiol,* 66**,** 477-519.

TU, L., SANTARELLI, V., SHENG, Z., SKACH, W., PAIN, D. & DEUTSCH, C. 1996. Voltage-gated K+ channels contain multiple intersubunit association sites. *J Biol Chem,* 271**,** 18904-11.

VACHER, H., MOHAPATRA, D. P. & TRIMMER, J. S. 2008. Localization and targeting of voltage-dependent ion channels in mammalian central neurons. *Physiol Rev,* 88**,** 1407-47.

VALIYAVEETIL, F. I., LEONETTI, M., MUIR, T. W. & MACKINNON, R. 2006. Ion selectivity in a semisynthetic K+ channel locked in the conductive conformation. *Science,* 314**,** 1004-7.

VALIYAVEETIL, F. I., ZHOU, Y. & MACKINNON, R. 2002. Lipids in the structure, folding, and function of the KcsA K+ channel. *Biochemistry,* 41**,** 10771-7.

VAN MEER, G., VOELKER, D. R. & FEIGENSON, G. W. 2008. Membrane lipids: where they are and how they behave. *Nat Rev Mol Cell Biol,* 9**,** 112-24.

VEMURI, V. K. & MAKRIYANNIS, A. 2015. Medicinal chemistry of cannabinoids. *Clin Pharmacol Ther,* 97**,** 553-8.

VILLARROEL, A. & SCHWARZ, T. L. 1996. Inhibition of the Kv4 (Shal) family of transient K+ currents by arachidonic acid. *J Neurosci,* 16**,** 2522-32.

VISENTIN, S. & LEVI, G. 1998. Arachidonic acid-induced inhibition of microglial outward-rectifying K+ current. *Glia,* 22**,** 1-10.

WALKER, E. H., PACOLD, M. E., PERISIC, O., STEPHENS, L., HAWKINS, P. T., WYMANN, M. P. & WILLIAMS, R. L. 2000. Structural determinants of phosphoinositide 3-kinase inhibition by wortmannin, LY294002, quercetin, myricetin, and staurosporine. *Mol Cell,* 6**,** 909-19.

WAN, A. S., NGIAM, T. L., LEUNG, S. L., GO, M. L., FRANCISCO, C. G., FREIRE, R., HERNANDEZ, R., SALAZAR, J. A., SUAREZ, E., GARCIA, G. A. & ET AL. 1983. Long-acting contraceptive agents: levonorgestrel esters of unsaturated acids. *Steroids,* 41**,** 339-48.

WANG, H., KUNKEL, D. D., SCHWARTZKROIN, P. A. & TEMPEL, B. L. 1994. Localization of Kv1.1 and Kv1.2, two K channel proteins, to synaptic terminals, somata, and dendrites in the mouse brain. *J Neurosci,* 14**,** 4588-99.

WANG, W., KIM, H. J., LV, P., TEMPEL, B. & YAMOAH, E. N. 2013. Association of the Kv1 family of K+ channels and their functional blueprint in the properties of auditory neurons as revealed by genetic and functional analyses. *J Neurophysiol,* 110**,** 1751-64.

WARNECKE, A., SASSE, S., WENZEL, G. I., HOFFMANN, A., GROSS, G., PAASCHE, G., SCHEPER, V., REICH, U., ESSER, K. H., LENARZ, T., STOVER, T. & WISSEL, K. 2012. Stable release of BDNF from the fibroblast cell line NIH3T3 grown on silicone elastomers enhances survival of spiral ganglion cells in vitro and in vivo. *Hear Res,* 289**,** 86-97.

WEISZ, C., GLOWATZKI, E. & FUCHS, P. 2009. The postsynaptic function of type II cochlear afferents. *Nature,* 461**,** 1126-9.

WERKMAN, T. R., GUSTAFSON, T. A., ROGOWSKI, R. S., BLAUSTEIN, M. P. & ROGAWSKI, M. A. 1993. Tityustoxin-K alpha, a structurally novel and highly potent K+ channel peptide toxin, interacts with the alpha-dendrotoxin binding site on the cloned Kv1.2 K+ channel. *Mol Pharmacol,* 44**,** 430-6.

WHITLON, D. S., KETELS, K. V., COULSON, M. T., WILLIAMS, T., GROVER, M., EDPAO, W. & RICHTER, C. P. 2006. Survival and morphology of auditory neurons in dissociated cultures of newborn mouse spiral ganglion. *Neuroscience,* 138**,** 653-62.

WILKE, B. U., LINDNER, M., GREIFENBERG, L., ALBUS, A., KRONIMUS, Y., BUNEMANN, M., LEITNER, M. G. & OLIVER, D. 2014. Diacylglycerol mediates regulation of TASK potassium channels by Gq-coupled receptors. *Nat Commun,* 5**,** 5540.

WILLIAMS, S. R. & MITCHELL, S. J. 2008. Direct measurement of somatic voltage clamp errors in central neurons. *Nat Neurosci,* 11**,** 790-8.

WINLOVE, C. I. & ROBERTS, A. 2011. Pharmacology of currents underlying the different firing patterns of spinal sensory neurons and interneurons identified in vivo using multivariate analysis. *J Neurophysiol,* 105**,** 2487-500.

WINTER, I. M., ROBERTSON, D. & YATES, G. K. 1990. Diversity of characteristic frequency rate-intensity functions in guinea pig auditory nerve fibres. *Hear Res,* 45**,** 191-202.

WOLF, M. J., IZUMI, Y., ZORUMSKI, C. F. & GROSS, R. W. 1995. Long-term potentiation requires activation of calcium-independent phospholipase A2. *FEBS Lett,* 377**,** 358-62.

WRZESZCZ, A., STEFFENS, M., BALSTER, S., WARNECKE, A., DITTRICH, B., LENARZ, T. & REUTER, G. 2015. Hydrogel coated and dexamethasone releasing cochlear implants: quantification of fibrosis in guinea pigs and

evaluation of insertion forces in a human cochlea model. *J Biomed Mater Res B Appl Biomater,* 103**,** 169-78.

WU, J., DING, W. G., MATSUURA, H., TSUJI, K., ZANG, W. J. & HORIE, M. 2009. Inhibitory actions of the phosphatidylinositol 3-kinase inhibitor LY294002 on the human Kv1.5 channel. *Br J Pharmacol,* 156**,** 377-87.

WYMANN, M. P., BULGARELLI-LEVA, G., ZVELEBIL, M. J., PIROLA, L., VANHAESEBROECK, B., WATERFIELD, M. D. & PANAYOTOU, G. 1996. Wortmannin inactivates phosphoinositide 3-kinase by covalent modification of Lys-802, a residue involved in the phosphate transfer reaction. *Mol Cell Biol,* 16**,** 1722-33.

XIAO, Y. F., KANG, J. X., MORGAN, J. P. & LEAF, A. 1995. Blocking effects of polyunsaturated fatty acids on Na+ channels of neonatal rat ventricular myocytes. *Proc Natl Acad Sci U S A,* 92**,** 11000-4.

XIAO, Y. F., MA, L., WANG, S. Y., JOSEPHSON, M. E., WANG, G. K., MORGAN, J. P. & LEAF, A. 2006. Potent block of inactivation-deficient Na+ channels by n-3 polyunsaturated fatty acids. *Am J Physiol Cell Physiol,* 290**,** C362-70.

XIE, D., HU, P., XIAO, Z., WU, W., CHEN, Y. & XIA, K. 2007. Subunits of voltage-gated calcium channels in murine spiral ganglion cells. *Acta Otolaryngol,* 127**,** 8-12.

XU, J., YU, W., JAN, Y. N., JAN, L. Y. & LI, M. 1995. Assembly of voltage-gated potassium channels. Conserved hydrophilic motifs determine subfamily-specific interactions between the alpha-subunits. *J Biol Chem,* 270**,** 24761-8.

YANG, R. H., WANG, F., HOU, X. H., CAO, Z. P., WANG, B., XU, X. N. & HU, S. J. 2012. Dietary omega-3 polyunsaturated fatty acids improves learning performance of diabetic rats by regulating the neuron excitability. *Neuroscience,* 212**,** 93-103.

YANO, H., NAKANISHI, S., KIMURA, K., HANAI, N., SAITOH, Y., FUKUI, Y., NONOMURA, Y. & MATSUDA, Y. 1993. Inhibition of histamine secretion by wortmannin through the blockade of phosphatidylinositol 3-kinase in RBL-2H3 cells. *J Biol Chem,* 268**,** 25846-56.

YAROV-YAROVOY, V., DECAEN, P. G., WESTENBROEK, R. E., PAN, C. Y., SCHEUER, T., BAKER, D. & CATTERALL, W. A. 2012. Structural basis for gating charge movement in the voltage sensor of a sodium channel. *Proc Natl Acad Sci U S A,* 109**,** E93-102.

YATES, G. K., WINTER, I. M. & ROBERTSON, D. 1990. Basilar membrane nonlinearity determines auditory nerve rate-intensity functions and cochlear dynamic range. *Hear Res,* 45**,** 203-19.

YAWN, R., HUNTER, J. B., SWEENEY, A. D. & BENNETT, M. L. 2015. Cochlear implantation: a biomechanical prosthesis for hearing loss. *F1000Prime Rep,* 7**,** 45.

YE, Y., MACHADO, D. G. & KIM, D. O. 2000. Projection of the marginal shell of the anteroventral cochlear nucleus to olivocochlear neurons in the cat. *J Comp Neurol,* 420**,** 127-38.

YELLEN, G. 2002. The voltage-gated potassium channels and their relatives. *Nature,* 419**,** 35-42.

YI, E., ROUX, I. & GLOWATZKI, E. 2010. Dendritic HCN channels shape excitatory postsynaptic potentials at the inner hair cell afferent synapse in the mammalian cochlea. *J Neurophysiol,* 103**,** 2532-43.

YING, S. W., TIBBS, G. R., PICOLLO, A., ABBAS, S. Y., SANFORD, R. L., ACCARDI, A., HOFMANN, F., LUDWIG, A. & GOLDSTEIN, P. A. 2011. PIP2-mediated HCN3 channel gating is crucial for rhythmic burst firing in thalamic intergeniculate leaflet neurons. *J Neurosci,* 31**,** 10412-23.

ZAGOTTA, W. N., HOSHI, T. & ALDRICH, R. W. 1994a. Shaker potassium channel gating. III: Evaluation of kinetic models for activation. *J Gen Physiol,* 103**,** 321-62.

ZAGOTTA, W. N., HOSHI, T., DITTMAN, J. & ALDRICH, R. W. 1994b. Shaker potassium channel gating. II: Transitions in the activation pathway. *J Gen Physiol,* 103**,** 279-319.

ZAIKA, O., LARA, L. S., GAMPER, N., HILGEMANN, D. W., JAFFE, D. B. & SHAPIRO, M. S. 2006. Angiotensin II regulates neuronal excitability via phosphatidylinositol 4,5-bisphosphate-dependent modulation of Kv7 (M-type) K+ channels. *J Physiol,* 575**,** 49-67.

ZAYDMAN, M. A., SILVA, J. R., DELALOYE, K., LI, Y., LIANG, H., LARSSON, H. P., SHI, J. & CUI, J. 2013. Kv7.1 ion channels require a lipid to couple voltage sensing to pore opening. *Proc Natl Acad Sci U S A,* 110**,** 13180-5.

ZERANGUE, N., JAN, Y. N. & JAN, L. Y. 2000. An artificial tetramerization domain restores efficient assembly of functional Shaker channels lacking T1. *Proc Natl Acad Sci U S A,* 97**,** 3591-5.

ZHANG, H., CRACIUN, L. C., MIRSHAHI, T., ROHACS, T., LOPES, C. M., JIN, T. & LOGOTHETIS, D. E. 2003. PIP(2) activates KCNQ channels, and its hydrolysis underlies receptor-mediated inhibition of M currents. *Neuron,* 37**,** 963-75.

ZHANG, H., HE, C., YAN, X., MIRSHAHI, T. & LOGOTHETIS, D. E. 1999. Activation of inwardly rectifying K+ channels by distinct PtdIns(4,5)P2 interactions. *Nat Cell Biol,* 1**,** 183-8.

ZHANG, L., FOSTER, K., LI, Q. & MARTENS, J. R. 2007. S-acylation regulates Kv1.5 channel surface expression. *Am J Physiol Cell Physiol,* 293**,** C152-61.

ZHANG, Y., ZHANG, W., JOHNSTON, A. H., NEWMAN, T. A., PYYKKO, I. & ZOU, J. 2012. Targeted delivery of Tet1 peptide functionalized polymersomes to the rat cochlear nerve. *Int J Nanomedicine,* 7**,** 1015-22.

ZHOU, M. & MACKINNON, R. 2004. A mutant KcsA K(+) channel with altered conduction properties and selectivity filter ion distribution. *J Mol Biol,* 338**,** 839-46.

ZHOU, M., MORAIS-CABRAL, J. H., MANN, S. & MACKINNON, R. 2001a. Potassium channel receptor site for the inactivation gate and quaternary amine inhibitors. *Nature,* 411**,** 657-61.

ZHOU, Y. & MACKINNON, R. 2003. The occupancy of ions in the K+ selectivity filter: charge balance and coupling of ion binding to a protein conformational change underlie high conduction rates. *J Mol Biol,* 333**,** 965-75.

ZHOU, Y., MORAIS-CABRAL, J. H., KAUFMAN, A. & MACKINNON, R. 2001b. Chemistry of ion coordination and hydration revealed by a K+ channel-Fab complex at 2.0 A resolution. *Nature,* 414**,** 43-8.

ZHOU, Z., LIU, Q. & DAVIS, R. L. 2005. Complex regulation of spiral ganglion neuron firing patterns by neurotrophin-3. *J Neurosci,* 25**,** 7558-66.

ZHU, J., YAN, J. & THORNHILL, W. B. 2014. The Kv1.3 potassium channel is localized to the cis-Golgi and Kv1.6 is localized to the endoplasmic reticulum in rat astrocytes. *FEBS J,* 281**,** 3433-45.

ZUCCOTTI, A., LEE, S. C., CAMPANELLI, D., SINGER, W., SATHEESH, S. V., PATRIARCHI, T., GEISLER, H. S., KOPSCHALL, I., ROHBOCK, K., NOTHWANG, H. G., HU, J., HELL, J. W., SCHIMMANG, T., RUTTIGER, L. & KNIPPER, M. 2013. L-type CaV1.2 deletion in the cochlea but not in the brainstem reduces noise vulnerability: implication for CaV1.2-mediated control of cochlear BDNF expression. *Front Mol Neurosci,* 6**,** 20.